



ΕΛΛΗΝΙΚΗ ΔΗΜΟΚΡΑΤΙΑ
Εθνικό και Καποδιστριακό
Πανεπιστήμιο Αθηνών

NATIONAL AND KAPODISTRIAN UNIVERSITY OF ATHENS
MEDICAL SCHOOL, SECTOR OF BASIC MEDICAL SCIENCES LABORATORY OF
HISTOLOGY-EMBRYOLOGY
DIRECTOR: PROFESSOR VASSILIS G. GORGOULIS

**The role of the replication licensing factor CDC6 in oncogenesis: a study in
inducible cellular models**

PhD THESIS

Christos-Nektarios Zampetidis
Medical Doctor-Molecular Biologist

SUPERVISOR: Assistant Professor Sophia Havaki

ATHENS, GREECE, 2021



ΕΛΛΗΝΙΚΗ ΔΗΜΟΚΡΑΤΙΑ
Εθνικό και Καποδιστριακό
Πανεπιστήμιο Αθηνών

**NATIONAL AND KAPODISTRIAN UNIVERSITY OF ATHENS
MEDICAL SCHOOL, SECTOR OF BASIC MEDICAL SCIENCES LABORATORY OF
HISTOLOGY-EMBRYOLOGY**

DIRECTOR: PROFESSOR VASSILIS G. GORGOULIS

**The role of the replication licensing factor CDC6 in oncogenesis: a study in
inducible cellular models**

PhD THESIS

Christos-Nektarios Zampetidis

Medical Doctor-Molecular Biologist

SUPERVISOR: Assistant Professor Sophia Havaki

ATHENS, GREECE, 2021

Advisory Committee

Vassilis G. Gorgoulis, Professor-Director, Laboratory of Histology-Embryology, Medical School, National and Kapodistrian University of Athens, Athens, Greece

Alexandra Giatromanolaki, Professor, Medical School, Democritus University of Thrace, Alexandroupolis, Greece

Sophia Havaki (Supervisor), Assistant Professor, Laboratory of Histology Embryology, Medical School, National and Kapodistrian University of Athens, Athens, Greece

Examining Committee

Vassilis G. Gorgoulis, Professor-Director, Laboratory of Histology-Embryology, Medical School, National and Kapodistrian University of Athens, Athens, Greece

Kavantzias Nikolaos, Professor-Director, Department of Pathology, Medical School, National and Kapodistrian University of Athens, Athens, Greece

Alexandra Giatromanolaki, Professor, Department of Pathology, Medical School, Democritus University of Thrace, Alexandroupolis, Greece

Theodoros Troupis, Professor-Director of the Department of Anatomy, Medical School, National and Kapodistrian University of Athens, Athens, Greece

Athanasios Kotsinas, Associate Professor, Laboratory of Histology-Embryology, Medical School, National and Kapodistrian University of Athens, Athens, Greece

Konstantinos Evangelou, Associate Professor, Laboratory of Histology-Embryology, Medical School, National and Kapodistrian University of Athens, Athens, Greece

Sophia Havaki (Supervisor), Assistant Professor, Laboratory of Histology-Embryology, Medical School, National and Kapodistrian University of Athens

Dean of the Faculty of Medicine of Athens

Gerasimos Siasos, Professor of Cardiology, Medical School, National and Kapodistrian University of Athens, Athens, Greece

Date of submission for advisory committee registration: 24/04/2015

Date of advisory committee registration: 03/06/2015

Date of project's title submission: 01/07/2016

Date of PhD thesis submission: 21/12/2021

Ο ΟΡΚΟΣ ΤΟΥ ΙΠΠΟΚΡΑΤΟΥΣ

 ΜΝΥΜΙ ΑΠΟΛΛΥΝΑ ΙΗΤΡΟΝ, ΚΑΙ ΑΣΚΛΗΠΙΟΝ,
 ΚΑΙ ΥΓΕΙΑΝ, ΚΑΙ ΠΑΝΑΚΕΙΑΝ, ΚΑΙ ΘΕΟΥΣ ΠΑΝ
 ΤΑΣ ΤΕ ΚΑΙ ΠΑΣΑΣ, ΙΣΤΟΡΑΣ ΠΟΙΕΥΜΕΝΟΣ, ΕΠΙ
 ΤΕΛΕΑ ΠΟΙΗΣΕΙΝ ΚΑΤΑ ΔΥΝΑΜΙΝ ΚΑΙ ΚΡΙΣΙΝ ΕΜΗΝ
 ΟΡΚΟΝ ΤΟΝΔΕ ΚΑΙ ΞΥΓΓΡΑΦΗΝ ΤΗΝΔΕ· ΗΓΗΣΑΣΘ
 ΑΙ ΜΕΝ ΤΟΝ ΔΙΔΑΞΑΝΤΑ ΜΕ ΤΗΝ ΤΕΧΝΗΝ ΤΑΥΤΗ
 Ν ΙΣΑ ΓΕΝΕΤΗΣΙΝ ΕΜΟΙΣΙ, ΚΑΙ ΒΙΟΥ ΚΟΙΝΩΣΑΣΘΑΙ, Κ
 ΑΙ ΧΡΕΩΝ ΧΡΗΖΟΝΤΙ ΜΕΤΑΔΟΣΙΝ ΠΟΙΗΣΑΣΘΑΙ, Κ
 ΑΙ ΓΕΝΟΣ ΤΟ ΕΞ ΛΥΤΕΟΥ ΑΔΕΛΦΟΙΣ ΙΣΟΝ ΕΠΙΚΡΙΝ
 ΕΕΙΝ ΑΡΡΕΣΙ, ΚΑΙ ΔΙΔΑΞΕΙΝ ΤΗΝ ΤΕΧΝΗΝ ΤΑΥΤΗΝ,
 ΗΝ ΧΡΗΖΩΣΙ ΜΑΝΘΑΝΕΙΝ, ΑΝΕΥ ΜΙΣΘΟΥ ΚΑΙ ΞΥ
 ΓΓΡΑΦΗΣ, ΠΑΡΑΓΓΕΛΙΗΣ ΤΕ ΚΑΙ ΑΚΡΟΗΣΙΟΣ ΚΑΙ ΤΗΣ
 ΛΟΙΠΗΣ ΑΠΑΣΗΣ ΜΑΘΗΣΙΟΣ ΜΕΤΑΔΟΣΙΝ ΠΟΙΗΣΑΣ
 ΘΑΙ ΥΙΟΙΣΙ ΤΕ ΕΜΟΙΣΙ, ΚΑΙ ΤΟΙΣΙ ΤΟΥ ΕΜΕ ΔΙΔΑΞΑΝ
 ΤΟΣ, ΚΑΙ ΜΑΘΗΤΑΙΣΙ ΣΥΓΓΕΓΡΑΜΜΕΝΟΙΣΙ ΤΕ ΚΑΙ ΛΟ
 ΚΙΣΜΕΝΟΙΣ ΝΟΜΩ, ΙΗΤΡΙΚΩ, ΑΛΛΩ, ΔΕ ΟΥΔΕΝΙ·
 ΔΙΔΙΤΗΜΑΣΙ ΤΕ ΧΡΗΣΟΜΑΙ ΕΠ' ΩΦΕΛΕΙΗ, ΚΑΜΝΟ
 ΝΤΩΝ ΚΑΤΑ ΔΥΝΑΜΙΝ ΚΑΙ ΚΡΙΣΙΝ ΕΜΗΝ, ΕΠΙ ΔΗΛΗ
 ΣΕΙ ΔΕ ΚΑΙ ΑΔΙΚΗ, ΕΙΡΞΕΙΝ. ☒ ΟΥ ΔΩΣΩ ΔΕ ΟΥΔΕ
 ΦΑΡΜΑΚΟΝ ΟΥΔΕΝΙ ΑΙΤΗΘΕΙΣ ΘΑΝΑΣΙΜΟΝ, ΟΥΔΕΥ
 ΦΗΓΗΣΟΜΑΙ ΞΥΜΒΟΥΛΙΗΝ ΤΟΙΗΝΔΕ· ΟΜΟΙΩΣ ΔΕ ΟΥ
 ΔΕ ΓΥΝΑΙΚΙ ΠΕΣΣΟΝ ΦΘΟΡΙΟΝ ΔΩΣΩ. ☒ ΑΓΝΩΣ Δ
 Ε ΚΑΙ ΟΣΙΩΣ ΔΙΑΤΗΡΗΣΩ ΒΙΟΝ ΤΟΝ ΕΜΟΝ ΚΑΙ ΤΕΧΝ
 ΗΝ ΤΗΝ ΕΜΗΝ. ☒ ΟΥ ΤΕΜΕΩ ΔΕ ΟΥΔΕ ΜΗΝ ΛΙΘ
 ΙΛΩΤΑΣ, ΕΚΧΩΡΗΣΩ ΔΕ ΕΡΓΑΤΗΣΙΝ ΑΝΔΡΑΣΙ ΠΡ
 ΗΞΙΟΣ ΤΗΣΔΕ. ☒ ΕΣ ΟΙΚΙΑΣ ΔΕ ΟΚΟΣΑΣ ΑΝ ΕΣΩ,
 ΕΞΕΛΕΥΣΟΜΑΙ ΕΠ' ΩΦΕΛΕΙΗ, ΚΑΜΝΟΝΤΩΝ, ΕΚΤ
 ΟΣ ΕΩΝ ΠΑΣΗΣ ΑΔΙΚΗΣ ΕΚΟΥΣΙΗΣ ΚΑΙ ΦΘΟΡΙΗΣ, Τ
 ΗΣ ΤΕ ΑΛΛΗΣ ΚΑΙ ΑΦΡΟΔΙΣΙΩΝ ΕΡΓΩΝ ΕΠΙ ΤΕ ΓΥ
 ΝΑΙΚΕΙΩΝ ΣΩΜΑΤΩΝ ΚΑΙ ΑΝΔΡΩΝ, ΕΛΕΥΘΕΡ
 ΩΝ ΤΕ ΚΑΙ ΔΟΥΛΩΝ. ☒ Α Δ' ΑΝ ΕΝ ΘΕΡΑΠΕΙΑ,
 Η ΙΔΩ, Η ΔΚΟΥΣΩ, Η ΚΑΙ ΑΝΕΥ ΘΕΡΑΠΗΪΗΣ ΚΑΤΑ Β
 ΙΟΝ ΑΝΘΡΩΠΩΝ, Δ ΜΗ ΧΡΗ ΠΟΤΕ ΕΚΛΑΛΕΕΣΘΑΙ
 ΕΞΩ, ΣΙΓΗΣΟΜΑΙ, ΑΡΡΗΤΑ ΗΓΕΥΜΕΝΟΣ ΕΙΝΑΙ ΤΑ ΤΟ
 ΙΔΥΤΑ. ☒ ΟΡΚΟΝ ΜΕΝ ΟΥΝ ΜΟΙ ΤΟΝΔΕ ΕΠΙΤΕΛΕ
 Δ ΠΟΙΕΟΝΤΙ, ΚΑΙ ΜΗ ΞΥΓΧΕΟΝΤΙ, ΕΙΗ ΕΠΑΥΡΑΣΘ
 ΑΙ ΚΑΙ ΒΙΟΥ ΚΑΙ ΤΕΧΝΗΣ ΔΟΞΑΖΟΜΕΝΩ, ΠΑΡΑ Π
 ΔΣΙΝ ΑΝΘΡΩΠΟΙΣ ΕΣ ΤΟΝ ΔΙΕΙ ΧΡΟΝΟΝ· ΠΑΡΑΒΑΙ
 ΝΟΝΤΙ ΔΕ ΚΑΙ ΕΠΙΟΡΚΟΥΝΤΙ, ΤΑΝΑΝΤΙΑ ΤΟΥΤΕΩΝ.



Christos-Nektarios Zampetidis

Athens, Greece

Telephone:

Email: chzambo@yahoo.gr

Date of birth: 23/01/1991

Nationality: Hellenic (Greek)

EDUCATION QUALIFICATIONS

2015-2021 PhD in the Department of Histology-Embryology, Medical School of Athens, National Kapodistrian University of Athens (Athens, Greece). **PhD Thesis Project:** “The role of the pre-replicative complex (pre-RC) component, *Cdc6*, in autophagy and carcinogenesis.

Supervisors: Prof. Vassilis Gorgoulis, Dr. Sophia Havaki

2016-2021 Undergraduate Medical Studies, Medical School of Athens, National Kapodistrian University of Athens (Athens, Greece),
Grade: 8.25/10.

2013-2014 MSc “Reproductive and Developmental Biology”, Department of Surgery and Cancer, Division of Cancer, Imperial College London (London, UK), Grade: 2:1 (Merit/Upper Second Class).

Diploma Thesis Project: “c-Met inhibition as a strategy to overcome epithelial-mesenchymal transition (EMT) chemotherapy resistance in ovarian cancer cell lines” (Grade: Distinction/First Class).

Supervisor: Dr. Sarah Blagden

2008-2012 BSc in Department of Molecular Biology and Genetics, Democritus University of Thrace (Alexandroupolis, Greece), Grade: 7.64/10.

Diploma Thesis Project: “Silibinin: Chemopreventive properties and underlying molecular mechanisms using an *in vitro* preclinical model of metastatic pharyngeal carcinoma” (Grade: 10/10).

Supervisor: Dr. Aglaia Pappa

RESEARCH EXPERIENCE

2015-2021 PhD in the Department of Histology-Embryology, Medical School of Athens, National Kapodistrian University of Athens (Athens, Greece).

2014 MSc Thesis Project under the supervision of Dr. Sarah Blagden, Department of Surgery and Cancer, Division of Cancer, Imperial College London (London, UK).

2012 BSc Thesis Project under the supervision of Dr. Aglaia Pappa, Department of Molecular Biology and Genetics, Democritus University of Thrace (Alexandroupolis, Greece).

2010 Research assistant at the Department of Nuclear Medicine, Alexandroupolis University Hospital (Alexandroupolis, Greece).

LABORATORY EXPERIENCE

Cell culture:

- ✓ Mammalian normal and cancer cell lines
- ✓ Embryonic stem cells

Cell and Molecular Biology Assays:

- ✓ General molecular biology techniques (DNA/RNA/Protein isolation)
- ✓ Western Blotting
- ✓ ELISA
- ✓ PCR (conventional and RT)
- ✓ DNA fiber assay

Microscopy:

- ✓ Optical
- ✓ Confocal
- ✓ Electron

Immunochemical techniques:

- ✓ Immunochemistry
- ✓ Immunofluorescence

Nuclear Medicine Assays:

- ✓ Radioimmunoassay (RIA)
- ✓ Immunoradiometric assay (IRMA)

CLINICAL EXPERINECE

- ✓ Rotation in many different hospitals and departments as part of the Medical School Degree training (Internal Medicine, Surgery, Radiology, ENT, Ophthalmology, Urology, Orthopedics, Neurology, Cardiology, Respiratory Medicine, Intensive Care Unit, Psychiatry, Pediatrics, Gynecology).

PUBLICATIONS

- ✓ A recurrent chromosomal inversion suffices for driving escape from oncogene-induced senescence via subTAD reorganization (2021). **Zampetidis C.P.***, Galanos P.*, Angelopoulou A.*, Zhu Y., Polyzou Ai., Karamitros T., Kotsinas A., Lagopati N., Mourkioti I., Mirzazadeh R., Polyzos A., Garnerone S., Mizi A., Gusmao E.G., Sofiadis K., Gál Z., Larsen D.H., Pefani D.E., Demaria M., Tsirigos A., Crosetto N., Maya-Mendoza A., Papaspyropoulos A., Evangelou K., Bartek J., Papantonis A., Gorgoulis V.G. Mol Cell
- ✓ A prototypical non-malignant epithelial model to study genome dynamics and concurrently monitor micro-RNAs and proteins in situ during oncogene-induced senescence (2018). Komseli E.S., Pateras I.S., Krejsgaard T., Stawiski K., Rizou S.V., Polyzos A., Roumelioti F.M., Chiourea M., Mourkioti I., Paparouna E., **Zampetidis C.P.**, Gumeni S., Trougakos I.P., Pefani D.E., O'Neill E., Gagos S., Eliopoulos A.G., Fendler W., Chowdhury D., Bartek J., Gorgoulis V.G. BMC Genomics 19(1): 37
- ✓ Monitoring Autophagy Immunohistochemically and Ultrastructurally during Human Head and Neck Carcinogenesis. Relationship with the DNA Damage Response Pathway (2017). Havaki S.*, Vlachou V.*, **Zampetidis C.P.***, Selemenakis P., Kotsinas A., Mavrogonatou E., Rizou S.V., Kyrodimos E., Evangelou K., Kletsas D., Giatromanolaki A., Gorgoulis V.G. Int J Mol Sci 18(9)
- ✓ Unravelling a p73-regulated network: The role of a novel p73-dependent target, MIR3158, in cancer cell migration and invasiveness (2017). Galtsidis S., Logotheti S., Pavlopoulou A., **Zampetidis C.P.**, Papachristopoulou G., Scorilas A., Vojtesek B., Gorgoulis V., Zoumpourlis V. Caner Lett 388:96-106

STUDENTSHIPS/AWARDS

- ✓ Marie Curie Innovative Training Networks (MSCA-ITN) studentship for PhD related research (2017-2020)

LANGUAGE SKILLS

- ✓ Greek: Native speaker
- ✓ English: Working Proficiency C2 (MSc in the UK, IELTS Overall Band 7.5)
- ✓ French: Fluent B2 (DELFA1, A2, A3, A4)

Contents

Acknowledgements	13
Abstract (English)	15
Abstract (Greek)	18
Introduction	21
1.1 Cancer	22
1.1.1 Defining cancer.....	23
1.1.2 Benign and malignant tumors.....	23
1.1.3 Categorization of tumors based on embryonic origin and histology.....	24
1.1.4 Grading and staging of tumors.....	25
1.1.5 Carcinogenesis.....	25
1.1.6 Causes/Etiology of cancer.....	27
1.1.7 Commonly affected genes.....	28
1.1.8 Hallmarks of cancer.....	30
1.1.9 Emerging hallmarks of cancer.....	34
1.1.10 Enabling characteristics of cancer.....	35
1.2 Cell cycle	37
1.2.1 Checkpoints and cell cycle regulation.....	38
1.2.2 Cyclins and cell cycle regulation.....	38
1.2.3 Role of CDKs and CDKIs on cell cycle regulation.....	40

1.2.4 Cell cycle regulation by tumor suppressor genes.....	41
1.2.5 Cellular senescence.....	42
1.3 DNA replication.....	43
1.3.1 Origins of replication.....	44
1.3.2 Initiation of DNA replication.....	45
1.3.3 Replication checkpoints.....	46
1.3.4 The CDC6 replication licensing factor.....	47
1.3.5 CDC6 in other phases of the cell cycle.....	48
1.4 CDC6 in cancer progression.....	49
1.4.1 Molecular mechanisms implicated in CDC6 deregulation.....	51
1.4.2 Mechanisms through which CDC6 exerts oncogenic activity.....	53
1.4.3 CDC6 and senescence induction.....	55
Aim of PhD thesis.....	57
Materials and Methods.....	59
2.1 Methods.....	60
2.1.1 Cell lines and treatments.....	60
2.1.2 Plasmid generation.....	60
2.1.3 siRNA and plasmids transfection.....	60
2.1.4 Selection of escaped clones.....	61
2.1.5 Protein extraction, cell fractionation and immunoblot analysis.....	61
2.1.6 Immunofluorescence analysis.....	61
2.1.7 Immunocytochemistry.....	62

2.1.8 Cell growth analysis.....	63
2.1.9 3D (organotypic/organoid) culture.....	63
2.1.10 Senescence detection with SenTraGor.....	63
2.1.11 Invasion assay.....	64
2.1.12 Flow cytometry analysis (FACS) - Cell cycle analysis.....	64
2.1.13 5'-EU incorporation based nascent RNA assay.....	64
2.1.14 QIBC analysis.....	65
2.1.15 DR-GFP, SA-GFP and BIR-GFP reporter assays.....	66
2.1.16 DNA fiber fluorography (combing assay).....	66
2.1.17 Breaks Labeling In Situ and Sequencing (BLISS).....	66
2.1.18 Next Generation Sequencing and Bioinformatics analysis.....	67
2.1.19 RNA isolation, sequencing, and data analysis.....	67
2.1.20 Chromatin immunoprecipitation (ChIP), sequencing, and data analysis.....	68
2.1.21 Genome-wide chromosome conformation capture (Hi-C) and data analysis...	68
2.1.22 CRISPR/Cas9 inversion generation.....	69
2.1.23 Sanger sequencing.....	70
2.1.24 Survival data analysis.....	71
2.1.25 Quantification and statistical analysis.....	71
2.2 Materials.....	72
Results.....	79
3.1 Assessment of a cellular system recapitulating oncogene-induced senescence.....	80
3.1.1 Escaped cells acquire an EMT-like phenotype.....	85
3.1.2 CDC6 overexpression generates DNA damage and the lesions are repaired in an error-prone manner.....	86

3.1.3 Genomic alterations occurring early upon senescence contribute to the evasion- from-senescence phenotype and are found in the genome of escaped cells....	92
3.1.4 A large inversion in chromosome 3p encompasses the circadian transcription factor BHLHE40.....	98
3.1.5 BHLHE40 is pivotal for the maintenance of the escape phenotype.....	102
3.1.6 An artificially engineered inversion in chromosome 3p is sufficient for senescence bypass.....	103
3.1.7 Generation of a novel cellular system overexpressing BHLHE40 protein based on HBEC-CDC6/TetON cellular setting.....	108
3.1.8 BHLHE40 is up-regulated in a replication-dependent manner.....	110
3.1.9 BHLHE40 induction and escape from senescence occur due to chromatin Refolding.....	111
3.1.10 Human pancreatic ductal epithelial cells show a different behavior upon CDC6 Overexpression.....	112
3.2 CDC6 silencing as a strategy to inhibit cancer progression.....	113
3.2.1 CDC6 inhibition alters the cell cycle profile and induces senescence.....	116
3.2.2 MDA-MB-231 cells acquire a phenotype resembling mitotic catastrophe.....	117
3.2.3 MDA-MB-231 cells gradually accumulate in M phase.....	119
Discussion.....	123
References.....	129
Annex.....	146

Acknowledgements

First, I would like to express my personal gratitude to Professor Vassilis Gorgoulis for giving me the opportunity to work as a member in his group and for supporting me and guiding me throughout the course of this project, from inception to completion. The completion of this study could have not been possible without his expertise and his patience in working with me the past years.

I would also like to thank and acknowledge my advisory committee for their time and effort in providing me with assistance and encouragement. Special thanks to Dr. Sophia Havaki for undertaking the official position as supervisor of the present PhD thesis.

Furthermore, I would like to thank the examining committee for participating in my defense and helping me strengthen my thesis. I owe special thanks to Dr. Thanos Kotsinas for his invaluable help throughout the whole duration of this project. He was always available for providing his advice in every single step of this study. I would also like to thank Dr. Kostas Evangelou for his support during the writing of our recently published research article.

My second round of acknowledgements are devoted to the people who contributed to the publication of the research article related to this thesis. Prominent among these are Professor Jiri Bartek, Professor Argyris Papantonis, Dr. Panos Galanos and Ms. Andriani Angelopoulou for supporting the laboratory experiments of this project. In addition, I would like to thank Professor Jiri Bartek for accepting me in his laboratory at the Danish Cancer Society in Copenhagen, Denmark and also Dr. Panos Galanos and Mr. Giorgos Pappas for guiding me during my visit in Copenhagen. It would be an omission if I do not acknowledge all the members of our research group and the support I received during the course of this doctoral project.

Primary finding support for this project was provided by the European Union Horizon 2020 Research and Innovation Program under Marie Skłodowska-Curie grant agreement 722729 (SYNTRAIN).

Last but not least, I owe my parents a heartfelt thank you for their continued guidance, support and encouragement. I express my complete gratitude to them as their interest in my studies has propelled my motivation and given me the strength to further achieve.

Abstract

Homeostasis is a fundamental feature of single and multi-cellular organisms that is maintained by cellular responses that counteract a plethora of deleterious intrinsic and extrinsic signals (Lloyd et al. 2001). Aberrations in the modulating pathways that govern these responses result in excess of damage, functional defects and disease emergence, including cancer (Gorgoulis and Halazonetis 2010). In cancer cells, one of the most frequently affected cellular functions is the proper execution of the cell cycle, which under specific circumstances can produce genomic instability (Negrini et al. 2010). This established hallmark of cancer is closely related to the dysfunction of the replication licensing machinery (Petrakis et al. 2016).

Cell division cycle 6 (CDC6) is a pivotal molecule of this apparatus. Coordinated expression of CDC6, together with ORC and CDT1, facilitate timely loading of MCM2-7 onto the chromatin in G1 phase, forming the pre-replicative complex. This results in licensing of the replication origins once per cell cycle and ensuring the accurate duplication of the whole genome before cell division (Blow and Gillespie 2008). Moreover, CDC6 is engaged into the activation of checkpoints that regulate S phase and mitosis (Borlado and Mendez 2008).

Interestingly, accumulating amount of data supports that deregulated expression of CDC6 exerts oncogenic activity. Particularly, it is frequently overexpressed in cancer, usually from its earliest stages, and is associated with poor prognosis (Williams et al. 1998, Karakaidos et al. 2004, Lontos et al. 2007, Sideridou et al. 2011). CDC6 overexpression results in re-replication and eventually in DNA damage and genomic instability (Vaziri et al. 2003, Lontos et al. 2007, Sideridou et al. 2011, Walter et al. 2016). Subsequent activation of DNA damage response checkpoints triggers the antitumor barriers of senescence and apoptosis (Bartkova et al. 2006, Petrakis et al. 2016), while selective loss of p53 promotes malignant behavior (Karakaidos et al. 2004, Lontos et al. 2007, Halazonetis et al. 2008) and acquisition of mesenchymal traits through E-cadherin down-regulation, a hallmark of epithelial-to-mesenchymal transition (EMT) (Lontos et al. 2007, Sideridou et al. 2011). More recently, CDC6 has been

shown to be involved in the transcription of rRNA (Huang, Xu et al. 2016) and CXCL12 (Petrakis et al. 2016).

To investigate the role of CDC6 in oncogenesis our group has developed a prototypical non-malignant epithelial cellular system overexpressing CDC6 in an inducible manner in Human Bronchial Epithelial Cells (HBECs), a non-cancerous lung cell line (Komseli et al. 2018). The immortalization of the cells generated was achieved with a combined expression of human telomerase reverse transcriptase (hTERT) and an ectopic mutant cyclin dependent kinase 4 (CDK4), maintaining their epithelial phenotype and preserving intact the p53 checkpoint pathway (Ramirez et al., 2004). Thus, they represent a valuable tool for studying carcinogenesis, since the majority of malignancies have epithelial origin and lung cancer is among the most frequent cancer types in clinics.

CDC6 forced expression resulted in the activation of senescence after 6 days, whereas protracted overexpression enabled the cells to evade senescence in about 30 days, following CDC6 induction, resulting in the emergence of aggressive clones with high invasive potential (Komseli et al. 2018). Nevertheless, the events leading to the escape from senescence were not clear until now. Hence, the aim of the present PhD thesis is to interrogate for the mechanism(s) involved in this process.

Upon CDC6 induction, DNA damage occurred and subsequently repair mechanisms were triggered. However, the nature of the DNA repair pathways that were activated resulted in erroneous repair of the genome. Thus, genetic alterations occurred and among them, the most prominent defect discovered, is a large chromosomal inversion at chromosome 3p. The affected chromosomal locus located in this inversion, concerns the BHLHE40 coding locus. BHLHE40 is a transcription factor involved in the daily regulation of the circadian clock (Kato et al. 2014, Sato et al. 2016). Interestingly, this factor targets >68% of the differentially regulated genes found between the non-induced and the cells that escaped senescence. Furthermore, BHLHE40 is overexpressed in the escaped cells and plays a crucial role in the preservation of their phenotype, as its down-regulation induces cell death.

For this purpose, we decided to generate an artificial genetic inversion at chromosome 3p, mimicking the naturally selected inversion. As expected, the cells bearing the inversion bypassed senescence. Similar results were obtained after introducing a BHLHE40-expressing vector into the HBECs. Interestingly, remodeling of the BHLHE40 3D chromatin structure coincides with its activation.

The above mentioned results indicate that CDC6 can be a promising target for cancer inhibition. Given that CDC6 overexpression also correlates with adverse outcome in cancer patients, we down-regulated CDC6 in breast cancer cell lines that overexpress this replication licensing factor. Our results suggest that CDC6 abrogation induces DNA damage, cellular senescence and cell death. Importantly, cells were eliminated via mitotic catastrophe in the triple-negative cell line, which coincides with the abrogation of G2/M checkpoint.

Overall, the main aim of the present PhD thesis was to uncover the underlying mechanistic basis, responsible for the escape from oncogene-induced senescence. Early events occurring during the first few days of CDC6 induction proved to play a pivotal role in the escape phenomenon/process and particularly genetic alterations revealed to be of high importance for the emergence of aggressive cell clones. Among them an inversion in chromosome 3p led to the rearrangement of the 3D chromatin structure and to the subsequent overexpression of the BHLHE40 transcription factor. This event, finally, modified the expression pattern of a series of genes and hence promoted the escape from the anti-tumor barrier of senescence. Considering that CDC6 is a triggering event for malignant transformation and is also related to poor overall survival, inhibiting its function in cancer patients can be a promising therapeutic strategy. On the other hand, an alternative therapeutic approach could exploit the concurrent elimination of senescent cells with senolytic drugs, in parallel with the use of traditional chemotherapeutic schemes that are known to induce senescence.

Περίληψη

Η ομοιόσταση συνιστά θεμελιώδη ιδιότητα των οργανισμών και εξασφαλίζεται μέσω πληθώρας κυτταρικών αποπκρίσεων έναντι ενδογενών και εξωγενών παραγόντων. Η διαταραχή των μηχανισμών που ελέγχουν τις διαδικασίες αυτές οδηγεί στη συσσώρευση βλαβών και γενικά στην απορρύθμιση της κυτταρικής λειτουργίας με επακόλουθο την εμφάνιση νόσων, όπως ο καρκίνος. Στους όγκους παρατηρείται συχνά διατάραξη της ομαλής εξέλιξης του κυτταρικού κύκλου, που υπό προϋποθέσεις μπορεί να οδηγήσει στην πρόκληση γενωμικής αστάθειας. Η τελευταία έχει καθιερωθεί τα τελευταία χρόνια ως χαρακτηριστικό των καρκινικών κυττάρων και σχετίζεται στενά με την διαταραχή του μηχανισμού αδειοδότησης της αντιγραφής του DNA.

Ο παράγοντας CDC6 αποτελεί κύριο συστατικό αυτής της λειτουργίας. Το CDC6 μαζί με τις πρωτεΐνες ORC και CDT1 διευκολύνουν την στρατολόγηση των παραγόντων MCM2-7 στη χρωματίνη κατά την G1 φάση του κυτταρικού κύκλου, προκειμένου να σχηματιστεί το προ-αντιγραφικό σύμπλοκο. Έτσι η αδειοδότηση των θέσεων έναρξης της αντιγραφής θα συμβεί μια φορά ανά κυτταρικό κύκλο πράγμα το οποίο εξασφαλίζει την απρόσκοπτη αντιγραφή του γενετικού υλικού πριν την κυτταρική διαίρεση. Επίσης, το CDC6 συμμετέχει στα σημεία ελέγχου που ρυθμίζουν την φάση S του κυτταρικού κύκλου καθώς και την μίτωση.

Όλο και περισσότερα δεδομένα υποστηρίζουν ότι η απορρυθμισμένη έκφραση του CDC6 έχει ογκογόνο δυναμικό. Συγκεκριμένα, το CDC6 είναι συχνά υπερ-εκφρασμένο από τα αρχικά στάδια της καρκινογένεσης και συσχετίζεται με μειωμένο χρόνο ζωής των ασθενών. Επίσης, η υπερ-έκφραση του CDC6 έχει αποδειχθεί ότι οδηγεί σε επαναντιγραφή του DNA και τελικά σε βλάβη του γενετικού υλικού και γενωμική αστάθεια. Η επακόλουθη ενεργοποίηση των κυτταρικών μηχανισμών απόκρισης στην βλάβη του DNA πυροδοτεί τους αντικαρκινικούς φραγμούς της κυτταρικής γήρανσης και της απόπτωσης, ενώ η απώλεια του ογκο-κατασταλτικού γονιδίου p53 προωθεί την ανάπτυξη κακοήθειας και τελικά την επιθηλιο-μεσεγχυματική μετατροπή (EMT). Πιο πρόσφατα βρέθηκε ότι το CDC6 εμπλέκεται στην μεταγραφή του ριβοσωμικού RNA (rRNA).

Προκειμένου να μελετήσουμε τον ρόλο του CDC6 στην ογκογένεση η ερευνητική μας ομάδα ανέπτυξε ένα κυτταρικό σύστημα το οποίο έχει την δυνατότητα να υπερ-εκφράζει τον παράγοντα CDC6 μέσα σε αθανατοποιημένα φυσιολογικά κύτταρα βρογχικού επιθηλίου (Human Bronchial Epithelial Cells, HBECS). Η αθανατοποίηση των κυττάρων έγινε με συνδυαστική υπερ-έκφραση τελομεράσης και της πρωτεΐνης CDK4. Τα κύτταρα αυτά διατηρούν τον επιθηλιακό τους φαινότυπο και έχουν άθικτο το μονοπάτι ελέγχου μέσω του p53. Έτσι, αντιπροσωπεύουν ένα φυσιολογικό επιθηλιακό περιβάλλον και αποτελούν ένα πολύτιμο εργαλείο για τη μελέτη της καρκινογένεσης, καθώς η πλειοψηφία των κακοηθειών έχει επιθηλιακή προέλευση και συγκεκριμένα ο καρκίνος του πνεύμονα βρίσκεται μεταξύ των πιο συχνών τύπων καρκίνου στον άνθρωπο.

Η υπερ-έκφραση του CDC6 για 6 ημέρες είχε ως αποτέλεσμα την ενεργοποίηση της κυτταρικής γήρανσης, ενώ η παρατεταμένη υπερ-έκφρασή του καθιστά τα κύτταρα ικανά να διαφύγουν της κυτταρικής γήρανσης μετά από περίπου 30 ημέρες. Παρόλα αυτά, τα γεγονότα που οδηγούν στην διαφυγή από την κυτταρική γήρανση δεν είναι ξεκάθαρα. Ως εκ τούτου, ο σκοπός της παρούσας Διδακτορικής Διατριβής είναι να μελετήσει τους μηχανισμούς που συμμετέχουν σε αυτή την διαδικασία.

Σύντομα μετά την ενεργοποίηση του CDC6, εμφανίζονται βλάβες στο DNA και ως συνέπεια αυτού, οι επιδιορθωτικοί μηχανισμοί του DNA ενεργοποιούνται. Όμως, τα μονοπάτια επιδιόρθωσης που ενεργοποιήθηκαν οδήγησαν στην εμφάνιση λαθών κατά την επιδιόρθωση του γενετικού υλικού. Έτσι, γενετικές αλλοιώσεις προέκυψαν και μεταξύ αυτών η πιο αξιοσημείωτη είναι μια εκτεταμένη αναστροφή του γενετικού υλικού στο χρωμόσωμα 3. Η περιοχή του χρωμοσώματος που αντιστρέφεται, περιλαμβάνει το γονίδιο BHLHE40. Η πρωτεΐνη που κωδικοποιείται από αυτό το γονίδιο είναι ένας μεταγραφικός παράγοντας ο οποίος συμμετέχει στη ρύθμιση του κερκάδιου ρυθμού. Σημαντικό κρίνεται το γεγονός ότι ο παράγοντας BHLHE40 ρυθμίζει >68% των γονιδίων που εμφανίζουν διαφορετική έκφραση ανάμεσα στα κύτταρα πριν και μετά την διαφυγή από την γήρανση. Επιπρόσθετα, ο παράγοντας BHLHE40 υπερ-εκφράζεται στα κύτταρα που διαφεύγουν από την κυτταρική γήρανση και επίσης παίζει κεντρικό ρόλο στην διατήρηση του φαινοτύπου τους.

Για αυτό τον σκοπό, κατασκευάσαμε μια τεχνητή γενετική αναστροφή στο χρωμόσωμα 3, μιμούμενοι με αυτό τον τρόπο την αναστροφή που προέκυψε με φυσικό τρόπο. Όπως ήταν αναμενόμενο, τα κύτταρα που φέρουν την αναστροφή διαφεύγουν από την κυτταρική γήρανση. Παρόμοια αποτελέσματα παρήχθησαν κατόπιν εισαγωγής στα HBECs του γονιδίου BHLHE40. Είναι επίσης πολύ ενδιαφέρον να τονισθεί ότι η αναδιαμόρφωση της τρισδιάστατης διαμόρφωσης της χρωματίνης στην περιοχή του γονιδίου BHLHE40 συμπίπτει με την ενεργοποίησή του.

Τα προαναφερθέντα αποτελέσματα αποδεικνύουν ότι το CDC6 μπορεί να είναι ένας υποσχόμενος στόχος για την παρεμπόδιση της καρκινογένεσης. Δεδομένου ότι η υπερ-έκφραση του CDC6 συσχετίζεται επίσης με κακή πρόγνωση των ασθενών, βρήκαμε κυτταρικές σειρές μαστού που εκφράζουν σε περίσσεια τον εν λόγω παράγοντα και τον αποσιώπησαμε. Σύμφωνα με τα αποτελέσματά μας, η αποσιώπηση του CDC6 προκαλεί βλάβες στο DNA και ενεργοποιεί την κυτταρική γήρανση και την απόπτωση. Σημαντικό κρίνεται το γεγονός ότι τα κύτταρα προερχόμενα από τριπλό αρνητικό καρκίνο μαστού πέθαναν μέσω μιτωτικής καταστροφής, πράγμα το οποίο συμπίπτει και με την κατάργηση του σημείου ελέγχου των G2/M φάσεων του κυτταρικού κύκλου.

Συγκεντρωτικά, κατά την διάρκεια της παρούσας διδακτορικής διατριβής, ανακαλύφθηκε ο μηχανισμός που βρίσκεται πίσω από την διαφυγή από την επαγόμενη από την ενεργοποίηση ογκογονιδίων κυτταρική γήρανση. Γεγονότα που συμβαίνουν τις πρώτες ημέρες μετά την ενεργοποίηση του CDC6 αποδείχθηκαν ότι παίζουν καθοριστικό ρόλο στην διαφυγή και συγκεκριμένα οι γενετικές αλλοιώσεις είναι ιδιαίτερος σημαντικές στην εμφάνιση επιθετικών κυτταρικών κλώνων. Ανάμεσα τους μια αναστροφή στο χρωμόσωμα 3 οδήγησε στην αναδιαμόρφωση της τρισδιάστατης μορφής της χρωματίνης και επακόλουθα στην υπερ-έκφραση του μεταγραφικού παράγοντα BHLHE40. Αυτό με την σειρά του τροποποίησε την έκφραση μιας σειράς γονιδίων και με αυτό τον τρόπο προωθήθηκε η διαφυγή από τον αντικαρκινικό φραγμό της κυτταρικής γήρανσης. Γνωρίζοντας πλέον ότι το CDC6 είναι το γεγονός που πυροδότησε τον κακοήθη φαινότυπο και επίσης συσχετίζεται με μειωμένη επιβίωση των ασθενών, η φαρμακευτική του αποσιώπηση θα μπορούσε να είναι μια έξυπνη προσέγγιση για την θεραπεία του καρκίνου.

CHAPTER 1

INTRODUCTION

1.1 Cancer

Cancer is among the leading causes of death worldwide. According to World Health Organization (WHO), cancer ranks first or second leading cause of death before the age of 70 in 112 of 183 countries and is third or fourth in the remaining 23 countries based on available data. Although heart diseases were the leading cause of death in the past, a decline of heart-related deaths is observed the last few years. Among the 112 countries where cancer is the leading cause of death are included mainly developed countries such as European Union (EU) member states (including Greece), USA, Canada, Australia, Japan and China (Sung et al. 2021). This increase of cancer rates reflects the increasing aging of the global population as well as tobacco and alcohol use, consumption of unhealthy foods, physical inactivity and the increasing air pollution. Furthermore, chronic infections are also a responsible risk factor, particularly in low- and middle-income countries. Approximately 13% of cancers are attributed to several infections including *Helicobacter pylori*, human papilloma virus (HPV), hepatitis b virus (HBV), hepatitis c virus (HCV), human immunodeficiency virus (HIV) and Epstein-Barr virus (EBV). Particularly, tobacco use has been correlated with lung, colorectal, stomach and liver cancers; obesity and physical inactivity with breast and colorectal cancers and infections with liver, stomach and cervical cancers. However, a percentage of cancer cases could be avoided by applying certain precautionary measures such as not using tobacco, maintaining a healthy body weight and eating a healthy diet, doing physical activity and getting vaccinated against carcinogenic viruses e.g. HPV and HBV. In addition to the above, frequent medical screening is very important to diagnose cancer at early stages, which can result in higher survival rates as well as lower morbidity occurrence (<https://www.who.int/news-room/fact-sheets/detail/cancer>).

In Greece were diagnosed 64530 new cases in 2020 and 179828 5-year prevalent cases, whereas the estimated cancer deaths were 33166 in 2020. Lung cancer is the most frequent diagnosed cancer type in males followed by prostate, bladder, colorectal and pancreas. On the other hand, breast cancer is the most common diagnosed cancer type in females, whereas lung cancer ranks third among Greek women. Collectively in both genders, lung cancer is responsible for the majority of the newly diagnosed cancer

cases and also contributes to the majority of cancer-related mortality rates (<https://gco.iarc.fr/today/data/factsheets/populations/300-greece-fact-sheets.pdf>).

1.1.1 Defining cancer

The term cancer includes all the cases of malignant transformation. Malignant transformation is a term used to define the autonomous proliferation of cells which originally belong to the organism. This process is the result of perturbations to the control of cell growth, differentiation and apoptosis of normal cells leading to the development of tumors (Bocker et al 2007, Weinberg 2007). Initially, it was strongly believed that tumors are the result of an infection with an unknown factor. However, in the end of 19th century scientists were able to observe human tissue samples under light microscope and it was then, when a new theory emerged. According to that theory, cancer cells originate from patients' normal cells, as the organization and the morphology of tumor tissues resembles those of normal adjacent tissues. Indeed, this theory was validated the following years by comparing genetic markers of cancer and normal cells originating from the same tissue (Weinberg 2007).

1.1.2 Benign and malignant tumors

Tumors are classified as benign and malignant. This categorization of tumors is really important in the clinical practice and treatment. Benign tumors are mostly characterized by slow growth and they form a well-defined tissue mass which repels and compresses the surrounding normal tissues. They are of high grade differentiation, which means that they look similar to the normal tissue of origin, and they also consist of well-shaped cells (Bocker et al 2007).

Benign tumors are fully treated in most of the cases only by surgical removal. Hence, they are not generally lethal. The only rare exceptions are when a tumor damages surrounding tissues due to increasing compression or leads to the atrophy of vital organs or alternatively results in the overproduction and excretion of hormones or

metabolism byproducts which then perturb the normal function of the organism (Weinberg 2007).

The term cancer is used only for the malignant tumors. The basic characteristic of these tumors is that they invade adjacent tissues and thus spread to proximal organs. Furthermore, malignant cells possess the capability to invade into blood and lymph vessels. Hence, cancer cells are transferred to distant organs and develop secondary tumors, a process known as metastasis (Bocker et al 2007).

Concerning the histologic features of malignant tumors, these include the following nuclei and cytoplasmic atypias:

- 1) Increased number of mitoses
- 2) Cell heterogeneity
- 3) Heterogeneity of cell nuclei size and shape
- 4) Multiple nucleoli
- 5) Increased nuclear-cytoplasmic ratio

1.1.3 Categorization of tumors based on embryonic origin and histology

Regarding the embryonic origin, malignant tumors are separated in endodermal (lung, pancreas, liver, bile duct, bladder, digestive tract), mesodermal (blood, connective tissue, ovaries) and ectodermal (skin, neuronal tissue) (Weinberg 2007).

Based on the tissue origin, malignant tumors are divided in two major categories (Weinberg 2007):

- 1) Epithelial tumors or carcinomas, which originate from epithelial cells, are further divided in: a) squamous cell carcinomas e.g. skin cancer and b) adenocarcinomas e.g. lung and stomach cancers. Adenocarcinomas are the majority of malignant tumors and include tumors originating from endoderm, mesoderm and ectoderm.
- 2) Tumors of non-epithelial origin include:
 - ✓ sarcomas, tumors from mesenchymal origin cell (fibroblasts, osteoblasts, muscle cells, fat cells) that form connective and supportive tissue

- ✓ blood cells malignancies, which are further divided into leukemias and lymphomas
- ✓ Tumors of neuro-ectodermal origin which originate from neuronal cells e.g. gliomas, neuroblastomas.

Nevertheless, there are some tumor types which are not included in any of the above mentioned categories such as mesothelioma and small cell lung cancer.

1.1.4 Grading and staging of tumors

Tumor grading is correlated with the aggressiveness of the cancer and is related to the differentiation grade of cancer cells, nuclei atypias and number of mitoses in the tumor. According to the tumor grading system, tumors are separated as low, medium and high differentiation. Low differentiation tumors are phenotypically distinct from the tissue of origin, whereas high differentiated ones resemble the tissue of origin. Interestingly, tumors can be completely undifferentiated and thus difficult to determine the tissue of origin. The most undifferentiated tumors are the most aggressive ones (Bocker et al 2007).

Tumor staging defines the most appropriate therapeutic approach for each individual. The most widely used staging system is the TNM (tumor-node-metastasis). According to it, Tumor size (T), lymph Nodes invasion (N) and presence or absence of Metastasis (M) in distant sites are the three major criteria to choose the most suitable therapeutic scheme (Kumar et al. 2012).

1.1.5 Carcinogenesis

All the different forms of cancer share a common characteristic: cancer cells derive from normal cells. Given that cancer originates from normal tissue, then a process should transform normal into cancer cells. This process is known as malignant transformation or carcinogenesis.

Carcinogenesis is a multistep process that requires a series of genetic events to gradually transform one normal cell into a malignant one (Fearon and Vogelstein 1990) (**Figure 1**). The genome of the cells is altered at multiple sites. These alterations can vary from a single point mutation to a major chromosomal translocation. Part of these changes does not affect cells, while others lead cells to cell death or provide them with a growth advantage relatively to the adjacent normal cells. This process is called clonal evolution and renders cells more aggressive and more resistant to therapy (Luo et al. 2009).

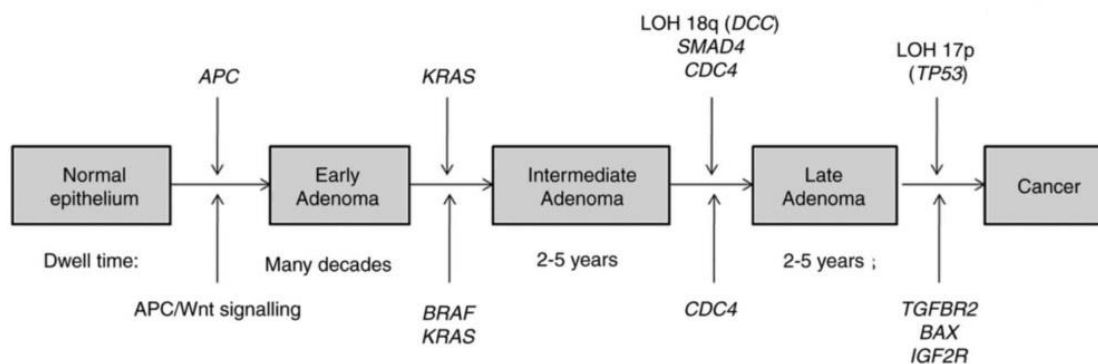


Figure 1. Colon adenocarcinoma development is a multistep process requiring a sequence of molecular events (Nguyen and Duong 2018).

The first stage of the carcinogenesis process is hyperplasia. At this stage, the difference between a hyperplastic and a normal tissue is the higher proliferation capacity, whereas the morphology and the organization of the hyperplastic tissue are similar to the normal counterpart. Thus, this is actually a benign form which is mostly not lethal for the individuals. The only exception is when the benign tumor disturbs the normal function of the tissue.

A second precancerous stage is metaplasia. Metaplasia is the substitution of a specific differentiated tissue type from another differentiated tissue type, which is not normally present in that organ site. A very characteristic example is the Barrett’s esophagus which involves the replacement of the squamous epithelial cells located in the lower esophagus by glandular epithelial cells, normally found in stomach. The site of metaplasia is a substrate for further malignant transformation.

The following stage of carcinogenesis is dysplasia that is characterized by cellular atypia. Cell size and morphology pronouncedly differs from that of normal tissue, the nucleus-cytoplasm ratio increases and the number of mitoses is higher. Nevertheless, dysplasia does not extend beyond basement membrane that separates epithelial cells from submucosa and hence it is considered a benign lesion.

Regarding the extent of cellular atypia, dysplasia is divided in low and high grade dysplasia. High grade dysplasia is often known as *in situ* carcinoma, a final stage before the rupture of the basement membrane and hence a transitional stage between benign and malignant lesions. From the moment that cancer cells can disrupt the basement membrane and further propagate in the blood and lymph vessels of the submucosa layer, the tumor acquires invasive properties and thus malignant potential (Weinberg 2007).

The final stage of malignant transformation and by far the most lethal for patients is the metastatic cancer. During that stage, cancer cells manage to propagate mostly through blood and lymph vessels and eventually form secondary tumors in distant sites of the body (Kumar et al. 2012). Metastasis is a complicated process which mainly requires the acquisition of mesenchymal traits through a process known as epithelial-to-mesenchymal transition (EMT) (Nieto et al. 2016).

1.1.6 Causes/etiology of cancer

Epidemiological studies have suggested the major role of both environmental factors and modern lifestyle, as certain cancer types are observed in different countries. Interestingly, immigration studies have highlighted the fact that immigrants tend to develop types of malignancies commonly observed in their host country, but not in their country of origin. As a result the importance of environmental factors in cancer emergence is superior to the genetic background. Needless to say that there are also inherited cancer types, however they constitute a minority (Jemal et al. 2011).

Among the environmental factors that damage the genetic material and thus promote carcinogenesis are radiation, chemical mutagens and oncogenic viruses. The

alterations that these factors cause to the genome emerge in the majority of the tumors, suggesting that they are crucial for the malignant transformation. To that end, genetic studies have proven that the majority of the most commonly mutated genes control and regulate critical cellular functions that are altered in cancer cells. These include cell proliferation and growth, cell division, programmed cell death (apoptosis), senescence as well as DNA damage and repair machinery (Hanahan and Weinberg 2011).

1.1.7 Commonly affected genes

The mostly affected genes, which dominate carcinogenesis, are distinguished in three major categories (Hanahan and Weinberg 2011, Kumar et al. 2012):

- 1) **Oncogenes.** Their overexpression promotes carcinogenesis through activation of signaling pathways that control cell proliferation and remain activated regardless of the presence or absence of extracellular signals. Initially, oncogenes were discovered in the genome of viruses, which had the capacity to generate tumors in animals and subsequently their homologs discovered in human tumors as well as new oncogenes.

Mechanisms of oncogene activation include:

- ✓ **Point mutations.** Typical example is the *RAS* oncogenes, which has been found to be mutated in a high number of cases of pancreatic and colon cancers. Constant activation of RAS signaling pathway promotes continuous cell proliferation.
- ✓ **Gene enhancement.** It involves an increase in gene copy number or of a chromosomal locus which then drives oncogene overexpression. For instance, *ERBB2* gene, which encodes for the human epidermal growth receptor 2 (HER2), when overexpressed is adversely related to breast cancer stage.
- ✓ **Chromosomal rearrangements.** It usually includes translocations between different chromosomes resulting in the activation of oncogenes or in the generation of chimeric proteins with altered characteristics. It is more commonly found in hematologic malignancies such as leukemias

and lymphomas. Typical paradigm is the Philadelphia chromosome in Chronic Myelogenous Leukemia (CML) and the responsible reciprocal translocation between chromosomes 9 and 22 drives the generation of the chimeric protein BCR-ABL, which behaves as a constantly activated kinase.

- 2) **Tumor suppressor genes.** Decreased expression of these genes is usually observed in cancer, thus highlighting their role in preventing cancer formation. They participate in signaling pathways which control cell proliferation and growth, as well as the activation of apoptosis and senescence.

Mechanisms of tumor suppressor genes inactivation include:

- ✓ **Point mutation.** This mutation type leads to the loss of function of the protein product or to the loss of protein domains due to the primary termination of the transcription process. Point mutations are more frequently involved in the inactivation of tumor suppressor genes than in the hyper-activation of oncogenes.
 - ✓ **Deletion of genes or larger chromosomal loci.** Loss of heterozygosity in cancer (loss of one allele) strongly implies the coding of a tumor suppressor gene by this specific locus.
 - ✓ **Epigenetic silencing.** A subset of tumor suppressor genes exhibits increased methylation of their promoters, which subsequently results in decreased or complete loss of their expression. Typical example is the gene which encodes for the cell cycle inhibitor p16^{INK4}.
- 3) **“Caretaker” genes.** They participate on mechanisms which contribute to genome integrity. These genes mainly participate in the following mechanisms:
- ✓ DNA damage response pathway (DDR)
 - ✓ DNA repair pathway
 - ✓ Pathways implicated in the inactivation or elimination of factors responsible for causing DNA lesions.

Perturbation in the expression of these genes accelerates the acquisition of new mutations and contributes to genomic instability.

1.1.8 Hallmarks of cancer

Elucidation of the molecular and genetic pathways that participate in the malignant transformation process and are affected by the perturbed expression of genes, made possible the discovery of the basic alterations that cells acquire during carcinogenesis. Based on research discoveries until 2011, Hanahan and Weinberg defined the following hallmarks of cancer (Hanahan and Weinberg 2000, Hanahan and Weinberg 2011)

(Figure 2):

- 1) **Sustained proliferative signaling.** Fundamental trait of cancer cells is the sustained and constant proliferation. To this end, normal cells should initially lose their dependence on normal extracellular signals that activate cell proliferation. Subsequently, perturbed extracellular mitogenic signals can promote proliferation. However, such signals are hard to study as their production relies on adjacent cells or the extracellular matrix. An alternative way to sustain proliferation is the deregulation of intracellular mitogenic pathways. Oncogenes constitute deregulated genes which participate in these pathways as signal receptors or as signal transducers, for instance *RAS* oncogenes.
- 2) **Evasion from tumor suppressor genes.** The aforementioned constant activation of proliferation and growth signaling pathways is the one side of the coin. On the other side, loss of function of tumor suppressor genes plays a major role in carcinogenesis. Typical examples are the *Rb* and *TP53* tumor suppressor genes which control and tightly regulate cell proliferation (*RB*) or activate apoptosis and senescence pathways proportionally to the extent of cellular stress (*p53*).
- 3) **Resisting cell death.** Programmed cell death, known as apoptosis, is a very important cellular mechanism which is activated upon stress factors release under conditions such as DNA damage, decrease of necessary metabolites e.g. amino acids and nucleotides, decreased levels of survival signals. Apoptosis activation ensures the extinction of severely damaged cells and thus forming a barrier against carcinogenesis. Cancer cells evade apoptosis through the loss of genes that normally activate apoptosis. Loss of the *TP53* gene, which encodes for the *p53* protein, results in increased expression of antiapoptotic proteins (e.g.

Bcl2, Bcl-X_L, Bcl-w) or decreased expression of proapoptotic proteins (e.g. Bak, Bax, Bim, Noxa, Puma).

In contrast to apoptosis, necrotic cell death promotes malignant transformation, due to release of inflammation and survival factors.

Autophagy is a process that is responsible for the recycling of cells metabolites in order to promote cell survival. It is probably an alternative pathway to apoptosis, as it is activated by proteins participating in apoptosis activation. Nonetheless, the role of autophagy in carcinogenesis remains unclear, as in the first stages impedes carcinogenesis, however in later stages protects cancer cells by promoting their survival.

- 4) **Replicative immortality.** Normal cells undergo a certain number of cell divisions before they stop dividing. Subsequently, cells enter a replicative senescence state and then enter a process known as crisis, which involves cell death. Cells predominantly cease dividing due to telomere shortening. Telomeres are protective sequences of DNA located in the chromosome endings and ensure the proper replication and the avoidance of chromosomes ends merging. Telomerase, the responsible enzyme for regenerating telomeres, is inactivated in normal cells. However, telomerase has been found to be reactivated in cancer cells allowing unlimited divisions, a process known as immortalization. Although immortalization is a first step required for the transformation of a normal into a cancer cell, recent studies have shown that telomerase reactivation is a late event during the malignant transformation and thus it is not observed in precancerous lesions.

Barring the above mentioned hallmarks, additional traits can give cancer cells new properties and hence contribute to tumor aggressiveness. Such traits are mostly present in the invasive and metastatic malignancies and briefly are the following:

- ✓ **Angiogenesis.** This process is responsible for the generation of new blood vessels in order to provide a tumor with essential nutrients and oxygen and hence sustain its growth. Angiogenesis includes the overexpression of factors, such as Vascular Endothelial Growth Factor (VEGF), which promotes the formation of new vessels.

- ✓ **Invasiveness.** Crucial step for the further evolution of cancer is the invasion of the basement membrane from cancer cells, which results in their expansion into deeper layers of the tissue that are rich in blood and lymph vessels. Invasion into blood and lymph vessels dramatically increases the metastasis potential. EMT is a fundamental cellular process which facilitates cancer cell invasion. Cancer cells acquire mesenchymal characteristics, such as loss of extracellular and intercellular connections through loss of adhesion molecules (e.g. E-cadherin). EMT is the first step required for metastasis. In addition, two distinct modes have been implicated in cancer cell invasion. “Collective invasion” involves a subset of cells invading en masse and is characteristic of squamous cell carcinomas. The “amoeboid” form of invasion still remains unclear and includes the invasion of cancer cells through existing interstices of the extracellular matrix rather than creating a path for themselves.
- ✓ **Metastasis.** Metastasis presupposes the invasion of cancer cells into blood and lymph vessels, delivery of cancer cells via circulation to distant organ sites, exit from vessels and formation of micrometastases, which will eventually develop in metastatic tumors. EMT facilitates the entrance into blood and lymph vessels through the acquisition of mesenchymal features. However, establishment of metastatic tumors probably requires the reacquisition of the epithelial characteristics and the adjustment to the environment of the new tissue. To this end, valuable is the contribution of a process opposite to EMT, known as mesenchymal-to-epithelial transition (MET). Although detailed knowledge of both EMT and MET pathways has not yet been acquired, it gets more and more obvious that tumor stromal cells, such as fibroblasts, and cells of the immune system (macrophages) are stimulated by cancer cells and secrete factors that promote survival and inflammation and thus contribute to cancer evolution.

Additional mechanisms which help cancer evolution and have been discovered in the cancerous environment include evasion from the immune system surveillance, up-regulation of inflammation factors, and a shift in cell metabolism towards aerobic

glycolysis (Warburg effect); thus conferring cancer cells the capability to survive in the anaerobic environment of a rapidly growing tumor. Finally, perturbation of the DDR pathway leads to genomic instability, which favors the accumulation of mutations in the genome.

Normally, DDR pathway effectors ensure that the number of spontaneous mutations due to DNA replication machinery mistakes remains quite low. DDR pathway is also activated in response to mutations caused by mutagenic factors. Therefore, accumulation of mutations requires both protracted exposure to mutagenic factors and defective function of mechanisms that control the integrity of the genome, finally leading to genomic instability. Though some stochastic mutations can potentially give a survival advantage to cells and thus initiate carcinogenesis, loss of genome surveillance mechanisms favors genomic instability, which characterizes advancement of cancer evolution.

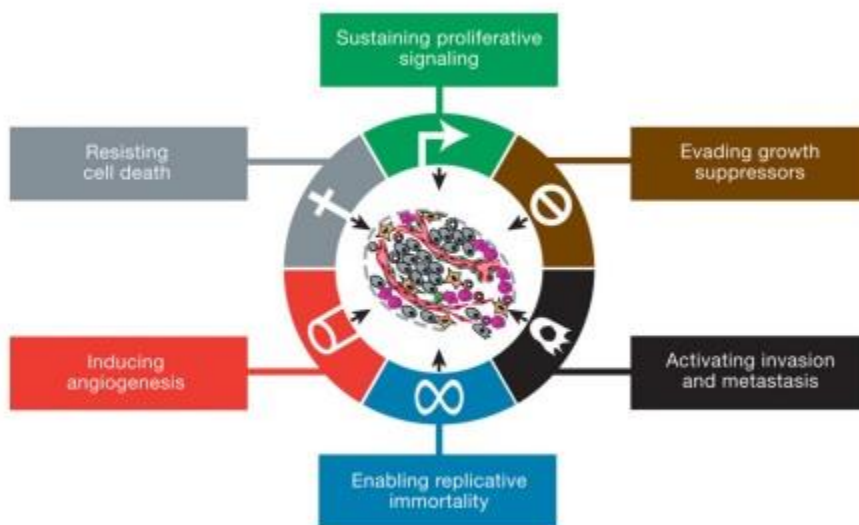


Figure 2.Hallmarks of cancer (Hanahan and Weinberg 2011)

1.1.9 Emerging hallmarks of cancer

The accumulation of research data resulted in the appearance of two additional properties of carcinogenesis. These emerging hallmarks are the following (Hanahan and Weinberg 2011) (**Figure 3**):

1) Reprogramming of cell metabolism

The rapid proliferation of cancer cells requires the adjustment of cell metabolism in order to possess the necessary amount of energy. Warburg first observed that cancer cells produce lactate regardless of oxygen levels (Warburg 1930), which means that malignant cells are based on aerobic glycolysis.

Cancer cells heavily depend on glycolysis due to the oxygen-deprived environment that dominates tumors. Tumor cells acquire the ability to compensate the reduced energy efficiency of glycolysis compared to oxidative phosphorylation. Frequently two distinct metabolic populations are present in tumors: one based on glycolysis and produces lactate and a second one which uses the lactate and undergoes oxidative phosphorylation. This combination is the most efficient for environments with different oxygen concentrations (Hanahan and Weinberg 2011).

2) Evasion from immune system surveillance

The immune system has the ability to resist or even inhibit the emerging neoplasms, late stage tumors and micrometastases. It is obvious that tumors have acquired the ability to evade the immune system's recognition and destruction capability (Hanahan and Weinberg 2011).

Particularly, the escape from immune system requires the decrease or complete loss of Major Histocompatibility Complex (MHC) class I, which are necessary for the recognition of cancer cells from cytotoxic

T lymphocytes (CTLs). Furthermore, cancer cells can inactivate CTLs and natural killer (NK) cells by secreting several inhibitory factors, such as Tumor Growth Factor- β (TGF- β). Finally, the recruitment of T regulatory cells (Tregs) and the Myeloid-Derived Suppressor Cells (MDSCs) also inhibit the cytotoxic action of CTLs.

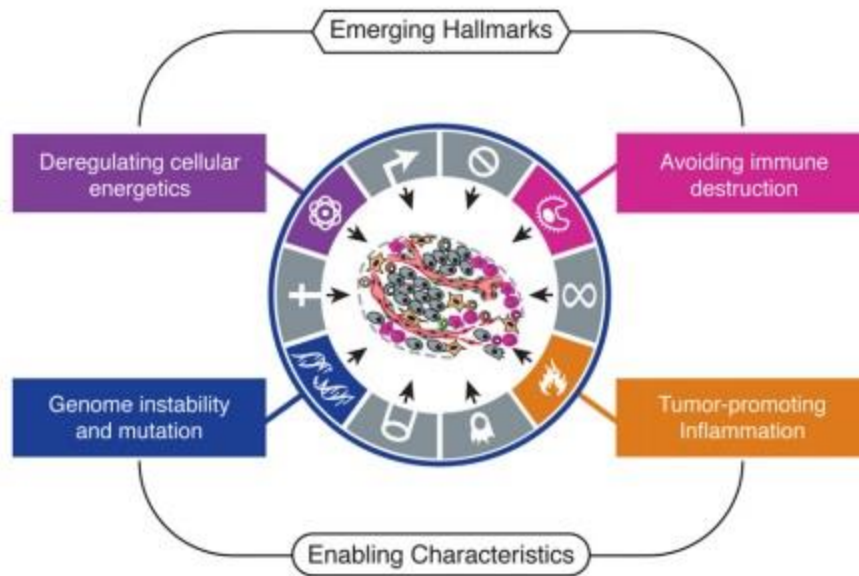


Figure 3.Emerging hallmarks and enabling characteristics of cancer (Hanahan and Weinberg 2011).

1.1.10 Enabling characteristics of cancer

There are some additional events, which contribute to the acquisition of the aforementioned hallmarks of cancer, and are briefly described below (Hanahan and Weinberg 2011) (**Figure 3**):

1) Genomic instability

The acquisition of the above mentioned hallmarks of cancer strongly depends on the consecutive alterations occurring in the cells' genome which provides them with an evolutionary advantage. Nonetheless, cells possess a regulatory system to strictly control the DNA damage repair process, which keeps the mutational burden extremely low. However, genomic instability promotes the emergence and further development of cancer cells.

Genomic instability is caused by perturbations in the genes that are responsible for DNA stability (Jackson and Bartek 2009) or alternatively, by telomeres shortening, which

provokes karyotypic instability and is related to deletion or enhancement of chromosome regions (Artandi and DePinho 2010).

According to the oncogene-induced DNA damage model for cancer development, the activation of oncogenes in sporadic cancers generates replication stress which in turn leads to formation of DNA DSBs. This continuous formation of DSBs promotes genomic instability and as a result cancer development (Halazonetis et al. 2008) (**Figure 4**).

Consequently, in familial cancer syndromes genomic instability may be the initiating event, whereas in sporadic cases of cancer activation of oncogenes induces replication stress, which subsequently leads to genomic instability (Negri et al. 2010).

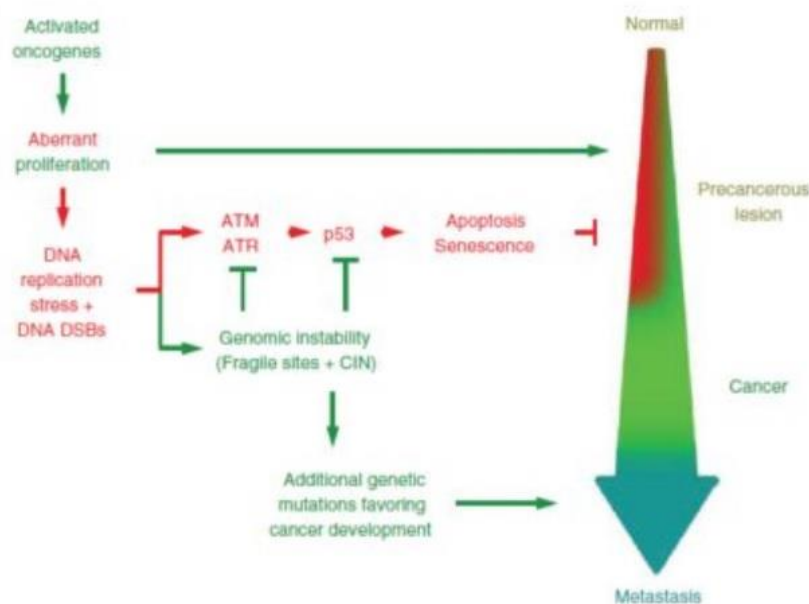


Figure 4. Oncogene-induced DNA damage model for cancer development. The activation of oncogenes induce replication stress which in turn results in genomic instability and the activation of the anti-tumor barriers of apoptosis and senescence. Mutations accumulation and loss of p53 protein lead to the bypass of the anti-tumor barriers and thus promote carcinogenesis (Halazonetis et al. 2008).

2) Tumor-promoting inflammation

It is widely known that cancer lesions are accompanied by inflammatory reactions and involve cells implicated in both innate and adaptive immunity responses. Inflammation is

a natural effort of the immune system to eliminate cancer, which paradoxically has a positive impact on cancer progression and mediates the acquisition of cancer hallmarks. Particularly, inflammation provides the tumor with bioactive molecules, including growth factors, which enhance cell proliferation, survival factors, pro-angiogenic factors and enzymes which modify extracellular matrix and thus facilitate angiogenesis and metastasis. Furthermore, inflammatory cells produce reactive oxygen species (ROS), which are mutagenic for their adjacent cancer cells and hence they accelerate malignant transformation (Colotta et al. 2009, DeNardo et al. 2010, Grivennikov et al. 2010).

1.2 Cell cycle

Cell cycle is the cellular process which results in the generation of two new daughter cells identical to the progenitor cell. This process requires the duplication of the genome through tightly regulated subsequent phases. To guarantee the fidelity of cell division, cell cycle includes surveillance mechanisms, known as checkpoints, between distinct phases. The aim is to ensure the integrity of the duplicated genetic material of cells and broadly of the organism. Loss of control results in abnormal development and cancer evolution.

The cell cycle consists of 4 distinct phases, named as G1, S, G2 and M. G1 (first gap) is the phase during which cells express genes accordingly to their needs and prepare themselves for S phase. During S (synthesis) phase DNA is duplicated in order to proceed into the next one with intact genetic material. In parallel, centrosome, a structure responsible for the correct separation of sister chromatids during M phase, is duplicated. Subsequently in G2 (second gap) phase, the necessary proteins for the separation of sister chromatids (mitosis) and the division of the cell (cytokinesis) are synthesized. Furthermore, during G2 phase, cells communicate with the intra- and extracellular environment to ensure genome integrity as well as the appropriate conditions to proceed into the next phase. M (mitosis) phase is a series of 5 distinct steps (prophase, prometaphase, metaphase, anaphase and telophase), which

eventually results in the separation of sister chromatids as well as cytoplasm and subcellular organelles in order to generate two new cells (Harvey et al. 2007).

1.2.1 Checkpoints and cell cycle regulation

During the cell cycle process molecular mechanisms are activated to control the faultless proceeding of the cycle in each constitutive phase. Cell cycle checkpoints are necessary because any mistakes occurring can potentially lead to cell malfunction and therefore malignant transformation. Checkpoints are mainly activated at the border between two alternate phases. Important checkpoints are the G1/S and G2/M and cyclin-dependent kinases (CDKs) are the main mediators of these mechanisms. CDKs are enzymes which add negative charged phosphate groups in proteins and are activated by Cyclins. Cyclins are proteins stably synthesized and degraded during cell cycle. Assembly and disassembly of Cyclins with CDKs are responsible for both the entry and the exit from each phase. Briefly, there are 4 groups of Cyclins: G1, G1/S, S and mitotic Cyclins participating on G1 phase, G1/S transition, S phase and mitosis respectively. G1 and G1/S Cyclins bind to CDKs during G1 phase permitting the exit from G1 and the subsequent entry in S phase. S phase Cyclins connect to CDKs and thus promote the initiation of DNA synthesis. Mitotic Cyclins gradually increase during G2 phase. As soon as they become abundant, bind to CDKs and they form the Mitosis Promoting Factor (MPF) complex. This complex licenses the cell to enter M phase. As soon as Cyclins are degraded and MPF is inactivated, cell divides and the newly emerged cells enter G1 phase (Garrett 2001).

1.2.2 Cyclins and cell cycle regulation

Cyclins are categorized proportionally to the cell cycle phase in which they participate in. Cyclins D (D1, D2 and D3) family members participate in G1 phase and regulate the entry from G₀ (quiescent phase) to G1 phase. They are activated by growth factors and extracellular stimuli through the Ras-GTPase signaling pathway. Cyclins D binds to CDK4 and CDK6 kinases and promotes the entry to S phase (Coverley et al. 2002). The

Cyclin D/CDK4 complex promotes Cyclin E expression. Cyclin E and Cyclin A independently bind to CDK2 and facilitate the entry to S phase by phosphorylating and thus inactivating the RB protein. The latter event activates the E2F family of transcription factors. Particularly, Cyclin E stimulates the formation of the replication complex by interacting with CDC6. Cyclin A triggers DNA synthesis and simultaneously inhibits the formation of new replication complexes. Cyclins B1 and B2 are responsible for M phase. In collaboration with MPF, they regulate the mitotic spindle assembly and the correct placement of sister chromatids onto the spindle (Hochegger et al. 2008) (Figure 5).

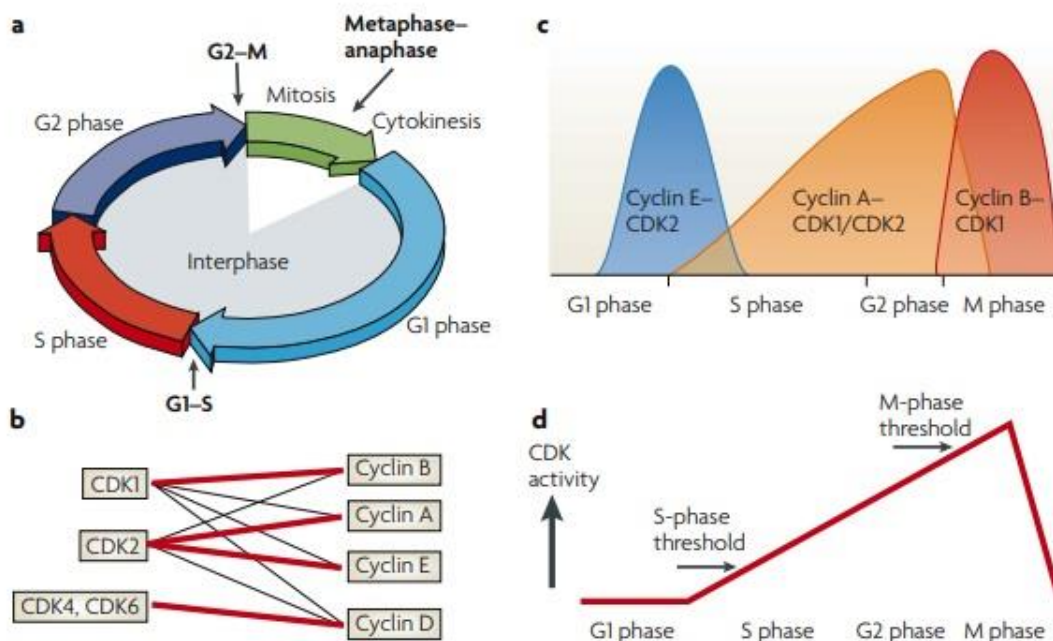


Figure 5. Cell cycle regulation. a) Cell cycle phases. DNA replication occurs during S phase, whereas cell division takes place at the M phase of the cell cycle. b) CDK1 and CDK2 bind to various Cyclins (A, B, D and E), while CDK4 and CDK6 bind exclusively to Cyclin D. Red lines represent the more frequent combinations. c) The Cyclin E-CDK2 complex triggers S phase, Cyclin A-CDK1/CDK2 complexes regulate the exit from S phase and Cyclin B-CDK1 heterodimer is responsible for mitosis. d) Increase of CDKs activity favors the entry in S phase, while the transition in M phase requires lower CDKs activity (Hochegger et al. 2008).

1.2.3 Role of CDKs and CDKIs on cell cycle regulation

Regulation of CDKs from Cyclins depends also on inhibitor proteins. Wee1 is a kinase, whereas Cdc25 is a phosphatase, both exerting inhibitory role during cell cycle. These two enzymes are responsible for the regulation of mitosis. Proteins that inhibit the Cyclin-CDK complex are known as CDK inhibitory proteins, which are further divided in CIPs and INK4s. CIPs inhibit CDK1, CDK2, CDK4 and CDK6, whereas INK4s inhibit CDK4 and CDK6 proteins (Malumbres and Barbacid 2009).

Typical examples of CIPs are p21^{Cip1/WAF1}, p27^{KIP1} and p57^{KIP2}. Each of these proteins plays role in different cell cycle phases. For instance, p21^{Cip1/WAF1} is activated by the tumor suppressor protein p53 as a response to DNA damage stimuli and inhibits cell cycle progression. INK4s include p14^{INK4ARF}, p15^{INK4B}, p16^{INK4A} and p18^{INK4C}. Among these proteins p16^{INK4A} is an established tumor suppressor protein, as its loss promotes carcinogenesis (Malumbres and Barbacid 2009).

Cells undergo cell cycle as a response to extracellular stimuli, such as growth factors. The latter induce the expression of genes, separated further in early- or delayed-response genes. Early-response genes activate transcription factors or act as transcription factors themselves and activate the expression of delayed-response genes, such as Cyclin-CDK complexes.

Proto-oncogene *myc* belongs to the early-response genes and activates Cyclin D gene, the SCF (Skp1/Cullin/F-box) complex genes and the E2F family genes. Subsequently, Cyclin D activates G1-CDK complexes. SCF complex degrades p27^{KIP1} in order to activate G1-CDK complexes. In parallel, E2F family proteins induce S phase-related genes, such as Cyclins A and E, CDK2, CDC6 and CDT1 (Li et al. 2003).

Degradation of Cyclins takes place during the cell cycle process and is mediated by ubiquitin ligases complexes. Typical paradigms of such complexes are SCF, which regulates the G1/S transition and the Anaphase Promoting Complex/Cyclosome (APC/C) complex that regulates the expression levels of M phase Cyclins. One fundamental role of APC/C is the transition from metaphase to anaphase (Manchado et al 2010).

1.2.4 Cell cycle regulation by tumor suppressor genes

Tumor suppressor genes regulate the cell cycle by halting its progress in case of damage. Therefore, cells repair damage before progressing in subsequent phases. Hence, loss of tumor suppressor genes renders cells prone to irreparable damage and as a consequence prone to cancer. Two typical examples of tumor suppressor proteins are the RB and p53 proteins. RB inhibits the entry to S phase, whereas p53 suppress S phase progression and entry to G2 phase.

As mentioned above, E2F induces the expression of cyclins A and E and also the expression of CDK2, which are necessary for S phase progression. E2F binds to and inactivates RB. However, RB phosphorylation diminishes its binding capacity to E2F, which contributes to the induction of its transcriptional activity. Normally, RB is phosphorylated at the early S phase, while it is not phosphorylated in mitosis and early G1 phase. The G1-CDK complex phosphorylates RB in order to release E2F and regulate its target genes expression. As soon as E2F activates the S-CDK complex, the latter preserves the phosphorylation status of RB and consequently the cell progress to genome duplication (Tsolli et al. 2001, Stevaux and Dyson 2002).

The p53 protein controls the DNA replication process and is activated by DNA damage. Under normal conditions, p53 is regulated by MDM2. Particularly, MDM2 binds to and degrades p53. As soon as DNA damage occurs, ATM and Chk2 kinases phosphorylate p53 and hence prevent the interaction between p53 and MDM2. Then, p53 induces CDKN1A expression, which encodes the p21^{Cip1/WAF1} protein, an inhibitor of cell cycle progression upon DNA damage.

Overall, the two aforementioned tumor suppressor genes are very important for the integrity of the genome. Deregulation of these factors leads to cancer development. Generally, perturbations in the DNA replication mechanism, known as DNA replication stress, predisposes for genomic instability that is an established hallmark of cancer.

1.2.5 Cellular senescence

DNA damage leads to activation of the DDR pathway under normal conditions. The potential cell fate is: a) temporary inhibition of cell cycle to repair the damage or b) apoptosis in case of extensive damage or c) senescence induction, which is generally considered as an irreversible inhibition of the cell cycle (Campisi and d'Adda di Fagagna 2007). It is worth mentioning that not only the damage extent is implicated in senescence induction, but also the affected cell type. Generally, apoptosis is more frequent in epithelial cells, while senescence in stromal cells (Georgakopoulou et al. 2016).

Senescence is triggered both *in vitro* and *in vivo* by various stimuli:

- ✓ Shortening of telomeres induces replicating senescence. As mentioned above, telomeres are short DNA sequences which cover and protect the chromosome endings. Extensive shortening of telomeres makes chromosome endings vulnerable to DNA damaging factors and finally activates the DDR pathway and replicating senescence (Takai et al. 2003, d'Adda di Fagagna et al. 2004, Herbig et al. 2004). Cancer cells activate telomerase and thus evade senescence caused by telomere shortening (see also 1.1.8). Nonetheless, telomerase does not inhibit senescence activation due to other causality (Chen et al. 2001).
- ✓ Treatment of cancer with chemotherapeutic agents induces senescence mainly through the generation of DNA double strand breaks (DSBs). This phenomenon is known as therapy-induced senescence. Triggering of the p53 pathway is mostly responsible for this type of senescence (Di Leonardo et al. 1994, Herbig et al. 2004).
- ✓ Oncogene activation during carcinogenesis induces a distinct type of senescence, known as oncogene-induced senescence. Oncogenes cause replication stress and thus activate the DDR pathway due to DNA damage (Bartkova et al. 2005, Bartkova et al. 2006, DiMicco et al. 2006). In addition, *in vivo* studies support that oncogene-induced senescence is present in precancerous lesions acting as an anti-tumor barrier (Braig et al. 2005, Chen et

al. 2005, Collado et al. 2005, Lazzerini et al. 2005, Michaloglou et al. 2005, Bartkova et al. 2006, Di Micco et al. 2006).

- ✓ Stress induced by ROS or protracted cytokines signaling, such as interferon β or TGF- β has been shown to trigger senescence (stress-induced senescence) (Campisi et al. 2007, Campisi et al. 2014, Salama et al. 2014). Likewise, stress induction during epithelial cell culture activates senescence through the p16^{INK4A} pathway, regardless of telomeres length. This highlights the fact that inactivation of p16^{INK4A} is necessary for the immortalization of normal epithelial cells (Kiyono et al. 1998, Ramirez et al. 2001).
- ✓ Furthermore, factors that affect histones, such as histones deacetylases, can alter the expression of various genes leading to cellular senescence (Campisi and d'Adda di Fagagna 2007).
- ✓ Finally, a distinct type of senescence emerged recently. This type of senescence is induced by AKT and results in the stabilization of the p53 protein independently of DNA damage. AKT induces senescence through MDM2 nucleolar sequestration. Thus, p53 is stabilized and activates senescence (Aistle et al. 2012).

1.3 DNA replication

DNA replication is a fundamental process, as it is a prerequisite for cell division. Thus, cells inherit the correct amount of genetic material to the newly emerged cells. DNA replication ensures that DNA is transferred unaltered among generations and takes place strictly once during the S phase of the cell cycle (Blow and Dutta 2005).

DNA replication is a tightly regulated process and is controlled by a high number of enzymes capable of ensuring the accuracy and speed of the whole procedure. The fidelity of DNA duplication is controlled by protein networks, which are activated upon DNA double strand breaks or single-stranded DNA (ssDNA) breaks occurrence at certain timepoints throughout the cell cycle (checkpoints). For this purpose, these proteins inhibit the progress of DNA forks, but they also facilitate the restart of DNA replication as soon as the damage has been repaired (Branzei and Folani 2010).

Replisome, a dynamic protein complex, is the main mediator of DNA replication, which is further divided into three distinct phases: the initiation phase, the elongation phase and finally the termination phase (Baker and Bell 1998). The mechanisms of initiation and elongation phases do not differ between the eukaryotic and prokaryotic organisms. In contrast, concerning the termination phase, prokaryotic organisms require Tus proteins (terminus utilization substance), whereas in eukaryotic organisms the respective process is based on telomerase (Greider and Blackburn 1987).

1.3.1 Origins of replication

The initiation of DNA replication does not occur on random sites throughout the genome, but on specific locations, known as origins of replication (ORI).

The number of ORIs depends on the size of the genome, which varies among different species. For instance, bacteria and archaea possess one circular molecule of DNA with a single ORI (Barry and Bell 2006, Skarstad and Katayama 2013). In addition, various viruses also possess a single ORI (Hoeben and Uil, 2013). On the other hand, in eukaryotic organisms there are numerous ORIs in order to ensure the timely replication of the genome, which is larger compared to prokaryotic organisms. Particularly, the yeast genome encompasses 400 ORIs and the human genome between 30000 and 50000 ORIs (Cvetic and Walter 2005, Mechali 2010, O'Donnell et al. 2013).

Importantly, yeast ORIs bear a specific sequence of 100-200 base pairs (bp), which includes a conserved region of 11bp, whereas in metazoa this sequence is not well defined (Mechali 2010, Leonard and Mechali 2013). In higher eukaryotes, ORIs are organized in replicons which are activated at different time points throughout S phase (O'Donnell et al. 2013). According to Cayrou and colleagues, only one in five ORIs of a replicon is used in each cell cycle (Cayrou et al. 2011), however dormant origins can be activated in case of necessity (Branzei and Foiani 2005, Woodward et al. 2006).

1.3.2 Initiation of DNA replication

Initiation of DNA replication is the first important step for genome duplication and consists of 2 distinct stages: the origin licensing and the origin firing which are triggered at different time points (Kaplan 2016). They are strictly regulated events, which are determined by periodical fluctuations of CDK levels (Petrakis et al. 2016).

DNA replication licensing occurs following the end of M phase and throughout the G1 phase when pre-replicative complexes (pre-RCs) are formed. The hexamer origin recognition complex (ORC) first binds to ORIs in order to recruit the replication licensing factors (RLFs) CDC6 and CDT1. Subsequently, RLFs mediate the recruitment of 2 hexamer helicase complexes, known as minichromosome maintenance 2-7 (MCM 2-7) (DePamphilis et al. 2006).

Origin firing occurs as soon as cell enters the S phase (G1/S transition), where the activated CDK and DDK kinases convert the pre-RC into pre-initiation complex (pre-IC). This requires the recruitment of additional factors, such as CDC45, Sld2 (homologous to human RECQ4), Sld3 (homologous to human Treslin), Dpb11 (homologous to human TOPBP1), GINS complex [consists of Sld5, Psf1, Psf2, and Psf3 subunits (Takayama et al. 2003)], MCM10 and DNA polymerases α/ϵ (Tanaka and Araki 2013). Thus, origin firing is the conversion of the inactivated pre-RC into two activated pre-IC complexes which then leads to the unwinding of DNA double helix at ORIs. This results in symmetric and bidirectional move of the replisome until the replication of DNA is complete (Teer and Dutta 2006, O'Donnell et al. 2013) (**Figure 6**).

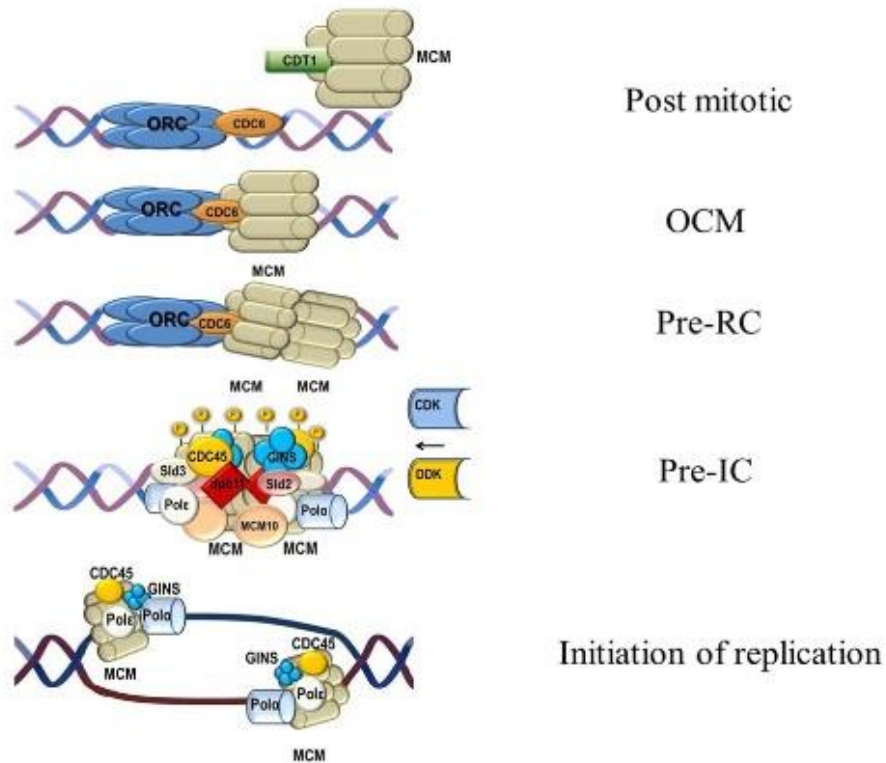


Figure 6. Initiation of DNA replication. Replication licensing includes the binding of the ORC-CDC6 complex to ORIs and the subsequent recruitment of CDT1 and MCM 2-7 complex. Next, pre-RC complex is formed after the binding of a second MCM 2-7 complex. MCM 2-7 is activated by DDK kinases. The activated MCM 2-7 complex with additional factors (CDC45, GINS, Sld2, Sld3, Dpb11, polymerases α/ϵ) form the pre-IC (Petrakis et al. 2016).

1.3.3 Replication checkpoints

The replication process is strictly controlled to ensure that the genome is precisely duplicated once in every cell cycle. Initially, pre-RC assembly is supervised by licensing checkpoint, which in case of an error diminishes the activity of cyclin E-CDK2 complex and thus inhibits the entry into S phase until the error is repaired (Feng et al. 2003, Machida and Dutta 2005, Liu et al. 2009, Nevis et al. 2009). Following MCM 2-7 recruitment, ORC, CDC6 and CDT1 are either degraded by proteasomes, or transferred outside the nucleus or are inhibited by specific molecules, such as Geminin, an inhibitor of CDT1. Hence, the re-licensing of ORIs during the same cell cycle and DNA re-

replication are avoided. This is very important as DNA re-replication leads to replication stress and thus threatens genome integrity. Furthermore, RLFs degradation or inactivation promotes the re-organization of pre-RCs after mitosis completion (Hills and Diffley 2014).

Interestingly, according to previous studies, in some regions of the human genome, replication is not completed until the cells enter mitosis (Lukas et al. 2011, Naim et al. 2013, Moreno et al. 2016). These specific regions are visible in the form of “ultrathin anaphase fibers”, known as ultrafine anaphase bridges and are separated between the newly emerged cells. During G1 phase they are covered with 53BP1 proteins, forming structures known as nuclear bodies. These structures protect the bridges until they complete replication in the upcoming S phase. Furthermore, there is a negative correlation between ultrafine anaphase bridges and ORIs. As the number of ORIs increases, the amount of under-replicated DNA decreases. Supportively, 53BP1 selectively binds to DNA regions poor in ORIs (Moreno et al. 2016).

1.3.4 The CDC6 replication licensing factor

CDC6 belongs to the family of AAA⁺ ATP hydrolases (ATPases associated with a variety of cellular activities) and is correlated with ORC1 protein and to a lesser extent with ORC4, ORC5 and MCM 2-7 proteins (Neuwald et al. 1999) (**Figure 7**). The regulation of its activity plays major role on the formation of the pre-RC complex during cell cycle process. Various studies support that CDC6 function depends on its capability to bind and hydrolyze nucleotides. If CDC6 is unable to bind ATP, then the cell cannot enter S phase, whereas the inability of CDC6 to hydrolyze ATP inhibits the completion of S phase (Tsaraklides and Bell 2010). The phosphorylation of CDC6 from CDK in S phase results in its transfer from cytoplasm to the nucleus. However, during mitosis, CDC6 is degraded by the APC/C^{CDH1} complex (Mailand and Diffley 2005). Most recent data suggest that CDC6 is also degraded through CUL4-DDB1^{CDT2} pathway upon interaction with proliferating cell nuclear antigen (PCNA) (Clijsters and Wolthuis 2014), as well as via the interaction of SCF^{Cyclin F} with the 93-100 amino acid residues of CDC6

protein (Walter et al. 2016). The above mentioned mechanisms are necessary in order for the cell to avoid DNA re-replication (Liu et al. 2000,Walter et al. 2016).

The carboxyl-terminus of CDC6 protein encompasses a Winged-Helix domain, which is frequently found in transcription factors. Previous studies have shown that this region mediates protein interactions among CDC6 and other AAA⁺ ATPases of pre-RC complex and is the substrate for MCM 2-7 complex (Jeruzalmi et al. 2001).

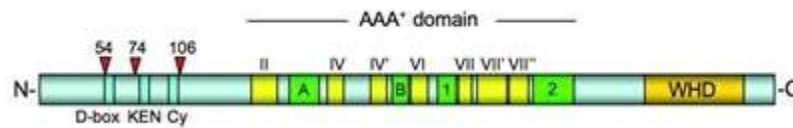


Figure 7.CDC6 protein. Red arrows indicate three serine residues targets for CDKs phosphorylation (Borlado and Mendez 2008).

1.3.5 CDC6 in other phases of the cell cycle

Mammalian cells do not eliminate CDC6 in S and G2 phases. Thus, alternative mechanisms are responsible to prevent DNA re-replication. One such mechanism involves the inactivation of ORC1 through polyubiquitination by SCF^{Skp2} and subsequent degradation by proteasome (Mendez et al. 2002), or by monoubiquitination and dissociation from chromatin (Li et al. 2002). In addition, mammalian cells can alternatively regulate the proteolytic degradation of CDT1 by SCF^{Skp2} or the CUL4-DDB1^{Cdt2} ubiquitin ligases. CDT1 is also regulated through Geminin inhibition, as mentioned above (Fujita 2006).

CDC6 overexpression in G2 cells results in G2 arrest and thus the cells do not progress into mitosis. This unexpected CDC6 function involves the activation of checkpoint kinase Chk1, a molecule that plays a pivotal role in the G2/M checkpoint pathway. ATM/ATR kinases phosphorylate and activate Chk2/Chk1 kinases; hence ATM/ATR activation by CDC6 would activate the pathway. Interestingly, the use of caffeine, an ATM/ATR inhibitor, does not alleviate mitotic block, which indicates a direct interaction between CDC6 and Chk1 (Borlado and Mendez 2008).Furthermore, a study conducted

in *S. pombe* revealed that during an S phase arrest, CDC18 (CDC6 mammalian homolog) recruits Rad3-Rad26 complex on the chromatin (ATR/ATRIP mammalian homologs) to maintain mitotic block (Hermand et al. 2007). In line with the aforementioned results, CDC6-depleted cells do not activate ATR-Chk1 checkpoint. Hence, cells progress into mitosis and undergo aberrant chromosomal segregation (Lau et al. 2002). Overall, CDC6 proved to be an important mediator of the S-M checkpoint by preventing mitosis progression before DNA replication is complete (**Figure 8**).

Concerning mitosis per se, increasing evidence suggest that CDC6 is also a pivotal mediator of cell division. Notably, CDC6 in combination with Plk1 and CDK1 regulates the activity of separases. Thus, CDC6 depletion leads to chromosome missegregation (Yim et al. 2010, Youn et al. 2020).

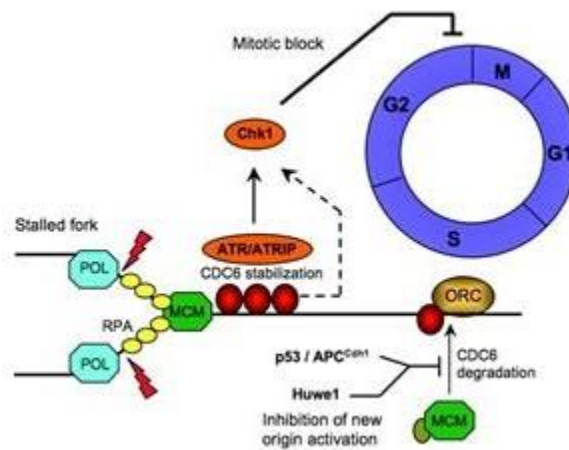


Figure 8. Functions of CDC6 throughout the cell cycle (Borlado and Mendez 2008).

1.4 CDC6 in cancer progression

The strict regulation of DNA replication is very important for the proper development of multicellular organisms, as the deregulation of this process has been linked to more than 40 human diseases including cancer (Borlado and Mendez 2008). RLFs are the first intracellular mediators which detect the increased mitogenic signals and their

deregulation is one of the commonest cancer characteristics and appears early during the carcinogenesis process (Pettrakis et al. 2016).

Indeed a series of *in vivo* studies have shown high CDC6 levels in various cancer types (Ohta et al. 2001, Bonds et al. 2002, Karakaidos et al. 2004, Xouri et al. 2004, Bravou et al. 2005, Murphy et al. 2005, Pinyol et al. 2006, Lontos et al. 2007, Sideridou et al. 2011). Particularly, high CDC6 levels emerge in 55% of brain cancers (Ohta et al. 2001), 50% of non-small cell lung cancers (NSCLC), which also correlates with poor prognosis in combination with p53 loss (Karakaidos et al. 2004), in lymphomas (Pinyol et al. 2006), cervix cancer (Bonds et al. 2002, Murphy et al. 2005), in colon and gastric cancers and finally in head and neck cancers (Sideridou et al. 2011). Furthermore, CDC6 high levels are also observed in precancerous stages and particularly in dysplastic lesions of lung, colon and head and neck origin (Lontos et al. 2007). Interestingly, high CDC6 levels are not related to increased proliferation of cancer cells in NSCLC (Karakaidos et al. 2004). Notably, in hyperplastic stage, which is characterized by uncontrolled cell proliferation, high CDC6 levels are not detected (Lontos et al. 2007). Thus, CDC6 is not up-regulated due to the increased proliferation rate, but due to the perturbed expression or regulation of CDC6 protein levels (Lau et al. 2010, Das et al. 2013, Hua et al. 2014) (**Figure 9**).

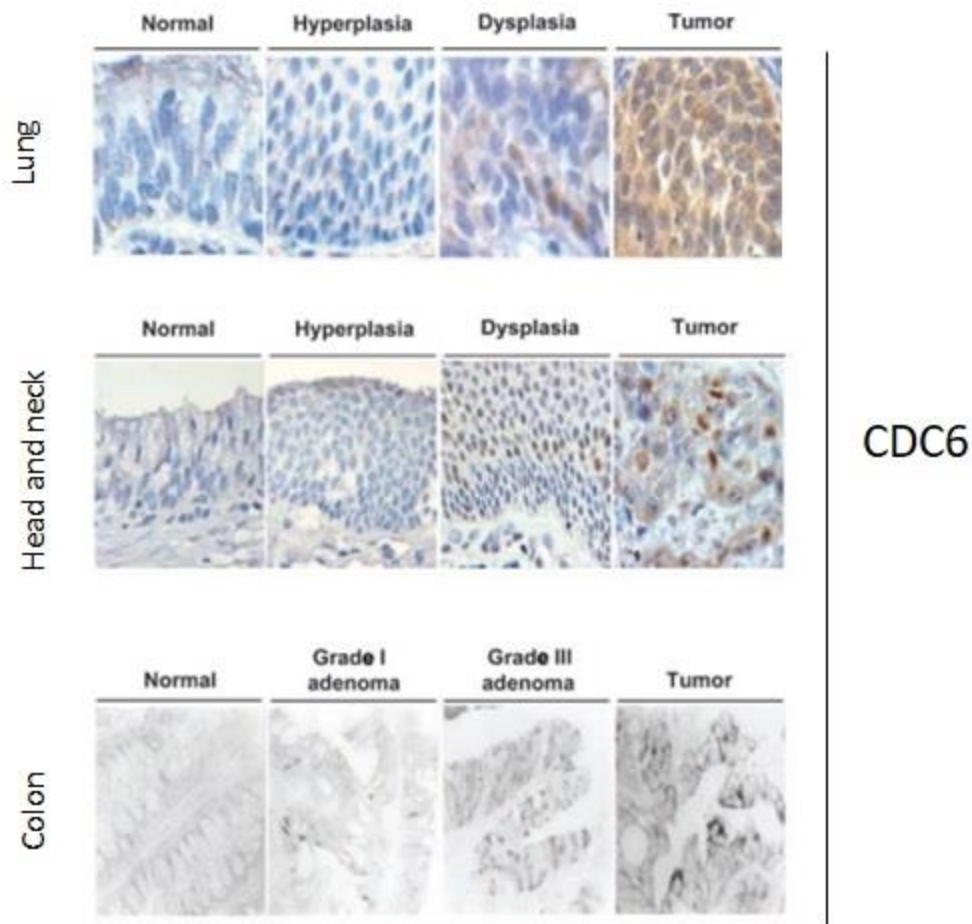


Figure 9. Increase of CDC6 levels from normal tissue to full blown cancer covering the whole spectrum of malignant transformation (modified from Lontos et al. 2007).

1.4.1 Molecular mechanisms implicated in CDC6 deregulation

Given that CDC6 is a pivotal factor for DNA replication licensing process, its overexpression in precancerous and cancerous lesions should be attributed to increasing cell proliferation. Nonetheless, the fact that CDC6 is not correlated with the Ki67 proliferation marker in combination with the fact that CDC6 is not detected in hyperplasias (Lontos et al. 2007), implies that the expression or the regulation of the expression of CDC6 is deregulated. Various molecular events contribute to CDC6 overexpression in cancer. First, the overproduction of transcription factors E2F1/2 due

to the deregulation of pRB-E2F pathway in cancer, leads to CDC6 overexpression (Gorgoulis et al. 2002, Zacharatos et al. 2004, Tsantoulis et al. 2005, Evangelou et al. 2008). Second, the enhanced expression of *CDC6* gene is a frequent event that contributes to its overexpression (Liontos et al. 2007). Notably, *CDC6* gene is located on 17q21.3 locus in proximity with the *ErbB2* gene (encodes for HER2), which is frequently amplified in tumors (Jacot et al. 2013, Krishnamurti et al. 2014, Martin et al. 2014, Mar et al. 2015). Consequently, *CDC6* enhancement could be a subsequent event of *ErbB2* amplification. Furthermore, a third mechanism which contributes to *CDC6* abundance in tumors is the production of an mRNA isoform which lacks part of its 3' untranslated region (3' UTR). This site is a target for micro-RNAs (miR25, miR541, miR92a/b) responsible for *CDC6* degradation and thus its loss results in increased mRNA stability and in turn higher protein levels (Akman et al. 2012, Petrakis et al. 2016) (**Figure 10**). Finally, a more recently proposed mechanism is related to perturbations of *CDC6* degradation. Briefly, the E3 ligase CUL4-DDB1-CDT2 ubiquitin complex is responsible for the degradation of *CDC6*, CDT1, p21^{WAF1/CIP1} protein, as well as other factors that participate on S phase. Accumulation of p21^{WAF1/CIP1} inhibits *CDC6* degradation due to the saturation of the responsible enzymes (Galanos et al. 2016).

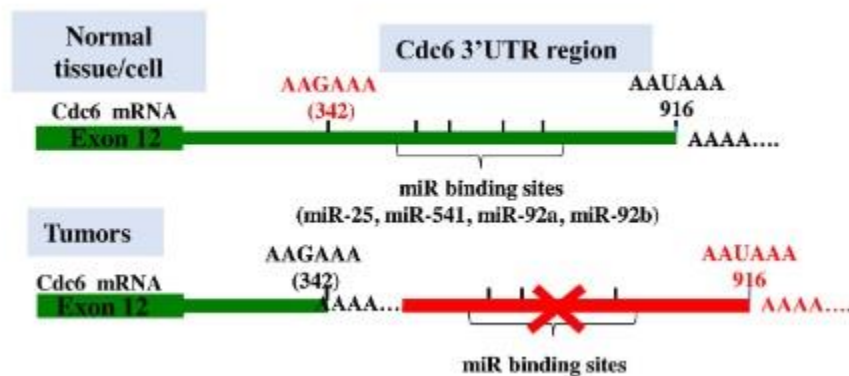


Figure 10. The role of 3'UTR in *CDC6* mRNA stability. Shortening of 3'UTR due to polyadenylation at an alternative site deprives the *CDC6* mRNA from miRs binding sites. Thus, regulatory miRs cannot bind to *CDC6* mRNA and facilitate its degradation.

Although CDC6 normally displays characteristic fluctuations during cell cycle, the above mentioned mechanisms contribute to the deregulation of CDC6 levels (Ho and Dowdy 2002). This results in CDC6 protein accumulation with detrimental effects (Petrakis et al. 2016).

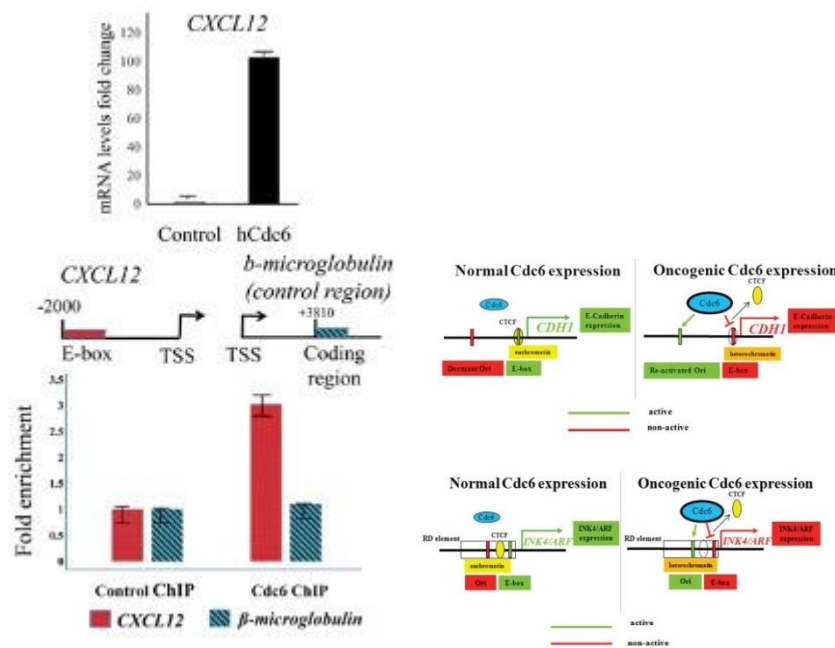
1.4.2 Mechanisms through which CDC6 exerts oncogenic activity

CDC6 overexpression promotes carcinogenesis. According to the oncogene-induced DNA damage model for cancer development, CDC6 deregulation activates the apoptosis and senescence anticancer barriers through the induction of DDR pathway (Bartkova et al 2006, Halazonetis et al. 2008). The activation of this mechanism occurs due to DNA re-replication and the subsequent replication stress induction. The continuous CDC6 overexpression provokes genomic instability, which in turn results in loss of tumor suppressor genes (e.g. TP53) and finally the bypass of antitumor barriers and cancer progression (Halazonetis et al 2008).

Additional findings also support the oncogenic role of CDC6. Briefly, non-cancerous cells that originate from mice papillomas (P1 cells), transformed with CDC6 possess a subpopulation which overexpresses CDC6 and also acquires a CD44^{high}/CD24^{low} antigenic profile (Petrakis et al. 2012), characteristic of stem cells (Mani et al. 2008). Injection of these cells into Severe Combined Immunodeficiency (SCID) mice results in tumor formations at injections sites. However, only the cells that overexpress CDC6 are capable of generating tumors, thus further highlighting the oncogenic role of CDC6 (Liontos et al. 2007).

Furthermore, CDC6 exert oncogenic activity through transcriptional regulation. Specifically, CDC6, when aberrantly overexpressed, binds to the promoter of E-cadherin gene (*CDH1*) resulting in the displacement of the transcriptional regulatory factor CTCF and of histone H2A.Z from *CDH1* promoter, resulting in heterochromatinization and silencing of this gene. Loss of E-cadherin is an event that mediates EMT (Sideridou et al 2011).

Additionally, CDC6 inhibits INK4/ARF locus at transcriptional level, which encodes for 3 tumor suppressor proteins (p16^{INK4A}, p14/ARF, p15^{INK4B}) (Sideridou et al. 2011). In addition, high-throughput assays revealed that the promoters of genes, which are deregulated after CDC6 overexpression in the P1 cell line comprise CTCF binding sites (Pettrakis et al. 2012). For instance, *CXCL12* gene, which encodes for SD-1 (Stromal derived factor-1) chemokine, is related to cancer progression and metastasis development (Sun et al. 2010). Supportively, subsequent chromatin immunoprecipitation (ChIP) experiments proved that CDC6 binds to *CXCL12* promoter (Pettrakis et al. 2016). Finally, more recent data revealed that CDC6 interacts with B23 (nucleophosmin, NPM) and is transferred to nucleolus. There, CDC6 binds to the promoter of ribosomal DNA (rDNA) and through ATP hydrolysis contributes to the recruitment of RNA polymerase I to activate rDNA transcription (Huang et al. 2016) (Figure 11).



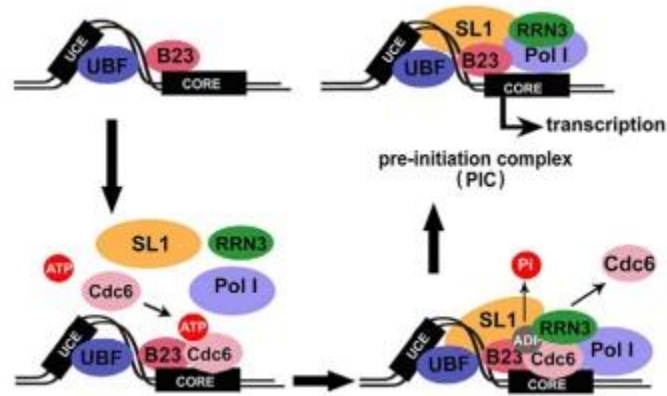
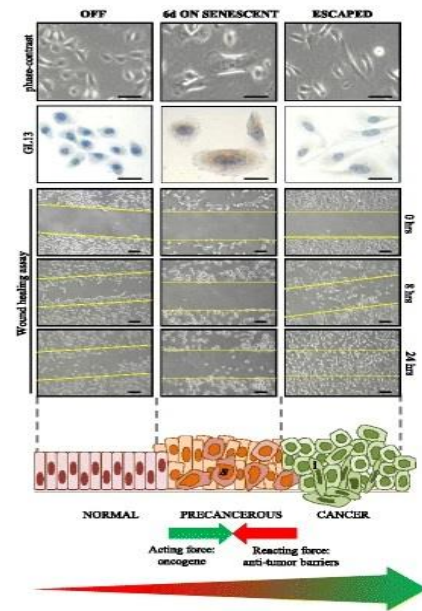


Figure 11. Mechanisms through which CDC6 regulates transcription. CDC6 overexpression inhibits the transcription of *CDH1* and *INK4/ARF* genetic loci by displacing CTCF and thus inducing the heterochromatinization of their promoters (Sideridou et al. 2011). In contrast, it induces the transcription of rDNA and *CXCL12* gene (Huang et al. 2016, Petrakis et al. 2016).

1.4.3 Cdc6 and senescence induction

Recent data published by Komseli and colleagues (Komseli et al. 2018) highlight the role of CDC6 in oncogene-induced senescence. The authors used a non-cancerous human bronchial epithelial cell line (HBECEs) as a model to study CDC6 overexpression. Upon CDC6 overexpression cells enter senescence at day 3, whereas they fully senesce at day 6 following overexpression. This finding is in accordance with a previous study which suggested that CDC6 overexpression in human fibroblasts induces senescence in a DDR-dependent manner (Bartkova et al. 2006). The most intriguing result of Komseli and co-authors research is the emergence of a fraction of proliferating cells after a protracted stalled growth phase which lasted for about a month. This implies that a subpopulation of cells managed to escape from the senescence growth arrest. Interestingly, the escaped population acquired an aggressive phenotype indicative of malignant transformation (**Figure 12**).

Figure 12. Overexpression of CDC6 in non-cancerous human bronchial epithelial cells (HBECs). CDC6 overexpression induces senescence, while protracted overexpression leads to senescence evasion and the acquisition of aggressive features, mimicking malignant transformation (Komseli et al. 2018).



Aim of PhD thesis

CDC6 is a pivotal factor for DNA replication licensing and along with ORC and CDT1 proteins leads to the upload and binding of MCM 2-7 helicases onto chromatin to form the pre-RC complex. This results in ORIs licensing during the S phase of the cell cycle. Hence, the CDC6 function is connected to S phase regulation. However, CDC6 has also been proved to participate in the regulation of mitosis and plays a precisely central role in the S-M checkpoint (Blow and Gillespie 2008, Borlado and Mendez 2008).

On the other hand, CDC6 deregulation has a cancer promoting role. CDC6 levels are increased from the early stages of carcinogenesis in a plethora of cancer types. In addition, aberrant CDC6 overexpression is highly correlated with adverse prognosis (Karakaidos et al. 2004, Lontos et al. 2007, Sideridou et al. 2011).

CDC6 is implicated in malignant progression through either transcriptional regulation or DNA re-replication. Regarding its transcriptional role, CDC6 inhibits the transcription of tumor suppressor genes which encode for the *INK4/ARF* locus proteins as well as the gene which expresses E-cadherin, a protein which characterizes epithelial cells (Sideridou et al. 2011). E-cadherin loss predisposes to EMT (Nieto et al. 2016). More recently, CDC6 has been shown to activate the transcription of *CXCL12*, which encodes for the chemokine SDF-1 that plays a metastasis promoting role (Petrakis et al. 2016).

Concerning the role of CDC6 on the deregulation of DNA replication, the overexpression of this RLF generates replication stress due to DNA re-replication (Vaziri et al. 2003, Lontos et al. 2007, Sideridou et al. 2011, Walter et al. 2016). Replication stress results in DNA damage and genomic instability, which in turn contributes to cancer progression (Halazonetis et al. 2008, Negrini et al. 2010).

Our group recently suggested that CDC6 overexpression *in vitro* induces senescence in a normal bronchial epithelial cellular setting. Interestingly, protracted expression of CDC6 protein resulted in the emergence of a subpopulation which evades senescence and re-enters cell cycle. Nonetheless, this population is not identical to the initial one

and has acquired an aggressive phenotype with malignant potential (Komseli et al. 2018).

However, the mechanisms which are responsible for senescence evasion have not been clarified yet. Hence, the aim of the present PhD thesis is to investigate the molecular events which contribute to the senescence-evading phenotype. For this purpose, human bronchial epithelial cells which overexpress CDC6 in an inducible manner were employed. In addition, a CDC6 depletion strategy was applied in breast cancer cell lines in order to address the issue whether CDC6 can be an attractive target for selective inhibition in the context of cancer therapy.

CHAPTER 2

MATERIALS & METHODS

2.1 METHODS

2.1.1 Cell lines and treatments

HBEC-CDC6/TetON (Komseli et al. 2018) and HPDEC-CDC6/TetON (supplied by Prof. Townsend) cell lines were maintained in Keratinocyte-Serum-Free Medium supplemented with 50µg/ml Bovine Pituitary Extract and 5ng/ml hEGF at 37°C and 5% CO₂. *CDC6* induction was conducted by treatment of the cell culture with 1 µg/ml doxycycline hyclate (DOX) (Sigma). Where applied 5,6-dichloro-1-β-D-ribofuranosylbenzimidazole (DRB) was used at a final concentration of 100µM and it was added directly in the growth media for the indicated time periods. The cell lines used in this study were not found in the database of commonly misidentified cell lines that is maintained by ICLAC and NCBI Biosample. Its identity has been authenticated by STR profiling and is regularly tested for mycoplasma.

2.1.2 Plasmid generation

The pcDNA3-HA-BHLHE40 vector was obtained from Addgene (cat No 110154). The neomycin resistance cassette was replaced with a hygromycin coding one. The hygro insert was amplified through fusion-PCR from a pcDNA3 Hygro HA Akt2 vector (Addgene Cat No 16000). Moreover, a pcDNA3 Hygro vector with no insert was generated for mock experiments.

2.1.3 siRNA and plasmids transfections

For BHLHE40 silencing two different cocktails of 3 unique siRNA duplexes - 2 nmol each from OriGene Technologies, Inc, (Cat No SR305619) and from Thermo Fisher Scientific (#1299001: HSS112516, HSS112517, HSS112518) were employed respectively, to secure off-target effects. For *CDC6* silencing 3 unique siRNA 2nmol each from Thermo Fisher Scientific were used (#1299001: HSS101647, HSS101648, HSS101649). siRNA gene silencing was performed following the manufacturer's instructions. More specifically, 3×10⁵ cells plated in 60mm dishes were transfected using Invitrogen Lipofectamine RNAiMAX Transfection Reagent with the appropriate RNAi

pool (set of three siRNAs) or the corresponding RNAi negative control. Cells were harvested 48h after transfection for further analysis.

2.1.4 Selection of escaped clones

Initially, 5×10^5 cells were plated. One day after the plating, CDC6 expression is induced by adding doxycycline in the culture media. Following the induction, cells fully senesce at day 6. At about day 30, senescence-evading cells start forming roughly 50 distinct colonies. Eventually, colonies were collected and they were transferred to 6-well plates, where they independently propagated.

2.1.5 Protein extraction, cell fractionation and immunoblot analysis

Thirty micrograms of protein from total extracts per sample were adjusted with Laemmli buffer and loaded on acrylamide/bis-acrylamide gels. Gel electrophoresis, transfer to PVDF membrane and signal development with chemiluminescence have been described before. Horse Radish Peroxidase conjugated anti-mouse and anti-rabbit secondary antibodies (1:1000 dilution) (Cell Signaling) were used. Primary antibodies utilized were: anti-CDC6 (mouse, Santa Cruz, sc9964, 1:500), anti-BHLHE40 (mouse, Santa Cruz, sc101023, 1:200), anti-RAD52 (mouse, Santa Cruz, sc-365341, 1:100), anti-RAD51 (rabbit, Merck-Millipore, PC130, 1:100), anti-BRCA1 (mouse, Santa Cruz, sc6954, 1:500), anti-BRCA2 (mouse, Sigma (mfr. Calbiochem), OP95, 1:500), anti-p53 (mouse, Santa Cruz, DO7, 1:500), anti-MDM2 (mouse, Santa Cruz, SMP14, 1:500), anti-PER1 (rabbit, Abcam, ab136451, 1:500), anti- β -actin (rabbit, Cell Signaling, 4967L, 1:1000), anti-GAPDH (rabbit, Cell Signaling, 2118S, 1:2000), anti-vinculin (mouse, Sigma, V9131, 1:1000), anti-HA-Tag (C29F4 rabbit, Cell Signaling, 3724, 1:1000), anti-phospho-Chk1 (Ser345) (rabbit, Cell Signaling, 2348, 1:1000). All analyses were performed in triplicate.

2.1.6 Immunofluorescence analysis

Cells were seeded and grown on 12-mm diameter autoclaved glass coverslips. To identify RAD52, RPA70, 53BP1 and γ H2AX foci, cells were pre-extracted on ice with cold PBS containing 0.1% Triton X-100 for 5 min before fixation in 4% cold

formaldehyde solution for 15 min at room temperature. For the rest of the analyzed proteins, the pre-extraction step was skipped. When Click-iT EdU staining was performed, cells were incubated with 10 μ M EdU for 30 min, before fixation or pre-extraction. Detection of EdU was performed according to the manufacturer's recommendations (Click-iT Imaging Kit Alexa Fluor 647; Thermo Fisher Scientific, C10340) followed by incubation with primary antibodies. Cells were incubated with primary antibodies for 1 h at room temperature. Following washing steps with PBS, coverslips were incubated with the corresponding secondary antibodies (Thermo Fisher Scientific) supplemented with DAPI for an additional 1 h at room temperature before washed again and mounted. Image acquisition of multiple random fields was automated on a DM 6000 CFS Upright Microscope (Confocal Leica TCS SP5 II) or a ScanR screening station (Olympus) and analyzed with ScanR (Olympus) software, or a Zeiss AxioLab fluorescence microscope equipped with a Zeiss AxioCam MRm camera and Achroplan objectives, while image acquisition was performed with AxioVision software 4.7.1. In the case of RAD52, the representative images of foci formation were acquired with a confocal LSM800 Zeiss microscope and processed with its Blue ZEN software. Primary antibodies utilized were: anti-CDC6 (mouse, Santa Cruz, sc9964, 1:500), anti-RAD52 (sheep, MRC-PPU Reagents, 1:100, kind gift from Drs. Jiri and Claudia Lukas), anti-53BP1 (rabbit polyclonal, Abcam ab36823, 1:250), anti-CDH1 (E-cadherin) (rabbit monoclonal, Cell Signaling #3195S, 1:100), anti-Vimentin (mouse monoclonal, Sigma V6630, 1:100), anti-RPA70 (rabbit, Abcam, ab79398, 1:100). All analyses were performed in triplicate.

2.1.7 Immunocytochemistry

For immunocytochemistry analysis cells were grown on coverslips and fixed with 100% ice-cold methanol or 4% formaldehyde (prepared from paraformaldehyde) for 10 min and stored at 4°C until staining was performed. Following, cells were permeabilized with 0,3% Triton X-100 in PBS for 5 min at RT. A 10% fetal bovine serum and 3% bovine serum albumin in PBS solution was used as a blocking buffer for 1 h at RT. Primary antibodies were diluted in blocking buffer and incubated overnight at 4°C. Secondary antibodies were: anti-CDC6 (mouse, Santa Cruz, sc9964, 1:500), Ki-67 (rabbit, Abcam,

ab16667, 1:250), caspase-3 (rabbit, Cell Signaling, 9662, 1:500). Nuclear signal was evaluated as a positive one. A minimum of 100 cells were counted at high power optical field (x 400).

2.1.8 Cell growth analysis

HBEC cells were seeded at day 0 on 6-well plates at a density of 8×10^4 cells per well. Every day up to day 6, cells from one well at a time were trypsinized and counted using a standard Neubauer chamber (Marienfeld Superior, # 0640010).

2.1.9 3D (organotypic/organoid) culture

First, airway fibroblasts were embedded in type I collagen, allowing contraction of the gel mimicking the underlying submucosa, as previously described (Sato et al. 2006, Ramirez et al. 2003). Subsequently, positively selected HBEC-CDC6/TetON cells were seeded on top of the contracted layer and upon attachment of HBECs on the underlying stroma, the organotypic culture was submerged into Keratinocyte-Serum-Free Medium (#17005-075, Invitrogen) supplemented with 50 μ g/ml Bovine Pituitary Extract and 5ng/ml hEGF (#17005-075, Invitrogen) and then lifted to an air-liquid interface, while cell growth was performed at 37°C with 5% CO₂. Following, *CDC6* induction was performed as per the 2D culture medium. Finally, matrigels were collected at 6 and 30 days post-induction, formalin fixed and paraffin embedded. Sections were obtained and processed for hematoxylin-eosin and GL13 staining and immunohistochemical analysis as described in previous section.

2.1.10 Senescence detection with SenTraGor

Fixed cells mounted on coverslips were rinsed sequentially in 50% and 70% Ethanol for 5 minutes at room temperature, respectively. Then the coverslips were incubated with the SenTraGor solution for 10 minutes. Following washings with 50% Ethanol and TBS at room temperature, the anti-biotin antibody ([Hyb-8] ab201341 Abcam, diluted 1:30 in TBS) was applied for 60 minutes at 37°C. Subsequently the signal was developed using the Ultravision Quanto Detection System HRP DAB kit (Cat no: TL-125-QHD), according to the manufacturer's instructions. Finally cells were counterstained with

Hematoxylin (diluted 1:4 in deionized water) for 40 sec and observed under a light microscope.

2.1.11 Invasion assay

Cells were trypsinized and plated (1×10^5) into a cell invasion chamber (Corning, 354480) containing EGF-free medium and allowed to invade for 24h towards full medium. Cells were fixed with 4% paraformaldehyde, stained with Giemsa, photographed and counted. Data from three independent measurements were averaged, and the corresponding SDs are also reported.

2.1.12 Flow cytometry analysis (FACS) - Cell cycle analysis

Cell cycle analysis was determined using a BD FACSVerser (BD Biosciences), following EdU incorporation, as previously published [Galanos et al., 2016]. Briefly, cells were incubated with 10 μ M EdU for 30 min, and they were then fixed with 70% of ice cold ethanol and were incubated on ice for at least 30 min or kept at -20 °C until the day of staining and analysis. Afterwards, the samples were centrifuged (1500 rpm, 5 min at room temperature) and washed sequentially with PBS and PBS⁺ (PBS, 1% BSA and 0,1% Tween). Detection of EdU was performed according to the manufacturer's recommendations (Click-iT Imaging Kit Alexa Fluor 647; Thermo Fisher Scientific, C10340) and subsequently samples were incubated with Hoechst 33342 (1:1000 in PBS) followed by a final wash with PBS⁺. Cells were then analysed on BD FACSVerser (BD Biosciences) and acquired data were processed using the FlowJo software.

2.1.13 5'-EU incorporation based nascent RNA assay

In situ detection of nascent RNA was performed with the Click-iT Alexa Fluor 488 Imaging Kit (Thermo Fisher Scientific). Cells were incubated for 30 min in the presence of 0.5 mM 5-EU. Samples were fixed in 4% formaldehyde for 15 min and permeabilized in 0.5% Triton X-100 for 20 min at RT. Samples then processed according to the manufacturer's recommendation. Cells were analyzed using LSM780 or LSM710 (Carl Zeiss Microscopy) confocal microscopes and 5-EU nuclear intensity was quantified with the NIS-elements software (Nikon).

2.1.14 QIBC analysis

Quantitative image-based cytometry (QIBC) analysis (**Figure S2**) was performed essentially as previously described (Ochs et al., 2016). In brief, images were taken with a ScanR inverted microscope High-content Screening Station (Olympus) that was equipped with wide-field optics, a 20x, 0.75-NA (UPLSAPO 20x) dry objective, fast excitation and emission filter-wheel devices for DAPI, FITC, Cy3, and Cy5 wavelengths, an MT20 illumination system, and a digital monochrome Hamamatsu ORCA-R2 CCD camera. Images were obtained in an automated fashion with the ScanR acquisition software (Olympus, 2.6.1). Depending on cell confluency, 25 to 49 images were acquired containing at least 1,000 cells per condition. Acquisition times for the different channels were adjusted for non-saturated conditions in 12-bit dynamic range, and identical settings were applied to all the samples within one experiment. Images were processed and analyzed with ScanR analysis software. First, a dynamic background correction was applied to all images. The DAPI signal was then used for the generation of an intensity-threshold-based mask to identify individual nuclei as main objects. This mask was then applied to analyze pixel intensities in different channels for each individual nucleus. For analysis of DNA damage-induced foci, additional masks were generated by segmentation of the respective images into individual spots with intensity-based or spot-detector modules included in the software. Each focus was thereby defined as a sub-object, and this mask was used for quantification of pixel intensities in foci. After this segmentation of objects and sub-objects, the desired parameters for the different nuclei or foci were quantified, with single parameters (mean and total intensities, area, foci count, and foci intensities) as well as calculated parameters (sum of foci intensity per nucleus). These values were then exported and analyzed with TIBCO Software, version 5.0.0. This software was used to quantify absolute, median, and average values in cell populations and to generate all color-coded scatter plots. Within one experiment, similar cell numbers were compared for the different conditions (at least 1,000 cells), and for visualization low x-axis jittering was applied (random displacement along the x axis) to make overlapping markers visible. Primary antibodies utilized were: anti-53BP1 (rabbit, Abcam ab36823, 1:250), anti- γ H2AX (pSer139/140)

(rabbit, Abcam, ab36823, 1:100), anti-RPA (rabbit, Abcam, ab79398, 1:100), anti-RAD52 (sheep, MRC-PPU Reagents, 1:100, kind gift from Drs. Jiri and Claudia Lukas).

2.1.15 DR-GFP, SA-GFP and BIR-GFP reporter assays

HBEC-CDC6/TetON cells were transiently transfected with the GFP based reporter constructs for synthesis-dependent strand annealing (DR-GFP), single strand annealing (SA-GFP) and break induced replication (BIR-GFP). To monitor repair of I-SceI-generated DSBs, cells were transiently co-transfected with 1 µg of the I-SceI expression vector HA-ISceID44A (Addgene #59424) using the Effectene reagent (Qiagen). DSB repair efficiency upon *CDC6* induction was determined by quantifying GFP-positive cells via flow cytometry FACS Calibur (Becton Dickinson) 48h after transfection, under non-chromatinized conditions.

2.1.16 DNA fiber fluorography (combing assay)

HBEC-CDC6/TetON cells were grown in the presence or absence of doxycycline for the indicated time points and then pulsed-labeled with 25µM CldU for 20min, and then labelled with 250µM IdU for 20min (1:1000, I7125, Sigma-Aldrich). Cells were then harvested and lysed on glass slides in spreading buffer, DNA was denatured and stained using rat anti-BrdU/CldU (1:1000, C6891, B5002, Sigma-Aldrich) and mouse anti-IdU/BrdU (1:500, clone B44, Becton Dickinson) antibodies.

2.1.17 Breaks Labeling In Situ and Sequencing (BLISS)

The method consists of following main steps: i) upon harvesting of cells from multi-well plates, approx. 2 million cells were fixed in suspension with 4% formaldehyde for 10 min at room temperature, ii) DSBs ends were *in situ* blunted, iii) next they were tagged with dsDNA adapters containing sample barcodes, UMIS (unique molecular identifiers), RA5 adapter and T7 promoter, iv) tagged DSB ends were linearly amplified using *in vitro* transcription and v) the resulting RNA was used for library preparation and sequencing. BLISS data were analyzed as described below.

2.1.18 Next Generation Sequencing and Bioinformatics analysis

The library preparation and the whole genome sequencing were carried out in EMBL Genecore facility according to the Illumina platform. Whole genome sequencing was performed in non-induced and escaped cells achieving a 30x coverage of the human genome. Paired-end 2x100 bp was performed with the use of Illumina Hi-seq 2000. SAMtools *mpileup* and *bcftools* (Li et al 2009), *GATK tools*, the GATK source bundle and the GATK best practices guide (Van der Auwera et al, 2013), were used for identification and filtering of the SNPs and INDELS. Variations that were unique in the escaped cells were normalized based on the sequencing depth of each experiment. Copy number and structural variants were determined using MANTA (Chen et al. 2016) and annotated on the Human reference genome using ANNOVAR (Wang et al. 2010). As shared CNVs (or overlapped regions) we characterized the common intersected variations between the escaped replicates, (using `intersectBed -wa -u` from BEDtools), after extracting the variations that are present in the un-induced samples (`intersectBed -v`).

For BLISS data, DNA Double Stranded Breaks (DSBs) were normalized for total mapped reads and for the total number of used cells for each replicate. The aggregation of Unique Molecule Identifiers (UMIs) and the frequency of DSBs in various genomic regions were calculated using in-house R scripts (available on request).

BLISS signal data and CNV regions were compared with `intersectBed`, a subcommand from BEDtools suite in order to determine the distribution of expected overlaps. As a control we used a randomly selected set of loci by applying the `randomBed` and `shuffleBed` subcommands in order to permute these genomic locations repeatedly (10000 times).

2.1.19 RNA isolation, sequencing, and data analysis

6 days ON and senescence-bypass “inverted” HBECs were harvested in Trizol (Thermo Fisher Scientific, 15596026) and total RNA was isolated and DNase-treated using the Direct-zol RNA miniprep kit (Zymo Research) as per manufacturer’s instructions. cDNA libraries were next generated using the TruSeq RNA library kit (Illumina) via selection on poly(dT) beads. The resulting libraries were single-end sequenced to >50 million

reads on a HiSeq4000 platform (Illumina). Raw reads were mapped to the human genome (hg19) using STAR aligner (version 2.5.3a) (Dobin et al. 2013). Samtools (version 0.1.19) (Li et al. 2009) were used for data filtering and file format conversion, while HTseq count (version 0.5.4p3.) algorithm (Anders et al. 2015) was used to assign aligned reads to exons using the following command line «htseq-count -s no -m intersection -nonempty». Normalization of reads and removal of unwanted variation was performed with RUVseq (Risso et al. 2014).

2.1.20 Chromatin immunoprecipitation (ChIP), sequencing, and data analysis

ChIP was performed on 10-15 million cells crosslinked in 1% PFA/PBS at RT for 10 min, and quenched in 0.125M ice-cold glycine. ChIP material was prepared as previously described (Ford et al. 2014), and sonication was performed using a Bioruptor sonicator and adjusting fragment size to 200-500 bp. For the IP the following polyclonal antisera were used: anti-CTCF (61311, Active Motif), anti-H3K27ac (39133, Active Motif) and anti-BHLHE40 (#NB100-800, Novus Biologicals). ChIP-seq libraries were sequenced on a HiSeq4000 platform (Illumina) to at least 25 million reads per sample, and analyzed using the ENCODE pipeline (https://www.encodeproject.org/chip-seq/transcription_factor/).

2.1.21 Genome-wide chromosome conformation capture (Hi-C) and data analysis

In situ Hi-C on HBECs of different states and genotypes was performed and controlled for quality using the Arima Hi-C kit as per manufacturer's instructions. All resulting libraries that met the QC criteria set by the manufacturer were paired-end sequenced on a NovoSeq6000 platform (Illumina) to at least 0.5 billion reads. For data analysis, reads were mapped to the reference human genome (GRCh37/hg19) using Bowtie (ver. 23.4.1) (Langmead and Salzberg 2012) with the "--reorder" flag. Local mapping was used to increase mapping rates due to the inherent presence of chimeric reads. All preprocessing and downstream analysis was performed using HiCExplorer (ver. 3.2) (Ramirez et al. 2018) to remove unmappable reads, non-uniquely mapped reads and

low-mapping-quality reads, as well as duplicated pairs (i.e., starting and ending with exactly the same location), dangling-ends (i.e., digested but not ligated), self-circularized (i.e., reads pairing within <25 Kbp and facing outwards), same-fragment (i.e., read pair locating in the same restriction enzyme fragment) or self-ligated reads (i.e., having a restriction site in between the read pair within <800 bp). Next, genome-wide contact matrices were generated in the form of .cool files, in which the genome was binned into different sizes (resolution) — 10 kb, 20 kb, 50 kb and 100 kb — for different downstream usage. To facilitate comparison between different samples, all Hi-C interaction counts were normalized and then balanced using the Knight-Ruiz (KR) matrix balancing algorithm (Knight and Ruiz 2013). Hi-C matrices stored in .cool files were visualized using HiGlass (Kerpedjiev et al. 2018) as interactive heatmaps. To make zooming-in and -out possible, normalized and balanced .cool files at 10 Kbp resolution were converted to multi-resolution cooler files called .mcool files using Cooler (Abdennur and Mirny 2020). For calling A/B compartments, 100 kbp-resolution and Pearson-transformed matrices were used to calculate the first eigenvector, which was then integrated with own H3K27ac ChIP-seq data to mark A-compartments. TADs were assigned using 20 kbp-resolution matrices using the function embedded in HiCExplorer based on deduced z-scores and with a P-value cutoff of 0.01. Finally, loops we detected as previously described (Rao et al. 2014) by computing a negative binomial distribution of 10 kbp-resolution Hi-C data and using Anderson-Darling/Wilcoxon rank-sum tests and a P-value cutoff of 0.05; loop lengths were restricted to 0.1-2 Mbp (to avoid signal contamination from the diagonal of Hi-C matrices), and compared to CTCF ChIP-seq data to identify loops with CTCF-bound anchors.

2.1.22 CRISPR/Cas9 inversion generation

Design of gRNAs. Based on the WGS data (see corresponding section), 20-nt sgRNAs were designed around each breakpoint. Two complementary DNA oligos for each sgRNA were annealed generating 5'overhangs consisting of CACC(G) and AAAC. gRNA1 and gRNA2 were chosen due to high specificity and small distance from the exact breakpoints (listed in supplemental material). They were cloned into – Cas9 expression plasmids - pSpCas9(BB)-2A-GFP (PX458) and pU6-(BbsI)_CBh-Cas9-T2A-

mCherry, respectively, which had been already digested with BbsI. In this way, sgRNAs were integrated next to the gRNA scaffold of the particular vector (**see Zampetidis et al. 2021**).

Transfection and FACS sorting. HBECs were cultured in Keratinocyte (serum free medium) (#17005042) without antibiotics supplemented with 25 mg Bovine Pituitary Extract and 2.5 µg EGF, Human Recombinant. Delivery of 2.5µg from each plasmid, coding for one sgRNA and Cas9, was performed via double transfection of HBECs two days after plating 8×10^4 cells per well in a 6-well plate (reaching 80% confluency) with FuGENE® HD Transfection Reagent (Promega #E231A) (4:1 FuGENE® HD Transfection Reagent: DNA Ratio). FACS sorting of double positive (GFP and mCherry) cells gave rise to a large number of clones, subsequently cultured in 96-well plates.

DNA extraction and PCR screening. After harvesting cells from 96-well plates in 30 µl Trypsin/EDTA 1x (stock 10X, Thermo Fisher Scientific, #15400054), followed by a neutralization step with an equal volume of Trypsin Neutralizer Solution (Thermo Fisher Scientific, #R002100), half of the cells were lysed by adding 30 µl of Lysis Buffer (50 mM KCl, 10 mM TRIS pH: 8.3, 2.5 mM MgCl₂, 0.45% NP40 and 0.45% Tween20) containing Proteinase K (1 µl of 20 µg/µl Proteinase K for every 50 µl of Lysis Buffer), and heating for 45 min at 60°C followed by 10 min at 80°C to inactivate Proteinase K. The other half of the cells were kept in culture. 4µl of the lysate were used as genomic DNA for PCR. Two pairs of forward and reverse primer were designed around each breakpoint (**see Zampetidis et al. 2021**). PCR product of F1/R1 and F2/R2 manifest the wild type genomic DNA, while F1/F2 and R1/R2 give product in case that the area has been inverted. PCR products were submitted for Sanger sequencing verification (see below).

2.1.23 Sanger sequencing

PCR products were purified using the QIAquick PCR Purification Kit (#28104) and submitted for Sanger sequencing. Parental HBEC-CDC6/TetON cells were used as a reference. Primers and full Sanger sequences are available in **Zampetidis et al 2021**.

2.1.24 Survival data analysis

Data on survival analysis was obtained from a public database Kaplan-Meier plotter (<http://www.kmplot.com>) (Nagy et al. 2018), except for breast and prostate cancer data for which a separate Log-rank (Mantel-Cox) survival analysis, with Bonferroni correction, was performed on data retrieved from Metabric and TCGA, respectively.

2.1.25 Quantification and statistical analysis

Two-tailed unpaired Student's t-test was employed to compare data obtained by DNA fiber fluorography, QIBC assay, immunofluorescence imaging, reporter assays and differences in cell proliferation and invasion assay. Super Exact test was used to assess whether common CNVs were significantly more than expected by chance. The hypergeometric test was applied to estimate the significance of the up-regulated genes which were identified as both BHLHE40 target genes and differentially expressed genes during escape. Fisher's exact test was used to assess the significance of the increased cell death in FACS-based cell cycle profiling and in the immunostaining for Caspase-3. Wilcoxon-Mann-Whitney test was used to examine changes in the distribution of lengths for the loops observed.

2.2 MATERIALS

REAGENT or RESOURCE	SOURCE	IDENTIFIER
Antibodies		
Mouse anti-CDC6	Santa Cruz	sc9964
Mouse anti-BHLHE40	Santa Cruz	sc101023
Mouse anti-BRCA1	Santa Cruz	sc6954
Mouse anti-BRCA2	Sigma (mfr. Calbiochem)	OP95
Mouse anti-Vinculin	Sigma	V9131
Rabbit anti-RAD51	Merck-Millipore	PC130
Mouse anti-RAD52	Santa Cruz	sc365341
Sheep anti-RAD52	MRC-PPU Reagents, University of Dundee, Scotland	Supplied by Dr. Claudia and Jiri Lukas
Rabbit anti-RPA70	Abcam	ab79398
Mouse anti-gH2AX (pSer139/140)	Abcam	ab22551
Mouse anti-p53	Santa Cruz	DO7
Mouse anti-MDM2	Santa Cruz	SMP14
Rabbit anti-PER1	Abcam	ab136451
Rabbit anti- β -actin	Cell Signaling Technology	4967L
Rabbit anti-GAPDH	Cell Signaling Technology	2118S
Rabbit-anti-HA-tag	Cell Signaling Technology	C29F4
Rabbit anti-53BP1	Abcam	ab36823
Rabbit anti-CDH1	Cell Signaling Technology	3195S
Mouse anti-Vimentin	Sigma	V6630
Rabbit anti-H3K27ac	Active Motif	39133

Rabbit anti-H3K27me3	Active Motif	39155
Rabbit anti-Ki-67	Abcam	ab16667
Rabbit anti-caspase 3	Cell Signaling	9662
Rabbit anti-CTCF	Active Motif	61311
Rabbit anti-phospho-Chk1 (Ser 345)	Cell Signaling	2348
Horse Radish Peroxidase-conjugated anti-mouse	Cell Signaling Technology	7076P2
Horse Radish Peroxidase-conjugated anti-rabbit	Cell Signaling Technology	7074S
Alexa Fluor 488 donkey anti-rabbit	Abcam	ab150073
Alexa Fluor 568 goat anti-mouse	Abcam	ab175473
Rat anti-BrdU/CldU	Bio-rad (former AbD Serotec)	OBT0030
Mouse anti-IdU/BrdU	Becton Dickinson	347580 (clone B44)
Chemicals, peptides, and recombinant proteins		
Keratinocyte-Serum Free medium	Invitrogen	17005-075
Bovine pituitary extract + human epidermal growth factor (hEGF)	Invitrogen	37000-015
Doxycycline	Sigma	D9891-5G
BamHI	NEB	R0136S
SmaI	NEB	R0141S
BbSI	NEB	R0539S
5,6-dichloro-1- β -D-ribofuranosylbenzimidazole (DRB)	Merck	287891
Laemmli buffer	Merck	38733
polyvinylidene fluoride (PVDF) membrane	Macherey-Nagel	741260
Clarity Western ECL Substrate	Bio-rad	1705060
SenTraGor™	Supplied by Lab Supplies Scientific	N/A

5-ethynyl-2'-deoxyuridine (EdU)	Invitrogen	A10044
diamidino-2-phenylindole (DAPI)	Thermo Fisher Scientific	62248
5-Iodo-2'-deoxyuridine (IdU)	Sigma-Aldrich	I7125
5-Chloro-2'-deoxyuridine (CldU)	Sigma-Aldrich	C6891
5-bromo-2'-deoxyuridine (BrdU)	Sigma-Aldrich	B5002
Effectene Transfection Reagent	Qiagen	301425
Trizol	Thermo Fisher Scientific	15596026
Phosphate Buffer Saline (PBS) 1X	biowest	L0615-500
Triton X-100	Acros Organics	327372500
FuGENE® HD Transfection Reagent	Promega	E2311
Trypsin/ Ethylenediaminetetraacetic acid (EDTA) 10x	Thermo Fisher Scientific	15400054
Trypsin Neutralizer Solution	Thermo Fisher Scientific	R002100
Fetal Bovine Serum (FBS)	Gibco	10270-106
Bovine Serum Albumin (BSA)	Applichem	A1391
Proteinase K	Thermo Fisher Scientific	AM2548
Paraformaldehyde (PFA)	Merck	104005
Glycine	Applichem	A1067
Lipofectamine RNAiMAX Transfection Reagent	Thermo Fisher Scientific	13778150
Critical commercial assays		
Click-iT Alexa Fluor 647 Imaging Kit	Thermo Fisher Scientific	C10340
Direct-zol RNA miniprep kit	Zymo Research	R2050
TruSeq RNA library kit	Illumina	RS-122-2001
Arima Hi-C kit	Arima Genomics	A51008-ARI

QIAquick PCR Purification Kit	QIAGEN	28104
Experimental models: Cell lines		
HBEC-CDC6 Tet-ON	Ramirez et al., 2003 Komseli et al., 2018	Supplied by Liloglou T. (parental cells known as HBEC-3KT) Constructed by our group
HPDEC-CDC6 Tet-ON	Furukawa et al., 1996	Supplied and Townsend P.
Oligonucleotides		
Primers for the screening of inverted clones	Zampetidis et al. 2021	N/A
Primers and full Sanger sequences	Zampetidis et al. 2021	N/A
gRNA1	Zampetidis et al. 2021	N/A
gRNA2	Zampetidis et al. 2021	N/A
siRNA cocktail targeting BHLHE40	Origene	Cat No SR305619
siRNA cocktail targeting BHLHE40	Thermo Fisher Scientific	Cat No 1299001: HSS112516, HSS112517, HSS112518
siRNA cocktail targeting CDC6	Thermo Fisher Scientific	Cat No 1299001: HSS101647 HSS101648 HSS101649
Recombinant DNA		
pcDNA3-HA-BHLHE40	Addgene	110154

pcDNA3 Hygro HA Akt2	Addgene	16000
DR-GFP	Stark J.M. et al., 2004	Supplied by Halazonetis T.
BIR-GFP	Sotiriou et al., 2016	Supplied by Halazonetis T.
SA-GFP	Stark J.M. et al., 2004	Supplied by Halazonetis T.
HA-ISceID44A	Galanos P. et al., 2018	Supplied by Soutoglou E.
pSpCas9(BB)-2A-GFP (PX458)	Addgene	48138
pU6-(BbsI)_CBh-Cas9-T2A-mCherry	Addgene	64324
Software and algorithms		
ScanR automated image acquisition and analysis software (Olympus, 3.1)	Olympus	https://www.olympus-lifescience.com/en/microscopes/inverted/scanr/
TIBCO Spotfire Analyst, version 10.10.3	Tibco Software	https://perkinelmerinformatics.com/products/exclusive-reseller/tibco-spotfire/
STAR aligner (version 2.5.3a)	Dobin et al, 2013	https://github.com/alexdobin/STAR

Samtools (version 0.1.19)	Li et al., 2009	http://samtools.sourceforge.net/
HTseq count (version 0.5.4p3.)	Anders et al, 2015	https://htseq.readthedocs.io/en/master/history.html
RUVseq	Risso et al., 2014	https://rdrr.io/bioc/RUVSeq/man/RUVr.html
DESeq	Anders, 2010	https://www.bioconductor.org/packages//2.10/bioc/html/DESeq.html
BWA-MEM	Li and Durbin, 2010	http://bio-bwa.sourceforge.net/
MACS2 (ver. 2.1.2)	Zhang et al., 2008	https://pypi.org/project/MACS2/
Bowtie (ver. 2.3.4.1)	Langmead and Salzberg, 2012	https://sourceforge.net/projects/bowtie-bio/files/bowtie2/2.3.4.1/
HiCExplorer (ver. 3.2)	Ramirez et al., 2018	https://github.com/deeptools/HiCExplorer

Knight-Ruiz (KR) matrix balancing algorithm	Knight and Ruiz, 2013	https://github.com/deeptools/Knight-Ruiz-Matrix-balancing-algorithm
HiGlass	Kerpedjiev et al., 2018	https://higlass.io/
Cooler	Abdennur and Mirny, 2020	https://github.com/open2c/cooler
MANTA	Chen et al., 2016	https://github.com/Illumina/manta
ANNOVAR	Wang et al., 2010	https://annovar.openbioinformatics.org/en/latest/
<i>bcftools</i>	Li et al., 2009	https://github.com/samtools/bcftools
<i>GATK tools</i>	Van der Auwera et al., 2013	https://gatk.broadinstitute.org/hc/en-us
Other		
Matrigel Invasion Chambers	Corning	354480
Neubauer glass chamber	Marienfeld Superior	0640010

Table 1. List of materials

CHAPTER 3
RESULTS

3.1 Assessment of a cellular system recapitulating oncogene-induced senescence and cancer evolution

Our group recently developed and described a cellular setting based on the non-cancerous cell line HBECs, which carries a CDC6-TetON overexpression cassette (HBEC/CDC6-TetON) (Komseli et al. 2018). Importantly, the HBEC cell line is of epithelial origin resembling the majority of cancer types and like normal cells is free of mutation burden found in cancer cells (Stratton et al. 2009, Goodspeed et al. 2016).

The RLF CDC6 was chosen as the preferred oncogenic stimulus because, first, CDC6 is a key component of the replication licensing machinery and it is frequently deregulated from pre-cancerous stages and precisely the stage of dysplasia (Karakaidos et al. 2004, Liontos et al. 2007, Sideridou et al. 2011, Petrakis et al. 2016). Furthermore, CDC6 has been proven to be a more powerful inducer of senescence compared to other oncogenes, such as RAS or BRAF (Patel et al. 2016). Interestingly, its overexpression has been linked with poor patient survival in a variety of cancer types (**Figure 13A**).

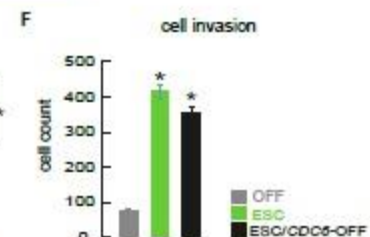
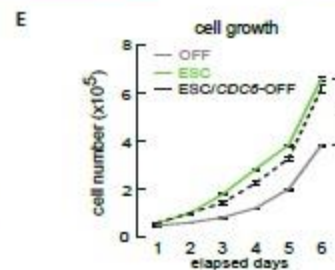
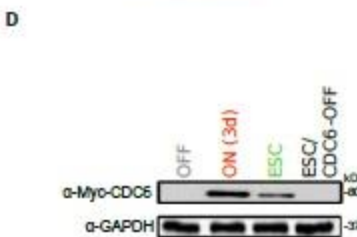
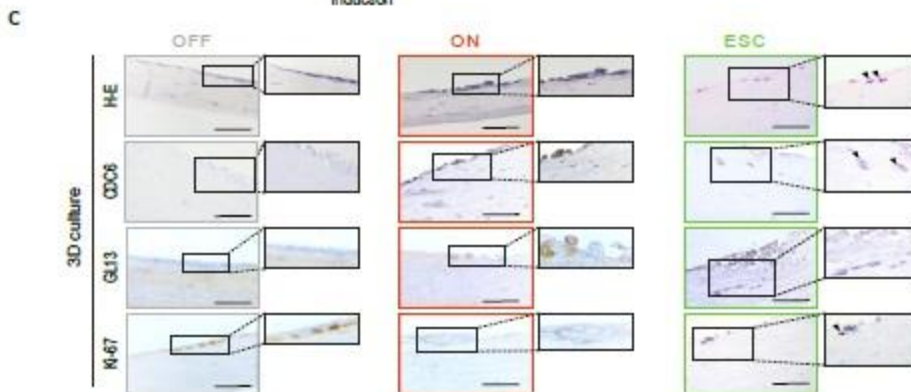
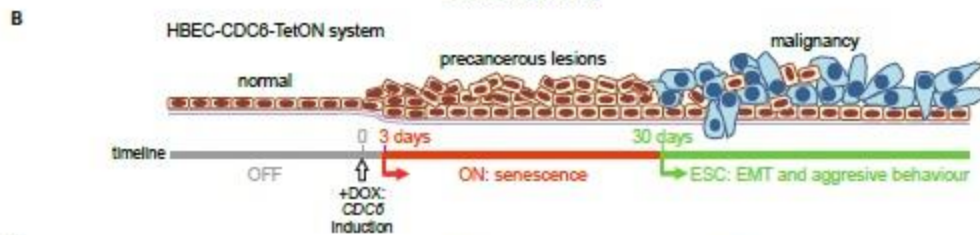
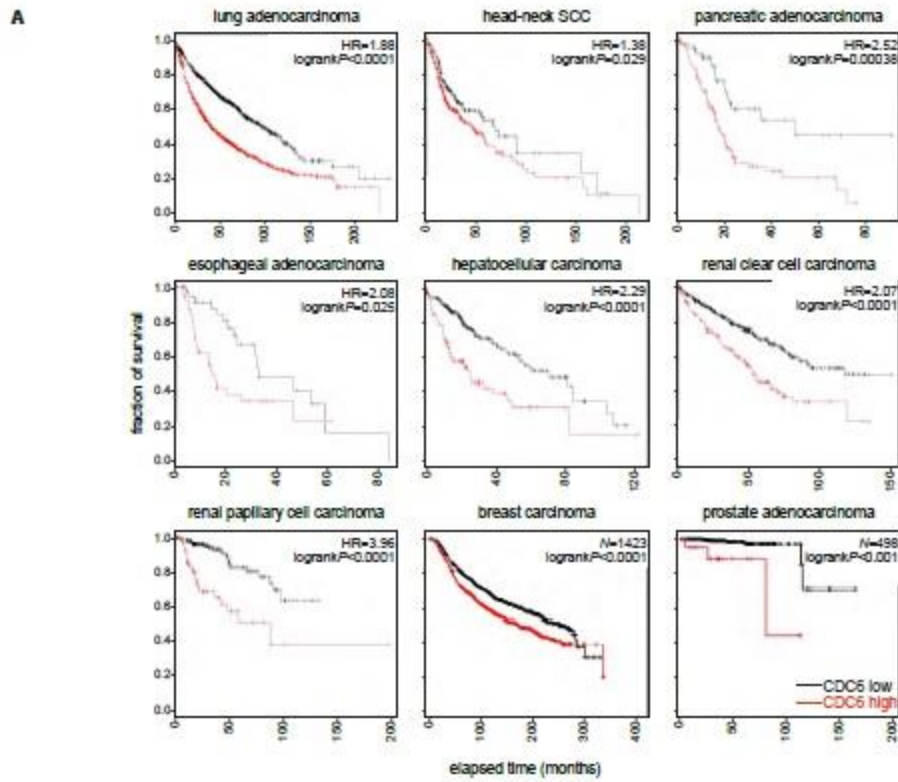


Figure 13. CDC6 overexpression is correlated with adverse prognosis for cancer patients and is a driving force for escape from oncogene-induced senescence.

(A) Kaplan-Meier survival plots generated using public data from tumors stratified as “high” (red line) or “low” CDC6-expressing (black line; <http://www.kmplot.com>). Plots for breast and prostate tumors were generated using data from Metabric and TCGA, respectively.

(B) A human bronchial epithelial cell (HBEC) CDC6/TetON cellular system recapitulating successive stages of cancer evolution (Komseli et al. 2018).

(C) Representative images of HBECs grown in 3D organotypic conditions and immunostained for H-E (hematoxylin-eosin), CDC6, SenTraGor and Ki-67 following the timeline in panel B. Non-induced cells (OFF) recapitulate the upper respiratory epithelium. Upon CDC6 induction, cells enter senescence and form spheroids. Prolonged CDC6 induction gives rise to escaped (ESC) cells with an EMT phenotype (arrowheads) and renewed proliferative capacity (arrowhead in Ki-67-stained ESC cells) that invade the supporting collagen matrix (arrowheads in CDC6-stained ESC cells).

(D) Western blots showing changing levels of induced CDC6 in HBECs.

(E) Line plots quantifying sustained proliferation (mean \pm S.D.; n=3) of ESC/CDC6-OFF cells. *: significantly different to OFF: P<0.05, unpaired two-tailed Student’s t-test.

(F) Bar plots quantifying cell invasion capacity (mean \pm S.D.; n=3) of ESC/CDC6-OFF cells. *: significantly different to OFF: P<0.05, unpaired two-tailed Student’s t-test.

According to our working hypothesis, the activation of the CDC6-TetON cassette, by adding doxycycline in cells’ culture medium, resulted in increased CDC6 levels (oncogene activation), which in turn causes DNA damage (Phase I). As a result, DNA repair pathways are activated and at least a fraction of cells repair their damage in an error-prone manner (Phase II) (Bartkova et al. 2006, Galanos et al. 2016, Galanos et al. 2018). The erroneous repair then increases the burden of genetic alterations (Phase III), while a subset of these variations play a major role in the subsequent escape from

oncogene-induced senescence giving birth to transformed cells with malignant potential (Phase IV) (**Figure 14A**).

As mentioned above, we used the HBEC-CDC6/TetON cellular system in which CDC6 is overexpressed under the control of tetracycline antibiotics. CDC6 is a rapid and massive inducer of senescence (<6 days) in both 2D and 3D cell culture conditions (**Figure 14B-C, 13C**). However, after a reasonably short time period (~30 days) senescent cells escape from senescence (**Figure 14B, 13B**) (Komseli et al. 2018). Interestingly, shutting off CDC6 induction does not result in phenotype reversal. Thus, molecular alterations obtained after CDC6 overexpression are permanent and independent of CDC6 retaining activity (**Figure 14B, 13D**). Overall, this evolutionary experiment recapitulates the malignant transformation process.

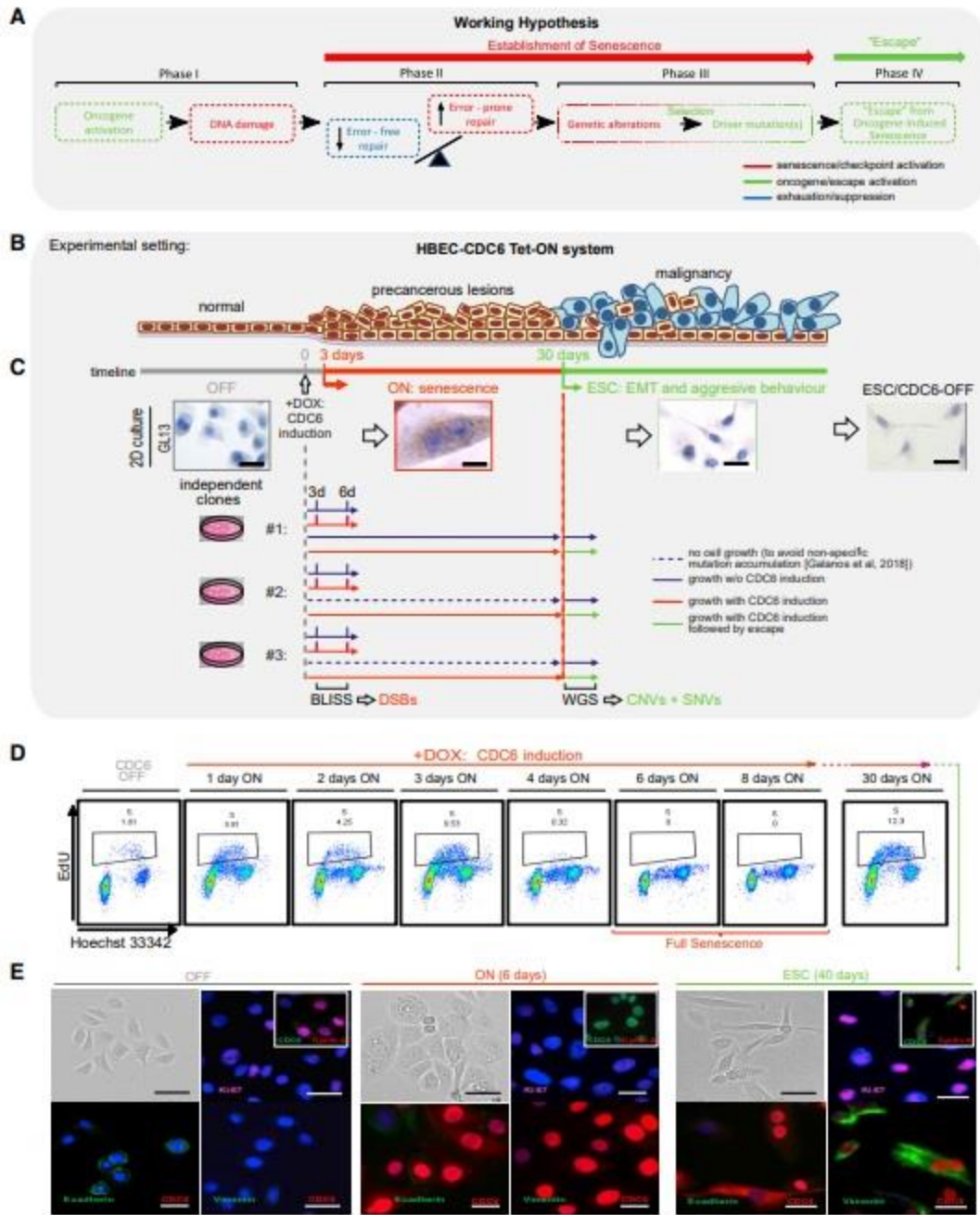


Figure 14. Working hypothesis and preliminary results showing the escape from oncogene-induced senescence.

(A) Working hypothesis, based on our cancer development model (Halazonetis et al. 2008), to address the aim of this study: that accumulating DNA damage traits during oncogene-induced

senescence (OIS) will be selected and should appear in escaped cells as functionally meaningful genetic defects.

(B) A human bronchial epithelial cell (HBEC) CDC6/TetON cellular system recapitulating successive stages of cancer evolution (Komseli et al. 2018).

(C) Representative images of HBECs grown in 2D culture and stained for SenTraGor. CDC6 induction drives cells into senescence (ON). After ~30 days, a subset of cells escapes senescence (ESC) to re-enter the cell cycle and adopt an EMT phenotype. Shutting-off CDC6 in ESC cells (ESC/CDC6-OFF) does not reverse this phenotype. Overview of three independent escape experiments. BLISS was performed to identify DSBs occurring after 3 or 6 days of CDC6 induction. Then, whole-genome sequencing (WGS) was applied on ESC cells to map genetic alterations in respect to damage that occurred at early time points. OFF cells that served as controls for WGS analysis were only initiated for culture at the time when escaped cells emerged to avoid non-specific accumulation of genetic alterations in the prolonged stationary period of senescent ON cells.

(D) FACS-based cell cycle analysis of HBECs at different time points, following EdU incorporation and CDC6 induction, demonstrating progressive S phase reduction, acquisition of senescence and escape.

(E) Representative phase contrast views and immune-detection of epithelial (E-cadherin) and mesenchymal markers (Vimentin) in HBECs showing that escape from senescence (ESC) coincides with epithelial-to-mesenchymal transition.

3.1.1 Escaped cells acquire an EMT-like phenotype

We conducted three independent experiments in order to exclude the possibility that escape from senescence is a stochastic event (**Figure 14C**). Indeed, in all three experimental settings a fraction of cells (~50 colonies from 5×10^5 cells) re-entered the cell cycle after a time period during which cell proliferation completely ceased (**Figure 14D**). Interestingly, escaped cells acquired EMT features, as depicted by the loss of the epithelial marker E-cadherin followed by the up-regulation of the mesenchymal marker

Vimentin (**Figure 14C-E**). Escaped cells also produced tumors upon subcutaneous injection into nude mice (**Figure 14F**). Furthermore, bioinformatics analysis showed that the escaped cells express a unique signature which is a combination of embryonic stem cell-like, epithelial, mesenchymal-like and MYC-dependent markers (**Figure 14G**). As mentioned before, after CDC6 was switched off, cells preserve their phenotype and also retain their growth and invasion capacity intact (**Figure 14B-C, 14D-F**). All the aforementioned results are in line with our working hypothesis.

3.1.2 CDC6 overexpression generates DNA damage and the lesions are repaired in an error-prone manner

According to the oncogene-induced DNA damage model, the overexpression of an oncogene can induce first replication stress which then leads to the accumulation of DNA breaks (Halazonetis et al. 2008). For this purpose, we performed Breaks Labeling In-Situ and Sequencing (BLISS) analysis (Yan et al. 2017) at different time points after CDC6 overexpression (**Figure 14C**). Particularly, using this assay we recorded DSBs accumulation at 3 and 6 days post-induction. Notably, there was a tremendous increase of DSBs at 3 days post-overexpression and a reduction of about 50% at day 6, indicative of a repair process that took place between days 3 and 6 (**Figure 15A**).

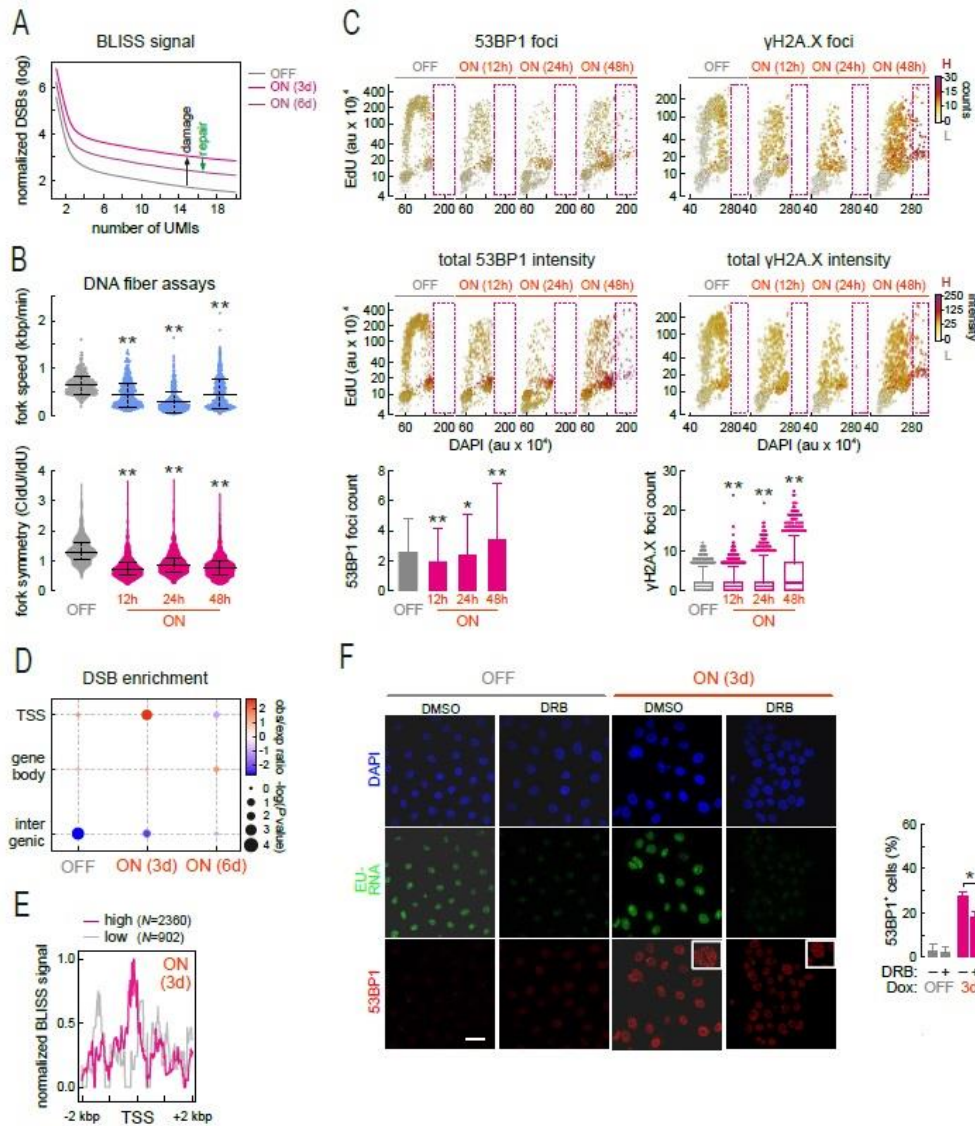


Figure 15. CDC6 overexpression causes DNA double strand breaks (DSBs) and alters replication dynamics.

(A) BLISS data generated at the time points indicated after CDC6 activation show strongest DSBs accumulation at 3 days followed by about 50% reduction at day 6, indicative of DNA repair (UMIs: unique molecular identifiers).

(B) Violin plots depicting DNA fiber fluorography results show decreased fork rate progression and asymmetry at the time points indicated. **: significantly different to OFF; $P < 0.01$, Student's t-test (\pm S.D.; $n=3$).

(C) Quantitative image-based cytometry of HBECs at the time points indicated, shows cell cycle distribution of single cells based on cyclin A and DAPI levels (au: arbitrary units). Foci counts (top) and 53BP1 and γ H2AX levels (middle) are indicated by color-coding. Bar graphs (bottom) show population means (\pm S.D.). Dashed rectangles indicate accumulation of cells with DNA content $>4N$. **: significantly different to OFF; $P < 0.01$, Student's t-test (\pm S.D.; $n=3$); H: high level, L: low levels.

(D) Dot plot showing increased frequency of DSBs at gene Transcription Start Sites(TSSs) based on BLISS data.

(E) Histogram showing BLISS-defined DSBs enrichment at gene TSSs upon CDC6 induction.

(F) Representative immunofluorescence imaging (left) of EU-labeled nascent RNA and 53BP1 foci in control HBECs (DMSO) or DRB-treated HBECs to inhibit transcription (DRB) at the times indicated. Bar graphs (right) show the percentage (\pm S.D.; $n=3$) of cells with 53BP1 foci. *: significantly different to OFF; $P < 0.05$, two-tailed unpaired Student's t-test.

Following the observed DSBs formation, a key question is which mechanisms are responsible for DSBs generation. First, by applying DNA fibers assay, we found perturbations in the DNA replication process in the form of reduced fork speed and increased fork asymmetry following CDC6 induction (**Figure 15B**). Moreover, as it was expected, there was an increase in the DNA damage markers 53BP1 and γ H2AX foci number and intensity reflecting the increase in DSBs. Importantly, an increased DNA content ($>4N$) occurred, suggesting re-replication (**Figure 15C, 16**). An additional interesting finding was that DSBs were mostly enriched at transcription start sites (TSSs) (**Figure 15D-E**). Hence, we assumed that replication-transcription collision might be another mechanism of DSBs formation at these positions. To prove our claim, we performed global transcriptional inhibition by using DRB (5,6-dichloro-1-beta-D-ribofuranosylbenzimidazole), an RNAPII inhibitor. Indeed, reduced DNA damage levels occurred upon DRB inhibition (**Figure 15F**). Overall, we suggest that the aforementioned mechanisms contribute to the emergence of DSBs upon CDC6

induction in our non-cancerous cellular setting, in agreement with the Phase I of our working hypothesis (**Figure 14A**).

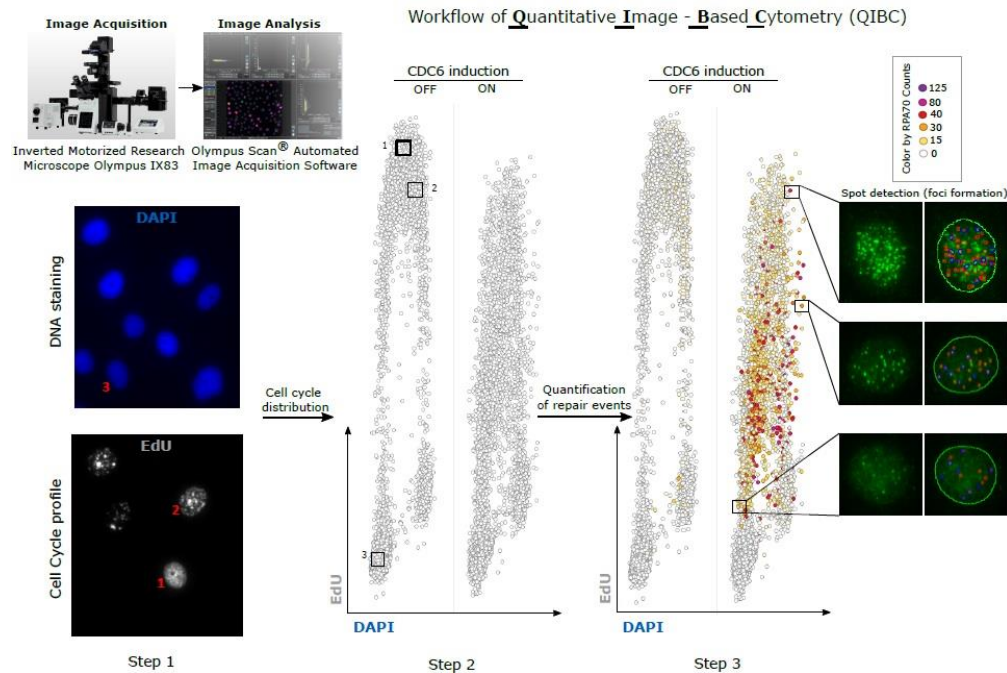


Figure 16. Schematic depiction of quantitative image-based cytometry (QIBC) workflow.

This high-content fluorescent technique allows the measurement of different parameters of nuclear repair factors during the cell cycle. The experiment consists of 3 steps. Cells expressing CDC6 in various timepoints (compared to the non-induced cells ‘OFF’) that are growing on coverslips are incubated with 5-ethynyl-2’-deoxyuridine (EdU), the nucleotide analog, for 30min before pre-extraction and fixation. As step1 of the method, clickit chemistry is performed and then cells are stained for DAPI and a specific DNA damage or/and Replication Stress-marker. Step 2 consists of the image acquisition using a fully-motorized automated wide-field microscope. Cells are plotted according to the cycle distribution based on DAPI and EdU signal and every dot represents a single cell. At the 3rd step, fluorescent signals associated with DNA damage or/and replication stress marker are quantified and expressed as a heat map (on the right corner of the 2nd set of plots). 5000 cells are analyzed for each condition typically. Scale bar, 10µm. Further specifications can be found in the methods section and as described previously (Toledo et al. 2013).

Subsequently, we investigated the validity of Phase II of our working hypothesis. To determine the choice of repair pathway for the CDC6-induced DNA breaks, we first estimated the levels of replication stress. For this purpose, we counted RPA foci, a single-strand DNA binding factor and a marker of replication stress (Gorgoulis et al. 2018) (**Figure 17Ai-ii, 16**). As expected, RPA foci robustly increased, which implies that DNA repair mainly takes place via homologous recombination (HR) during S phase. However, key components of the synthesis-dependent-strand-annealing (SDSA) (the main error-free pathway) like RAD51, BRCA1 and BRCA2 are diminished at day 3 following CDC6 induction (**Figure 17Bi-ii**). In contrast, RAD52 protein levels and foci increase between days 3 and 6 after CDC6 induction (**Figure 17Bii, 17Ci-iii**). Collectively, these results indicate that a shift from SDSA to break-induced-replication (BIR) and single-strand-annealing pathways (SSA) occurs (Wu et al. 2008, Galanos et al. 2016, Ochs et al. 2016, Galanos et al. 2018, Gorgoulis et al, 2018). Both BIR and SSA pathways are highly error-prone and this contributes to genomic instability and cancer progression (Galanos et al. 2018, Sotiriou et al. 2018). To examine whether BIR and SSA pathways are activated in a RAD52-dependent manner, we used specific plasmid reporters for BIR, SSA and SDSA pathways in a “RAD52 wild-type environment” versus “RAD52 defective environment”. Eventually, BIR and SSA mechanisms proved to be responsible for DNA repair in a RAD52-dependent manner upon CDC6 overexpression, whereas SDSA repair pathway is inactive in a CDC6-overexpressing environment regardless of RAD52 levels (**Figure 17D**).

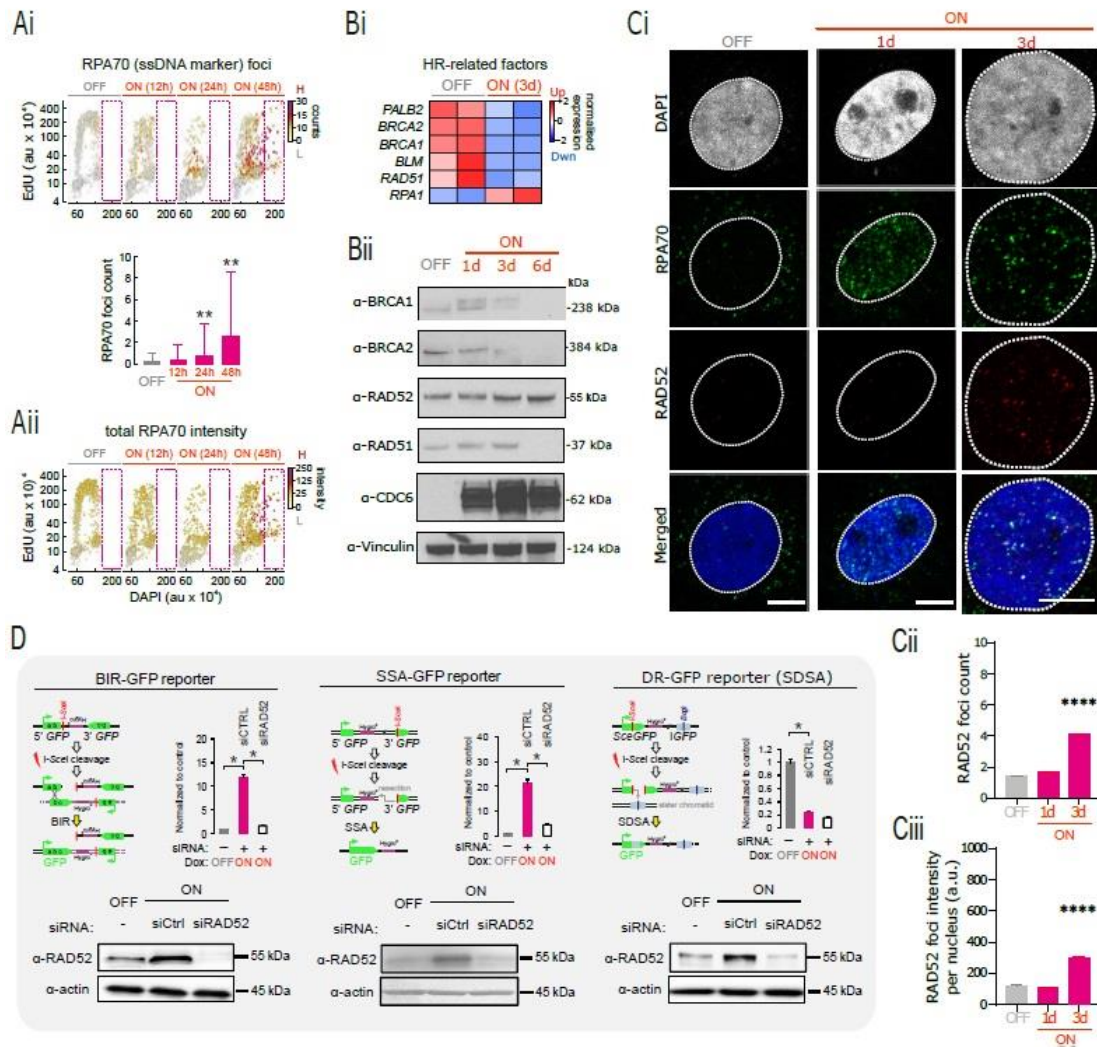


Figure 17. Protracted CDC6 expression results in replication stress and error-prone DNA repair.

(Ai-ii) Quantitative image-based cytometry of HBECs, at the time points indicated, shows cell cycle distribution of single cells based on cyclin A and DAPI levels (au: arbitrary units). Foci counts (top) and RPA70 levels (bottom) are color-coded. Bar graphs (middle) show population means (\pm S.D.; n=3). Dashed rectangles denote accumulation of cells with DNA content > 4N. **: significantly different to OFF; $P < 0.01$, unpaired two-tailed Student's t-test; H: high level, L: low levels.

(Bi-ii) Heatmap and western blots showing reduction in the expression levels of the genes involved in error-free homologous recombination (HR) DNA repair upon CDC6 induction in HBECs (ON). Up: up-regulated, Dwn: down-regulated.

(C) i. Immunofluorescence imaging of RAD52 and RPA70 upon CDC6 overexpression in ON cells. ii-iii. Bar graphs depict RAD52 mean foci count and foci intensity per nucleus, respectively. ****: significantly different to OFF; $P < 0.0001$, unpaired two-tailed Student's t-test.

(D) Reporter assays demonstrating increase (\pm S.D.; $n=3$) in RAD52-dependent break-induced replication (BIR; left) and in single-strand annealing repair of DSBs (SSA; middle). Error-free repair monitored by a synthesis-dependent strand annealing reporter (SDSA; right) is suppressed. Western blots (below) show RAD52 expression levels. *: $P < 0.05$, unpaired two-tailed Student's t-test. Repair is monitored 3 days after CDC6 induction.

3.1.3 Genetic alterations occurring early upon senescence contribute to the evasion-from-senescence phenotype and are found in the genome of escaped cells

Although the cells remain in a senescent state, after ~4 weeks a fraction of cells re-entered cell cycle and escaped clones emerged (**Figure 14B-E, 13B-C**). To exclude the possibility of a random event, we employed three replicates. Escaped clones emerged in all three replicates (**Figure 14C**) and we performed whole-genome sequencing (WGS), comparing the non-induced with the escaped cells. WGS revealed different types of single nucleotide variations (SNVs) and copy number variations (CNVs) (**Figure 18A, 19A, see Zampetidis et al. 2021**). Regarding SNVs distribution, they took a “kataegis” form throughout the genome and interestingly a mutation signature emerged in our escaped clones resembling the “signature 15” which is connected to mismatch defects seen in stomach and lung cancers (Alexandrov et al. 2013) (**Figure 19B-C**). Furthermore, escaped cells bear mutations in *MUC16* and *NEB* genes, which are among the most frequently mutated genes in cancer (**Figure 19D**). Interestingly, *MUC16* is also known as *CA125*, a well-established marker for various cancer types

including lung tumors and both mutations are correlated with adverse prognosis in cancer patients (Chugh et al. 2015, Kufe 2009, Mazzoccoli et al. 2017) (**Figure 19E-F**). Notably, no mutations were detected in the *TP53* gene, which is the most frequently altered gene in various cancer types (Zhu et al 2020). However, MDM2 mRNA and protein levels increase in the escaped cells. MDM2 is a negative regulator of p53; hence its up-regulation results in p53 decreased levels (**Figure 20A**).

(B) Pie charts showing the distribution of the 58 CNVs shared by all the three replicates (see Zampetidis et al. 2021). *: significantly more than expected by chance; $P < 0.0001$, Super Exact test.

(C) Circos plot of the type and location of all shared CNVs from panel B, alongside any differentially-expressed genes they harbor in ESC cells (*confirmed by RT-qPCR, not in RNA-seq data). Outer circle: human reference karyotype; Inner circle: distribution of the 58 CNVs across the genome.

(D) Superimposing DSB coordinates, as defined by BLISS, with the breakpoints of the shared CNVs from panel B, shows overlap in 51 out of the 58 cases. The inversion in 3p26.1 is magnified.

Regarding CNVs, while large numbers were found per each replicate, interestingly 58 CNVs were commonly shared among the three escaped clones. These include inversions, translocations, deletions, insertions and duplications and they are distributed in all chromosomes (**Figure 18A-C**). Aligning the breakpoints' genomic positions of these CNVs (confirmed also by Sanger sequencing) to DSBs coordinates obtained by BLISS revealed that 51 out of the 58 common CNVs overlapped with DSBs (**Figure 18D, see Zampetidis et al. 2021**). Collectively, all the above mentioned events suggest that genomic instability is a crucial element for evading oncogene-induced senescence and is in line with Phase III of our working hypothesis (**Figure 13A**).

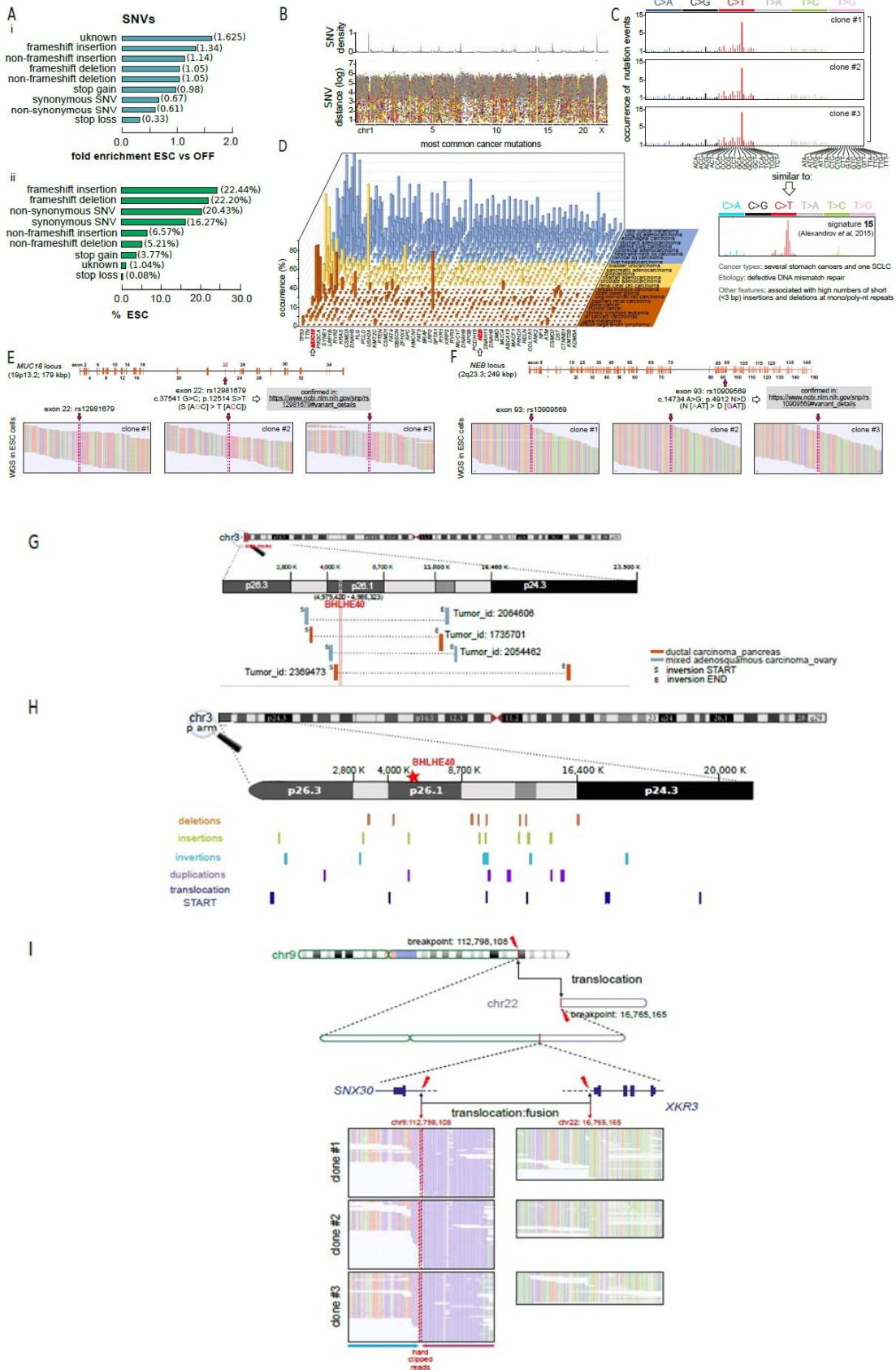


Figure 19. CDC6-driven single nucleotide variant (SNVs) landscapes in ESC cells and publicly available alterations at chr3 in human malignancies.

(A) Bar plots showing the type and relative enrichment, as fold (i) versus OFF and percentage (ii) of SNVs in ESC cells using WGS data.

(B) WGS-derived SNVs density plots aligned to a “kataegis” SNV distribution in ESC genomes.

(C) Bar plots showing the occurrence of specific SNVs in each of the three independent replicates that represent a CDC6-specific mutational signature similar to that previously reported for stomach cancer and one small lung cell carcinoma (Alexandrov et al. 2013).

(D) Two of the top 50 most frequent mutations observed in cancer specimens in MUC16 and NEB (arrows) were consistently recapitulated in our CDC6-driven cancer evolution model.

(E) MUC16 encodes an established biomarker for diagnosis of many cancers, including lung (the origin of our HBEC model). The identified mutation maps to exon 22 (arrow) in a domain associated with protein stabilization and previously confirmed (see SNPdb: rs12981679).

(F) As in panel E, but for the NEB locus encoding the actin-binding protein nebulin with a mutation in exon 93 also previously confirmed in cancer (see SNPdb: rs10909569).

(G) Inversions affecting the BHLHE40 locus in human malignancies. Graph depicting recorded inversions in human tumors that encompass the BHLHE40 locus.

(H) Map of previously reported genetic aberrations surrounding the BHLHE40 locus. Graph depicting various chromosome 3p alterations nearby the BHLHE40 locus found in various human malignancies and extracted from public repositories.

(I) A reciprocal translocation involving chr9 and 22 among the ESC-shared CNVs. WGS data describing the translocation breakpoints in ESC cells connecting chr9 and 22 (Valencia et al. *Advances in Hematology* 2009, Ramachandran et al. *Front Oncol* 2019). Hard clipped and discordantly mapped reads are indicated for all three replicates.

3.1.4 A large inversion in chromosome 3p encompasses the circadian transcription factor BHLHE40

Among the 58 common CNVs we noticed a >3.7 Mbp-long heterozygous balanced inversion in the short arm of chromosome 3p (**Figure 18B-D**). Interestingly, the inverted region contains the *BHLHE40* locus (basic-helix-loop-helix member 40, also known as *DEC1*) (**Figure 18D, 21A**), which encodes a transcription factor belonging to the CLOCK (*circadian locomotor output cycles kaput*) protein family and plays a major role in daily circadian rhythm oscillations (Kato et al. 2014, Sato et al. 2016). Importantly, ChIP-seq data from ENCODE highlight that BHLHE40 is a master transcriptional regulator in the human genome by binding and regulating >15500 genes (Rouillard et al. 2016), including cell cycle regulators (**Figure 21B**). Of note, ~68.8% of the genes of the differentially-expressed genes in escaped cells are direct BHLHE40 targets, comprising regulators of pivotal cellular processes, such as cell cycle, DNA replication and repair (**Figure 20B**). Moreover, ~80.8% of the up-regulated genes are both BHLHE40 target genes and differentially expressed genes during escape from senescence (**Figure 21C**). Interestingly, MDM2, the main negative regulator of p53, is also a target of BHLHE40 (**Figure 20C**).

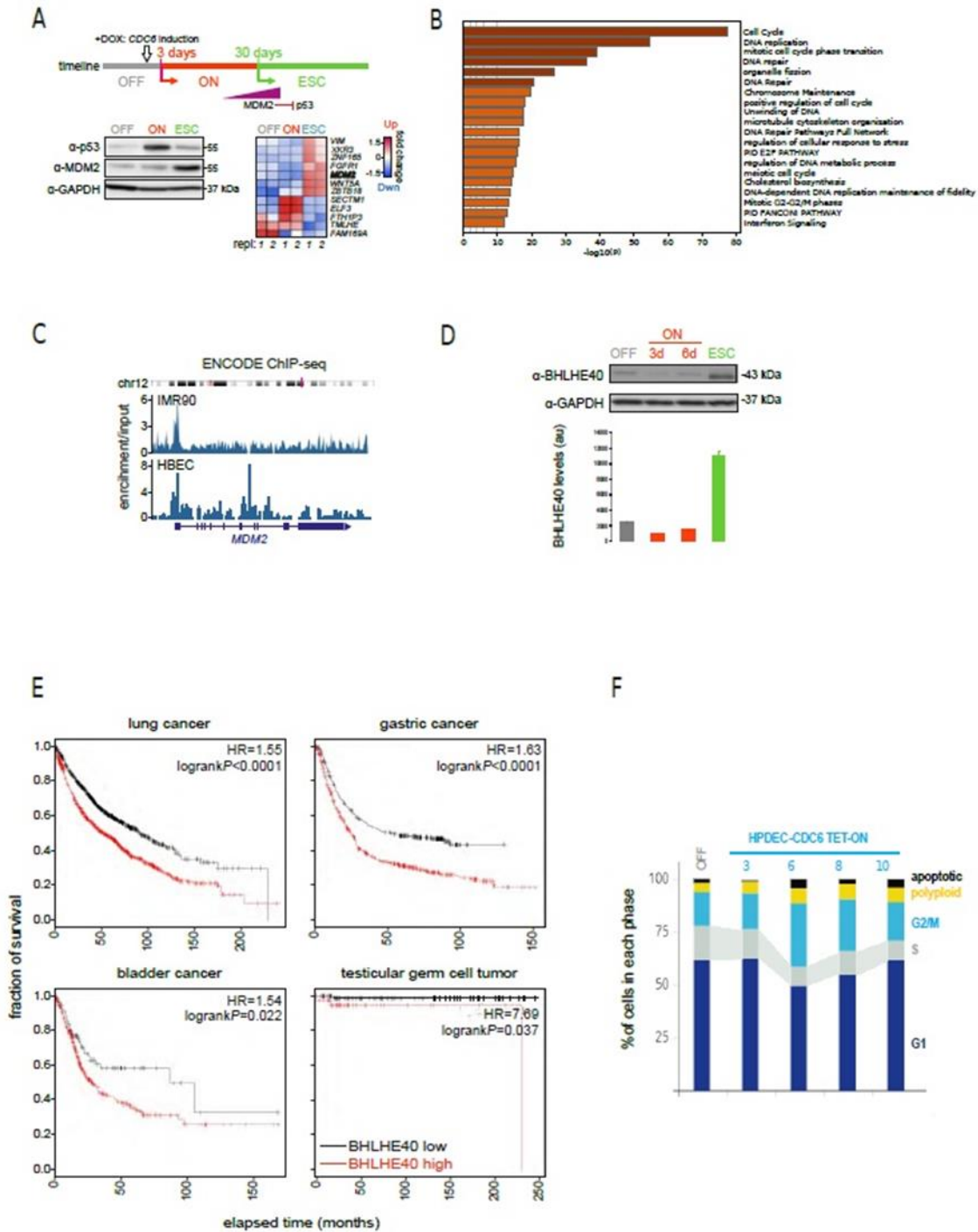


Figure 20. BHLHE40 gene targets in ESC cells and cancer patients survival according to BHLHE40 levels of expression.

(A) MDM2 is a BHLHE40 target upregulated in ESC cells. Western blots and RNA-seq data confirm MDM2 upregulation and p53 suppression in ESC cells.

(B) Western blots showing changing BHLHE40 levels in OFF, ON and ESC cells.

(C) Genome browser views of BHLHE40 ENCODE ChIP-seq data from IMR90 and own data from HBECs cells showing binding to the MDM2 locus.

(D) Bar graphs from gene ontology and pathway analysis showing a log₁₀ (P - value) enrichment of genes identified as both BHLHE40 targets and differentially expressed during escape (**see also Figure 21**).

(E) BHLHE40 overexpression in malignancies is associated with poor survival. Kaplan-Meier survival plots generated using available data (<http://www.kmplot.com>) from tumors stratified as “high” (red) or “low” BHLHE40-expressing.

(F) Cell cycle analysis in an HPDEC-based CDC6-Tet-ON system. FACS-based cell cycle analysis of HPDECs demonstrating no absence of S phase at different days after CDC6 induction.

Regarding the escaped clones, transcriptome data revealed that BHLHE40 is highly up-regulated, whereas PER1/2, which encode the circadian factors periodins (Yamada and Miyamoto 2005, Wood et al. 2009, Kato et al. 2014, Sato et al. 2016), are in contrast repressed (**Figure 21D**). Supportively, BHLHE40 protein levels also increase in the escaped clones (**Figure 20D, 21D**). Collectively, these results suggest that BHLHE40 is a pivotal molecule for promoting escape from senescence. This is in line with the fact that circadian machinery regulates cell cycle progression; hence its deregulation can directly affect cell cycle checkpoints and promote malignant transformation (Hunt and Sassone-Corsi 2007, Masri et al. 2013). Notably, 38 genes, which encode for replication machinery components, are strongly up-regulated in escaped cells and also bound by BHLHE40, such as BLM, GINS1-4, MCM2-10, PCNA, POLE (**Figure 21B, E**).

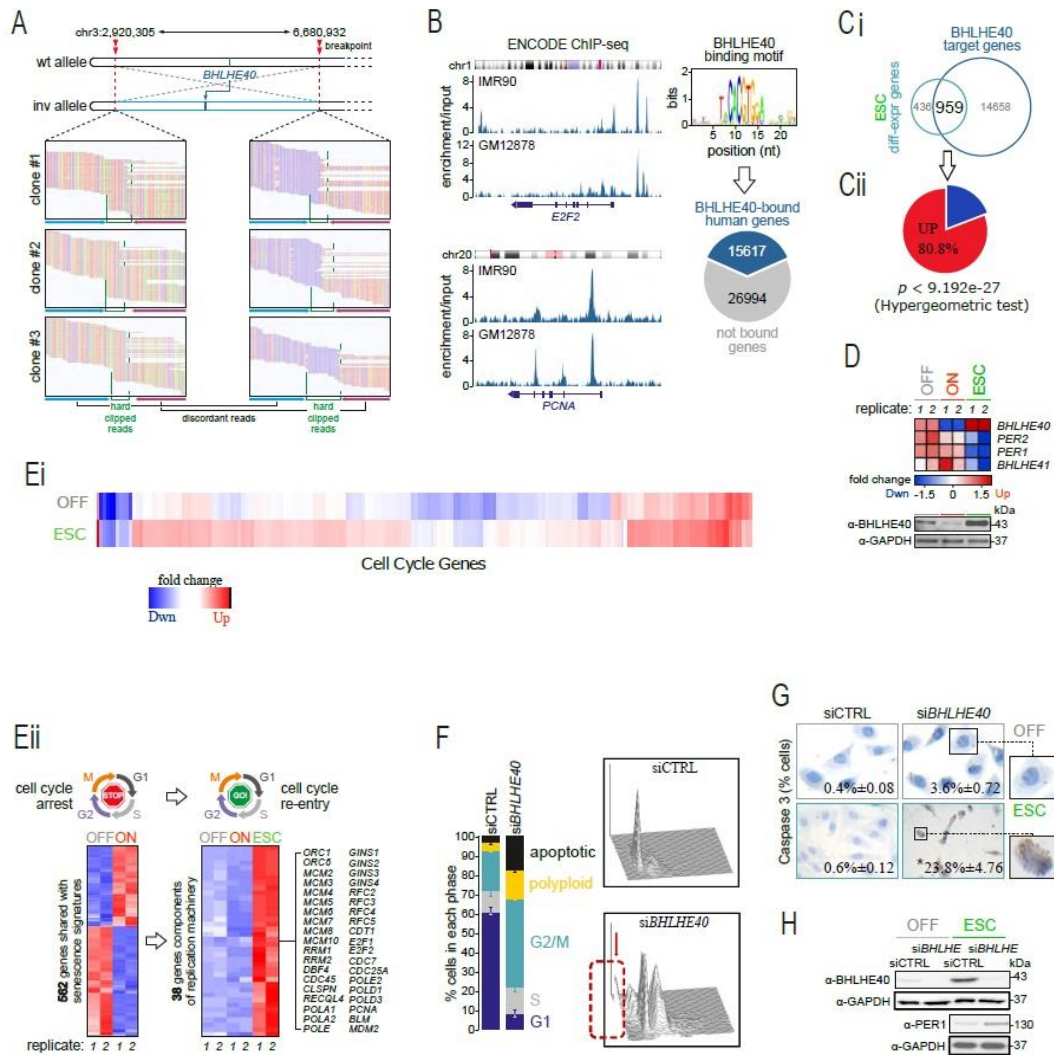


Figure 21. BHLHE40 harbored in the chr3 inversion is essential for “escape” phenotype maintenance.

(A) WGS data around the chr3 inversion breakpoints in ESC cells. Hard clipped (green lines) and discordantly mapped reads (blue/purple arrows) are indicated for all three replicates.

(B) Representative genome browser views (left) of BHLHE40 ENCODE ChIP-seq data from IMR90 and GM12878 cells in the E2F2 and PCNA loci. This data was used to infer the BHLHE40 binding motif logo, and to assign 36.7% of all human genes as its direct targets (Pertea et al. 2018).

(C) i. Venn diagram showing 68.8% of all genes differentially-expressed in ESC cells also being BHLHE40 targets according to ChIP-seq data. ii. Pie chart representing the significant percentage of the up-regulated genes, which are identified as both BHLHE40 target genes and differentially expressed genes during escape. $P < 9.192e-27$, Hypergeometric test.

(D) Heatmap of RNA-seq data shows BHLHE40, but not other circadian genes like PER1/2, being selectively upregulated in ESC cells.

(E) i. Heatmap depicting the fold change expression of cell cycle genes between the “escape” and “OFF” condition. Fold change cut-off 2.0 and P -adjust < 0.05 . ii. Heatmap (left) showing that 25.3% of the 2220 differentially-expressed genes in ON cells are shared with reported senescence signatures (Hernandez-Segura et al., 2017). Of these, 38 encode replication machinery components (right) and are strongly induced in ESC cells. Up: up-regulated, Dwn: down-regulated.

(F) FACS-based cell cycle profiling of control (siCTRL) and BHLHE40-knockdown (siBHLHE40) cells showing significantly altered cell cycle progression and increased cell death (red arrow pointing dashed line) (\pm S.D.; $n=3$). *significantly more than in control: $P < 0.001$, Fisher’s exact test.

(G) Representative images of control (siCTRL) and BHLHE40-knockdown cells (siBHLHE40) immunostained for Caspase-3. Inset numbers indicate the percentage of positive cells (from a minimum of 100 cells counted in each condition). *: $P < 0.01$, Fisher’s exact test.

(H) Western blots showing reciprocal changes in BHLHE40 and PER1 levels upon BHLHE40-knockdown in ESC cells, thought to drive apoptosis (Hunt and Sassone-Corsi 2007).

3.1.5 BHLHE40 is pivotal for the maintenance of the escaped phenotype

To examine if BHLHE40 is crucial for the escape from senescence, we used two different settings of siRNAs to silence this gene in escaped cells. This resulted in deregulated cell cycle profile and increased cell death in escaped cells (**Figure 21F**) in a caspase-3 dependent manner (**Figure 21G**). In contrast, in the non-induced cells

there was no increase in cell death as shown via caspase-3 staining (**Figure 21G**). Interestingly, BHLHE40 silencing resulted in the up-regulation of PER1 in escaped clones (**Figure 21H**); a factor known to promote apoptosis in cells (Gery et al. 2006, Hunt and Sassone-Corsi 2007). Collectively, the aforementioned results indicate that BHLHE40 is crucial for the maintenance of the escape phenotype. Regarding the clinical impact of BHLHE40 up-regulation, it has been shown that its overexpression correlated with adverse clinical outcome in many malignancies, including lung cancer (**Figure 20E**). Importantly, our cellular model originated from bronchial tissue. Moreover, BHLHE40 is often prone to genetic aberrations in various human cancer types (**Figure 19G-H**).

Along with the observed BHLHE40 inversion, a reciprocal translocation involving chromosomes 9 and 22 was also found in all three escaped populations (**Figure 19I**). This aberration is typically identified in chronic myelogenous leukemia (CML) (Valencia et al. Advances in Hematology 2009, Chandran et al. Front Oncol 2019), suggesting an additional event mimicking *in vivo* alterations. Finally, the remaining commonly shared CNVs include genes that have been associated with the senescence process (**see Zampetidis et al. 2021**). Overall, these findings are in accordance with the Phase III of the working hypothesis (**Figure 13A**).

3.1.6 An artificially engineered inversion in chromosome 3p is sufficient for senescence bypass

Our next question was whether the inversion in chromosome 3p promotes escape from senescence through BHLHE40 re-induction. In other words, we examined if genetic alterations occurred upon the first days of CDC6 induction are maintained in the escaped cells and are pertinent to the escape phenomenon. To answer this, we first tested BHLHE40 levels at several time points, including non-induced cells, days 3 and 6 after CDC6 induction and escaped cells. Baseline levels in non-induced cells are initially decreased upon CDC6 induction, however are pronouncedly up-regulated in the escaped clones (**Figure 20D**). Interestingly, after a vast decrease at day 3 of CDC6

overexpression, BHLHE40 levels partially increased by day 6. This probably coincides with the time of the chromosome 3p inversion, as error-prone DNA repair has already been activated at that time point (**Figure 14A**).

Subsequently, we decided to generate an artificial inversion mimicking the inversion that spontaneously occurred. For this purpose, we used CRISPR-Cas 9 in non-induced HBECs (**Figure 22A**) and we targeted sequences within 72 (at 2,920,305) and 50 bp (at 6,680,932) of the inversion breakpoints previously mapped using WGS (**Figure 18C-D**). Finally, we developed two distinct clones carrying this 3.7-Mbp heterozygous inversion (**Figure 22Bi, 23A**) and we performed ChIP-seq to record the binding sites of BHLHE40 throughout the genome. Notably, we found 2,576 peaks harboring the BHLHE40 binding motif, which mostly overlap gene promoters (**Figure 22C-B**).

Next, we further tested the newly acquired inverted clones. Interestingly, non-induced inverted cells had lost their epithelial traits and had acquired spindle morphology. In support to this result, inverted cells exhibited low E-cadherin and high Vimentin levels (**Figure 23B**). All the above suggest a metastable state indicative of trans-differentiating cells (Nieto et al. 2016).

In line with our hypothesis, the clones carrying the inversion did not completely cease to proliferate nor did they enter senescence upon CDC6 overexpression. In contrast, the cells initially lowered their proliferating rate until they bypassed the senescence barrier (**Figure 22Bii-iii, 23C-D**). This implies that the metastable state is energy-demanding, hence the cells slow down their propagation in order to adapt at this condition.

Alternatively, DDR activation can be responsible for the low S-phase percentage; however it is not adequate to activate senescence in this cell context (**Figure 22Biv- v**). Importantly, senescence-bypassed cells exhibit increased growth rate and invasive capacity resembling the non-inverted induced HBECs (**Figure 23E-F**).

Although non-inverted cells express lower levels of BHLHE40 upon CDC6 overexpression (**Figure 23G**), both inverted clones overexpressed BHLHE40 (**Figure 22Bvi, 23H**) and this overexpression drives the rapid bypass from a metastable state and forces the expression of genes that promote senescence suppression and cell

cycle re-entry (**Figure 22E, 23I**). As negative controls we used CRISPR-Cas9 cells, which failed to acquire the inversion. In support to the above, these cells did enter senescence as shown by SenTraGor staining and low Ki-67 levels, a well-established cell proliferation marker (**Figure 22F**). In summary, the artificial inversion in chromosome 3p is adequate to drive BHLHE40 overexpression and thus senescence-bypass in response to oncogenic stimulus provided by CDC6 induction. This is consistent with the Phase IV of our working hypothesis (**Figure 13A**).

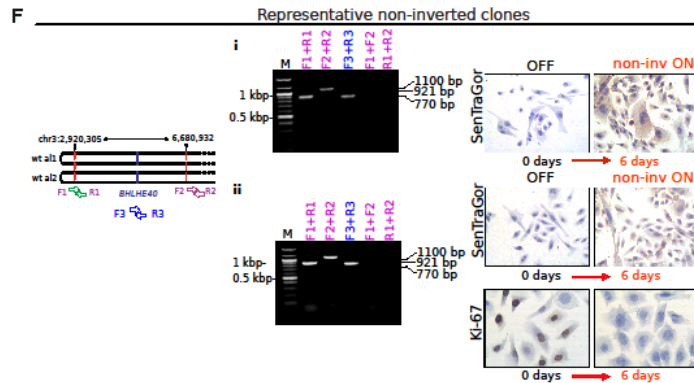
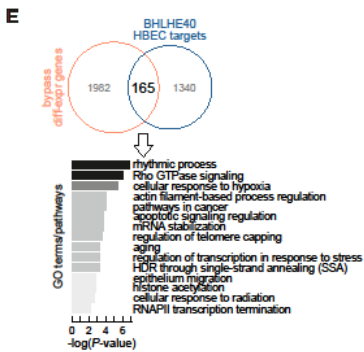
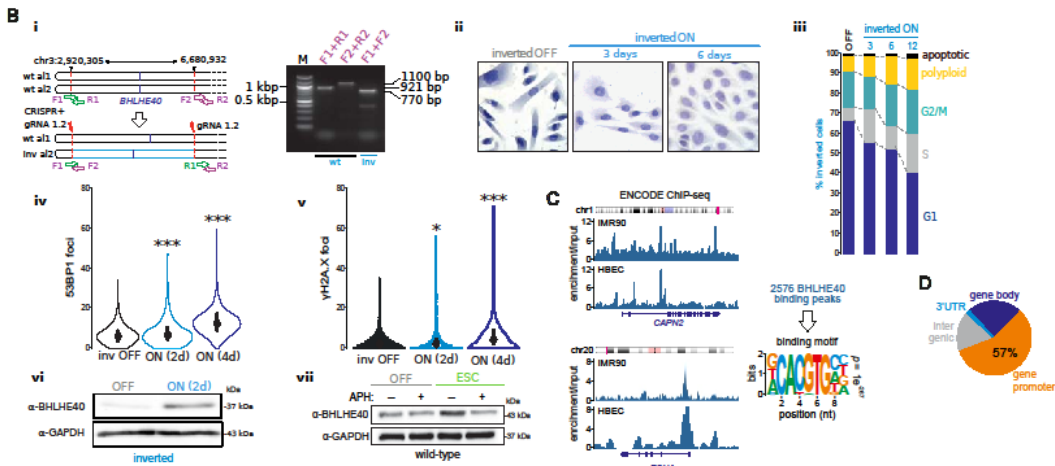
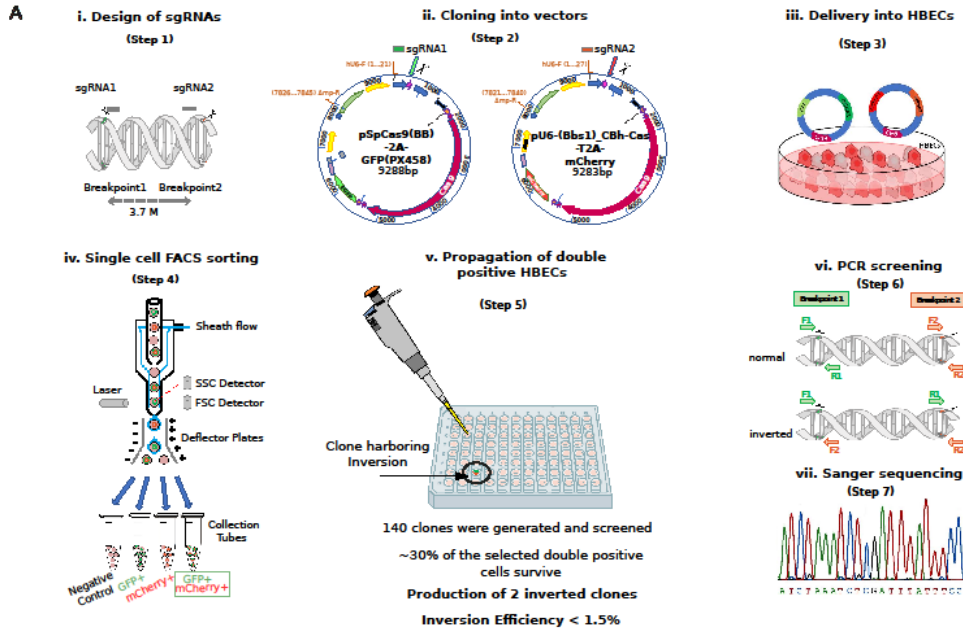


Figure 22. Flow diagram of method to generate and validate an inversion in the short arm of chr3 based on CRISPR/Cas-9 editing procedure and additional CRISPR-generated clones with or without the chr3 inversion.

(A) CRISPR experimental strategy:

- i.** Design of sgRNAs near the breakpoints, as identified by WGS (72 bp from breakpoint 1 and 50 bp from breakpoint 2).
- ii.** Cloning of sgRNA1 and sgRNA2 into vectors expressing Cas9 and GFP or mCherry, respectively.
- iii.** Co-transfection of both vectors into HBECS.
- iv.** Single-cell FACS sorting to separate the double positive cells (GFP+/mCherry+).
- v.** Plating of double positive single cells in 96-well plates. Only 30% of the plated double positive cells finally survive.
- vi.** Design of primers around each breakpoint (F1/R1 around breakpoint 1 and F2/R2 around breakpoint 2) for PCR screening of the clones harboring the inversion. The inversion is identified by successful F1/F2 and R1/R2 amplification. Among the clones that survived and propagated, the inversion efficiency was less than 2%.
- vii.** Sanger sequencing validation is performed on the PCR products of the inverted clones.

(B) (i) PCR and Sanger sequencing validation of a second clone carrying a CRISPR-generated 3.7-Mbp heterozygous inversion in chr3 that closely mimics that discovered using WGS. (ii) Representative images of OFF and 3-/6-day ON “inverted” cells stained with SenTraGor and demonstrating senescence-bypass. (iii) FACS analysis of this “inverted” clone indicating increasing S phase at different days after CDC6 induction. (iv) Violin plots depicting 53BP1 foci accumulation upon CDC6 induction in “inverted” cells. *: significantly different to OFF; $P < 0.05$, ***: significantly different to OFF; $P < 0.001$, unpaired two-tailed Student’s t-test (\pm S.D.; $n=3$). (v) As in subpanel iv, but for γ H2A.X foci. (vi) Western blots showing BHLHE40 overexpression upon CDC6-induction; GAPDH provides a loading control. (vii) As in subpanel

vi, but showing the effect of aphidicolin (APH) treatment on BHLHE40 levels in wild-type OFF and ESC cells.

(C) Representative genome browser views of BHLHE40 ChIP-seq signal from IMR90 (ENCODE data) and HBECs (own data) in the CAPN2 and PCNA loci. The motif deduced from the 2576 ChIP-seq peaks matches the BHLHE40 one (top right).

(D) Pie chart showing genomic distribution of the BHLHE40 ChIP-seq peaks. 57% of peaks are promoter-proximal.

(E) Venn diagram (top) showing the overlap of BHLHE40 gene targets in inverted HBECs with genes differentially-expressed upon senescence bypass. This overlap is more than expected by chance (hypergeometric test; P-value < 10⁻⁶). The GO terms/pathways associated with these 165 genes are presented as a bar graph of enrichment P-value (-log; bottom).

(F) Representative (i,ii) PCR verified 6-day ON non-inverted clones cells stained with SenTraGor demonstrating senescence and no proliferation (negative Ki-67 immunostaining).

3.1.7 Generation of a novel cellular system overexpressing BHLHE40 protein based on HBEC-CDC6/TetON cellular setting

To support the notion that BHLHE40 is sufficient for bypassing senescence, we developed a cellular setting which stably overexpresses BHLHE40. To engineer this system, we used as basis the HBEC-CDC6/TetON cell line. As we expected, BHLHE40 is overexpressed regardless the induction of CDC6 and led to senescence-bypass upon CDC6 overexpression (**Figure 23J**). Interestingly, these cells adopt a metastable state similar to the inverted clones and their proliferating rate reduced for a short period of time. However, they never cease to proliferate and quickly bypass senescence. As negative control, we used mock cells in which we had introduced an empty vector without the gene of interest (**Figure 23J**). Notably, the non-induced cells demonstrated a spindle-like morphology resembling the non-induced inverted clones. This result strongly suggests that BHLHE40 drives escape from senescence and is in line with the Phase IV of our hypothesis (**Figure 13A**).

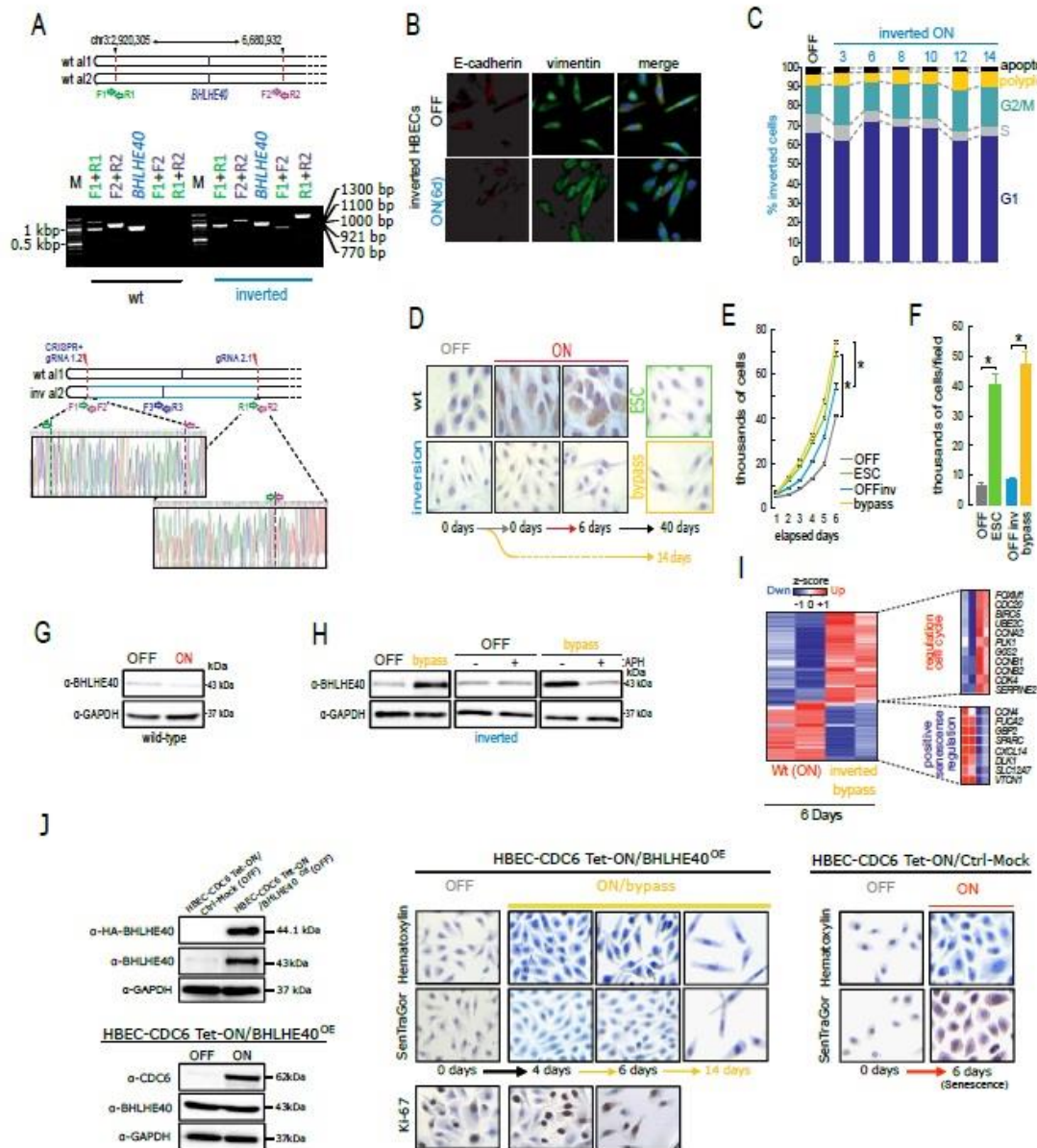


Figure 23. The 3.7-Mbp inversion in chr3 suffices for bypassing CDC6-induced senescence.

(A) PCR and Sanger sequencing validation of a CRISPR-generated 3.7-Mbp heterozygous inversion in chr3 that closely mimics that discovered in ESC cells using WGS (wt: wild-type).

(B) Immunodetection of epithelial (E-cadherin) and mesenchymal markers (vimentin) in inverted OFF and 6-day ON cells is reminiscent of cells undergoing trans-differentiation.

(C) FACS-based cell cycle analysis in inverted cells at different time points after CDC6 induction (\pm S.D.; n=3).

(D) Representative images of OFF, ON, and ESC or bypass (bottom) cells stained with SenTraGor to assess senescence-bypass in inverted (yellow color defined) compared to wild-type (red and green color defined) cells.

(E) Plots depicting mean proliferation (\pm S.D.; n=3) in the different states of wild-type and inverted cells. *: significantly different to OFF; $P < 0.05$, unpaired two-tailed Student's t-test.

(F) As in panel E, but quantifying cell invasion capacity (\pm S.D.; n=3). *: significantly different to OFF; $P < 0.05$, unpaired two-tailed Student's t-test.

(G) Western blots showing BHLHE40 suppression upon CDC6-induction in wild-type cells. GAPDH provides a loading control.

(H) Left: As in panel G, but showing strong BHLHE40 re-expression upon CDC6-induction in cells carrying the CRISPR-generated inversion. Middle/right: Blots showing aphidicolin (APH) treatment suppresses CDC6-driven BHLHE40 re-expression in inverted bypass cells. GAPDH provides a loading control.

(I) Heatmap of gene expression data depicting inverse patterns for cell cycle and senescence regulators between 6-day CDC6-ON wild-type and bypass inverted cells.

(J) Left: Western blots showing BHLHE40 overexpression (BHLHE40OE) in transfected wild-type cells. GAPDH provides a loading control. Right: Representative images of OFF, ON, and bypass cells stained with SenTraGor to assess senescence-bypass in CDC6-ON BHLHE40OE compared to wild-type cells. Ki-67 staining for cell proliferation. α -HA: anti-hemagglutinin.

3.1.8 BHLHE40 is up-regulated in a replication-dependent manner

Given that transcription strongly depends on replication (S phase dependence) (Fisher and Mechali 2003) and in combination with the fact that replication origins can be activated from replication stress (Courtot et al. 2018), we decided to investigate if

replication affects gene transcription in our settings. For this purpose, non-inverted cells and inverted clones treated with aphidicolin, a well-established DNA replication inhibitor. As we speculated, performing aphidicolin treatment in non-inverted escaped cells and bypassed inverted clones resulted in the reduction of BHLHE40 protein levels (**Figure 22Bvii, 23H**). In contrast, non-induced/non-inverted and non-induced/inverted clones did not show significant change in BHLHE40 levels (**Figure 22Bvii, 23H**). Taken together, these results indicate that altered replication dynamics can lead to gene expression changes driving bypass from senescence.

3.1.9 BHLHE40 induction and escape from senescence occur due to chromatin refolding

To test whether three-dimensional (3D) chromosome architecture can also explain BHLHE40 up-regulation, we investigated 3D reorganization in the extended BHLHE40 genetic locus. For this purpose, we used the inverted HBECs to generate high-resolution Hi-C maps from non-induced and senescence-bypass cells (**see Zampetidis et al. 2021**). Genome-wide comparison of this data revealed that senescence-bypass cells exhibit an increase in sub-Mbp interactions (**Figure 24A**), accompanied by changes in the identity of compartments. Approximately 10% of A- or B-compartments switch to B or A, respectively, and this switching explains a considerable fraction (almost 50%) of the gene expression changes that underlie senescence bypass (**Figure 24B**). However, only marginal changes to topologically-associating domain positions (TADs; Beagan and Phillips-Cremins 2020) were found (**Figure 24C**). These effects are, for the most part, the converse of what was observed for cells transitioning into oncogene-induced senescence (Chandra et al. 2015, Criscione et al. 2016).

Looking specifically into the 3D organization of chromatin around the inversion region on chromosome 3p, we made three key observations. First, that BHLHE40 resides in one of the two centrally-located TADs of this extended locus; the long-range contacts of which do not change between non-induced and senescence-bypass cells (**Figure 24D**). Second, we found the emergence of new loops in this 4-Mbp region,

which contribute to the enhanced insulation of the two central TADs from one another (**Figure 24D, circles**). Third, we found that strong loop emergence coincided with the strengthening and broadening of the small A-compartment harboring BHLHE40, which is in line with its more potent activation (**Figure 24D, bottom**).

Given these effects in the BHLHE40 domain, we speculated that changes to genome-wide CTCF loops might explain the changes underlying senescence bypass. Indeed, subtracting non-induced from senescence-bypass Hi-C data revealed new long-range contacts emerging (**Figure 24E**). Across all chromosomes ~3500 new loops arise, while ~2150 specific to non-induced cells are lost (**Figure 24F**). In line with our subtracted maps, senescence-bypass specific loops are on average larger than non-induced specific ones (**Figure 24G**). Interestingly, and exactly as in the case of the BHLHE40 domain, these senescence-bypass specific loops arise at positions of existing insulation that become markedly strengthened. At the same time, insulation at the anchors of the non-induced cells specific loops shows little fluctuation (**Figure 24H**). Together, this type of changes suggests rewiring of regulatory gene-enhancer interactions.

3.1.10 Human pancreatic ductal epithelial cells show a different behavior upon CDC6 overexpression

To examine whether p53 down-regulation via MDM2 is crucial for escape from senescence we recruited human pancreatic ductal epithelial cells (HPDECs) that carry an inducible CDC6 construct identical to HBECs. HPDECs have been immortalized via HPV16-E6 transduction and hence p53 function is inactivated in this setting (Ouyang et al. 2000). Indeed, although HPDECs reduce their proliferation capacity, they never completely cease to proliferate and eventually bypass senescence similarly to the inverted and BHLHE40-overexpressing cells (**Figure20F**).

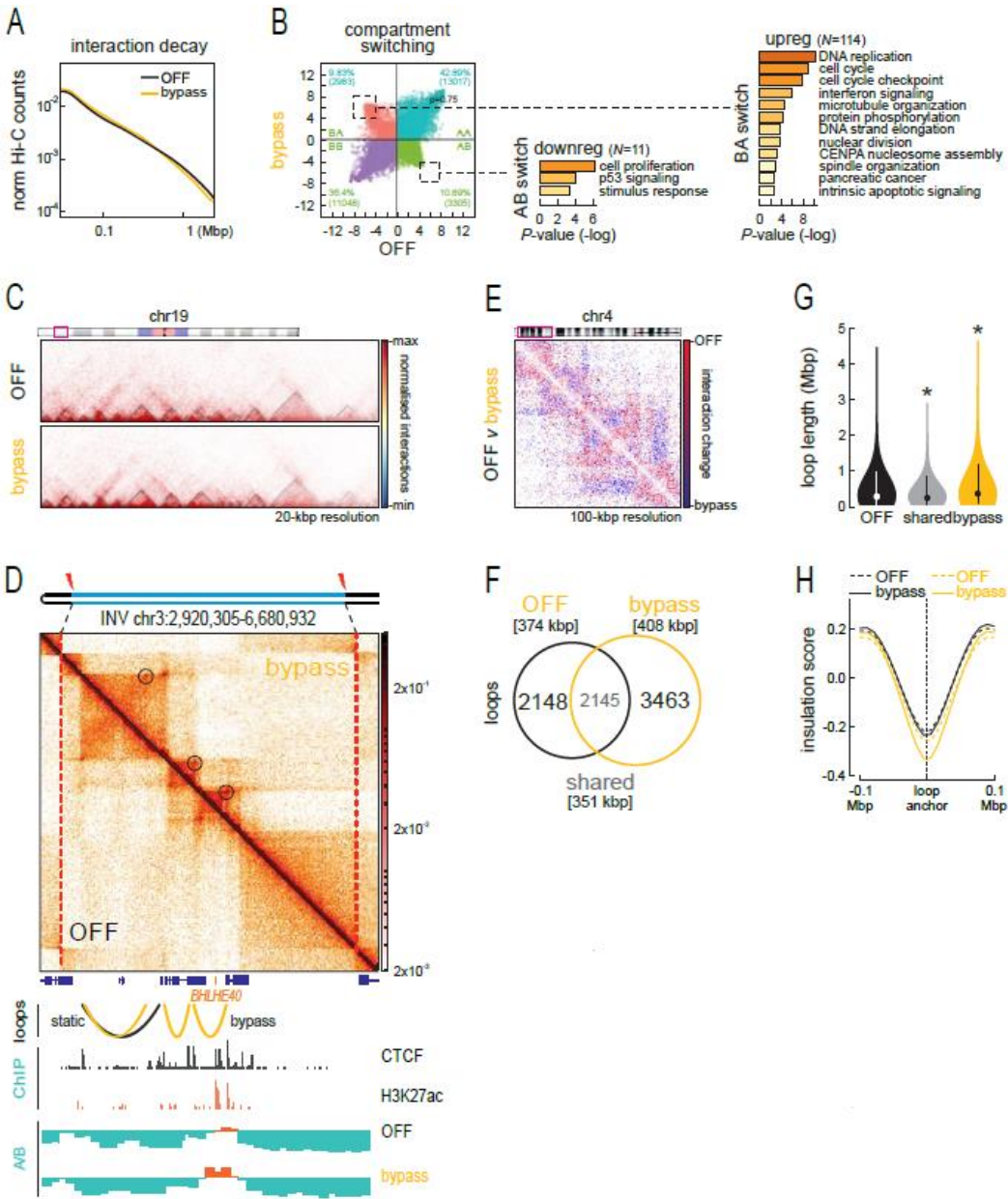


Figure 24. Analysis of spatial chromatin interactions in inverted non-induced and senescence-bypass cells.

(A) Line plot showing mean interaction strength decay (Hi-C counts) in relation to increasing separation of interacting fragments in non-induced (OFF) (black) and senescence-bypass (bypass) inverted cells (yellow).

(B) Changes in A/B-compartments in senescence-bypass versus non-induced Hi-C data. Strong B-to-A and A-to-B switching (dotted squares) are indicated, and the GO terms associated with differentially-expressed genes embedded in each switched domain.

(C) Exemplary Hi-C heatmaps from OFF and bypass cells showing negligible changes in TAD positions for a subregion on chromosome 19.

(D) Composite Hi-C heatmap depicting interactions from non-induced (bottom) and bypass inverted cells (top) in the region harboring BHLHE40 on chromosome 3p. The data is aligned to CTCF and H3K27ac ChIP-seq data from normal non-induced HBECs, as well as to A/B-compartment positions from non-induced and senescence-bypass cells. CTCF-anchored loops emerging upon senescence bypass are denoted on the Hi-C map (circles) and aligned below (yellow arches).

(E) Subtracted Hi-C heatmap showing changes in interactions upon transition from non-induced to senescence-bypass “inverted” cells for a subregion on chromosome 4.

(F) Venn diagram showing the number of loops unique to non-induced and senescence-bypass inverted cells or shared. Median loop lengths (square brackets) are indicated.

(G) Violin plots showing distribution of lengths for the loops from panel H. *: significantly different to non-induced; P-value <0.05, Wilcoxon-Mann-Whitney test.

(H) Line plots showing mean insulation of chromatin interactions in the 200 kbp around loop anchors unique to non-induced (black) or senescence-bypass inverted loops (yellow) using Hi-C data from non-induced (dotted lines) and senescence-bypass cells (solid lines).

(I) Update on the DNA damage model for cancer development (Halazonetis et al. 2008). Cells respond to oncogenic stimuli by eliciting senescence as an anti-tumor barrier. The high DNA damage (DSBs) burden amassing during senescence engages error-prone repair mechanisms. Consequently, genetic aberrations accumulate with concurrent chromatin remodeling that provide a “pool” of genomic defects, from which those that facilitate escape from senescence, cell cycle re-entry and aggressive features are selected and maintained.

3.2 CDC6 silencing as a strategy to inhibit cancer progression

Our results so far indicate that CDC6 is a crucial molecule for cancer development. It has the potential to drive malignant transformation in a non-cancerous cellular setting. Briefly, CDC6 overexpression in normal bronchial epithelial cells robustly induces senescence in less than 6 days. Nevertheless, senescence induction proved to be a reversible state and, as a result, a subset of cells overcome the senescence barrier and gives rise to aggressive clones with increased invasive potential. This, in combination with the fact that CDC6 has been found to be overexpressed in various cancer types, prompted us to investigate the impact of CDC6-silencing in breast cancer cell lines.

For this purpose, we recruited two breast cancer cell lines, namely MCF-7 and MDA-MB-231. MCF-7 scores positive for estrogen and progesterone receptors (ER⁺/PR⁺) and negative for HER2 expression. On the other hand, MDA-MB-231 is negative for HER2, but also negative for estrogen and progesterone receptors expression (triple-negative breast cancer, TNBC). Furthermore, MCF-7 expresses wild-type p53 protein, while MDA-MB-231 bears a p53 gain-of-function mutation and also has a higher invasive and metastatic potential compared to MCF-7. Importantly, both cell lines overexpress CDC6 protein and siRNA-mediated silencing proved to be a successful strategy to inhibit CDC6 protein expression (**Figure 25**).

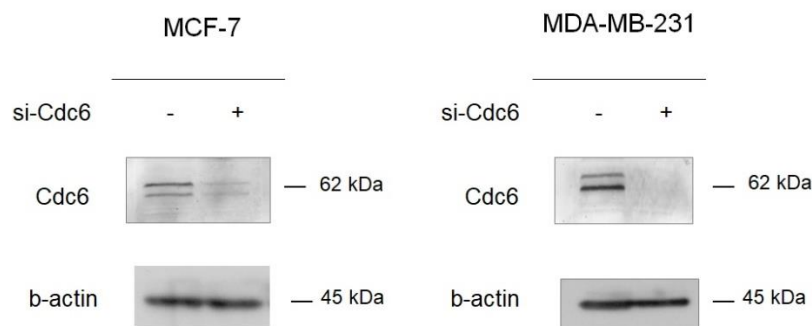


Figure 25. CDC6-silencing in MCF-7 and MDA-MB-231 cell lines for 6 days.

3.2.1 CDC6 inhibition alters the cell cycle profile and induces senescence

Next, we examined the cell cycle distribution and the cell morphology upon CDC6 inhibition. Interestingly, FACS analysis upon CDC6 down-regulation results in the following observations (**Figure 26**):

- 1) MCF-7 cells accumulate in G1 and G2/M phases
- 2) MDA-MB-231 cells accumulate mostly in G2/M phases
- 3) Cell death is increased in both cell lines.

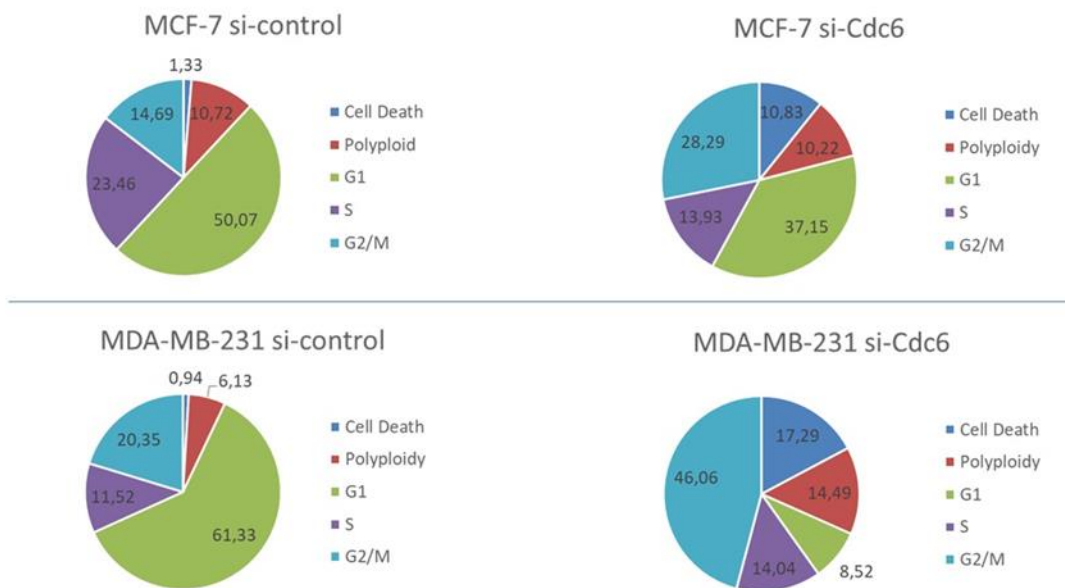


Figure 26. FACS sorting in MCF-7 and MDA-MB-231 cells reveals a reduction in the proliferation rate and an increase in cell death in both cell lines.

Simultaneously we also observed a typical senescence morphology. Thus, the cells were subsequently stained with SenTraGor and as expected the staining was positive for senescence induction (**Figure 27**).

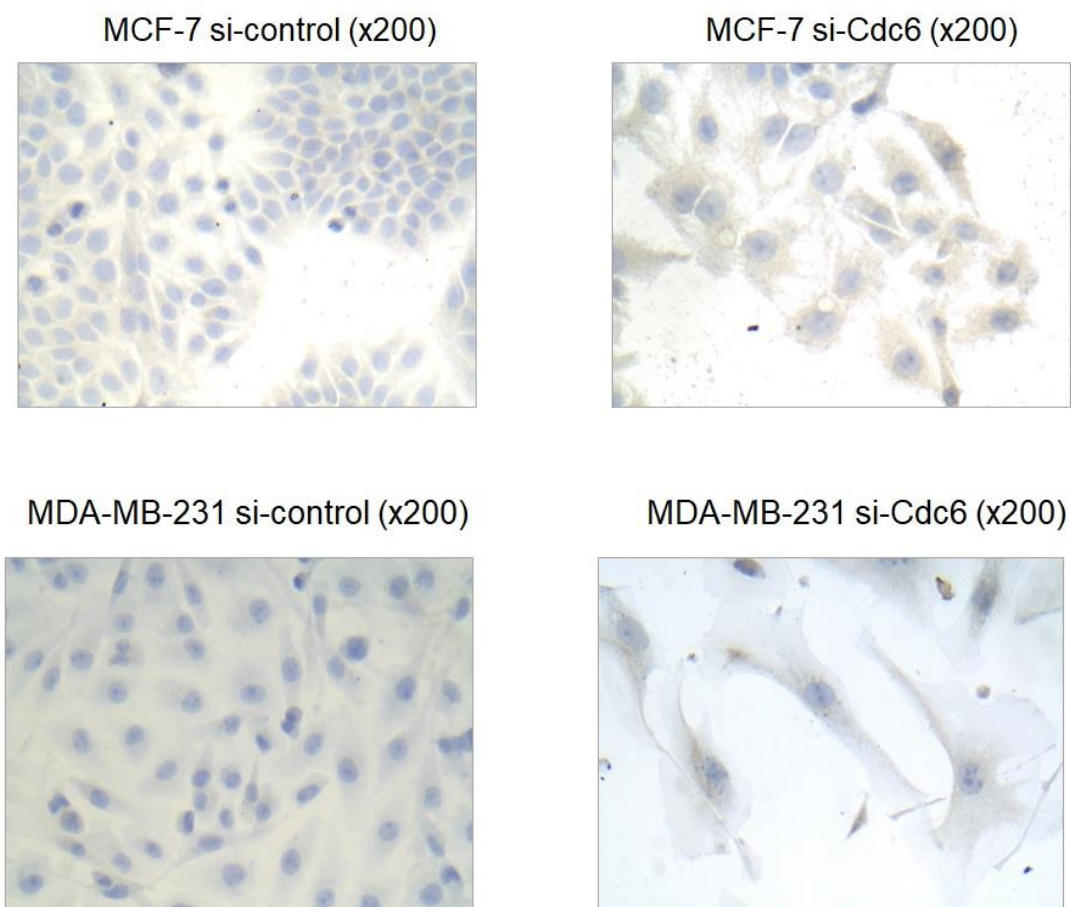


Figure 27. MCF-7 and MDA-MB-231 cells stained with SenTraGor 6 days upon CDC6-silencing.

3.2.2 MDA-MB-231 cells acquire a phenotype resembling mitotic catastrophe

Strikingly, MDA-MB-231 cells, while senescent, acquire a phenotype with several micronuclei (**Figure 28A**). Examining the MDA-MB-231 CDC6-silenced cells we noted that Cyclin B1 increased, while LATS1 levels were reduced (**Figure 28B**). Importantly, although 53BP1 foci emerged in MCF-7 cells, in MDA-MB231 cell line 53BP1 foci were not observed upon CDC6 inhibition (**Figure 28C**). Together, the above mentioned

results suggest that MDA-MB-231 cells accumulate in M phase and are eliminated via mitotic catastrophe in a caspase dependent or independent manner (**Figure 28D**).

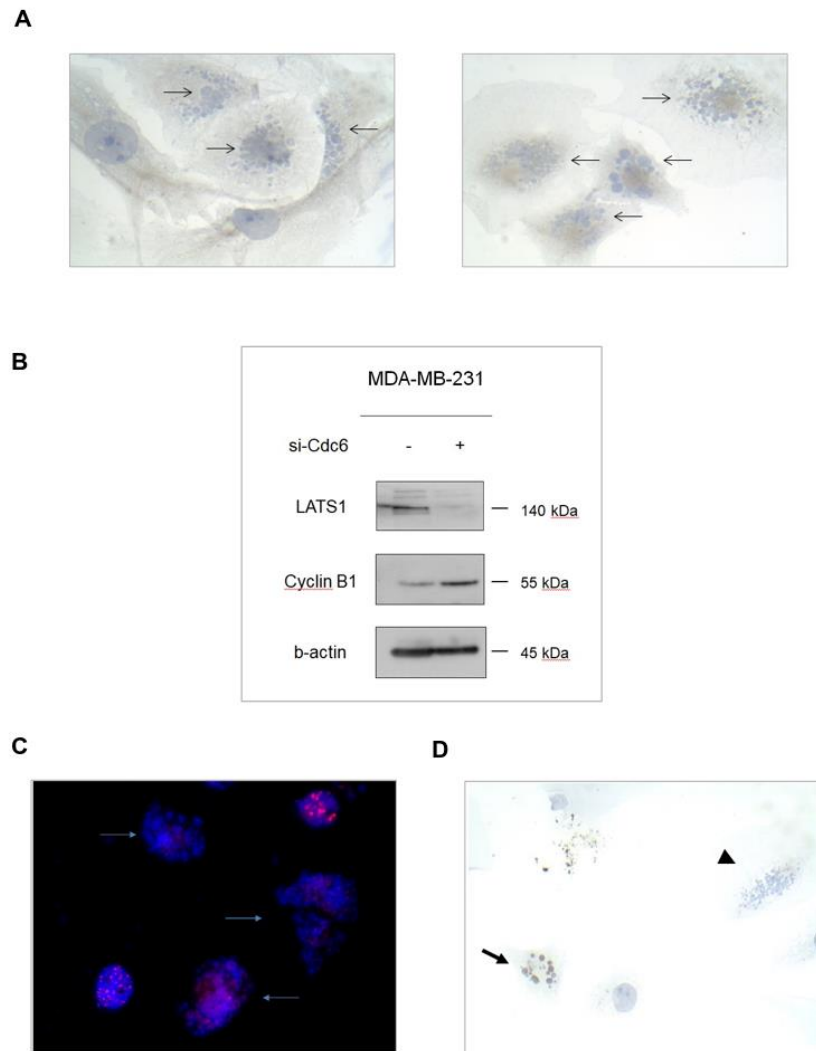


Figure 28. MDA-MB-231 cells express mitotic markers and die through mitotic catastrophe upon CDC6 down-regulation.

(A) Mitotic catastrophe phenotype of MDA-MB-231 cells (arrows), while they are positive for SenTraGor staining.

(B) Western blots assessing Cyclin B and LATS1 levels.

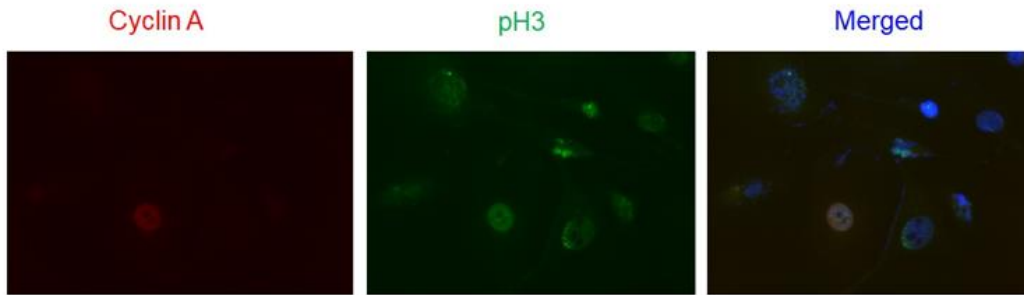
- (C) Immunofluorescence against 53BP1 supports the fact that MDA-MB-231 cells are arrested in mitosis. Arrows indicate cells with mitotic catastrophe phenotype.
- (D) Caspase-3 staining for MDA-MB-231 CDC6-silenced cells.

Given that CDC6 plays a role in the stability of Chk1 (Borlado and Mendez 2008), a major component of the G2/M checkpoint, we speculated that protracted CDC6 silencing destabilizes Chk1. This combined with the fact that CDC6 down-regulation results in DNA under-replication (Lau et al.2006), suggests that cells can proceed in M phase with under-replicated DNA and finally are eliminated via mitotic catastrophe. Furthermore, CDC6 silencing perturbs mitotic assembly and centrosome duplication, further contributing to mitotic catastrophe emergence (Youn et al 2020).

3.2.3 MDA-MB-231 cells gradually accumulate in M phase

Subsequently, we tested whether accumulation in mitosis is a dynamic phenomenon and occurs in due course after CDC6 down-regulation. To examine this, we used as markers Cyclin A and phosphorylated histone 3 (pH3). Cyclin A negative/pH3 positive cells were marked as positive for M phase (**Figure 29A**). This experimental setting eventually revealed that cells gradually accumulate in mitosis 4 days upon CDC6 silencing (**Figure 29B**).

A



B

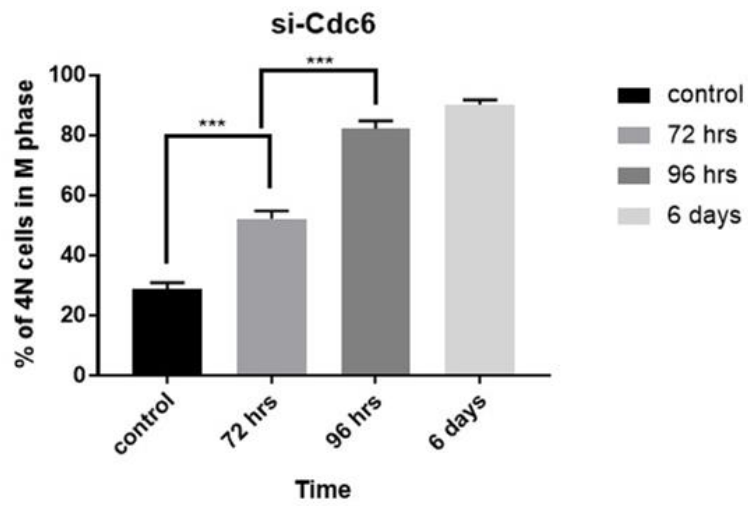


Figure 29. Immunofluorescence against Cyclin A and pH3 showed that MDA-MB-231 cells gradually enter mitosis since day 4 after CDC6-silencing.

(A) Representative pictures for Cyclin A and pH3 immunofluorescence.

(B) Bar graph showing the percentage of cells entering mitosis after CDC6-silencing.

Nonetheless, at day 6 after CDC6 inhibition cells express higher phosphorylated (and thus activated) Chk1 levels compared to the untreated cells (**Figure 30A**). This is in contrast with the M phase accumulation, as Chk1 constitutes a central regulator of the G2/M checkpoint. Thus, we speculated that there is a distinct role for Chk1 during mitosis. In line with the above, phosphorylated Chk1 levels significantly decreased at day 3 of silencing, whereas its levels were restored the day after (**Figure 30B**). This implies that Chk1 destabilization initially allows cells to proceed to mitosis and then Chk1 is up-regulated in mitotic cells. To further examine this hypothesis, we synchronized MDA-MB-231 cells in mitosis and we assessed phosphorylated Chk1 levels upon hydroxyurea (HU) treatment. As expected, mitotic cells express high levels of phosphorylated protein (**Figure 30C**), highlighting an undiscovered role of Chk1 during mitosis.

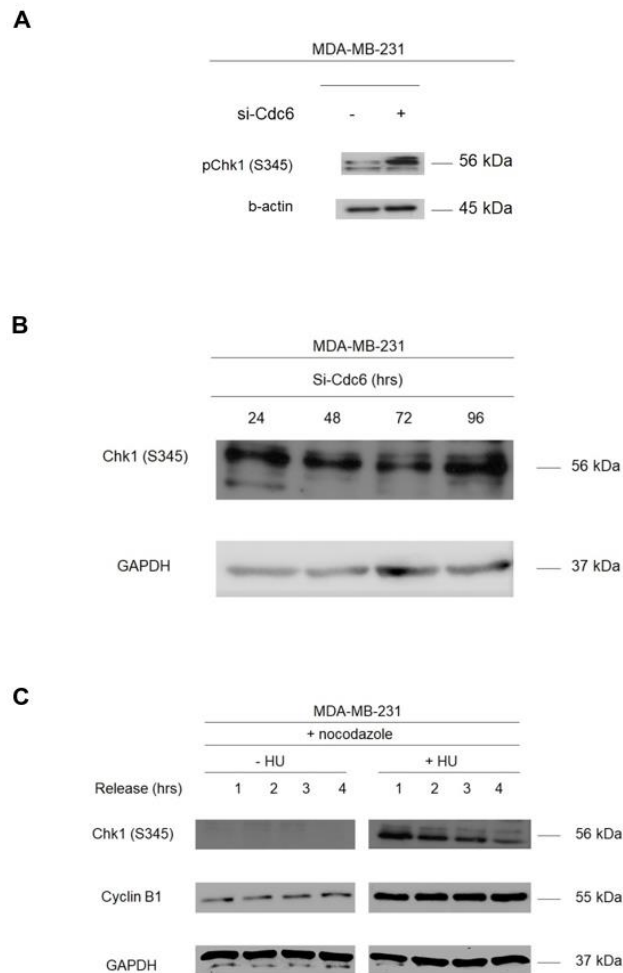


Figure 30. Chk1 abrogation drives entry into mitosis, however stressed mitotic cells re-express Chk1.

(A) Phospho-Chk1 is elevated at day 6 after CDC6 down-regulation

(B) Phospho-Chk1 expression is gradually decreased until day 3 following CDC6-silencing but the day after increases.

Phospho-Chk1 levels are increased in nocodazole-treated MDA-MB-231 cells. HU used as a replication stress inducer, mimicking CDC6-silencing conditions

CHAPTER 4

DISCUSSION

CDC6 is a fundamental component of the DNA replication process and its expression is strictly regulated during cell cycle. This precise regulation ensures that genome is replicated only once per cell cycle (Blow and Gillespie 2008). CDC6 deregulation has been described in different cancer types from the earliest stages of cancer progression (Karakaidos et al. 2004, Lontos et al. 2007, Sideridou et al. 2011, Petrakis et al. 2016). Specifically, CDC6 is implicated in cancer development and progression in two different ways. First, its overexpression in cancerous and pre-cancerous cell lines triggers replication stress, genomic instability and eventually leads to malignant biological behavior (Lontos et al. 2007, Sideridou et al. 2011, Galanos et al. 2016, Walter et al. 2016, Komseli et al. 2018). In addition, CDC6 plays a role as a transcriptional regulator of significant genes (Sideridou et al. 2011, Petrakis et al. 2015, Huang et al. 2016). Interestingly, CDC6 as a member of the AAA⁺ ATPase family (Neuwald et al. 1999) possesses the structural characteristics which can explain this biological function.

Given that CDC6 is strongly correlated with cancer development and progression, a question arising is to what extent CDC6 up-regulation is a subsequent event of increased proliferation rate of cancer cells or whether it can be an inaugural event of malignant transformation. Nonetheless, it has been demonstrated that there is no connection between expression of CDC6 and Ki-67 proliferation marker. Also, CDC6 levels are not increased at the stage of hyperplasia, which is characterized by rapidly proliferating cells (Lontos et al. 2007). Importantly, CDC6 overexpression in HBEC cell line ceased cell proliferation and induced senescence for a protracted time period. Hence, CDC6 overexpression is closely connected to oncogenesis.

Interestingly, two recent publications from our research group highlighted the role of CDC6 in malignant transformation. Firstly, Galanos and colleagues suggested that p21-protracted overexpression results in escape from senescence in a CDC6-dependent manner (Galanos et al. 2016). Subsequently, Komseli and coauthors proved that CDC6 overexpression in HBECs drives escape from senescence and this results in the emergence of malignant clones with increased invasive potential (Komseli et al. 2018). However, the latter work did not reveal the mechanistic basis underlying this phenomenon/outcome.

In the present PhD thesis, we present for the first time mechanistic evidence on how DNA lesions acquired early upon entry into oncogene-induced senescence can drive the subsequent escape from senescence. We employed the normal HBEC cell line as the tool and CDC6 as the triggering oncogenic insult. Upon CDC6 induction, DSBs occur genome-wide as early as 3 days. Notably, we observed that replication-transcription collision plays a role on DSBs formation. However, these DSBs are predominantly repaired in an error-prone manner. These misrepaired lesions are essential for the establishment and/or maintenance of the escaped clones. To confirm that, we demonstrated that BIR and SSA error-prone repair mechanisms are responsible for DNA repair in a RAD52-dependent manner, whereas error-free SDSA repair pathway has low efficiency in the CDC6-overexpressing environment regardless of RAD52 levels.

Interestingly, the observed SNVs took a “kataegis” form and the mutation signature of the escaped clones resembled previously discovered signatures in specific tumors derived from patients (Alexandrov et al. 2013). Another prerequisite for malignant transformation is p53 inactivation (Halazonetis et al. 2008). Nevertheless, in our model *TP53* locus itself is not mutated, but was abrogated via MDM2 up-regulation. To confirm this hypothesis, we used the HPDEC-CDC6/TetON cellular model in which p53 function is suppressed via HPV16-E6 transduction (Ouyang et al. 2000). As anticipated, HPDECs bypassed senescence upon CDC6 induction.

A prominent and recurrent feature that drove our attention in escaped clones was the 3.7-Mbp heterozygous inversion on chromosome 3p. While essentially all types of structural aberrations have been functionally linked to cancer development (Stratton et al. 2009, Danieli and Papantonis 2020), inversions confer particular properties regarding their selection. Their predominantly heterozygous nature allows for lower recombination rates and thus, for selective maintenance (Puig et al. 2015, Wellenreuther and Bernatchez 2018). Accordingly, the *BHLHE40* gene harbored in our 3.7-Mbp inversion encodes a circadian transcription factor known for controlling a large number of human genes and a variety of cellular processes, including cell cycle (Hunt and Sassone-Corsi 2007, Wood et al. 2009, Kato et al. 2014, Sato et al. 2016). Moreover, it also correlated

with adverse prognosis in various malignancies. In our system, control of key differentially-regulated genes in escaped cells can be attributed to BHLHE40. Remodeling of the BHLHE40 containing topological domain via the emergence of *de novo* loops coincided with its activation.

To assess the significance of the acquired inversion in BHLHE40 and further in escape from senescence we designed the following strategy:

First, we investigated the impact of the inversion on BHLHE40 expression and then we silenced BHLHE40 in escaped cells. As predicted, BHLHE40 silencing resulted in increased cell death in escaped cells. Hence, we further decided to recapitulate this genetic alteration by artificially generating this specific inversion via CRISPR/Cas9 technology. Interestingly, the newly acquired inverted cell line did not enter senescence upon CDC6 induction, validating our hypothesis.

To further clarify whether BHLHE40 is the responsible factor for senescence-bypass, we introduced a BHLHE40-carrying vector into the HBEC-CDC6/TetON cellular setting. Indeed, BHLHE40 stable overexpression resulted in senescence-bypass upon CDC6 activation. Hence, the aforementioned experimental results highlight that the inversion on chromosome 3p renders BHLHE40 a pivotal molecule for the escape from senescence phenomenon/condition.

Overall, CDC6 activation is a crucial mediator for the development of a stressogenic environment which triggers genomic instability. The present work highlights that the stress-induced aberrations acquired early into the cancer evolution process, constitute the genetic basis for the subsequent malignant transformation.

The converging point of the aforementioned list of events is CDC6 overexpression. Hence, this replication licensing factor can be an attractive target for cancer inhibition. For this purpose, we performed a targeted CDC6 silencing by using siRNA technology in breast cancer cell lines. MCF-7 and MDA-MB-231 cell lines were selected, as they express high levels of CDC6 protein and they represent two different breast cancer subtypes; ER⁺/PR⁺ and triple-negative breast cancers respectively. Of note, CDC6 up-regulation is correlated with adverse outcome in breast cancer patients.

Interestingly, artificial CDC6 silencing activated senescence in both cell lines and significantly increased the cell death rates. Moreover, in the triple-negative cell line, CDC6 inactivation not only triggered senescence, but also provoked cell death via a characteristic cell death subtype, known as mitotic catastrophe. The latter was not an unexpected event though. CDC6 has been found to play a critical role not only in DNA replication, but also in the G2/M checkpoint of the cell cycle (Borlado and Mendez 2008). Thus, we speculate that CDC6 abrogation has two distinct outcomes. First, as expected, it suppresses DNA replication. Second, it abolishes the G2/M checkpoint and thus cells with under-replicated DNA enter M phase. As a result, the cells cannot tolerate the stress and consequently are eliminated via mitotic catastrophe.

To further examine mechanistic details on how this cell death type occurred, we validated that G2/M checkpoint is abrogated in MDA-MB-231 cells. Interestingly, upon accumulation in mitosis, phospho-Chk1, a marker of G2/M checkpoint pathway, increased. Hence, we demonstrated that phospho-Chk1 can be activated in mitosis, exerting probably a different mode of action.

The major difference between the two breast cell lines is the type of cell death route followed. While MCF-7 cells were eliminated through apoptosis, MDA-MB-231 cells succumbed by mitotic catastrophe both in a caspase-dependent or independent manner. We speculate that p53 is the pivotal molecule which prevents mitotic catastrophe, as MCF-7 cells express wild-type p53, whereas MDA-MB-231 harbor a mutated form. Hence, this scenario warrants further future investigation. Overall, CDC6 seems a promising factor for targeting in order to halt cancer progression, but as mentioned additional studies are required to clarify its exploitation for triggering cancer cell death.

Taken together, our work suggests that the genetic events which take place in the early stages of the oncogene-induced senescence can eventually lead to further malignant transformation. Hence, targeting senescent cells can be of major clinical importance, by eliminating a potential source of recurrence. Conclusively, the elimination of senescent cells with senolytics (Zhu et al. 2015, Childs et al. 2015, Gorgoulis et al. 2019, Myriantopoulos et al. 2019) may be a therapeutic choice alternative to CDC6 inhibition.

Regarding the limitations of the present study, we cannot exclude the possibility that BHLHE40 activation and the subsequent escape from senescence can also occur independently of the genomic inversion showed herein. Probably other undiscovered mechanisms can be involved in this phenomenon. Finally, although BHLHE40 is the effector connecting replication machinery with the circadian clock, further work is needed to understand and reveal the full spectrum of underlying mechanisms.

CHAPTER 5

REFERENCES

Abdennur N., Mirny L.A. (2020) Cooler: scalable storage for Hi-C data and other genomically labeled arrays. *Bioinformatics* 36, 311-316.

Akman B.H., Can T., Erson-Bensan A.E. (2012) Estrogen-induced upregulation and 3'-UTR shortening of CDC6. *Nucleic Acids Res* 40, 10679-10688.

Alexandrov L.B., Nik-Zainal S., Wedge D.C., Aparicio S.A., Behjati S., Biankin A.V., et al. (2013) Signatures of mutational processes in human cancer. *Nature* 500, 415-421.

Anders S., Huber W. (2010) Differential expression analysis for sequence count data. *Genome Biology* 11, R106.

Anders S., Pyl P.T., Huber W. (2015) HTSeq-a Python framework to work with high-throughput sequencing data. *Bioinformatics* 31, 166-169.

Artandi S.E., DePinho R.A. (2010). Telomeres and telomerase in cancer. *Carcinogenesis* 31, 9-18.

Astle M.V., Hannan K.M., Ng P.Y., Lee R.S., George A.J., Hsu A.K. et al. (2012) AKT induces senescence in human cells via mTORC1 and p53 in the absence of DNA damage: implications for targeting mTOR during malignancy. *Oncogene* 31, 1949-1962.

Baker T.A., Bell S.P. (1998) Polymerases and the replisome: machines within machines. *Cell* 92, 295-305.

Barry E.R., Bell S.D. (2006) DNA replication in the archaea. *Microbiol Mol Biol Rev* 70, 876-887.

Bartkova J., Rezaei N., Liontos M., Karakaidos P., Kletsas D., Issaeva N., et al. (2006) Oncogene-induced senescence is part of the tumorigenesis barrier imposed by DNA damage checkpoints. *Nature* 444, 633-637.

Beagan J.A., Phillips-Cremins J.E. (2020). On the existence and functionality of topologically associating domains. *Nat. Genet.* 52, 8-16.

Blow J.J., Dutta A. (2005) Preventing re-replication of chromosomal DNA. *Nat Rev Mol Cell Biol* 6, 476-486.

Bocker W., Denk H., Heitz P.U. (2007) *Pathology*. Athens, Broken Hill Publishers.

Bonds L., Baker P., Gup C., Shroyer K.R. (2002) Immunohistochemical localization of cdc6 in squamous and glandular neoplasia of the uterine cervix. *Arch Pathol Lab Med* 126, 1164-1168.

Borlado L.R., Mendez J. (2008). CDC6: from DNA replication to cell cycle checkpoints and oncogenesis. *Carcinogenesis* 29, 237-243.

Braig M., Lee S., Loddenkemper C., Rudolph C., Peters A.H., Schlegelberger B., Stein H., Dorken B., Jenuwein T. and Schmitt C.A. (2005) Oncogene-induced senescence as an initial barrier in lymphoma development. *Nature* 436, 660-665.

Branzei D., Foiani M. (2005) The DNA damage response during DNA replication. *Curr Opin Cell Biol* 17, 568-575.

Branzei D., Foiani M. (2010) Maintaining genome stability at the replication fork. *Nat Rev Mol Cell Biol* 11, 208-219.

Bravou V., Nishitani H., Song S.Y., Taraviras S., Varakis J. (2005) Expression of the licensing factors, Cdt1 and Geminin, in human colon cancer. *Int J Oncol* 27, 1511-1518.

Campisi J., d'Adda di Fagagna F. (2007) Cellular senescence: when bad things happen to good cells. *Nat Rev Mol Cell Biol* 8, 729-740.

Campisi J., Robert L. (2014) Cell senescence: role in aging and age-related diseases. *Interdiscip Top Gerontol* 39, 45-61.

Cayrou C., Coulombe P., Vigneron A., Stanojcic S., Ganier O., Peiffer I. et al. (2011) Genome-scale analysis of metazoan replication origins reveals their organization in specific but flexible sites defined by conserved features. *Genome Res* 21, 1438-1449.

Chandra T., Ewels P.A., Schoenfelder S., Furlan-Magaril M., Wingett S.W., Kirschner K., et al. (2015) Global reorganization of the nuclear landscape in senescent cells. *Cell Rep.* 10, 471-483.

Chen X., Schulz-Trieglaff O., Shaw R., Barnes B., Schlesinger F., Källberg M., et al. (2016) Manta: rapid detection of structural variants and indels for germline and cancer sequencing applications. *Bioinformatics* 32, 1220-1222.

Chen Z., Trotman L.C., Shaffer D., Lin H.K., Dotan Z.A., Niki M., et al. (2005) Crucial role of p53-dependent cellular senescence in suppression of Pten-deficient tumorigenesis. *Nature* 436, 725-730.

Childs B.G., Durik M., Baker D.J., van Deursen J.M. (2015). Cellular senescence in aging and age-related disease: from mechanisms to therapy. *Nat. Med.* 21, 1424-1435.

Chugh S., Gnanapragassam V.S., Jain M., Rachagani S., Ponnusamy M.P., Batra S.K. (2015) Pathobiological implications of mucin glycans in cancer: Sweet poison and novel targets. *Biochim. Biophys. Acta* 1856, 211-225.

Clijsters L., Wolthuis R. (2014) PIP-box-mediated degradation prohibits re-accumulation of Cdc6 during S phase. *J Cell Sci* 127, 1336-134.

Collado M., Gil J., Efeyan A., Guerra C., Schuhmacher A.J., Barradas M., et al. (2005) Tumour biology: senescence in premalignant tumours. *Nature* 436, 642.

Colotta F., Allavena P., Sica A., Garlanda C., Mantovani A. (2009) Cancer-related inflammation, the seventh hallmark of cancer: links to genetic instability. *Carcinogenesis* 30, 1073-1081.

Courtot L., Hoffmann J.S., Bergoglio V. (2018) The protective role of dormant origins in response to replicative stress. *Int J Mol Sci* 19, 3569.

Coverley D., Laman H., Laskey R.A. (2002) Distinct roles for cyclins E and A during DNA replication complex assembly and activation. *Nat Cell Biol* 4, 523-528.

Criscione. S.W., Cecco. M., Siranosian B., Zhang Y., Kreiling. J., Sedivy J., et al. (2016) Reorganization of chromosome architecture in replicative cellular senescence. *Sci Adv* 32, 751-761.

Cvetic C., Walter J.C. (2005) Eukaryotic origins of DNA replication: could you please be more specific? *Semin Cell Dev Biol* 16, 343-353.

d'Adda di Fagagna F., Teo S.H., Jackson S.P. (2004) Functional links between telomeres and proteins of the DNA-damage response. *Genes Dev* 18, 1781-1799

Danieli A., Papantonis A. (2020) Spatial genome architecture and the emergence of malignancy. *Hum Mol Genet* 29, R197-204.

Das M., Prasad S.B., Yadav S.S., Govardhan H.B., Pandey L.K., Singh S. et al. (2013) Over expression of minichromosome maintenance genes is clinically correlated to cervical carcinogenesis. *PLoS One* 8, e69607.

DeNardo D.G., Andreu P., Coussens L.M. (2010) Interactions between lymphocytes and myeloid cells regulate pro- versus anti-tumor immunity. *Cancer Metastasis Rev* 29, 309-316.

DePamphilis M.L., Blow J.J., Ghosh S., Saha T., Noguchi K., Vassilev A. (2006) Regulating the licensing of DNA replication origins in metazoa. *Curr Opin Cell Biol* 18, 231-239.

Di Leonardo A., Linke S.P., Clarkin K., Wahl G.M. (1994) DNA damage triggers a prolonged p53-dependent G1 arrest and long-term induction of Cip1 in normal human fibroblasts. *Genes Dev* 8, 2540-2551.

Di Micco R., Fumagalli M., Cicalese A., Piccinin S., Gasparini P., Luise C., et al. (2006) Oncogene-induced senescence is a DNA damage response triggered by DNA hyper-replication. *Nature* 444, 638-642.

Dobin A., Davis C.A., Schlesinger F., Drenkow J., Zaleski C., Jha, S., et al. (2013) STAR: ultrafast universal RNA-seq aligner. *Bioinformatics* 29, 15-21.

Evangelou K., Kotsinas A., Mariolis-Sapsakos T., Giannopoulos A., Tsantoulis P.K., Constantinides C. et al. (2008) E2F-1 overexpression correlates with decreased proliferation and better prognosis in adenocarcinomas of Barrett oesophagus. *J Clin Pathol* 61, 601-605.

Fearon E.R. and Vogelstein B. (1990) A genetic model for colorectal tumorigenesis. *Cell* 61, 759-767.

Feng D., Tu Z., Wu W., Liang C. (2003) Inhibiting the expression of DNA replication-initiation proteins induces apoptosis in human cancer cells. *Cancer Res* 63, 7356-7364.

Fisher D., Mechali M. (2003) Vertebrate HoxB Gene Expression Requires DNA Replication. *EMBO J.* 22, 3737-3748.

Ford E., Nikopoulou C., Kokkalis A., Thanos D. (2014) A method for generating highly multiplexed ChIP-seq libraries. *BMC Res. Notes* 7, 312.

Fujita M. (2006) Cdt1 revisited: complex and tight regulation during the cell cycle and consequences of deregulation in mammalian cells. *Cell Div* 1, 22.

Galanos P., Vougas K., Walter D., Polyzos A., Maya-Mendoza A., Haagensen E.J., et al. (2016) Chronic p53-independent p21 expression causes genomic instability by deregulating replication licensing. *Nat. Cell Biol.* 18, 777-789.

Galanos P., Pappas G., Polyzos A., Kotsinas A., Svolaki I., Giakoumakis N.N., et al. (2018) Mutational signatures reveal the role of RAD52 in p53-independent p21-driven genomic instability. *Genome Biol.* 19, 37.

Garrett M.D. (2001) Cell cycle control and cancer. *Curr Sci* 81, 515-522.

Georgakopoulou E., Evangelou K., Havaki S., Townsend P., Kanavaros P., Gorgoulis V.G. (2016) Apoptosis or senescence? Which exit route do epithelial cells and fibroblasts preferentially follow? *Mech Ageing Dev* 156, 17-24.

Gery S., Komatsu N., Baldjyan L., Yu A., Koo D., Koeffler H.P. (2006) The circadian gene *per1* plays an important role in cell growth and DNA damage control in human cancer cells. *Mol Cell* 22, 375-382.

Goodspeed A., Heiser L.M., Gray J.W., Costello J.C. (2016) Tumor-Derived Cell Lines as Molecular Models of Cancer Pharmacogenomics. *Mol. Cancer Res.* 14, 3-13.

Gorgoulis V., Adams P.D., Alimonti A., Bennett D.C., Bischof O., Bishop C., et al. (2019) Cellular senescence: defining a path forward. *Cell* 179, 813-827.

Gorgoulis V.G., Zacharatos P., Mariatos G., Kotsinas A., Bouda M., Kletsas D. et al. (2002) Transcription factor E2F-1 acts as a growth-promoting factor and is associated with adverse prognosis in non-small cell lung carcinomas. *J Pathol* 198, 142-156.

Gorgoulis V.G., Pefani D.E., Pateras I.S., Trougakos I.P. (2018) Integrating the DNA damage and protein stress responses during cancer development and treatment. *J. Pathol.* 246, 12-40.

Greider C.W., Blackburn E.H. (1987) The telomere terminal transferase of *Tetrahymena* is a ribonucleoprotein enzyme with two kinds of primer specificity. *Cell* 51, 887-898.

Grivennikov S.I., Greten F.R., Karin M. (2010) Immunity, inflammation and cancer. *Cell* 140, 883-899.

Halazonetis T.D., Gorgoulis V.G., Bartek J. (2008) An oncogene-induced DNA damage model for cancer development. *Science* 319, 1352-1355.

Hanahan D., Weinberg R.A. (2000) The hallmarks of cancer *Cell* 100, 57-70.

Hanahan D., Weinberg R.A. (2011) Hallmarks of cancer: the next generation. *Cell* 144, 646-674.

Harvey L.A.B., Kaiser C.A., Krieger M., Scott M.P., Bretscher A., Ploegh H et al. (2007) *Molecular Cell Biology*. 6th Edition.

Herbig U., Jobling W.A., Chen B.P., Chen D.J., Sedivy J.M. (2004) Telomere shortening triggers senescence of human cells through a pathway involving ATM, p53, and p21(CIP1), but not p16(INK4a). *Mol Cell* 14, 501-513.

Hermans D., Nurse P. (2007) Cdc18 enforces long-term maintenance of the S phase checkpoint by anchoring the Rad3-Rad26 complex to chromatin. *Mol Cell* 26, 553-563.

Hills S.A., Diffley J.F. (2014) DNA replication and oncogene-induced replicative stress. *Curr Biol.* 24, R435-44.

Ho A., Dowdy S.F. (2002) Regulation of G(1) cell-cycle progression by oncogenes and tumor suppressor genes. *Curr Opin Genet Dev* 12, 47-52.

Hochegger H., Takeda S., Hunt T. (2008) Cyclin-dependent kinases and cell cycle transitions: does one fit all? *Nat Rev Mol Cell Biol* 9, 910-916.

Hoeben R.C., Uil T.G. (2013) Adenovirus DNA replication. *Cold Spring Harb Perspect Biol* 5, a013003.

Hua C., Zhao G., Li Y., Bie L. (2014) Minichromosome Maintenance (MCM) Family as potential diagnostic and prognostic tumor markers for human gliomas. *BMC Cancer* 14, 526.

Huang S., Xu X., Wang G., Lu G., Xie W., Tao W. et al. (2016) DNA replication initiator Cdc6 also regulates ribosomal DNA transcription initiation. *J Cell Sci* 129, 1429-1440.

Hunt T., Sassone-Corsi P. (2007) Riding tandem: circadian clocks and the cell cycle. *Cell* 129, 461-464.

Jacot W., Fiche M., Zaman K., Wolfer A., Lamy P.J. (2013) The HER2 amplicon in breast cancer: Topoisomerase IIA and beyond. *Biochim Biophys Acta* 1836, 146-157.

Jemal A., Bray F., Center M.M., Ferlay J., Ward E, Forman D. (2011) Global cancer statistics. *CA Cancer J Clin* 61, 69-90.

Jeruzalmi D., Yurieva O., Zhao Y., Young M., Stewart J., Hingorani M. et al. (2001). Mechanism of processivity clamp opening by the delta subunit wrench of the clamp loader complex of E. coli DNA polymerase III. *Cell*, 106, 417-428.

Karakaidos P., Taraviras S., Vassiliou L.V., Zacharatos P., Kastrinakis N., Kougiou D., et al. (2004) Overexpression of the replication licensing regulators hCdt1 and hCdc6 characterizes a subset of non-small-cell lung carcinomas. *Am J Pathol* 165, 1351-1365.

Kaplan D.L. (2016) The initiation of DNA replication in Eukaryotes. Switzerland, Springer international publishing.

Kato Y., Kawamoto T., Fujimoto K., Noshiro M. (2014) DEC1/STRA13/SHARP2 and DEC2/SHARP1 coordinate physiological processes, including circadian rhythms in response to environmental stimuli. *Curr Top Dev Biol* 110, 339-372.

Kerpedjiev, P., Abdennur, N., Lekschas, F. et al. (2018) HiGlass: web-based visual exploration and analysis of genome interaction maps. *Genome Biol* 19, 125.

Kiyono T., Foster S.A., Koop J.I., McDougall J.K., Galloway D.A., Klingelhutz A.J. (1998) Both Rb/p16INK4a inactivation and telomerase activity are required to immortalize human epithelial cells. *Nature* 396, 84-88.

Knight P.A., Ruiz D. (2013) A fast algorithm for matrix balancing. *IMA Journal of Numerical Analysis* 33, 1029–1047.

Komseli E.S., Pateras I.S., Krejsgaard T., Stawiski K., Rizou S.V., Polyzos A., et al. (2018) A prototypical non-malignant epithelial model to study genome dynamics and concurrently monitor micro-RNAs and proteins in situ during oncogene-induced senescence. *BMC Genomics* 19, 37.

Krishnamurti U., Silverman J.F. (2014) HER2 in breast cancer: a review and update. *Adv Anat Pathol* 21, 100-107.

Kufe D.W. (2009) Mucins in cancer: function, prognosis and therapy. *Nat Rev Cancer* 9, 874-85.

Kumar V., Abbas A., Aster J. (2012) *Robbins Basic Pathology*, Elsevier.

Langmead B., Salzberg SL. (2012) Fast gapped-read alignment with Bowtie 2. *Nat. Methods* 9, 357-359.

Lau E., Zhu C., Abraham R.T., Jiang W. (2006). The functional role of Cdc6 in S-G2/M in mammalian cells. *EMBO Rep* 7, 425-430.

Lau K.M., Chan Q.K., Pang J.C., Li K.K., Yeung W.W., Chung N.Y. et al. (2010) Minichromosome maintenance proteins 2, 3 and 7 in medulloblastoma: overexpression and involvement in regulation of cell migration and invasion. *Oncogene* 29, 5475-5489.

Lazzerini Denchi E., Attwooll C, Pasini D. Helin K. (2005) Deregulated E2F activity induces hyperplasia and senescence-like features in the mouse pituitary gland. *Mol Cell Biol* 25, 2660-2672.

Leonard A.C., Mechali M. (2013) DNA replication origins. *Cold Spring Harb Perspect Biol* 5, a010116.

Li C.J., DePamphilis M.L. (2002). Mammalian Orc1 protein is selectively released from chromatin and ubiquitinated during the S-to-M transition in the cell division cycle. *Mol Cell Biol* 22, 105-116.

- Li H., Handsaker B., Wysoker A., Fennell T., Ruan J., Homer N., et al. (2009) The sequence alignment/map format and SAMtools. *Bioinformatics* 25, 2078-2079.
- Li X., Zhao Q., Liao R., Sun P., Wu X. (2003) The SCF(Skp2) ubiquitin ligase complex interacts with the human replication licensing factor Cdt1 and regulates Cdt1 degradation. *JBC*, 278, 30854-30858.
- Liontos M., Koutsami M., Sideridou M., Evangelou K., Kletsas D., Levy B., et al. (2007) Deregulated overexpression of hCdt1 and hCdc6 promotes malignant behavior. *Cancer Res.* 67, 10899-10909.
- Liu J., Smith C.L., DeRyckere D., DeAngelis K., Martin G.S., Berger J.M. (2000) Structure and function of Cdc6/Cdc18: implications for origin recognition and checkpoint control. *Mol Cell*, 6, 637-648.
- Liu P., Slater D.M., Lenburg M., Nevis K., Cook J.G., Vaziri C. (2009) Replication licensing promotes cyclin D1 expression and G1 progression in untransformed human cells. *Cell Cycle* 8, 125-136.
- Lukas C., Savic V., Bekker-Jensen S., Doil C., Neumann B., Pedersen R.S. (2011) 53BP1 nuclear bodies form around DNA lesions generated by mitotic transmission of chromosomes under replication stress. *Nat Cell Biol* 13, 243-253.
- Luo J., Solimini N.L., Elledge S.J. (2009) Principles of cancer therapy: oncogene and non-oncogene addiction. *Cell* 136, 823-837.
- Machida Y.J., Dutta A. (2005) Cellular checkpoint mechanisms monitoring proper initiation of DNA replication. *J Biol Chem* 280, 6253-6256.
- Mailand N., Diffley J.F. (2005) CDKs promote DNA replication origin licensing in human cells by protecting Cdc6 from APC/C-dependent proteolysis. *Cell* 122, 915-926.
- Malumbres M., Barbacid M. 2009. Cell cycle, CDKs and cancer: a changing paradigm. *Nat Rev* 9, 53-166.

Manchado E., Eguren M., Malumbres, M. (2010) The anaphase-promoting complex/cyclosome (APC/C): cell-cycle-dependent and -independent functions. *Biochem Soc Trans* 38, 65-71.

Mani S.A., Guo W., Liao M.J., Eaton E.N., Ayyanan A., Zhou A.Y. et al. (2008) The epithelial-mesenchymal transition generates cells with properties of stem cells. *Cell* 133, 704-715.

Mar N., Vredenburg J.J., Wasser J.S. (2015) Targeting HER2 in the treatment of non-small cell lung cancer. *Lung Cancer* 87, 220-225.

Martin V., Cappuzzo F., Mazzucchelli L., Frattini M. (2014) HER2 in solid tumors: more than 10 years under the microscope; where are we now? *Future Oncol* 10, 1469-1486.

Masri S., Cervantes M., Sassone-Corsi P. (2013) The circadian clock and cell cycle: interconnected biological circuits. *Curr. Opin. Cell Biol.* 25, 730-734.

Mazzoccoli G., Castellana S., Carella M., Palumbo O., Tiberio C., Fusilli C., et al. (2017) A primary tumor gene expression signature identifies a crucial role played by tumor stroma myofibroblasts in lymph node involvement in oral squamous cell carcinoma. *Oncotarget* 8, 104913-104927.

Mechali M. (2010) Eukaryotic DNA replication origins: many choices for appropriate answers. *Nat Rev Mol Cell Biol* 11, 728-738.

Mendez J., Zou-Yang X.H., Kim S.Y., Hidaka M., Tansey W.P., Stillman B. (2002) Human origin recognition complex large subunit is degraded by ubiquitin-mediated proteolysis after initiation of DNA replication. *Mol Cell* 9, 481-491.

Michaloglou C., Vredeveld L.C., Soengas M.S., Denoyelle C., Kuilman T., van der Horst C.M., et al. (2005) BRAF^{E600}-associated senescence-like cell cycle arrest of human naevi. *Nature* 436, 720-724.

Moreno A., Carrington J.T., Albergante L., Al Mamun M., Haagensen E.J., Komseli E.S., et al. (2016) Unreplicated DNA remaining from unperturbed S phases passes through mitosis for resolution in daughter cells. *Proc. Natl. Acad. Sci. U.S.A.* 113: 5757-64.

Murphy N., Ring M., Heffron C.C., King B., Killalea A.G., Hughes C. et al. (2005) p16INK4A, CDC6, and MCM5: predictive biomarkers in cervical preinvasive neoplasia and cervical cancer. *J Clin Pathol*, 58, 525-534.

Myrianthopoulos V., Evangelou K., Vasileiou P.V.S., Cooks T., Vassilakopoulos T.P., Pangalis G.A., et al. (2019) Senescence and senotherapeutics: a new field in cancer therapy. *Pharmacol. Ther.* 193, 31-49.

Nagy A., Lániczky A., Menyhárt O., Gyórfy B. (2018) Validation of miRNA prognostic power in hepatocellular carcinoma using expression data of independent datasets. *Sci. Rep.* 8, 9227.

Naim V., Wilhelm T., Debatisse M., Rosselli F. (2013) ERCC1 and MUS81-EME1 promote sister chromatid separation by processing late replication intermediates at common fragile sites during mitosis. *Nat Cell Biol* 15, 1008-1015.

Negrini S., Gorgoulis V.G., Halazonetis T.D. (2010) Genomic instability—an evolving hallmark of cancer. *Nat. Rev. Mol. Cell. Biol.* 11, 220-28.

Neuwald A.F., Aravind L., Spouge J.L., Koonin E.V. (1999) AAA+: A class of chaperone-like ATPases associated with the assembly, operation, and disassembly of protein complexes. *Genome Res* 9, 27-43.

Nevis K.R., Cordeiro-Stone M., J.G. Cook (2009) Origin licensing and p53 status regulate Cdk2 activity during G(1). *Cell Cycle* 8, 1952-1963.

Nguyen H.T., Duong H.Q. (2018). The molecular characteristics of colorectal cancer: Implications for diagnosis and therapy. *Oncology Letters* 16, 9-18.

Nieto M.A., Huang R.Y., Jackson R.A., Thiery J.P. (2016) EMT: 2016. *Cell* 166, 21-45.

Ochs F., Somyajit K., Altmeyer M., Rask M.B., Lukas J., Lukas C. (2016) 53BP1 fosters fidelity of homology-directed DNA repair. *Nat. Struct. Mol. Biol.* 23, 714-721.

O'Donnell M. Langston L., Stillman B. (2013) Principles and concepts of DNA replication in bacteria, archaea, and eukarya. *Cold Spring Harb Perspect Biol* 5(7).

Ohta S., Koide M., Tokuyama T., Yokota N., Nishizawa S., Namba H. (2001) Cdc6 expression as a marker of proliferative activity in brain tumors. *Oncol Rep* 8, 1063-1066.

Ouyang H., Mou L.J., Luk C., Liu N., Karaskova J., Squire J., et al. (2000) Immortal human pancreatic duct epithelial cell lines with near normal genotype and phenotype. *Am. J. Pathol.* 157, 1623-1631.

Patel P.L., Suram A., Mirani N., Bischof O., Herbig U. (2016) Derepression of hTERT gene expression promotes escape from oncogene-induced cellular senescence. *Proc. Natl. Acad. Sci. U.S.A.* 113, E5024-5033.

Petrakis T.G., Vougas K., Gorgoulis V.G. (2012) Cdc6: a multi-functional molecular switch with critical role in carcinogenesis. *Transcription* 3, 124-129.

Petrakis T.G., Komseli E.S., Papaioannou M., Vougas K., Polyzos A., Myrianthopoulos V., et al. (2016) Exploring and exploiting the systemic effects of deregulated replication licensing. *Semin Cancer Biol.* 37-38, 3-15.

Pinyol M., Salaverria I., Bea S., Fernandez V., Colomo L., Campo E., Jares P. (2006), Unbalanced expression of licensing DNA replication factors occurs in a subset of mantle cell lymphomas with genomic instability. *Int J Can* 119, 2768-2774.

Puig M., Casillas S., Villatoro S., Cáceres M. (2015) Human inversions and their functional consequences. *Brief Funct Genomics* 14, 369-379.

Ramachandran RK, Geetha N, Sakthivel KM, Kumar RS, Krishna KMNJ, Sreedharan H. (2019) Impact of Additional Chromosomal Aberrations on the Disease Progression of Chronic Myelogenous Leukemia. *Front Oncol* 9, 88-99.

Ramirez R.D., Morales C.P., Herbert B.S., Rohde J.M., Passons C., Shay J.W., Wright W.E. (2001) Putative telomere-independent mechanisms of replicative aging reflect inadequate growth conditions. *Genes Dev* 15, 398-403.

Ramirez R.D., Herbert B.S., Vaughan M.B., Zou Y., Gandia K., Morales C.P., et al. (2003) Bypass of telomere-dependent replicative senescence (M1) upon overexpression of Cdk4 in normal human epithelial cells. *Oncogene* 22, 433-444.

Rao S.S., Huntley M.H., Durand N.C., Stamenova E.K., Bochkov I.D., Robinson J.T., et al. (2014) A 3D map of the human genome at kilobase resolution reveals principles of chromatin looping. *Cell* 159, 1665-1680.

Risso D., Ngai J., Speed T. Dudoit S. (2014) Normalization of RNA-seq data using factor analysis of control genes or samples. *Nat. Biotechnol.* 32, 896-902.

Rouillard A.D., Gundersen G.W., Fernandez N.F., Wang Z., Monteiro C.D., McDermott M.G., et al. (2016) The harmonizome: a collection of processed datasets gathered to serve and mine knowledge about genes and proteins. *Database (Oxford)* pii, baw100.

Salama R., Sadaie M., Hoare M., Narita M. (2014) Cellular senescence and its effector programs. *Genes Dev* 28, 99-114.

Sato M., Vaughan M.B., Girard L., Peyton M., Lee W., Shames D.S., et al. (2006) Multiple oncogenic changes (K-RAS(V12), p53 knockdown, mutant EGFRs, p16 bypass, telomerase) are not sufficient to confer a full malignant phenotype on human bronchial epithelial cells. *Cancer Res.* 66, 2116-2128.

Sato F., Bhawal U.K., Yoshimura T., Muragaki Y. (2016) DEC1 and DEC2 crosstalk between circadian rhythm and tumor progression. *J. Cancer* 7, 153-159.

Sideridou M., Zakopoulou R., Evangelou K., Lontos M., Kotsinas A., Rampakakis E., et al. (2011) Cdc6 expression represses E-cadherin transcription and activates adjacent replication origins. *J. Cell Biol.* 195, 1123-1140.

Skarstad K., Katayama T. (2013) Regulating DNA replication in bacteria. *Cold Spring Harb Perspect Biol* 5, a012922.

Sotiriou S., Kamileri I., Lugli N., Evangelou K., Da-Re C., Huber F., et al. (2016) Mammalian RAD52 functions in break-induced replication repair of collapsed DNA replication forks. *Mol. Cell* 64, 1127-1134.

Stevaux O., Dyson N.J. (2002) A revised picture of the E2F transcriptional network and RB function. *Cur Opin* 14, 684-691.

Stratton M.R., Campbell P.J., Futreal P.A. (2009) The cancer genome. *Nature* 458, 719-724.

Sun X., Cheng G., Hao M., Zheng J., Zhou X., Zhang J. et al. (2010) CXCL12 / CXCR4 / CXCR7 chemokine axis and cancer progression. *Cancer Metastasis Rev* 29, 709-722.

Sung H., Ferlay J., Siegel R.L., Laversanne M., Soerjomataram I., Jemal A. et al. (2021). Global Cancer Statistics 2020: GLOBOCAN Estimates of Incidence and Mortality Worldwide for 36 Cancers in 185 Countries. *CA Cancer J Clin*, 71, 209-249.

Takai H., Smogorzewska A., de Lange T. (2003) DNA damage foci at dysfunctional telomeres. *Curr Biol* 13, 1549-1556.

Takayama Y., Kamimura Y., Okawa M., Muramatsu S., Sugino A., Araki H. (2003) GINS, a novel multiprotein complex required for chromosomal DNA replication in budding yeast. *Genes Dev* 17, 1153-1165.

Tanaka S., Araki H. (2013) Helicase activation and establishment of replication forks at chromosomal origins of replication. *Cold Spring Harb Perspect Biol* 5, a010371.

Teer J.K., Dutta A. (2006) Regulation of S phase. *Results Probl Cell Differ* 42, 31-63.

Tsakraklides V., Bell S.P. (2010) Dynamics of pre-replicative complex assembly. *JBC*, 85, 9437-9443.

Tsantoulis P.K., Gorgoulis V.G. (2005) Involvement of E2F transcription factor family in cancer. *Eur J Cancer* 41, 2403-2414.

Tsoli E., Gorgoulis V.G., Zacharatos P., Kotsinas A., Mariatos G., Kastrinakis N.G. et al. (2001) Low levels of p27 in association with deregulated p53-pRb protein status enhance tumor proliferation and chromosomal instability in non-small cell lung carcinomas. *Mol Med* 7, 418-429.

Valencia A, Cervera J, Such E, Barragán E, Bolufer P, Fuster O, Collado R, Martínez J, Sanz MA. (2009) Complex Variant t(9;22) Chromosome Translocations in Five Cases of Chronic Myeloid Leukemia. *Adv Hematol*. 2009, 187125.

Van der Auwera G.A., Carneiro M., Hartl C., Poplin R., del Angel G., Levy-Moonshine A., et al. (2013) From fastQ data to high-confidence variant calls: the genome analysis toolkit best practices pipeline. *Curr. Protoc. Bioinformatics* 43, 1-33.

Vaziri C., Saxena S., Jeon Y., Lee C., Murata K., Machida Y., et al. (2003) A p53-dependent-checkpoint pathway prevents re-replication. *Mol. Cell* 11, 997-1008.

Walter D., Hoffmann S., Komseli E.S., Rappsilber J., Gorgoulis V., Sorensen C.S. (2016) SCF(Cyclin F)-dependent degradation of CDC6 suppresses DNA re-replication. *Nat Commun* 7, 10530.

Wang K., Li M., Hakonarson H. (2010) ANNOVAR: functional annotation of genetic variants from high-throughput sequencing data. *Nucleic Acids Res.* 38, e164.

Warburg O.H. (1930) *The metabolism of tumours: Investigations from the Kaiser-Wilhelm Institute for Biology.* London, UK: Arnold Constable, Berlin-Dahlem.

Weinberg R. (2007) *The Biology of Cancer,* New York, Garland Press.

Wellenreuther M., Bernatchez L. (2018) Eco-evolutionary genomics of chromosomal inversions. *Trends Ecol. Evol.* 33, 427-440.

Wood P.A., Yang X., Hrushesky W.J. (2009) Clock genes and cancer. *Integr Cancer Ther.* 8, 303-308.

Woodward A.M., Gohler T., Luciani M.G., Oehlmann M., Ge X., Gartner A. et al. (2006) Excess Mcm2-7 license dormant origins of replication that can be used under conditions of replicative stress. *J Cell Biol* 173, 673-683.

Wu Y., Kantake N, Sugiyama T., Kowalczykowski S.C. (2008) Rad51 protein controls Rad52-mediated DNA annealing. *J Biol Chem* 283, 14883-92.

Xouri G., Lygerou Z., Nishitani H., Pachnis V., Nurse P., Taraviras S. (2004) Cdt1 and geminin are down-regulated upon cell cycle exit and are over-expressed in cancer-derived cell lines. *Eur J Biochem* 271, 3368-3378.

Yamada K., Miyamoto K. (2005) Basic helix-loop-helix transcription factors, BHLHB2 and BHLHB3; their gene expressions are regulated by multiple extracellular stimuli. *Front. Biosci.* 10, 3151-3171.

Yan W.X., Mirzazadeh R., Garnerone S., Scott D., Schneider M.W., Kallas T., et al. (2017) BLISS is a versatile and quantitative method for genome-wide profiling of DNA double-strand breaks. *Nat. Commun.* 8, 15058.

Yim H., Erikson R.L. (2010) Cell division cycle 6, a mitotic substrate of polo-like kinase 1, regulates chromosomal segregation mediated by cyclin-dependent kinase 1 and separase. *PNAS* 107, 19742-19747.

Youn Y., Lee J.C., Kim J., Kim J.H., Hwang J.H. (2020) Cdc6 disruption leads to centrosome abnormalities and chromosome instability in pancreatic cancer cells. *Sci Rep* 10, 16518.

Zacharatos P., Kotsinas A., Evangelou K., Karakaidos P., Vassiliou L.V., Rezaei N. et al. (2004) Distinct expression patterns of the transcription factor E2F-1 in relation to tumour growth parameters in common human carcinomas. *J Pathol* 203, 744-753.

Zampetidis C.P., Galanos P., Angelopoulou A., Zhu Y., Polyzou A., Karamitros T., et al. (2021) A recurrent chromosomal inversion suffices for driving escape from oncogene-induced senescence via subTAD reorganization. *Mol Cell* 81, 4907-4923.

Zhu G., Pan C., Bei J.X., Li B., Liang C., Xu Y., et al. (2020) Mutant p53 in Cancer Progression and Targeted Therapies. *Front Oncol.* 10, 595187.

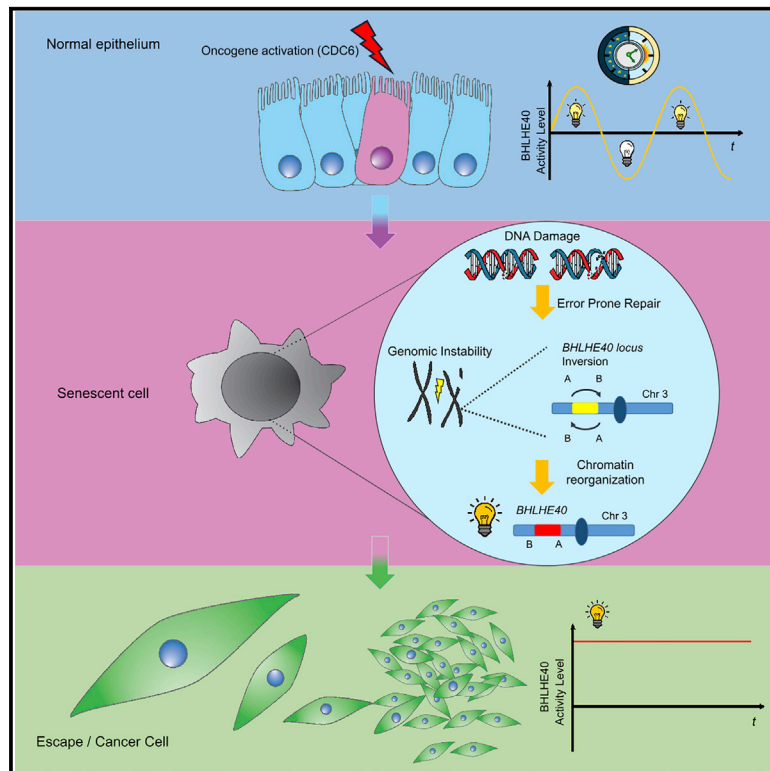
Zhu Y., Tchkonja T., Pirtskhalava T., Gower A., Ding H., Giorgadze N., et al. (2015) The Achilles' heel of senescent cells: from transcriptome to senolytic drugs. *Aging Cell* 14, 644-658.

CHAPTER 6

ANNEX

A recurrent chromosomal inversion suffices for driving escape from oncogene-induced senescence via subTAD reorganization

Graphical abstract



Highlights

- Oncogene-driven repair produces early genetic lesions, allowing escape from senescence
- Cells escaping senescence display mutational signatures observed in individuals with cancer
- A recurrent inversion harboring a circadian gene suffices for bypassing senescence
- Chromatin loop and compartment remodeling support the “escape” transcriptional program

Authors

Christos P. Zampetidis,
Panagiotis Galanos,
Andriani Angelopoulou, ..., Jiri Bartek,
Argyris Papantonis,
Vassilis G. Gorgoulis

Correspondence

panos@cancer.dk (P.G.),
jb@cancer.dk (J.B.),
argyris.papantonis@
med.uni-goettingen.de (A.P.),
vgorg@med.uoa.gr (V.G.G.)

In brief

Zampetidis et al. demonstrate that a recurrent chromosomal inversion harboring the circadian gene *BHLHE40* is sufficient to drive escape from oncogene-induced senescence. The inversion is the outcome of oncogene-mediated genomic instability followed by chromatin refolding changes that activate the gene, leading to cell cycle re-entry and aggressive behavior.

Article

A recurrent chromosomal inversion suffices for driving escape from oncogene-induced senescence via subTAD reorganization

Christos P. Zampetidis,^{1,17} Panagiotis Galanos,^{2,17,*} Andriani Angelopoulou,^{1,17} Yajie Zhu,³ Aikaterini Polyzou,¹ Timokratis Karamitros,⁴ Athanassios Kotsinas,¹ Nefeli Lagopati,¹ Ioanna Mourkioti,¹ Reza Mirzazadeh,⁵ Alexandros Polyzos,⁶ Silvano Garnerone,⁵ Athanasia Mizi,³ Eduardo G. Gusmao,³ Konstantinos Sofiadis,³ Zita Gál,⁷ Dorthe H. Larsen,⁷ Dafni-Eleftheria Pefani,⁸ Marco Demaria,⁹ Aristotelis Tsirigos,¹⁰ Nicola Crosetto,⁵ Apolinar Maya-Mendoza,¹¹ Angelos Paspaspyropoulos,¹ Konstantinos Evangelou,¹ Jiri Bartek,^{2,5,*} Argyris Papantonis,^{3,12,*} and Vassilis G. Gorgoulis^{1,13,14,15,16,18,*}

¹Molecular Carcinogenesis Group, Department of Histology and Embryology, Faculty of Medicine, National Kapodistrian University of Athens, 11527 Athens, Greece

²Genome Integrity Group, Danish Cancer Society Research Center, 2100 Copenhagen, Denmark

³Translational Epigenetics Group, Institute of Pathology, University Medical Center Göttingen, 37075 Göttingen, Germany

⁴Unit of Bioinformatics and Applied Genomics, Department of Microbiology, Hellenic Pasteur Institute, 11521 Athens, Greece

⁵Science for Life Laboratory, Division of Genome Biology, Department of Medical Biochemistry and Biophysics, Karolinska Institute, 171 77 Solna, Stockholm, Sweden

⁶Sanford I. Weill Department of Medicine, Sandra and Edward Meyer Cancer Center, Weill Cornell Medicine, New York, NY 10065, USA

⁷Nucleolar Stress and Disease Group, Danish Cancer Society Research Center, 2100 Copenhagen, Denmark

⁸Laboratories of Biology, Medical School, University of Patras, 26504 Rio, Greece

⁹University of Groningen (RUG), European Research Institute for the Biology of Aging (ERIBA), University Medical Center Groningen (UMCG), 9713 AV Groningen, the Netherlands

¹⁰Department of Pathology, NYU School of Medicine, New York, NY 10016, USA

¹¹DNA Replication and Cancer Group, Danish Cancer Society Research Center, 2100 Copenhagen, Denmark

¹²Center for Molecular Medicine Cologne (CMMC), University of Cologne, 50931 Cologne, Germany

¹³Biomedical Research Foundation, Academy of Athens, 11527 Athens, Greece

¹⁴Division of Cancer Sciences, School of Medical Sciences, Faculty of Biology, Medicine & Health, University of Manchester, M20 4GJ Manchester, UK

¹⁵Center for New Biotechnologies and Precision Medicine, Medical School, National and Kapodistrian University of Athens, 11527 Athens, Greece

¹⁶Faculty of Health and Medical Sciences, University of Surrey, Surrey GU2 7YH, UK

¹⁷These authors contributed equally

¹⁸Lead contact

*Correspondence: panos@cancer.dk (P.G.), jb@cancer.dk (J.B.), argyris.papantonis@med.uni-goettingen.de (A.P.), vgorg@med.uoa.gr (V.G.G.) <https://doi.org/10.1016/j.molcel.2021.10.017>

SUMMARY

Oncogene-induced senescence (OIS) is an inherent and important tumor suppressor mechanism. However, if not removed timely via immune surveillance, senescent cells also have detrimental effects. Although this has mostly been attributed to the senescence-associated secretory phenotype (SASP) of these cells, we recently proposed that “escape” from the senescent state is another unfavorable outcome. The mechanism underlying this phenomenon remains elusive. Here, we exploit genomic and functional data from a prototypical human epithelial cell model carrying an inducible *CDC6* oncogene to identify an early-acquired recurrent chromosomal inversion that harbors a locus encoding the circadian transcription factor *BHLHE40*. This inversion alone suffices for *BHLHE40* activation upon *CDC6* induction and driving cell cycle re-entry of senescent cells, and malignant transformation. Ectopic overexpression of *BHLHE40* prevented induction of *CDC6*-triggered senescence. We provide strong evidence in support of replication stress-induced genomic instability being a causative factor underlying “escape” from oncogene-induced senescence.

INTRODUCTION

According to the DNA damage model for cancer development, activated oncogenes trigger genomic instability that, at some

point, breaches the tumor-suppressing barriers of apoptosis and senescence to promote cancer development (Halazonetis et al., 2008). This model readily explains how emerging genomic instability in cancer leads to evasion of apoptosis via

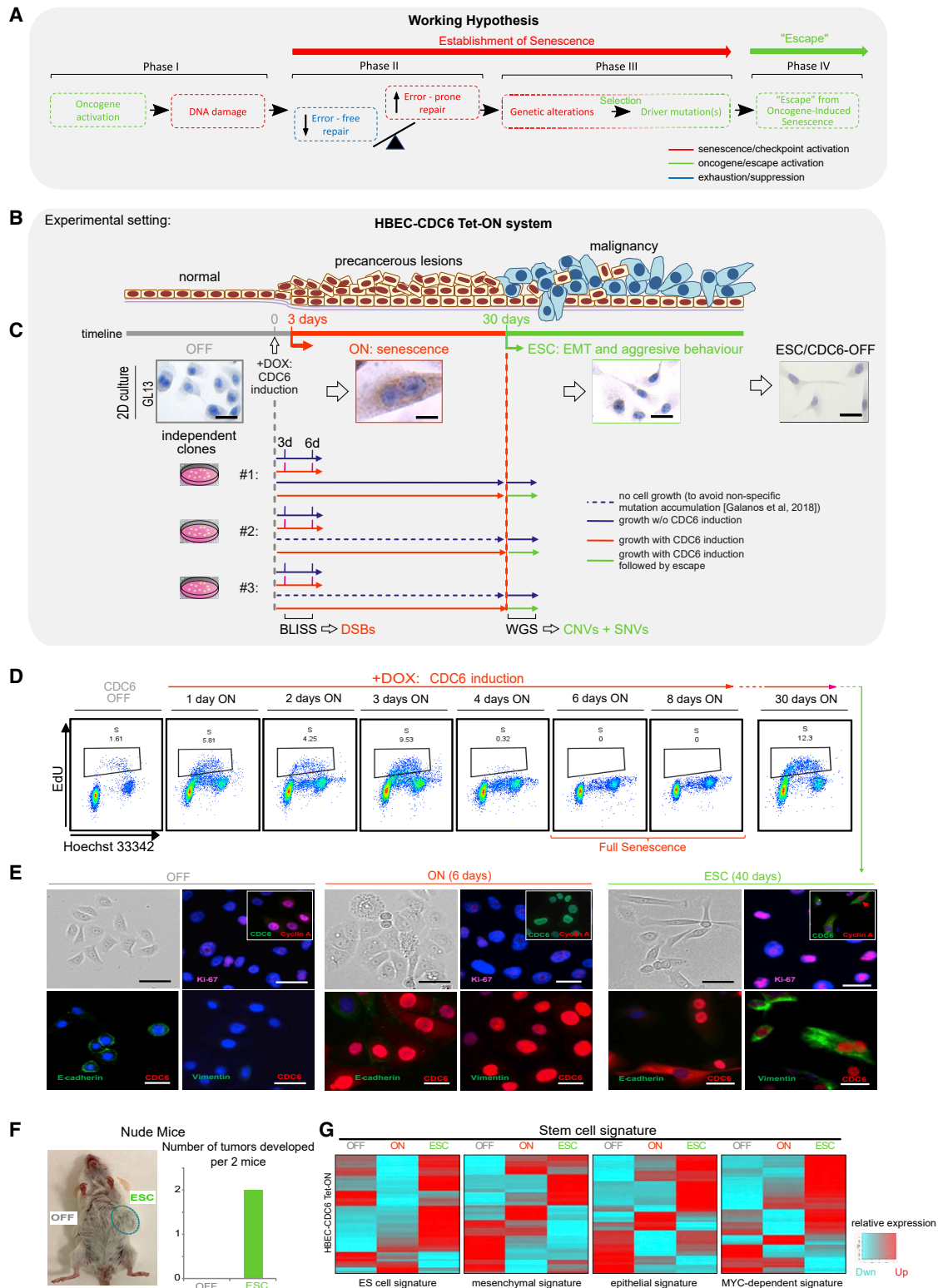


Figure 1. ESC from OIS

(A) Working hypothesis, based on our cancer development model (Halazonetis et al., 2008), to address the aim of this study: showing that accumulating DNA damage traits during oncogene-induced senescence (OIS) will be selected and should appear in ESC cells as functionally meaningful genetic defects.

(B) A human bronchial epithelial cell (HBEC) CDC6-TetON cellular system recapitulating successive stages of cancer evolution (Komseli et al., 2018).

(legend continued on next page)

accumulation of inactivating mutations at key signaling hubs and regulatory factors (Halazonetis et al., 2008; Negrini et al., 2010; Gorgoulis et al., 2018). It also provides the basis for considering senescence as an inherent barrier to tumor development in precancerous stages (Bartkova et al., 2006; Di Micco et al., 2006; Collado et al., 2005; Braig et al., 2005; Michaloglou et al., 2005; Chen et al., 2005). However, this model does not explain how cells “escape” from senescence and particularly how cells that have entered such a state of irreversible cell cycle arrest become able to breach this barrier and re-initiate proliferation.

Recently, we and others demonstrated that a subset of cells in a senescent population do re-enter the cell cycle, “escaping” senescence (Galanos et al., 2016, 2018; Yu et al., 2018; Milanovic et al., 2018; Patel et al., 2016). Such “escapee” cells adopt a more aggressive phenotype that closely mimics cancer development (Gorgoulis et al., 2019). The molecular mechanism underlying this “escape” phenomenon has not yet been deciphered.

Here we hypothesize that, if our cancer development model (Halazonetis et al., 2008) also applies to the “escape” phenomenon, then accumulating DNA damage traits during oncogene-induced senescence (OIS) would be selected and should appear in “escape” cells as functionally meaningful genetic aberrations (Figure 1A). To address this, we combine a prototypical human epithelial OIS cellular system with genomics and functional assays to present the first evidence in support of this hypothesis and discuss its clinical significance.

RESULTS

An OIS model recapitulating cancer evolution

We recently described a cellular system based on normal human bronchial epithelial cells (HBECs) carrying a *CDC6*-TetON overexpression cassette (Figure 1B; Moreno et al., 2016; Komseli et al., 2018). HBECs are of epithelial origin, like most common cancer types, and in their uninduced state (“OFF” in Figure 1B), they are free from the mutation burden found in cancer cells (Goodspeed et al., 2016; Stratton et al., 2009). This permits accurate detection of amassing DNA alterations during *CDC6*-induced senescence (“ON” state in Figure 1B).

The replication licensing factor *CDC6* was chosen as the inducible oncogenic stimulus because (1) as a key component of the replication licensing machinery integrating most mitogenic and oncogenic stimuli, it is frequently deregulated, also by gene

amplification, from the earliest stages of cancer (Karakaidos et al., 2004; Lontos et al., 2007; Sideridou et al., 2011; Petrakis et al., 2016); (2) compared to other tested oncogenes, such as *RAS* or *BRAF*, it is a more powerful inducer of senescence (Patel et al., 2016); and (3) its overexpression is linked to poor survival across common cancer types (Figure S1A).

Importantly, this system offers the advantage of prompt and quantitative senescence entry (< 6 days), followed by escape from senescence in a reasonably short time period (within ~30 days; escape [ESC]; Figures 1B and S1B; Moreno et al., 2016; Komseli et al., 2018). These transitions recapitulate the whole evolution course of malignant transformation and can be observed equally under 2D and 3D organotypic cell culture conditions (Figures 1B, 1C, and S1C). Thus, for our working hypothesis (Introduction) to be validated, the following sequence of steps (phases) initiated by an oncogenic insult are predicted to occur (Figure 1A).

First, shutting off *CDC6* overexpression in cells that have “escaped” senescence should not result in phenotype reversal, suggesting acquisition of permanent molecular alterations. Second, following *CDC6* induction, DNA double-strand breaks (DSBs) should form (phase I; Figure 1A), and at least a fraction of them should be repaired in an error-prone manner (phase II; Figure 1A). Third, some genomic alterations produced in the senescent state (phase III; Figure 1A) should be selected for to functionally facilitate ESC (phase IV; Figure 1A).

CDC6 expression is dispensable after EMT-like ESC from senescence

To exclude mapping of stochastic alterations, we conducted three independent evolution experiments (Figure 1C). In all three experiments, a fraction of cells (~50 colonies from 5×10^5 cells) re-entered the cell cycle after the protracted *CDC6*-induced senescent phase (Figure 1D; Videos S1 and S2). These ESC cells grew faster, were invasive, and adopted epithelial-to-mesenchymal transition (EMT) features (Figures 1C–1E and S1D–S1F; Videos S1 and S2) known to facilitate cancer progression (Nieto et al., 2016; Thiery et al., 2009). They also produced tumors upon injection into nude mice (Figure 1F). Moreover, bioinformatics analysis revealed that the ESC cells exhibited a mixed stem cell-like gene expression signature encompassing embryonic, epithelial, mesenchymal-like, and MYC-dependent markers (Ritschka et al., 2017; Wong et al., 2008; Kim et al., 2010; Ivanova et al., 2002; Chambers et al., 2007; Milanovic et al., 2018;

(C) Representative images of HBECs grown in 2D culture and stained for GL13 (SenTraGor). *CDC6* induction forces cells into senescence (ON). After ~30 days, a subset of cells “escape” senescence (ESC) to re-enter the cell cycle and adopt an EMT phenotype. Shutting off *CDC6* in ESC cells (ESC/*CDC6*-OFF) does not reverse this phenotype. Shown is an overview of three independent ESC experiments. BLISS was applied to identify DSBs occurring after 3 or 6 days of *CDC6* induction. Then, whole-genome sequencing (WGS) was performed on ESC cells to map genetic alterations with respect to damage that occurred at early time points. OFF cells that served as controls for WGS analysis were only initiated for culture when ESC cells emerged to avoid non-specific accumulation of genetic alterations in the prolonged stationary period of senescent ON cells. Scale bars: 20 μ m (OFF), 10 μ m (ON), and 20 μ m (ESC and ESC/*CDC6*-OFF).

(D) FACS-based cell cycle analysis of HBECs at different time points, following 5-ethynyl-2'-deoxyuridine (EdU) incorporation and *CDC6* induction, demonstrating progressive S-phase reduction, acquisition of senescence, and ESC.

(E) Representative phase contrast views and immunodetection of epithelial (E-cadherin) and mesenchymal markers (vimentin) in HBECs, showing that senescence “escape” (ESC) coincides with EMT. Scale bars: 20 μ m (OFF) and 15 μ m (ON and ESC).

(F) Tumorigenicity assay of ESC and OFF cells in severe combined immunodeficiency (SCID) mice and histological analysis of the tumors that developed (right).

(G) Heatmaps showing that ESC cells display a mixed stem cell-like gene expression signature consisting of embryonic, mesenchymal, epithelial, and Myc-dependent markers (for references, see text).

Figure 1G). Notably, switching off *CDC6* overexpression does not result in ESC phenotype reversal, preserving the growth and invasion capacity of the “escapee” cells, in line with our hypothesis (Figures 1B, 1C, and S1D–S1F).

DSBs occur early upon senescence entry and are repaired in an error-prone manner

We suspected that, as a licensing factor, deregulated *CDC6* would alter replication dynamics and induce replication stress. In turn, replication stress could lead to accumulation of breaks on the DNA (Halazonetis et al., 2008). To determine whether and to what extent DNA DSBs occur, we performed BLISS (breaks labeling *in situ* and sequencing) analysis (Yan et al., 2017) at different time points after *CDC6* overexpression (Figure 1C). BLISS data analysis verified DSBs emergence, with a dramatic increase 3 days after *CDC6*-induced senescence entry and an almost 50% reduction at the peak of senescence (day 6), suggesting that a repair process took place (Figure 2A).

To mechanistically explain DSB formation, we analyzed the classic markers of replication stress. We found strong aberrations in the form of reduced fork speed and asymmetry following *CDC6* induction (Figure 2B). In addition, the fraction of cells with increased DNA content (>4N) and DNA damage marker expression, indicative of re-replication (Galanos et al., 2018; Petrakis et al., 2016), increased progressively (Figures 1D, 2C, and S2). Given that DSBs detected by BLISS were particularly enriched at transcription start sites (TSSs) (Figures 2D and 2E; in agreement with previous observations by Gothe et al., 2019), we postulated that replication-transcription collisions could occur at these positions. In line with this, global inhibition of transcriptional elongation by RNA polymerase II (RNAPII) using 5,6-dichloro-1- β -D-ribofuranosylbenzimidazole (DRB) significantly reduced the levels of DNA damage response (DDR) (Figure 2F). Our results showed that overexpression of *CDC6* induced replication stress, accumulation of DSBs, and DNA damage response, validating phase I of our hypothesis (Figure 1A).

Next, we investigated the choice of repair pathway for the *CDC6*-induced DNA breaks. Concurrent with DSB emergence, we recorded a prompt (within ~24 h) and robust increase in RPA foci (Figures 3Ai, 3Aii, and S2), a single-strand DNA binding factor and surrogate marker for replication stress (Gorgoulis et al., 2018). This finding, in combination with our BLISS results, suggested that repair may take place predominantly via homologous recombination (HR) during S phase and before the peak of senescence establishment. However, the levels of key components of the main error-free HR pathway, synthesis-dependent strand annealing (SDSA), like *RAD51*, *BRCA1*, and *BRCA2*, are reduced after the third day of *CDC6* induction (Figures 3Bi and 3Bii). In contrast, *RAD52* levels and foci increased upon *CDC6* overexpression between days 3 and 6 (Figures 3Bii and 3Ci–3Ciii). Thus, in this conditional “BRCAness” environment with low *RAD51* levels (Wu et al., 2008; Ochs et al., 2016; Galanos et al., 2016, 2018; Gorgoulis et al., 2018;), DNA repair will predominantly rely on *RAD52* activity, which is central to break-induced-replication (BIR) and single-strand-annealing (SSA) repair pathways. BIR and SSA are highly error-prone mechanisms contributing to genomic instability and oncogenic transformation (Galanos et al., 2016, 2018; Sotiriou et al., 2016), and

we found them to be activated significantly in ON cells in a *RAD52*-dependent manner (Figure 3D). At the same time, SDSA processivity was reduced strongly, satisfying the requirement for phase II of our working hypothesis (Figure 1A), as we saw a shift from high- to low-fidelity DSB repair.

ESC cells harbor genomic alterations selected early upon senescence entry

Following a senescent period of ~4 weeks, ESC clones emerged in all three replicates (Figures 1B–1E, S1B, and S1C). To examine whether traits of DNA damage produced early in senescence are selected and maintained in ESC populations, we employed whole-genome sequencing (WGS). Compared with the non-induced cells, WGS uncovered a broad spectrum of single-nucleotide variants (SNVs) and copy number variants (CNVs) (Figures 4A and S3A; Table S1).

Chromosomal distribution of SNVs took a “kataegis” form, and we could deduce a mutation signature (Figures S3B and S3C) resembling the previously reported “signature 15” associated with mismatch defects seen in stomach and lung cancer (Alexandrov et al., 2013). Moreover, SNV analysis revealed that our “cancer evolution” model recapitulated two of the most frequently occurring cancer mutations, in *MUC16* and in *NEB* (Figures S3D–S3F), validating its relevance. Both mutations are associated with poor outcomes in individuals with cancer (Chugh et al., 2015; Kufe, 2009; Mazzocchi et al., 2017), with *MUC16* (also known as *CA125*) being an established marker for various cancer types, including lung cancer, that is most relevant to our cellular model. Although no mutations were found in the *TP53* gene, the most altered gene in cancer (Figure S3D; Zhu et al., 2020), its negative regulator, *MDM2*, increases in ESC cells, leading to its downregulation (Figure S4A), providing an alternative mode of p53 attenuation.

Finally, by interrogating the spectrum of recorded CNVs, we made two observations. First, as predicted by our model (Halazonetis et al., 2008; Tsantoulis et al., 2008), genetic alterations were located within common fragile sites (CFSs; Table S1). Second, 58 of ~344 CNVs per clone were shared by all three replicates (Figures 4A–4C; Table S1). Aligning the breakpoints flanking these CNVs, also confirmed by Sanger sequencing (Figure S5), with DSB coordinates obtained by BLISS resulted in a striking overlap for 51 of 58 of them (Figure 4D; Table S1). The cancer-specific mutational signature (Figure S3C), recapitulation of the *MUC16* and *NEB* mutations seen in affected individuals (Figures S3D–S3F), and the 58 shared CNVs identified in ESC cells (Figures 4B and 4C; Table S1) all point to genomic instability as a decisive determinant for “escaping” OIS. These observations are in agreement with phase III of our hypothesis (Figure 1A).

A large chromosomal inversion uncovers a circadian transcription factor as regulator of ESC

A fundamental question of our working hypothesis is whether genetic alterations obtained early in senescence are functionally relevant for ESC from the OIS state (Introduction). We noticed a more than 3.7-Mbp-long heterozygous balanced inversion in the short arm of chromosome 3 (chr3) in our list of 58 recurring CNVs (Figures 4B–4D and 5A; Table S2). Notably, the breaks flanking this inversion were not more prominent compared with

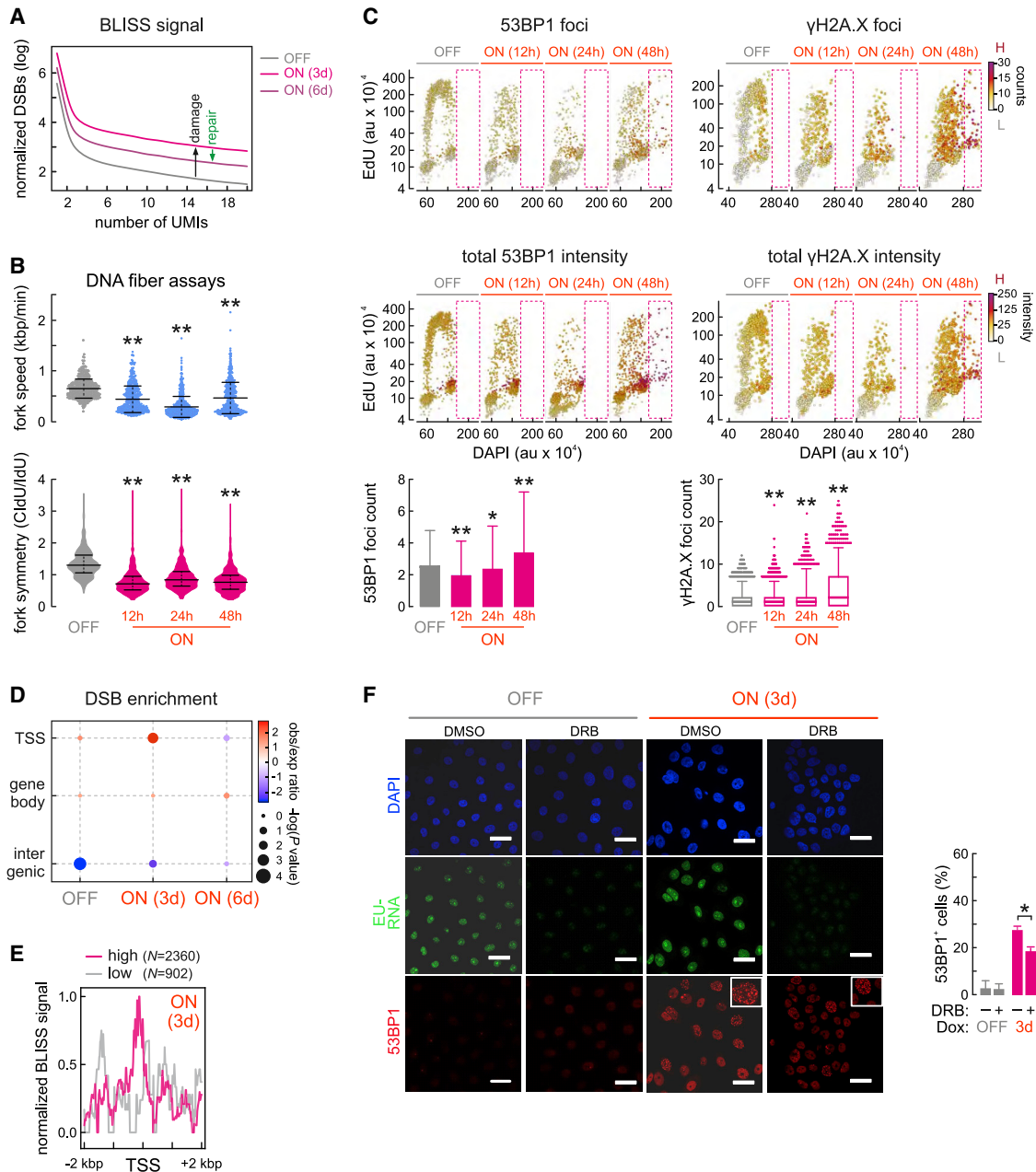


Figure 2. CDC6 induces DNA double-strand breaks (DSBs) and alters replication dynamics

(A) BLISS data generated at the indicated time points after *CDC6* activation show strongest DSBs accumulation at 3 days, followed by 50% reduction at day 6, indicative of DNA repair (UMI, unique molecular identifier).

(B) Violin plots of DNA fiber fluorography results show decreased fork progression rate and asymmetry at the indicated time points. Significantly different from OFF, ** $p < 0.01$; Student's t test (\pm SD, $n = 3$).

(C) Quantitative image-based cytometry of HBECCs at the indicated time points, showing cell cycle distribution of single cells based on EdU and DAPI levels (a.u., arbitrary unit). Focus counts (top) and 53BP1 and γ H2AX levels (center) are indicated by color coding. Bar graphs (bottom) show population means (\pm SD). Dashed rectangles indicate accumulation of cells with DNA content of more than 4N. Significantly different from OFF, ** $p < 0.01$; Student's t test (\pm SD, $n = 3$). H, high level; L, low level.

(D) Dot plot showing increased frequency of DSBs at gene TSSs based on BLISS data.

(E) Histogram showing BLISS-defined DSB enrichment at gene TSSs upon *CDC6* induction.

(F) Representative immunofluorescence imaging (left) of EU-labeled nascent RNA and 53BP1 foci in control HBECCs (DMSO) or DRB-treated HBECCs to inhibit transcription (DRB) at the indicated times. Bar graphs (right) show the percentage (\pm SD, $n = 3$) of cells with 53BP1 foci. Significantly different from OFF, * $p < 0.05$; two-tailed unpaired Student's t test. Scale bar, 20 μ m.

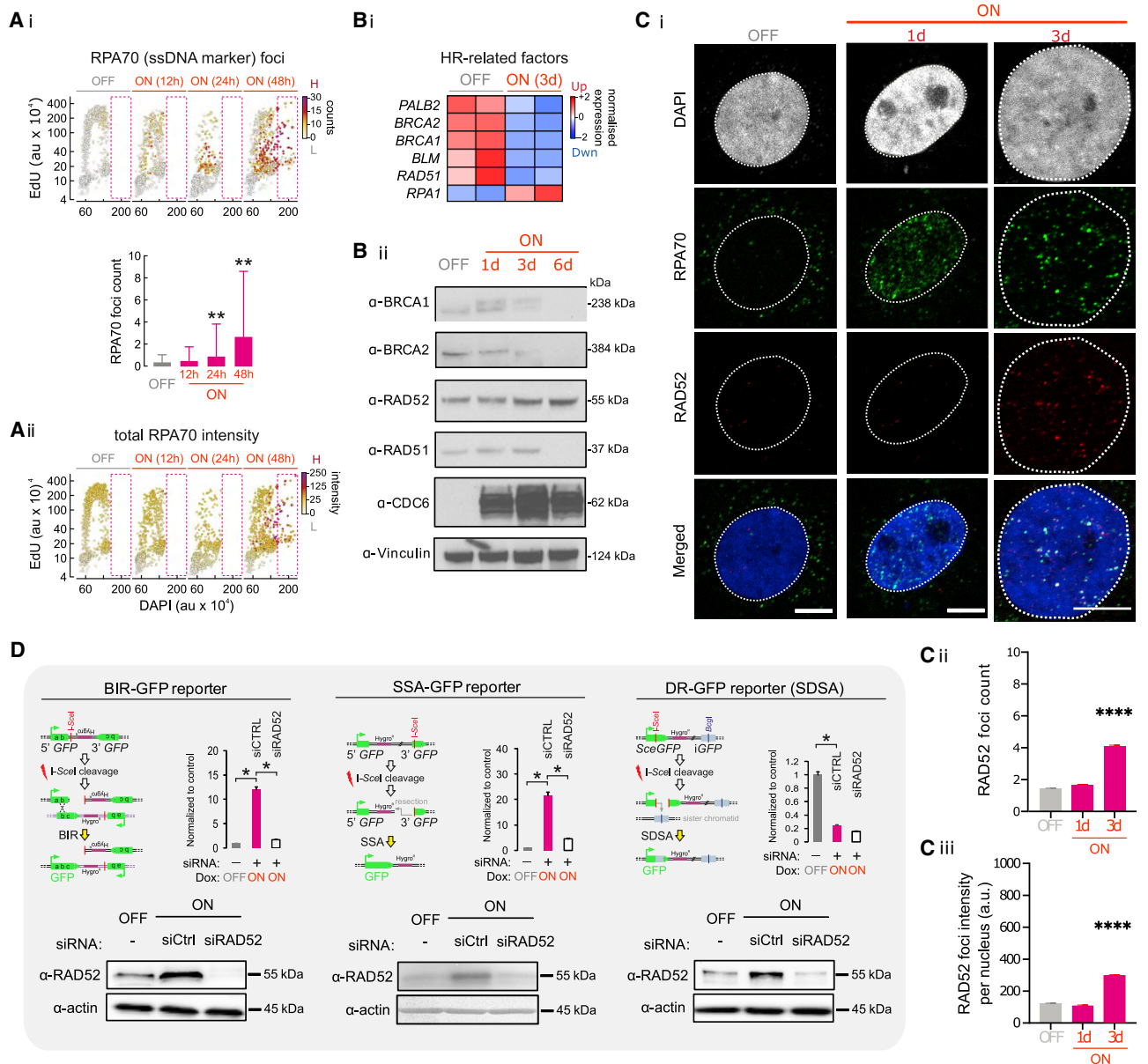


Figure 3. Sustained *CDC6* expression induces replication stress and error-prone DNA repair

(A i and A ii) Quantitative image-based cytometry of HBECs at the indicated time points shows cell cycle distribution of single cells based on EdU and DAPI levels. Focus counts (top) and RPA70 levels (bottom) are color coded. Bar graphs (center) show population means (\pm SD, $n = 3$). Dashed rectangles denote accumulation of cells with DNA content of more than 4N. Significantly different from OFF, $**p < 0.01$; unpaired two-tailed Student's *t* test.

(B i and B ii) Heatmap and western blots showing reduction in the expression levels of the genes involved in error-free homologous recombination (HR) DNA repair upon *CDC6* induction in HBECs (ON). Up, upregulated; Dwn, downregulated.

(C) Immunofluorescence imaging of RAD52 and RPA70 upon *CDC6* overexpression in ON cells (i). Bar graphs depict RAD52 mean focus count (ii) and focus intensity (iii) per nucleus, respectively. Significantly different from OFF, $****p < 0.0001$, unpaired two-tailed Student's *t* test. Scale bar, 7 μ m.

(D) Reporter assays demonstrating an increase (\pm SD, $n = 3$) in RAD52-dependent break-induced replication (BIR; left) and in single-strand annealing (SSA) repair of DSBs (center). Error-free repair monitored by a synthesis-dependent strand annealing (SDSA) reporter (right) is suppressed. Western blots (bottom) depict RAD52 expression levels. $*p < 0.05$, unpaired two-tailed Student's *t* test. Repair is monitored 3 days after *CDC6* induction.

the breakpoints of the other shared CNVs (Figure 4D) (see [Next Generation Sequencing and Bioinformatics analysis](#) for BLISS signal assessment). Naturally occurring inversions are generally less susceptible to further recombination, which suggests that genes within such structural variants are selectively “protected”

(Wellenreuther and Bernatchez, 2018). This HBEc-specific inversion encompasses the *BHLHE40* (basic helix-loop-helix family member 40, also known as *DEC1*) locus (Figure 5A), which encodes a transcription factor belonging to the CLOCK (circadian locomotor output cycles kaput) protein family and regulates

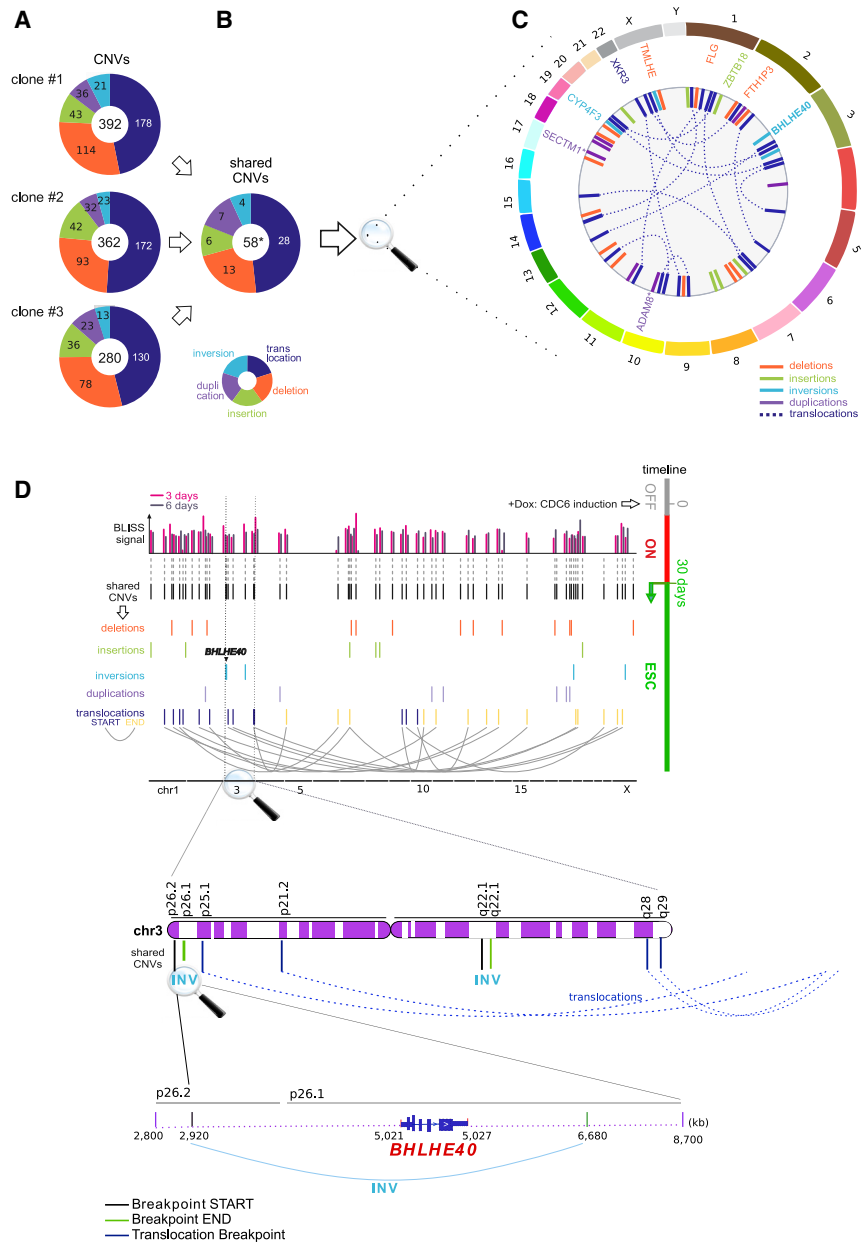


Figure 4. ESC cells harbor recurrent copy number variations (CNVs) aligning with DSBs

(A) Pie charts showing the distribution of CNVs identified in each of three independent replicates in five categories.

(B) Pie charts showing the distribution of the 58 CNVs shared by all the three replicates (Table S1). Significantly more than expected by chance, * $p < 0.0001$; super exact test.

(C) Circos plot of the type and location of all shared CNVs from (B), alongside any differentially expressed genes they harbor in ESC cells (*, confirmed by qRT-PCR, not in RNA sequencing [RNA-seq] data). Outer circle, human reference karyotype; inner circle, distribution of the 58 CNVs across the genome.

(D) Superimposing DSB coordinates, as defined by BLISS, with the breakpoints of the shared CNVs from (B) shows overlap in 51 of the 58 cases. The inversion in 3p26.1 is magnified.

circadian factors (Yamada and Miyamoto, 2005; Wood et al., 2009; Kato et al., 2014; Sato et al., 2016), and *BHLHE41* are suppressed (Figure 5D). This suggests a direct role of *BHLHE40* in promoting ESC. In fact, the circadian circuitry governs, among other processes, cell cycle progression. Therefore, its deregulation affects cell cycle checkpoints and can lead to cancer (Hunt and Sassone-Corsi, 2007; Masri et al., 2013). Looking into genes encoding replication machinery components, we found 38 key ones that are strongly reactivated in ESC cells and bound by *BHLHE40* (e.g., *BLM*, *GINS1-GINS4*, *MCM2-MCM10*, *PCNA*, and *POLE*; Figures 5B and 5E). Among these was also *MDM2*, the main negative regulator of *p53* (Figures 5E, S4A, and S4D).

To test the functional significance of *BHLHE40* in our working hypothesis, we silenced this gene in ESC cells using small interfering RNAs (siRNAs). This led to a deregulated cell cycle profile and increased cell death, as shown via fluorescence-activated cell sorting (FACS) (from $1.89\% \pm 0.8\%$ cells to $21.25\% \pm 0.3\%$; Figure 5F) and caspase-3 staining (Figure 5G), respectively. Notably, *BHLHE40* silencing also led to upregulation of *PER1* (Figure 5H), known to sensitize cells to apoptosis (Gery et al., 2006; Hunt and Sassone-Corsi, 2007). These results show that *BHLHE40* upregulation is necessary for maintenance of the ESC phenotype. *BHLHE40* is also relevant for clinical outcomes because its overexpression is associated with adverse effects on survival in various malignancies, including lung cancer (Figure S4E). Notably, the chromosomal region containing *BHLHE40* is prone to genetic aberrations in human malignancies (Figures S3G and S3H; Table S2). Apart from the

daily circadian rhythm oscillations (Kato et al., 2014; Sato et al., 2016). Publicly available ENCODE chromatin immunoprecipitation sequencing (ChIP-seq) data reveal that *BHLHE40* exhibits strong and ubiquitous binding across the genome and regulates more than 15,500 human genes (Rouillard et al., 2016), including many cell cycle regulators (Figure 5B).

Notably, ~69% of the genes found to be differentially expressed upon ESC from senescence are reported direct *BHLHE40* targets, most of them being cell cycle, DNA replication, and repair regulators (Figures 5C and S4B; Tables S4 and S5). Our transcriptome data showed that *BHLHE40* is strongly upregulated in ESC cells (also at the protein level; Figure S4C), whereas *PER1/2*, which encode periodins, the key

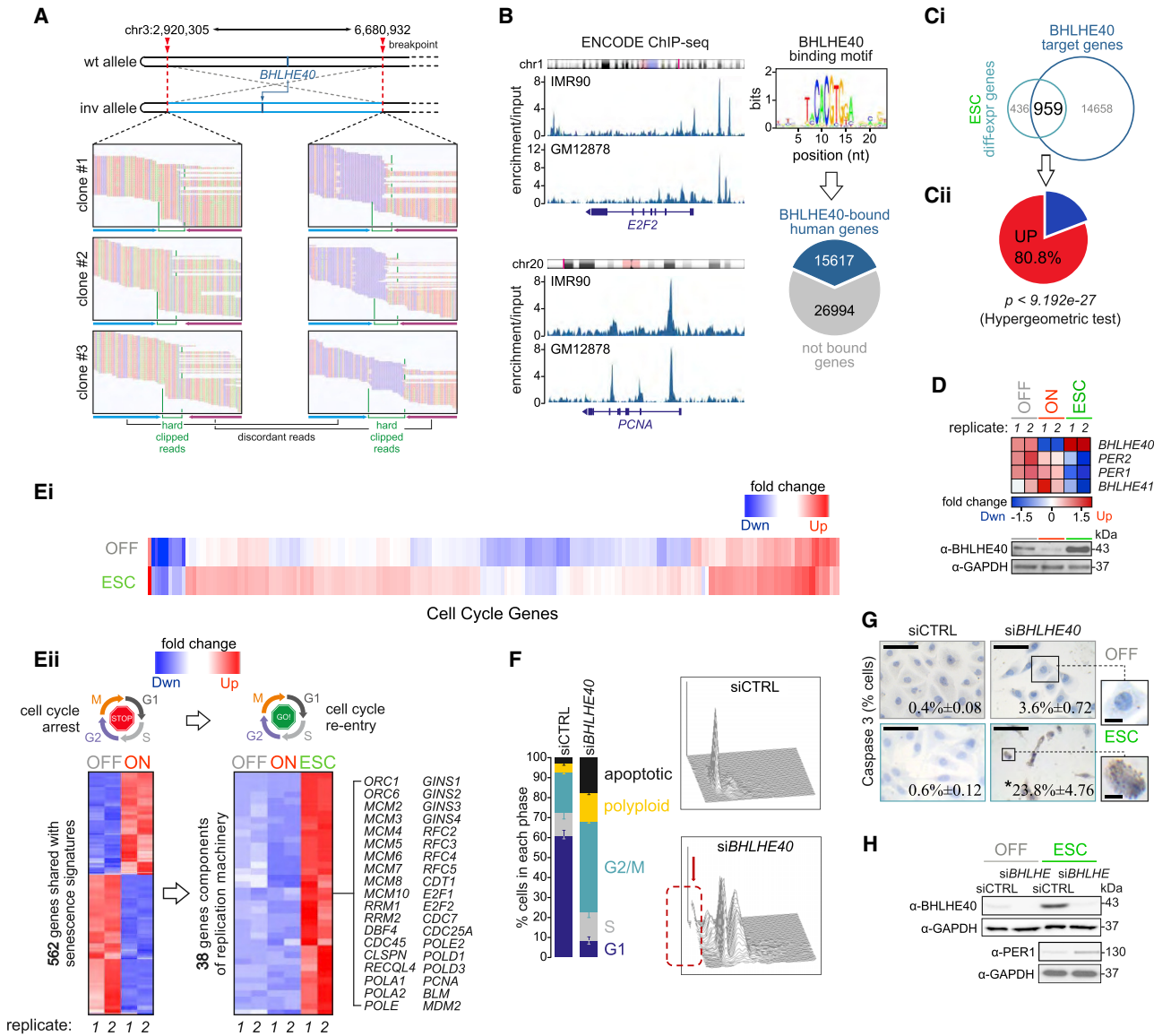


Figure 5. BHLHE40 harbored in the chr3 inversion is essential for ESC phenotype maintenance

(A) WGS data around the chr3 inversion breakpoints in ESC cells. Hard clipped (green lines) and discordantly mapped reads (blue/purple arrows) are indicated for all three replicates.

(B) Representative genome browser views (left) of BHLHE40 ENCODE ChIP-seq data from IMR90 and GM12878 cells in the *E2F2* and *PCNA* loci. These data were used to infer the BHLHE40 binding motif logo and to assign 36.7% of all human genes as its direct targets (Perteau et al., 2018).

(C) Venn diagram showing that 68.8% of all genes differentially expressed in ESC cells are also BHLHE40 targets according to ChIP-seq data (i). A pie chart shows the significant percentage of the upregulated genes that are identified as BHLHE40 target genes and differentially expressed genes during ESC (ii). $p < 9.192e-27$, hypergeometric test.

(D) Heatmap of RNA-seq data shows *BHLHE40*, but not other circadian genes like *PER1/2*, being selectively upregulated in ESC cells.

(E) Heatmap depicting the fold change expression of cell cycle genes between the ESC and “OFF” conditions (i). Fold change cutoff, 2.0; and p -adjust < 0.05 . A heatmap (left) shows that 25.3% of the 2,220 differentially expressed genes in ON cells are shared with reported senescence signatures (Hernandez-Segura et al., 2017) (ii). Of these, 38 encode replication machinery components (right) and are strongly induced in ESC cells.

(F) FACS-based cell cycle profiling of control (siCTRL) and *BHLHE40* knockdown (siBHLHE40) cells showing significantly altered cell cycle progression and increased cell death (red arrow pointing to the dashed line) (\pm SD, $n = 3$). Significantly more than in control, $*p < 0.001$; Fisher’s exact test.

(G) Representative images of siCTRL and siBHLHE40 cells immunostained for caspase-3. Inset numbers indicate the percentage of positive cells (from a minimum of 100 cells counted under each condition). $*p < 0.01$, Fisher’s exact test. Scale bars, 25 μ m and 5 μ m (insets).

(H) Western blots showing reciprocal changes in BHLHE40 and PER1 levels upon *BHLHE40* knockdown in ESC cells, thought to drive apoptosis (Hunt and Sassone-Corsi, 2007).

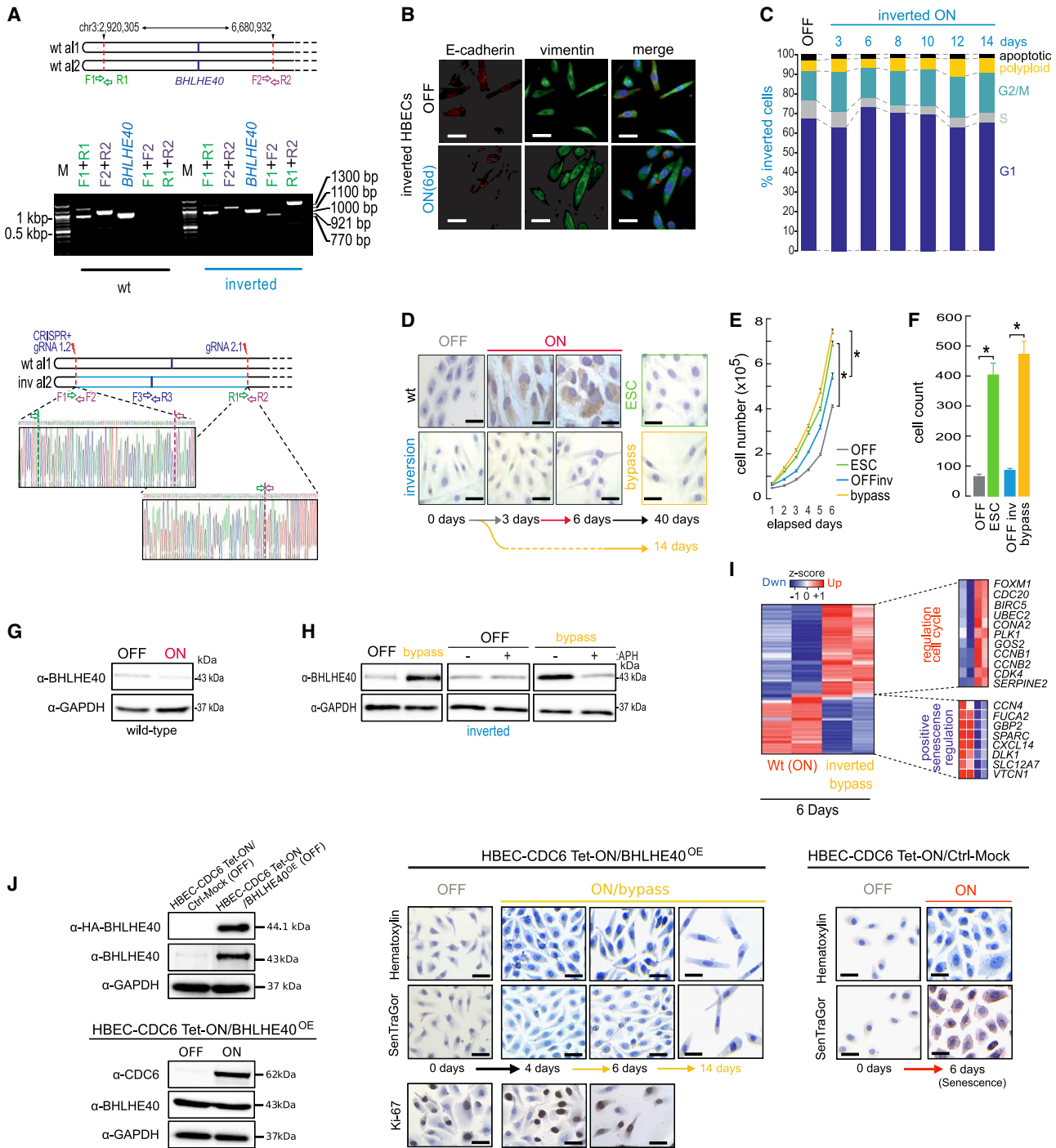


Figure 6. The 3.7-Mbp inversion in chr3 suffices for bypassing CDC6-induced senescence

(A) PCR and Sanger sequencing validation of a CRISPR-generated 3.7-Mbp heterozygous inversion in chr3 that closely mimics that discovered in ESC cells using WGS (WT, wild type). Sanger sequences are available in [Table S4D](#).

(B) Immunodetection of epithelial (E-cadherin) and mesenchymal markers (vimentin) in “inverted” OFF and 6-day ON cells is reminiscent of cells undergoing *trans*-differentiation. Scale bar, 15 μ m.

(C) FACS-based cell cycle analysis in “inverted” cells at different time points after *CDC6* induction (\pm SD, n = 3).

(D) Representative images of OFF, ON, and ESC or “bypass” (bottom) cells stained with SenTraGor to assess senescence bypass in “inverted” (yellow color defined) compared with WT (red and green color defined) cells. Scale bar, 15 μ m.

(E) Plots depicting mean proliferation (\pm SD, n = 3) in the different states of WT and “inverted” cells. Significantly different from OFF, *p < 0.05; unpaired two-tailed Student’s t test.

(legend continued on next page)

BHLHE40 inversion, which occurs *in vivo* (Figure S3G) and appears to be central in the ESC phenomenon, a variant of the reciprocal translocation involving chromosomes 9 and 22 typically identified in chronic myelogenous leukemia (CML) (Valencia et al., 2009; Krishna Chandran et al., 2019), was also shared by all three ESC populations (Figure S3I). Finally, all genes localized in the remaining shared CNVs have been associated with the senescence process (for details, see Table S2B). These findings are also consistent with phase III of our hypothesis (Figure 1A).

A CRISPR-generated inversion in chr3 suffices for senescence bypass

We next tested whether genetic alterations, obtained early upon senescence entry and maintained in ESC cells, are functionally relevant to this transition. In other words, does the inversion in chr3 facilitate ESC by promoting *BHLHE40* re-induction in response to oncogenic stimuli? To answer this, we first examined *BHLHE40* protein levels along a time course from OFF to ESC cells. Baseline levels in OFF cells are reduced upon *CDC6* induction but increased markedly in the ESC state (Figure S4C). Interestingly, *BHLHE40* suppression was partially alleviated by day 6 (Figure S4C). This coincides with the window of error-prone DSB repair (Figure 2A) and, thus, with the presumed acquisition time of the chr3 inversion.

Next we used CRISPR-Cas9 editing in HBECs (Figure S6A) to target sequences within 72 (at 2,920,305) and 50 bp (at 6,680,932) of the inversion breakpoints mapped previously using WGS (Figures 4C and 4D). We generated two independent clones carrying this 3.7-Mbp heterozygous inversion (Figures 6A and S6Bi) and used ChIP-seq to map the binding sites of *BHLHE40* genome wide. We discovered 2,576 robust peaks harboring the *BHLHE40* binding motif and mostly overlapping gene promoters (Figures S6C and S6D).

Notably, “inverted” cells demonstrated loss of epithelial features with accentuated spindle morphology, low E-cadherin and emergent vimentin expression (Figure 6B), reminiscent of the metastable state characterizing cells undergoing *trans*-differentiation (Nieto et al., 2016). Strikingly, and in accordance with our hypothesis, upon *CDC6* induction, the clones carrying this inversion never ceased to proliferate, nor did they acquire morphological features of senescence, supporting the notion that they bypass the senescence barrier (Figures 6C, 6D, S6Bii, and S6Biii). Notably, at the initial phases of *CDC6* induction, the observed low S-phase cell percentages can be attributed to the particularly energy-demanding state of this metastable phenotype (Nieto et al., 2016) and/or to DDR activation (Figures S6Biv and S6Bv). This is nevertheless not adequate for triggering senescence in this cell context (Figures 6B–6D).

Soon after this “slow growth” phase (Figures 6C and S6Biii), inverted cells progressively increase their growth rate and invasion capacity (Figures 6E and 6F).

Critically, both inverted clones overexpressed *BHLHE40* upon *CDC6* induction (Figures 6G, 6H, and S6Bvi), and this overexpression appears to drive gene expression changes that favor senescence suppression and cell cycle re-entry (Figures 6I and S6E). Indeed, stable overexpression of *BHLHE40* in the wild-type HBEC-*CDC6*-TetON system led to bypass of senescence upon *CDC6* activation as well (Figure 6J). Non-induced cells stably harboring high levels of *BHLHE40* (Figure 6J) demonstrated a spindle-like morphology, similar to non-induced inverted cells (Figures 6B and 6D). As negative controls, CRISPR-Cas9-engineered cells that failed to acquire the desired inversion did enter senescence upon *CDC6* induction (Figure S6F). A single inversion in one of the alleles harboring *BHLHE40* suffices for driving constitutive expression of this circadian transcription factor in response to oncogenic stimulation and ESC from senescence (phase IV of the working hypothesis; Figure 1A).

Genomic instability-mediated chromatin refolding underlies *BHLHE40* induction and ESC from senescence

It is now understood that changes in three-dimensional (3D) chromosome architecture, like those caused by inversions, may mechanistically explain disease manifestation, including cancer (Ibrahim and Mundlos, 2020). To test whether this can also explain *BHLHE40* upregulation, we investigated 3D reorganization in the extended *BHLHE40* locus. We used our “inverted” HBECs to generate high-resolution Hi-C maps from OFF and “senescence-bypass” cells (Table S4A). Genome-wide comparison of these data revealed that “bypass” cells exhibit an increase in sub-Mbp interactions (Figure 7A), accompanied by changes in the identity of compartments. Approximately 10% of A- or B-compartments switch to B or A, respectively, and this switching explains a considerable fraction (almost 50%) of the gene expression changes that underlie senescence bypass (Figure 7B). However, only marginal changes to topologically associating domain (TAD) positions (Beagan and Phillips-Cremins, 2020) were found (Figure 7C). These effects are, for the most part, the converse of what was observed for cells transitioning into senescence (Zirkel et al., 2018).

Looking specifically into the 3D organization of chromatin around the inversion region on chr3, we made three key observations. First, *BHLHE40* resides in one of the two centrally located TADs of this extended locus, whose long-range contacts do not change between OFF and “bypass” cells (Figure 7D). Thus, we can rule out the “classic” scenario of *BHLHE40* re-expression because of ectopic contacts with enhancers in adjacent TADs

(F) As in (E) but quantifying cell invasion capacity (\pm SD, $n = 3$). Significantly different from OFF, * $p < 0.05$; unpaired two-tailed Student's t test.

(G) Western blots showing *BHLHE40* suppression upon *CDC6* induction in WT cells. GAPDH is a loading control.

(H) Left: as in (G) but showing strong *BHLHE40* re-expression upon *CDC6* induction in cells carrying the CRISPR-generated inversion. Center/right: blots showing that aphidicolin (APH) treatment suppresses *CDC6*-driven *BHLHE40* re-expression in “inverted” bypass cells. GAPDH is a loading control.

(I) Heatmap of gene expression data depicting inverse patterns for cell cycle and senescence regulators between 6-day *CDC6*-ON WT and bypass “inverted” cells.

(J) Left: western blots showing *BHLHE40* overexpression (*BHLHE40*^{OE}) in transfected WT cells. GAPDH is a loading control. Right: representative images of OFF, ON, and “bypass” cells stained with SenTraGor to assess senescence bypass in *CDC6*-ON *BHLHE40*^{OE} compared with WT cells. Ki-67 staining for cell proliferation was performed. α -HA, anti-hemagglutinin. Scale bar, 20 μ m.

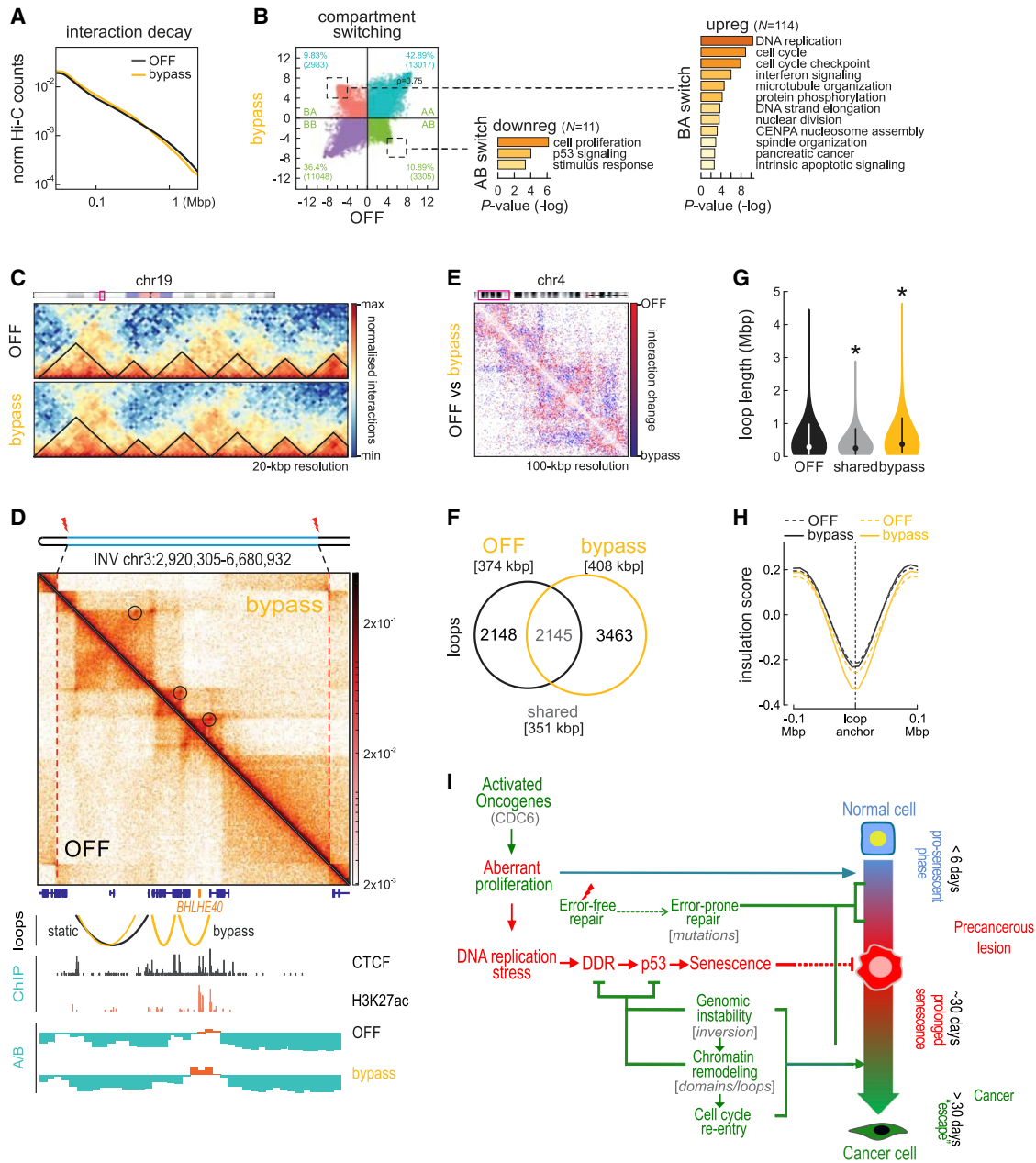


Figure 7. Analysis of spatial chromatin interactions in “inverted” OFF and bypass cells

- (A) Line plot showing mean interaction strength decay (HiC counts) in relation to increasing separation of interacting fragments in OFF (black) and bypass “inverted” cells (yellow).
- (B) Changes in A/B-compartments in bypass versus OFF HiC data. Strong B-to-A and A-to-B switching (dotted squares) is indicated, and the GO terms associated with differentially expressed genes embedded in each switched domain are shown.
- (C) Exemplary HiC heatmaps from OFF and bypass cells showing negligible changes in TAD positions for a subregion on chr19.
- (D) Composite HiC heatmap depicting interactions from OFF (bottom) and bypass “inverted” cells (top) in the region harboring *BHLHE40* on chr3. The data are aligned with CTCF and H3K27ac ChIP-seq data from normal OFF HBECs as well as with A/B-compartment positions from OFF and bypass cells. CTCF-anchored loops emerging upon senescence bypass are denoted on the HiC map (circles) and aligned below (yellow arches).
- (E) Subtracted HiC heatmap showing changes in interactions upon transition from OFF to bypass “inverted” cells for a subregion on chr4.
- (F) Venn diagram showing the number of loops unique to OFF and bypass “inverted” cells or shared. Median loop lengths (square brackets) are indicated.
- (G) Violin plots showing distribution of lengths for the loops from (H). Significantly different from OFF, * $p < 0.05$; Wilcoxon-Mann-Whitney test.
- (H) Line plots showing mean insulation of chromatin interactions in the 200 kbp around loop anchors unique to OFF (black) or bypass “inverted” loops (yellow) using HiC data from OFF (dotted lines) and bypass cells (solid lines).

(legend continued on next page)

(Ibrahim and Mundlos, 2020). Second, we found emergence of new loops in this 4-Mbp region that contribute to the enhanced insulation of the two central TADs from one another (Figure 7D, circles). Strikingly, a survey of this same 4-Mbp region encompassing *BHLHE40* in publicly available Hi-C data showed that these two centrally located TADs appear fused in normal tissue but well insulated in cancer cells (Figures S7A and S7B), mirroring our OFF and “bypass” data, respectively. Third, we found that strong loop emergence coincided with strengthening and broadening of the small A-compartment harboring *BHLHE40*, which is in line with its more potent activation Figure 7D, bottom).

Given these effects in the *BHLHE40* domain, we speculated that changes to CTCF loops genome-wide might explain the changes underlying senescence bypass. Indeed, subtracting OFF from “bypass” Hi-C data revealed new long-range contacts emerging (Figure 7E). Across all chromosomes, ~3,500 new loops arise, whereas ~2,150 specific to OFF cells are lost (Figure 7F). In line with our subtracted maps, bypass-specific loops are, on average, larger than OFF-specific ones (Figure 7G). Interestingly, and exactly as in the case of the *BHLHE40* domain, these bypass-specific loops arise at positions of existing insulation that become markedly strengthened. At the same time, insulation at the anchors of OFF-specific loops shows little fluctuation (Figure 7H). These types of changes suggests rewiring of regulatory gene-enhancer interactions. To cite two characteristic examples, we see emergence of bypass-specific loops in loci suppressed upon senescence bypass. In both cases, these loops trap the two genes, *RRM2* and *NCAPG* (involved in replication and mitosis, respectively), between adjacent insulated domains to mediate their downregulation (Figures S7C and S7D; Table S3). In contrast, *LAP3* finds itself within an emerging bypass-specific loop and is induced (Figure S7D).

Furthermore, given that replication origins in mammals are not defined by specific sequences but by structural chromatin context (Antequera, 2004; Cvetič and Walter, 2005), we reasoned that changes in chromatin segment orientation could additionally reorganize the replication process and, in turn, affect gene transcription (Lin et al., 2003; Chen et al., 2019; Fisher and Méchali 2003). The dependence of transcription on replication (S phase dependence) has been demonstrated in various developmental procedures (Fisher and Méchali 2003). This, combined with the fact that replication origins can be activated because of replication stress (Courtot et al., 2018), like that induced by *CDC6* overexpression (Petrakis et al., 2016; Hills and Diffley 2014), prompted us to investigate whether *BHLHE40* upregulation is linked to replication. Indeed, treating bypass “inverted” cells with aphidicolin markedly reduced the protein levels of *BHLHE40*, which was not the case for OFF cells (Figure 6H). Likewise, wild-type ESC but not OFF cells responded in exactly the same way to aphidicolin by suppressing *BHLHE40* levels (Figure S6Bvii). Such 3D reorganization events can explain gene expression changes leading to senescence bypass.

DISCUSSION

Entry into senescence is a ubiquitous physiological stress response, and it is also triggered by oncogene activation to serve as a tumor-suppressing mechanism (Gorgoulis et al., 2019). Still, as with any form of senescence, if the resulting cells are not removed from their niche in a timely manner, then an undesirable pro-tumorigenic facet can arise (Rodier and Campisi, 2011; Muñoz-Espin and Serrano, 2014; Gorgoulis et al., 2018; 2019). This adverse effect has been attributed to the SASP, the secretory cocktail senescence cells release into their surroundings to trigger chronic inflammation (Gorgoulis et al., 2019; Coppé et al., 2010). However, recent reports by us and others have documented that some cells can “escape” this state of OIS to initiate malignancy (Galanos et al., 2016; Komseli et al., 2018; Milanovic et al., 2018; Patel et al., 2016; Yu et al., 2018), but the molecular mechanisms underlying such an ESC still remain obscure.

Here we present the first mechanistic evidence of how DNA lesions acquired early upon entry into OIS can drive this phenomenon of ESC. We exploit normal HBECs driven to senescence by overexpressing the *CDC6* oncogene. From the populations of these senescent cells, mesenchymal-like, aggressively proliferating cells eventually emerge within ~30 days. Thus, we can essentially mimic “cancer evolution” to find that (1) forced *CDC6* expression induces DSBs genome wide as early as 3 days of senescence entry; (2) these DSBs are repaired predominantly in an error-prone manner; and (3) misrepaired lesions are actively selected during this “cancer evolution” time course and appear to be essential for establishment and/or maintenance of the ESC clones (Figure 7I).

Large genomic cancer studies have shown that the path to malignancy is not uniquely defined but needs to fulfill particular milestones that allow the aggressive and unhindered proliferation capacity of cancer cells (Gorgoulis et al., 2018). We propose that this also applies to ESC from senescence. Indeed, our independent ESC clones display recurrent structural and sequence variants that are linked to their phenotype; for example, precise recapitulation of frequent cancer mutations in *MUC16* and *NEB* or the resemblance of the ESC SNV signature to that discovered previously in tumors in affected individuals (Alexandrov et al., 2013). Another prerequisite for HBEC ESC and for most examples of malignant transformation (Aylon and Oren, 2011) is inactivation of the p53 response (Halazonetis et al., 2008). This also seems to occur in our model—not via *CDC6*-dependent mutation of the *TP53* locus itself but indirectly via MDM2 upregulation to disable p53. This course of events is not confined to the bronchial epithelium but can be recapitulated in human pancreatic duct epithelial cells (HPDECs) that carry an inducible *CDC6* construct and in which p53 function is inactivated via HPV16-E6 transduction (Ouyang et al., 2000). This is a relevant cell system because *CDC6* overexpression and senescence are frequently detected in precancerous pancreatic lesions

(I) Update of the DNA damage model for cancer development (Halazonetis et al., 2008). Cells respond to oncogenic stimuli by eliciting senescence as an anti-tumor barrier. The high DNA damage (DSBs) burden amassing during senescence engages error-prone repair mechanisms. Consequently, genetic aberrations accumulate with concurrent chromatin remodeling that provide a “pool” of genomic defects from which those that facilitate ESC from senescence, cell cycle re-entry, and aggressive features are selected and maintained.

(Myriantopoulos et al., 2019). As predicted, following *CDC6* induction, HPDECs follow a trajectory that bypasses senescence (Figure S4F).

A prominent and recurrent feature in our ESC clones is the 3.7-Mbp heterozygous inversion on chr3. Although essentially all types of structural aberrations have been functionally linked to cancer development (Stratton et al., 2009; Danieli and Pantonis, 2020), inversions confer particular properties regarding their selection. Their predominantly heterozygous nature allows lower recombination rates and, thus, selective maintenance so that the affected genes operate in an advantageous “enhanced” mode (Puig et al., 2015; Wellenreuther and Bernatchez, 2018). Accordingly, the *BHLHE40* gene harbored in our 3.7-Mbp inversion encodes a circadian transcription factor known for controlling a large number of human genes and a variety of processes, including the cell cycle (Hunt and Sassone-Corsi, 2007; Wood et al., 2009; Kato et al., 2014; Sato et al., 2016). In our system, control of key differentially regulated genes in ESC cells can be attributed to *BHLHE40*. Despite the fact that its expression has been linked to senescence (Colorado et al., 2005; Qian et al., 2008), dependence of this ESC phenomenon on *BHLHE40* can be explained by the following sequence of molecular events. Soon after senescence induction, between a 3- and 6-day time window, erroneous DNA repair establishes an inverted locus where this circadian gene is now responsive to *CDC6* overexpression and upregulated markedly. A major factor in this process appears to be CTCF and its ability to direct loop formation along chromosomes (Rada-Iglesias et al., 2018; Braccioli and de Wit, 2019). Remodeling of the *BHLHE40* topological domain via emergence of *de novo* loops coincides with its activation. The resulting abundance of this potent transcription factor is reminiscent of an oncogenic stimulus that can only exert its pro-tumorigenic potential when relieved of the senescence barrier. Such a mode of action would then explain contentious reports showing that *BHLHE40* triggers senescence or supports cell proliferation, EMT, tumor formation, and poor survival (Sato et al., 2016; Yamada and Miyamoto, 2005; Qian et al., 2008). It can also explain ESC-relevant gene expression changes that correlate with loop rewiring, in line with the proposed role of *BHLHE40* in regulating CTCF binding genome wide (Hu et al., 2020).

Our work suggests that it is in the early phase of OIS that the “genetic seeds” of the forthcoming malignant transformation are “planted” in chromosomes (Figure 7I). Whether ESC will always be the inevitable destiny of a subset of cells or whether there are cell-autonomous or non-cell-autonomous factors that can dictate this fate remains to be elucidated. The prospect that senescent cells can escape from their non-proliferative state may have far-reaching implications. Hence, targeting senescent cells can be of major clinical importance by eliminating a potential source of recurrence. In light of the expanding field of senotherapeutics (Zhu et al., 2015; Childs et al., 2015; Gorgoulis et al., 2019; Myriantopoulos et al., 2019), this may inspire future therapeutic choices.

Limitations of the study

Our study provides evidence that OIS is a time window during which DNA lesions repaired poorly because of replication stress

are seeded throughout the genome. Some of these are further selected because they allow a subset of cells to “escape” senescence and re-enter cell cycle progression. Particularly, we identified *BHLHE40*, a circadian rhythm gene, as a key driver of cell cycle re-entry and malignant transformation of originally senescent cells. *BHLHE40* activation is a result of a large inversion harboring its locus. However, it remains unclear whether the chromatin refolding changes we recorded upon its induction are causal or the readout of gene activation. Moreover, we cannot rule out the possibility that escape from senescence can also occur independent of such a genomic inversion and via some other mechanism, which would still likely involve *BHLHE40* activation. Finally, although our data suggest that *BHLHE40* is an effector linking replication coordination with circadian rhythms, further work is warranted to understand the underlying mechanisms.

STAR★METHODS

Detailed methods are provided in the online version of this paper and include the following:

- KEY RESOURCES TABLE
- RESOURCE AVAILABILITY
 - Lead contact
 - Materials availability
 - Data and code availability
- EXPERIMENTAL MODEL AND SUBJECT DETAILS
- METHOD DETAILS
 - Plasmid generation
 - siRNA and plasmid transfections
 - Selection of escaped clones
 - Protein extraction, cell fractionation and immunoblot analysis
 - Immunofluorescence analysis
 - Immunocytochemistry
 - Cell growth analysis
 - 3D (organotypic) culture
 - Senescence detection with SenTraGor
 - Invasion assay
 - Tumorigenicity assay
 - Flow cytometry analysis (FACS) - Cell Cycle analysis
 - 5'-EU incorporation based nascent RNA assay
 - QIBC analysis
 - DR-GFP, SA-GFP and BIR-GFP reporter assays
 - DNA fiber fluorography (combing assay)
 - Breaks Labeling *In Situ* and Sequencing (BLISS)
 - Next Generation Sequencing and Bioinformatics analysis
 - RNA isolation, sequencing, and data analysis
 - Chromatin immunoprecipitation (ChIP), sequencing, and data analysis
 - Genome-wide chromosome conformation capture (Hi-C) and data analysis
 - CRISPR/Cas9 inversion generation
 - Sanger sequencing
 - Survival data analysis
- QUANTIFICATION AND STATISTICAL ANALYSIS

SUPPLEMENTAL INFORMATION

Supplemental information can be found online at <https://doi.org/10.1016/j.molcel.2021.10.017>.

ACKNOWLEDGMENTS

We would like to thank Dr. Panagiota Kafasla for technical support. We are also thankful to Dr. Claudia and Jiri Lukas for providing an additional antibody against RAD52 for better representation of focus formation. V.G.G. and C.P.Z. are financially supported by the European Union Horizon 2020 Research and Innovation Program under Marie Skłodowska-Curie grant agreement 722729 (SYNTRAIN). V.G.G. is also supported by the National Public Investment Program of the Ministry of Development and Investment/General Secretariat for Research and Technology in the framework of the Flagship Initiative to address SARS-CoV-2 (2020ΣΕ01300001); the Welfare Foundation for Social & Cultural Sciences (KIKPE), Athens, Greece; a H. Pappas donation; grants 775 (Hippo) and 3782 (PACOREL) from the Hellenic Foundation for Research and Innovation (HFRI); and NKUA-SARG grant 70/3/8916. This work is also co-financed by Greece and the European Union (European Social Fund [ESF]) through the Operational Program “Human Resources Development, Education and Lifelong Learning” in the context of the project “Reinforcement of Postdoctoral Researchers—2nd Cycle” (MIS-5033021), implemented by the State Scholarships Foundation (IKY). A.P. is supported by the Deutsche Forschungsgemeinschaft via the Clinical Research Unit KFO5002 project grant (CO 1568/2-1) and the Priority Program SPP2202 (grant PA 2456/11-1). Y.Z. is also supported by the IMPRS “Molecular Biology” Program (GGNB), part of the Göttingen Graduate Center for Neurosciences, Biophysics and Molecular Biosciences (GGNB). P.G. is supported by the Danish Cancer Society (R167-A11068) and the Lundbeck Foundation (R322-2019-2577). Z.G. is supported by the Novo Nordisk Foundation (0052647), and D.H.L. is supported by the Independent Research Fund Denmark (8045-00057A) and the Danish Cancer Society. J.B. and his team were supported by the Danish Cancer Society (R204-A12617-B153), the Novo Nordisk Foundation (16854), the Danish National Research Foundation (Project CARD, DNRF 125), the Swedish Research Council (VR-MH 2014-46602-117891-30) and the Cancerfonden (170176).

AUTHOR CONTRIBUTIONS

C.P.Z., P.G., A.A., I.M., N.L., and K.E., cell culture and manipulation, immunoblots, FACS, immunofluorescence analysis, immunocytochemistry, SenTraGor staining, PCR, and 3D cell culture; P.G. and Z.G., QIBC analysis; C.P.Z., invasion and tumorigenicity assays; C.P.Z., P.G., and A.M.-M., combing assays; A.A., Y.Z., A.M., E.G.G., and K.S., ChIP-seq, Hi-C, CRISPR-Cas9 editing, and RNA-seq; D.E.P., EU assay; R.M., S.G., and N.C., BLISS; A.K., T.K., Y.Z., E.G.G., A.T., A. Polyzos, and A. Polyzou, bioinformatics analyses; A. Paspapoulos, A.K., T.K., A.T., and A. Polyzou, survival analyses; C.P.Z., P.G., A.A., A.K., A. Paspapoulos, D.H.L., M.D., K.E., J.B., A. Papantonis, and V.G.G., data analysis and interpretation and manuscript preparation; P.G., J.B., A. Papantonis, and V.G.G., experimental design, supervision and project funding, and manuscript writing with input from all co-authors.

DECLARATION OF INTERESTS

The authors declare no competing interests.

Received: January 14, 2021

Revised: July 14, 2021

Accepted: October 16, 2021

Published: November 17, 2021

REFERENCES

Abdennur, N., and Mirny, L.A. (2020). Cooler: scalable storage for Hi-C data and other genomically labeled arrays. *Bioinformatics* 36, 311–316.

Alexandrov, L.B., Nik-Zainal, S., Wedge, D.C., Aparicio, S.A., Behjati, S., Biankin, A.V., Bignell, G.R., Bolli, N., Borg, A., Borresen-Dale, A.L., et al.; Australian Pancreatic Cancer Genome Initiative; ICGC Breast Cancer Consortium; ICGC MMML-Seq Consortium; ICGC PedBrain (2013). Signatures of mutational processes in human cancer. *Nature* 500, 415–421.

Anders, S., and Huber, W. (2010). Differential expression analysis for sequence count data. *Genome Biol.* 11, R106.

Anders, S., Pyl, P.T., and Huber, W. (2015). HTSeq—a Python framework to work with high-throughput sequencing data. *Bioinformatics* 31, 166–169.

Antequera, F. (2004). Genomic specification and epigenetic regulation of eukaryotic DNA replication origins. *EMBO J.* 23, 4365–4370.

Aylon, Y., and Oren, M. (2011). New plays in the p53 theater. *Curr. Opin. Genet. Dev.* 21, 86–92.

Bartkova, J., Rezaei, N., Liontos, M., Karakaidos, P., Kleitas, D., Issaeva, N., Vassiliou, L.V., Kolettas, E., Niforou, K., Zoumpourlis, V.C., et al. (2006). Oncogene-induced senescence is part of the tumorigenesis barrier imposed by DNA damage checkpoints. *Nature* 444, 633–637.

Beagan, J.A., and Phillips-Cremins, J.E. (2020). On the existence and functionality of topologically associating domains. *Nat. Genet.* 52, 8–16.

Bouwman, B.A.M., Agostini, F., Garamone, S., Petrosino, G., Gothe, H.J., Sayols, S., Moor, A.E., Itzkovitz, S., Bienko, M., Roukos, V., and Crosetto, N. (2020). Genome-wide detection of DNA double-strand breaks by in-suspension BLISS. *Nat. Protoc.* 15, 3894–3941.

Braccioli, L., and de Wit, E. (2019). CTCF: a Swiss-army knife for genome organization and transcription regulation. *Essays Biochem.* 63, 157–165.

Braig, M., Lee, S., Loddenkemper, C., Rudolph, C., Peters, A.H.F.M., Schlegelberger, B., Stein, H., Dörken, B., Jenwein, T., and Schmitt, C.A. (2005). Oncogene-induced senescence as an initial barrier in lymphoma development. *Nature* 436, 660–665.

Chambers, S.M., Boles, N.C., Lin, K.-Y.K., Tierney, M.P., Bowman, T.V., Bradfute, S.B., Chen, A.J., Merchant, A.A., Sirin, O., Weksberg, D.C., et al. (2007). Hematopoietic fingerprints: an expression database of stem cells and their progeny. *Cell Stem Cell* 1, 578–591.

Chen, Z., Trotman, L.C., Shaffer, D., Lin, H.K., Dotan, Z.A., Niki, M., Koutcher, J.A., Scher, H.I., Ludwig, T., Gerald, W., et al. (2005). Crucial role of p53-dependent cellular senescence in suppression of Pten-deficient tumorigenesis. *Nature* 436, 725–730.

Chen, X., Schulz-Trieglaff, O., Shaw, R., Barnes, B., Schlesinger, F., Källberg, M., Cox, A.J., Kruglyak, S., and Saunders, C.T. (2016). Manta: rapid detection of structural variants and indels for germline and cancer sequencing applications. *Bioinformatics* 32, 1220–1222.

Chen, Y.H., Keegan, S., Kahli, M., Tonzi, P., Fenyö, D., Huang, T.T., and Smith, D.J. (2019). Transcription shapes DNA replication initiation and termination in human cells. *Nat. Struct. Mol. Biol.* 26, 67–77.

Childs, B.G., Durik, M., Baker, D.J., and van Deursen, J.M. (2015). Cellular senescence in aging and age-related disease: from mechanisms to therapy. *Nat. Med.* 21, 1424–1435.

Chugh, S., Gnanapragassam, V.S., Jain, M., Rachagani, S., Ponnusamy, M.P., and Batra, S.K. (2015). Pathobiological implications of mucin glycans in cancer: Sweet poison and novel targets. *Biochim. Biophys. Acta* 1856, 211–225.

Collado, M., Gil, J., Efeyan, A., Guerra, C., Schuhmacher, A.J., Barradas, M., Benguría, A., Zaballos, A., Flores, J.M., Barbacid, M., et al. (2005). Tumour biology: senescence in premalignant tumours. *Nature* 436, 642.

Coppé, J.P., Desprez, P.Y., Krtolica, A., and Campisi, J. (2010). The senescence-associated secretory phenotype: the dark side of tumor suppression. *Annu. Rev. Pathol.* 5, 99–118.

Courtot, L., Hoffmann, J.S., and Bergoglio, V. (2018). The protective role of dormant origins in response to replicative stress. *Int. J. Mol. Sci.* 19, 3569.

Cvetic, C., and Walter, J.C. (2005). Eukaryotic origins of DNA replication: could you please be more specific? *Semin. Cell Dev. Biol.* 16, 343–353.

Danieli, A., and Papantonis, A. (2020). Spatial genome architecture and the emergence of malignancy. *Hum. Mol. Genet.* 29 (R2), R197–R204.

- Di Micco, R., Fumagalli, M., Cicalese, A., Piccinin, S., Gasparini, P., Luise, C., Schurra, C., Garre', M., Nuciforo, P.G., Bensimon, A., et al. (2006). Oncogene-induced senescence is a DNA damage response triggered by DNA hyper-replication. *Nature* **444**, 638–642.
- Dobin, A., Davis, C.A., Schlesinger, F., Drenkow, J., Zaleski, C., Jha, S., Batut, P., Chaisson, M., and Gingeras, T.R. (2013). STAR: ultrafast universal RNA-seq aligner. *Bioinformatics* **29**, 15–21.
- Evangelou, K., Lougiakis, N., Rizou, S.V., Kotsinas, A., Kletsas, D., Muñoz-Espín, D., Kastrinakis, N.G., Pouli, N., Marakos, P., Townsend, P., et al. (2017). Robust, universal biomarker assay to detect senescent cells in biological specimens. *Aging Cell* **16**, 192–197.
- Fisher, D., and Méchali, M. (2003). Vertebrate HoxB gene expression requires DNA replication. *EMBO J.* **22**, 3737–3748.
- Ford, E., Nikopoulou, C., Kokkalis, A., and Thanos, D. (2014). A method for generating highly multiplexed ChIP-seq libraries. *BMC Res. Notes* **7**, 312.
- Furukawa, T., Duguid, W.P., Rosenberg, L., Viallet, J., Galloway, D.A., and Tsao, M.S. (1996). Long-term culture and immortalization of epithelial cells from normal adult human pancreatic ducts transfected by the E6E7 gene of human papilloma virus 16. *Am. J. Pathol.* **148**, 1763–1770.
- Galanos, P., Vougas, K., Walter, D., Polyzos, A., Maya-Mendoza, A., Haagensen, E.J., Kokkalis, A., Roumelioti, F.M., Gagos, S., Tzetis, M., et al. (2016). Chronic p53-independent p21 expression causes genomic instability by deregulating replication licensing. *Nat. Cell Biol.* **18**, 777–789.
- Galanos, P., Pappas, G., Polyzos, A., Kotsinas, A., Svolaki, I., Giakoumakis, N.N., Glytsou, C., Pateras, I.S., Swain, U., Souliotis, V.L., et al. (2018). Mutational signatures reveal the role of RAD52 in p53-independent p21-driven genomic instability. *Genome Biol.* **19**, 37.
- Gery, S., Komatsu, N., Baldjyan, L., Yu, A., Koo, D., and Koeffler, H.P. (2006). The circadian gene *per1* plays an important role in cell growth and DNA damage control in human cancer cells. *Mol. Cell* **22**, 375–382.
- Goodspeed, A., Heiser, L.M., Gray, J.W., and Costello, J.C. (2016). Tumor-Derived Cell Lines as Molecular Models of Cancer Pharmacogenomics. *Mol. Cancer Res.* **14**, 3–13.
- Gorgoulis, V.G., Pefani, D.E., Pateras, I.S., and Trougakos, I.P. (2018). Integrating the DNA damage and protein stress responses during cancer development and treatment. *J. Pathol.* **246**, 12–40.
- Gorgoulis, V., Adams, P.D., Alimonti, A., Bennett, D.C., Bischof, O., Bishop, C., Campisi, J., Collado, M., Evangelou, K., Ferbeyre, G., et al. (2019). Cellular senescence: defining a path forward. *Cell* **179**, 813–827.
- Gothe, H.J., Bouwman, B.A.M., Gusmao, E.G., Piccinno, R., Petrosino, G., Sayols, S., Drechsel, O., Minneker, V., Josipovic, N., Mizi, A., et al. (2019). Spatial chromosome folding and active transcription drive DNA fragility and formation of oncogenic MLL translocations. *Mol. Cell* **75**, 267–283.e12.
- Halazonetis, T.D., Gorgoulis, V.G., and Bartek, J. (2008). An oncogene-induced DNA damage model for cancer development. *Science* **319**, 1352–1355.
- Hernandez-Segura, A., de Jong, T.V., Melov, S., Guryev, V., Campisi, J., and Demaria, M. (2017). Unmasking transcriptional heterogeneity in senescent cells. *Curr. Biol.* **27**, 2652–2660.e4.
- Hills, S.A., and Diffley, J.F. (2014). DNA replication and oncogene-induced replicative stress. *Curr. Biol.* **24**, R435–R444.
- Hu, G., Dong, X., Gong, S., Song, Y., Hutchins, A.P., and Yao, H. (2020). Systematic screening of CTCF binding partners identifies that BHLHE40 regulates CTCF genome-wide distribution and long-range chromatin interactions. *Nucleic Acids Res.* **48**, 9606–9620.
- Hunt, T., and Sassone-Corsi, P. (2007). Riding tandem: circadian clocks and the cell cycle. *Cell* **129**, 461–464.
- Ibrahim, D.M., and Mundlos, S. (2020). Three-dimensional chromatin in disease: What holds us together and what drives us apart? *Curr. Opin. Cell Biol.* **64**, 1–9.
- Ivanova, N.B., Dimos, J.T., Schaniel, C., Hackney, J.A., Moore, K.A., and Lemischka, I.R. (2002). A stem cell molecular signature. *Science* **298**, 601–604.
- Karakaidos, P., Taraviras, S., Vassiliou, L.V., Zacharatos, P., Kastrinakis, N.G., Kougiou, D., Kouloukoussa, M., Nishitani, H., Papavassiliou, A.G., Lygerou, Z., and Gorgoulis, V.G. (2004). Overexpression of the replication licensing regulators hCdt1 and hCdc6 characterizes a subset of non-small-cell lung carcinomas: synergistic effect with mutant p53 on tumor growth and chromosomal instability—evidence of E2F-1 transcriptional control over hCdt1. *Am. J. Pathol.* **165**, 1351–1365.
- Kato, Y., Kawamoto, T., Fujimoto, K., and Noshiro, M. (2014). DEC1/STRA13/SHARP2 and DEC2/SHARP1 coordinate physiological processes, including circadian rhythms in response to environmental stimuli. *Curr. Top. Dev. Biol.* **110**, 339–372.
- Kerpedjiev, P., Abdennur, N., Lekschas, F., McCallum, C., Dinkla, K., Strobel, H., Lubner, J.M., Ouellette, S.B., Azhir, A., Kumar, N., et al. (2018). HiGlass: web-based visual exploration and analysis of genome interaction maps. *Genome Biol.* **19**, 125.
- Kim, J., Woo, A.J., Chu, J., Snow, J.W., Fujiwara, Y., Kim, C.G., Cantor, A.B., and Orkin, S.H. (2010). A Myc network accounts for similarities between embryonic stem and cancer cell transcription programs. *Cell* **143**, 313–324.
- Knight, P.A., and Ruiz, D. (2013). A fast algorithm for matrix balancing. *IMA J. Numer. Anal.* **33**, 1029–1047.
- Kohli, J., Wang, B., Brandenburg, S.M., Basisty, N., Evangelou, K., Varela-Eirin, M., Campisi, J., Schilling, B., Gorgoulis, V., and Demaria, M. (2021). Algorithmic assessment of cellular senescence in experimental and clinical specimens. *Nat. Protoc.* **16**, 2471–2498.
- Komseli, E.S., Pateras, I.S., Krejsgaard, T., Stawiski, K., Rizou, S.V., Polyzos, A., Roumelioti, F.M., Chiourea, M., Mourkioti, I., Paparouna, E., et al. (2018). A prototypical non-malignant epithelial model to study genome dynamics and concurrently monitor micro-RNAs and proteins in situ during oncogene-induced senescence. *BMC Genomics* **19**, 37.
- Krishna Chandran, R., Geetha, N., Sakthivel, K.M., Suresh Kumar, R., Jagathnath Krishna, K.M.N., and Sreedharan, H. (2019). Impact of Additional Chromosomal Aberrations on the Disease Progression of Chronic Myelogenous Leukemia. *Front. Oncol.* **9**, 88–99.
- Kufe, D.W. (2009). Mucins in cancer: function, prognosis and therapy. *Nat. Rev. Cancer* **9**, 874–885.
- Lagopati, N., Kotsinas, A., Veroutis, D., Evangelou, K., Papaspyropoulos, A., Arfanis, M., Falaras, P., Kitsiou, P.V., Pateras, I., Bergonzini, A., et al. (2021). Biological Effect of Silver-modified Nanostructured Titanium Dioxide in Cancer. *Cancer Genomics Proteomics* **18** (3, Suppl), 425–439.
- Langmead, B., and Salzberg, S.L. (2012). Fast gapped-read alignment with Bowtie 2. *Nat. Methods* **9**, 357–359.
- Li, H., and Durbin, R. (2010). Fast and accurate long-read alignment with Burrows-Wheeler transform. *Bioinformatics* **26**, 589–595.
- Li, H., Handsaker, B., Wysoker, A., Fennell, T., Ruan, J., Homer, N., Marth, G., Abecasis, G., and Durbin, R.; 1000 Genome Project Data Processing Subgroup (2009). The sequence alignment/map format and SAMtools. *Bioinformatics* **25**, 2078–2079.
- Lin, C.M., Fu, H., Martinovsky, M., Bouhassira, E., and Aladjem, M.I. (2003). Dynamic alterations of replication timing in mammalian cells. *Curr. Biol.* **13**, 1019–1028.
- Liontos, M., Koutsami, M., Sideridou, M., Evangelou, K., Kletsas, D., Levy, B., Kotsinas, A., Nahum, O., Zoumpourlis, V., Kouloukoussa, M., et al. (2007). Deregulated overexpression of hCdt1 and hCdc6 promotes malignant behavior. *Cancer Res.* **67**, 10899–10909.
- Masri, S., Cervantes, M., and Sassone-Corsi, P. (2013). The circadian clock and cell cycle: interconnected biological circuits. *Curr. Opin. Cell Biol.* **25**, 730–734.
- Mazzoccoli, G., Castellana, S., Carella, M., Palumbo, O., Tiberio, C., Fusilli, C., Capocceffalo, D., Biagini, T., Mazza, T., and Lo Muzio, L. (2017). A primary tumor gene expression signature identifies a crucial role played by tumor stroma myofibroblasts in lymph node involvement in oral squamous cell carcinoma. *Oncotarget* **8**, 104913–104927.

- Michaloglou, C., Vredeveld, L.C., Soengas, M.S., Denoyelle, C., Kuilman, T., van der Horst, C.M., Majoor, D.M., Shay, J.W., Mooi, W.J., and Peeper, D.S. (2005). BRAFE600-associated senescence-like cell cycle arrest of human naevi. *Nature* 436, 720–724.
- Milanovic, M., Fan, D.N.Y., Belenki, D., Däbritz, J.H.M., Zhao, Z., Yu, Y., Dörr, J.R., Dimitrova, L., Lenze, D., Monteiro Barbosa, I.A., et al. (2018). Senescence-associated reprogramming promotes cancer stemness. *Nature* 553, 96–100.
- Moreno, A., Carrington, J.T., Albergante, L., Al Mamun, M., Haagensen, E.J., Komseli, E.S., Gorgoulis, V.G., Newman, T.J., and Blow, J.J. (2016). Unreplicated DNA remaining from unperturbed S phases passes through mitosis for resolution in daughter cells. *Proc. Natl. Acad. Sci. USA* 113, E5757–E5764.
- Muñoz-Espin, D., and Serrano, M. (2014). Cellular senescence: from physiology to pathology. *Nat. Rev. Mol. Cell Biol.* 15, 482–496.
- Myrianthopoulos, V., Evangelou, K., Vasileiou, P.V.S., Cooks, T., Vassilakopoulos, T.P., Pangalis, G.A., Kouloukoussa, M., Kittas, C., Georgakilas, A.G., and Gorgoulis, V.G. (2019). Senescence and senotherapeutics: a new field in cancer therapy. *Pharmacol. Ther.* 193, 31–49.
- Nagy, Á., Lánckzy, A., Menyhárt, O., and Györfy, B. (2018). Validation of miRNA prognostic power in hepatocellular carcinoma using expression data of independent datasets. *Sci. Rep.* 8, 9227.
- Negrini, S., Gorgoulis, V.G., and Halazonetis, T.D. (2010). Genomic instability—an evolving hallmark of cancer. *Nat. Rev. Mol. Cell Biol.* 11, 220–228.
- Nieto, M.A., Huang, R.Y., Jackson, R.A., and Thiery, J.P. (2016). EMT: 2016. *Cell* 166, 21–45.
- Ochs, F., Somyajit, K., Altmeyer, M., Rask, M.B., Lukas, J., and Lukas, C. (2016). 53BP1 fosters fidelity of homology-directed DNA repair. *Nat. Struct. Mol. Biol.* 23, 714–721.
- Ouyang, H., Mou, L.J., Luk, C., Liu, N., Karaskova, J., Squire, J., and Tsao, M.S. (2000). Immortal human pancreatic duct epithelial cell lines with near normal genotype and phenotype. *Am. J. Pathol.* 157, 1623–1631.
- Patel, P.L., Suram, A., Mirani, N., Bischof, O., and Herbig, U. (2016). Derepression of hTERT gene expression promotes escape from oncogene-induced cellular senescence. *Proc. Natl. Acad. Sci. USA* 113, E5024–E5033.
- Pertea, M., Shumate, A., Pertea, G., Varabyou, A., Breitwieser, F.P., Chang, Y.C., Madugundu, A.K., Pandey, A., and Salzberg, S.L. (2018). CHES: a new human gene catalog curated from thousands of large-scale RNA sequencing experiments reveals extensive transcriptional noise. *Genome Biol.* 19, 208.
- Petrakis, T.G., Komseli, E.S., Papaioannou, M., Vougas, K., Polyzos, A., Myrianthopoulos, V., Mikros, E., Trougakos, I.P., Thanos, D., Branzel, D., et al. (2016). Exploring and exploiting the systemic effects of deregulated replication licensing. *Semin. Cancer Biol.* 37–38, 3–15.
- Puig, M., Casillas, S., Villatoro, S., and Cáceres, M. (2015). Human inversions and their functional consequences. *Brief. Funct. Genomics* 14, 369–379.
- Qian, Y., Zhang, J., Yan, B., and Chen, X. (2008). DEC1, a basic helix-loop-helix transcription factor and a novel target gene of the p53 family, mediates p53-dependent premature senescence. *J. Biol. Chem.* 283, 2896–2905.
- Rada-Iglesias, A., Grosveld, F.G., and Papantonis, A. (2018). Forces driving the three-dimensional folding of eukaryotic genomes. *Mol. Syst. Biol.* 14, e8214.
- Ramirez, R.D., Herbert, B.S., Vaughan, M.B., Zou, Y., Gandia, K., Morales, C.P., Wright, W.E., and Shay, J.W. (2003). Bypass of telomere-dependent replicative senescence (M1) upon overexpression of Cdk4 in normal human epithelial cells. *Oncogene* 22, 433–444.
- Ramírez, F., Bhardwaj, V., Arrigoni, L., Lam, K.C., Grüning, B.A., Villaveces, J., Habermann, B., Akhtar, A., and Manke, T. (2018). High-resolution TADs reveal DNA sequences underlying genome organization in flies. *Nat. Commun.* 9, 189.
- Rao, S.S., Huntley, M.H., Durand, N.C., Stamenova, E.K., Bochkov, I.D., Robinson, J.T., Sanborn, A.L., Machol, I., Omer, A.D., Lander, E.S., and Aiden, E.L. (2014). A 3D map of the human genome at kilobase resolution reveals principles of chromatin looping. *Cell* 159, 1665–1680.
- Risso, D., Ngai, J., Speed, T.P., and Dudoit, S. (2014). Normalization of RNA-seq data using factor analysis of control genes or samples. *Nat. Biotechnol.* 32, 896–902.
- Ritschka, B., Storer, M., Mas, A., Heinzmann, F., Ortells, M.C., Morton, J.P., Sansom, O.J., Zender, L., and Keyes, W.M. (2017). The senescence-associated secretory phenotype induces cellular plasticity and tissue regeneration. *Genes Dev.* 31, 172–183.
- Rodier, F., and Campisi, J. (2011). Four faces of cellular senescence. *J. Cell Biol.* 192, 547–556.
- Rouillard, A.D., Gundersen, G.W., Fernandez, N.F., Wang, Z., Monteiro, C.D., McDermott, M.G., and Ma'ayan, A. (2016). The harmonizome: a collection of processed datasets gathered to serve and mine knowledge about genes and proteins. *Database (Oxford)* 2016, baw100.
- Sato, M., Vaughan, M.B., Girard, L., Peyton, M., Lee, W., Shames, D.S., Ramirez, R.D., Sunaga, N., Gazdar, A.F., Shay, J.W., and Minna, J.D. (2006). Multiple oncogenic changes (K-RAS(V12), p53 knockdown, mutant EGFRs, p16 bypass, telomerase) are not sufficient to confer a full malignant phenotype on human bronchial epithelial cells. *Cancer Res.* 66, 2116–2128.
- Sato, F., Bhawal, U.K., Yoshimura, T., and Muragaki, Y. (2016). DEC1 and DEC2 crosstalk between circadian rhythm and tumor progression. *J. Cancer* 7, 153–159.
- Sideridou, M., Zakopoulou, R., Evangelou, K., Liontos, M., Kotsinas, A., Rampakakis, E., Gagos, S., Kahata, K., Grabusic, K., Gkouskou, K., et al. (2011). Cdc6 expression represses E-cadherin transcription and activates adjacent replication origins. *J. Cell Biol.* 195, 1123–1140.
- Sotiriou, S.K., Kamileri, I., Lugli, N., Evangelou, K., Da-Ré, C., Huber, F., Padayachy, L., Tardy, S., Nicati, N.L., Barriot, S., et al. (2016). Mammalian RAD52 functions in break-induced replication repair of collapsed DNA replication forks. *Mol. Cell* 64, 1127–1134.
- Stark, J.M., Pierce, A.J., Oh, J., Pastink, A., and Jasin, M. (2004). Genetic steps of mammalian homologous repair with distinct mutagenic consequences. *Mol. Cell. Biol.* 24, 9305–9316.
- Stratton, M.R., Campbell, P.J., and Futreal, P.A. (2009). The cancer genome. *Nature* 458, 719–724.
- Thiery, J.P., Acloque, H., Huang, R.Y., and Nieto, M.A. (2009). Epithelial-mesenchymal transitions in development and disease. *Cell* 139, 871–890.
- Tsantoulis, P.K., Kotsinas, A., Sfrikakis, P.P., Evangelou, K., Sideridou, M., Levy, B., Mo, L., Kittas, C., Wu, X.R., Papavassiliou, A.G., and Gorgoulis, V.G. (2008). Oncogene-induced replication stress preferentially targets common fragile sites in preneoplastic lesions. A genome-wide study. *Oncogene* 27, 3256–3264.
- Valencia, A., Cervera, J., Such, E., Barragán, E., Bolufer, P., Fuster, O., Collado, R., Martínez, J., and Sanz, M.A. (2009). Complex Variant t(9;22) Chromosome Translocations in Five Cases of Chronic Myeloid Leukemia. *Adv. Hematol.* 2009, 187125.
- Van der Auwera, G.A., Carneiro, M.O., Hartl, C., Poplin, R., Del Angel, G., Levy-Moonshine, A., Jordan, T., Shakir, K., Roazen, D., Thibault, J., et al. (2013). From FASTQ data to high confidence variant calls: the Genome Analysis Toolkit best practices pipeline. *Curr. Protoc. Bioinformatics* 43, 10.1, 33.
- Wang, K., Li, M., and Hakonarson, H. (2010). ANNOVAR: functional annotation of genetic variants from high-throughput sequencing data. *Nucleic Acids Res.* 38, e164.
- Wellenreuther, M., and Bernatchez, L. (2018). Eco-evolutionary genomics of chromosomal inversions. *Trends Ecol. Evol.* 33, 427–440.
- Wong, D.J., Liu, H., Ridky, T.W., Cassarino, D., Segal, E., and Chang, H.Y. (2008). Module map of stem cell genes guides creation of epithelial cancer stem cells. *Cell Stem Cell* 2, 333–344.
- Wood, P.A., Yang, X., and Hrushesky, W.J. (2009). Clock genes and cancer. *Integr. Cancer Ther.* 8, 303–308.

Wu, Y., Kantake, N., Sugiyama, T., and Kowalczykowski, S.C. (2008). Rad51 protein controls Rad52-mediated DNA annealing. *J. Biol. Chem.* *283*, 14883–14892.

Yamada, K., and Miyamoto, K. (2005). Basic helix-loop-helix transcription factors, BHLHB2 and BHLHB3; their gene expressions are regulated by multiple extracellular stimuli. *Front. Biosci.* *10*, 3151–3171.

Yan, W.X., Mirzazadeh, R., Garnerone, S., Scott, D., Schneider, M.W., Kallas, T., Custodio, J., Wernersson, E., Li, Y., Gao, L., et al. (2017). BLISS is a versatile and quantitative method for genome-wide profiling of DNA double-strand breaks. *Nat. Commun.* *8*, 15058.

Yu, Y., Schleich, K., Yue, B., Ji, S., Lohneis, P., Kemper, K., Silvis, M.R., Qutob, N., van Rooijen, E., Werner-Klein, M., et al. (2018). Targeting the senescence-overriding cooperative activity of structurally unrelated H3K9 demethylases in melanoma. *Cancer Cell* *33*, 785.

Zhang, Y., Liu, T., Meyer, C.A., Eeckhoute, J., Johnson, D.S., Bernstein, B.E., Nusbaum, C., Myers, R.M., Brown, M., Li, W., and Liu, X.S. (2008). Model-based analysis of ChIP-Seq (MACS). *Genome Biol.* *9*, R137.

Zhu, Y., Tchkonina, T., Pirtskhalava, T., Gower, A.C., Ding, H., Giorgadze, N., Palmer, A.K., Ikeno, Y., Hubbard, G.B., Lenburg, M., et al. (2015). The Achilles' heel of senescent cells: from transcriptome to senolytic drugs. *Aging Cell* *14*, 644–658.

Zhu, G., Pan, C., Bei, J.X., Li, B., Liang, C., Xu, Y., and Fu, X. (2020). Mutant p53 in Cancer Progression and Targeted Therapies. *Front. Oncol.* *10*, 595187.

Zirke, A., Nikolic, M., Sofiadis, K., Mallm, G-P., Brackley, C.A., Gothe, H., Drechsel, O., Becker, C., Altmüller, J., and Josipovic, N. (2018). HMGB2 Loss upon Senescence Entry Disrupts Genomic Organization and Induces CTCF Clustering across Cell Types. *Mol Cell* *70*, 730–744.

STAR★METHODS

KEY RESOURCES TABLE

REAGENT or RESOURCE	SOURCE	IDENTIFIER
Antibodies		
Mouse anti-CDC6	Santa Cruz	Cat# sc-9964, RRID:AB_627236
Mouse anti-BHLHE40	Santa Cruz	Cat# sc-101023, RRID:AB_2065356
Mouse anti-BRCA1	Santa Cruz	Cat# sc-6954, RRID:AB_626761
Mouse anti-BRCA2	Sigma (mfr. Calbiochem)	Cat# OP95, RRID:AB_2067762
Mouse anti-Vinculin	Sigma	Cat# V9131, RRID:AB_477629
Rabbit anti-RAD51	Merck-Millipore	Cat# PC130, RRID:AB_2238184
Mouse anti-RAD52	Santa Cruz	Cat# sc-365341, RRID:AB_10851346
Sheep anti-RAD52	MRC-PPU Reagents, University of Dundee, Scotland	Supplied by Dr. Claudia and Jiri Lukas
Rabbit anti-RPA70	Abcam	Cat# ab79398, RRID:AB_1603759
Mouse anti- γ -H2AX (pSer139/140)	Abcam	Cat# ab22551, RRID:AB_447150
Mouse anti-p53	Santa Cruz	Cat# 18-7251, RRID:AB_86845
Mouse anti-MDM2	Santa Cruz	Cat# sc-965, RRID:AB_627920
Rabbit anti-PER1	Abcam	Cat# ab136451
Rabbit anti- β -actin	Cell Signaling Technology	Cat# 4967, RRID:AB_330288
Rabbit anti-GAPDH	Cell Signaling Technology	Cat# 2118, RRID:AB_561053
Rabbit anti-HA-tag	Cell Signaling Technology	Cat# 5017, RRID:AB_10693385
Rabbit anti-53BP1	Abcam	Cat# ab36823, RRID:AB_722497
Rabbit anti-CDH1	Cell Signaling Technology	Cat# 3195, RRID:AB_2291471
Mouse anti-Vimentin	Sigma	Cat# V6630, RRID:AB_477627
Rabbit anti-H3K27ac	Active Motif	Cat# 39133, RRID:AB_2561016
Rabbit anti-H3K27me3	Active Motif	Cat# 39155, RRID:AB_2561020
Rabbit anti-Ki-67	Abcam	Cat# ab16667, RRID:AB_302459
Rabbit anti-caspase 3	Cell Signaling	Cat# 9662, RRID:AB_331439
Rabbit anti-CTCF	Active Motif	Cat# 61311, RRID:AB_2614975
Horse Radish Peroxidase-conjugated anti-mouse	Cell Signaling Technology	Cat# 7076, RRID:AB_330924
Horse Radish Peroxidase-conjugated anti-rabbit	Cell Signaling Technology	Cat# 7074, RRID:AB_2099233
Alexa Fluor 488 donkey anti-rabbit	Abcam	Cat# ab150073, RRID:AB_2636877
Alexa Fluor 568 goat anti-mouse	Abcam	Cat# ab175473
Alexa Fluor 488 goat anti-mouse	Thermo Scientific Fischer	Cat# A-11029, RRID:AB_2534088
Alexa Fluor 568 goat anti-mouse	Thermo Scientific Fischer	Cat# A-11031, RRID:AB_144696
Alexa Fluor 488 goat anti-rabbit	Thermo Scientific Fischer	Cat# A-11034, RRID:AB_2576217
Alexa Fluor 568 goat anti-rabbit	Thermo Scientific Fischer	Cat# A-11036, RRID:AB_10563566
Alexa Fluor 568 donkey anti-sheep	Thermo Scientific Fischer	Cat# A-21099, RRID:AB_2535753
Rat anti-BrdU/CldU	Bio-rad (former AbD Serotec)	Cat# OBTO030, RRID:AB_609568
Mouse anti-IdU/BrdU	Becton Dickinson	Cat# 347580, RRID:AB_10015219
Chemicals, peptides, and recombinant proteins		
Keratinocyte-Serum Free medium	Invitrogen	17005-075
Bovine pituitary extract + human epidermal growth factor (hEGF)	Invitrogen	37000-015
Doxycycline	Sigma	D9891-5G

(Continued on next page)

Continued

REAGENT or RESOURCE	SOURCE	IDENTIFIER
BamHI	NEB	R0136S
SmaI	NEB	R0141S
BbSI	NEB	R0539S
5,6-dichloro-1- β -D-ribofuranosylbenzimidazole (DRB)	Merck	287891
Laemmli buffer	Merck	38733
polyvinylidene fluoride (PVDF) membrane	Macherey-Nagel	741260
Clarity Western ECL Substrate	Bio-rad	1705060
SenTraGor™	Supplied by Lab Supplies Scientific	N/A
5-ethynyl-2'-deoxyuridine (EdU)	Invitrogen	A10044
diamidino-2-phenylindole (DAPI)	Thermo Fisher Scientific	62248
5-Iodo-2'-deoxyuridine (IdU)	Sigma-Aldrich	I7125
5-Chloro-2'-deoxyuridine (CldU)	Sigma-Aldrich	C6891
5-bromo-2'-deoxyuridine (BrdU)	Sigma-Aldrich	B5002
Effectene Transfection Reagent	QIAGEN	301425
Trizol	Thermo Fisher Scientific	15596026
Phosphate Buffer Saline (PBS) 1X	Biowest	L0615-500
Triton X-100	Acros Organics	327372500
FuGENE® HD Transfection Reagent	Promega	E2311
Trypsin/ Ethylenediaminetetraacetic acid (EDTA) 10x	Thermo Fisher Scientific	15400054
Trypsin Neutralizer Solution	Thermo Fisher Scientific	R002100
Fetal Bovine Serum (FBS)	GIBCO	10270-106
Bovine Serum Albumin (BSA)	Applichem	A1391
Proteinase K	Thermo Fisher Scientific	AM2548
Paraformaldehyde (PFA)	Merck	104005
Glycine	Applichem	A1067
Lipofectamine RNAiMAX Transfection Reagent	Thermo Fisher Scientific	13778150
Critical commercial assays		
Click-iT Alexa Fluor 647 Imaging Kit	Thermo Fisher Scientific	C10340
Direct-zol RNA miniprep kit	Zymo Research	R2050
TruSeq RNA library kit	Illumina	RS-122-2001
Arima Hi-C kit	Arima Genomics	A51008-ARI
QIAquick PCR Purification Kit	QIAGEN	28104
Deposited data		
All Hi-C data have been uploaded on NCBI Gene Expression Omnibus repository	This paper	GSE163371
All other data have been uploaded on Sequence Read Archive	This paper	bioproject PRJNA685322
Raw data from Figures 1, 2, 3, 5, 6, S1, and S4–S6 were deposited on Mendeley	This paper	https://doi.org/10.17632/9dhvmhy98s.1
Experimental models: Cell lines		
HBEC-CDC6 Tet-ON	Ramirez et al., 2003 ; Komseli et al., 2018	Supplied by Liloglou T. (parental cells known as HBEC-3KT Constructed by our group)
HPDEC-CDC6 Tet-ON	Furukawa et al., 1996	Supplied by Townsend P.

(Continued on next page)

Continued

REAGENT or RESOURCE	SOURCE	IDENTIFIER
Oligonucleotides		
Primers for the screening of inverted clones, see Table S4	This paper	N/A
Primers and full Sanger sequences, see Table S4	This paper	N/A
gRNA1, see Table S4	This paper	N/A
gRNA2, see Table S4	This paper	N/A
siRNA cocktail targeting BHLHE40	Origene	Cat No SR305619
siRNA cocktail targeting BHLHE40	Thermo Fisher Scientific	Cat No 1299001; HSS112516, HSS112517, HSS112518
Recombinant DNA		
pcDNA3-HA-BHLHE40	Addgene	RRID:Addgene_110154
pcDNA3 Hygro HA Akt2	Addgene	RRID:Addgene_16000
DR-GFP	Stark et al., 2004	Supplied by Halazonetis T.
BIR-GFP	Sotiriou et al., 2016	Supplied by Halazonetis T.
SA-GFP	Stark et al., 2004	Supplied by Halazonetis T.
HA-ISceID44A	Galanos et al., 2018	Supplied by Soutoglou E.
pSpCas9(BB)-2A-GFP (PX458)	Addgene	RRID:Addgene_48138
pU6-(BbsI)_CBh-Cas9-T2A-mCherry	Addgene	RRID:Addgene_64324
Software and algorithms		
ScanR automated image acquisition and analysis software (Olympus, 3.1)	Olympus	https://www.olympus-lifescience.com/en/microscopes/inverted/scanr/
TIBCO Spotfire Analyst, version 10.10.3	Tibco Software	https://perkinelmerinformatics.com/products/exclusive-reseller/tibco-spotfire/
STAR aligner (version 2.5.3a)	Dobin et al., 2013	https://github.com/alexdobin/STAR
Samtools (version 0.1.19)	Li et al., 2009	http://samtools.sourceforge.net/
HTseq count (version 0.5.4p3.)	Anders et al., 2015	https://htseq.readthedocs.io/en/master/history.html
RUVseq	Risso et al., 2014	https://rdrr.io/bioc/RUVSeq/man/RUVr.html
DESeq	Anders and Huber, 2010	https://www.bioconductor.org/packages/2.10/bioc/html/DESeq.html
BWA-MEM	Li and Durbin, 2010	http://bio-bwa.sourceforge.net/
MACS2 (ver. 2.1.2)	Zhang et al., 2008	https://pypi.org/project/MACS2/
Bowtie (ver. 2.3.4.1)	Langmead and Salzberg, 2012	https://sourceforge.net/projects/bowtie-bio/files/bowtie2/2.3.4.1/
HiCExplorer (ver. 3.2)	Ramírez et al., 2018	https://github.com/deeptools/HiCExplorer
Knight-Ruiz (KR) matrix balancing algorithm	Knight and Ruiz, 2013	https://github.com/deeptools/Knight-Ruiz-Matrix-balancing-algorithm
HiGlass	Kerpedjiev et al., 2018	https://higlass.io/
Cooler	Abdennur and Mirny, 2020	https://github.com/open2c/cooler
MANTA	Chen et al., 2016	https://github.com/Illumina/manta
ANNOVAR	Wang et al., 2010	https://annovar.openbioinformatics.org/en/latest/
<i>Bcftools</i>	Li et al., 2009	https://github.com/samtools/bcftools
<i>GATK tools</i>	Van der Auwera et al., 2013	https://gatk.broadinstitute.org/hc/en-us
Other		
Matrigel Invasion Chambers	Corning	354480
Neubauer glass chamber	Mariefeld Superior	0640010
Kodak® BioMax® MS film	Merck	Z363030-50EA

RESOURCE AVAILABILITY

Lead contact

Further information and requests for resources and reagents should be directed to and will be fulfilled by the Lead Contact, Vassilis Gorgoulis (vgorg@med.uoa.gr)

Materials availability

This study did not generate any unique reagents.

Data and code availability

- All Hi-C data generated in this study have been deposited at GEO and are publicly available as of the date of publication. Accession numbers are listed in the [Key resources table](#). Original western blot images have been deposited at Mendeley and are publicly available as of the date of publication. The DOI is listed in the [Key resources table](#). Microscopy data reported in this paper will be shared by the lead contact upon request.
- This paper does not report original code.
- Any additional information required to reanalyze the data reported in this paper is available from the lead contact upon request.

All the Hi-C data generated in this study are available via the NCBI Gene Expression Omnibus repository under accession number GSE163371 (reviewer access token: *kfmxxuaxnklzqd*). All the other data are available via the Sequence Read Archive under bio-project PRJNA685322.

Raw data from [Figures 1, 2, 3, 5, 6, S1, and S4–S6](#) were deposited on Mendeley at [<https://doi.org/10.17632/9dhvmhy98s.1>].

EXPERIMENTAL MODEL AND SUBJECT DETAILS

Human female HBEC-CDC6 Tet-ON and HPDEC-CDC6 Tet-ON cell lines were maintained in Keratinocyte-Serum-Free Medium (17005-075, Invitrogen) supplemented with 50 μ g/ml Bovine Pituitary Extract and 5ng/ml hEGF (37000-015, Invitrogen) at 37°C and 5% CO₂ ([Komseli et al., 2018](#)). CDC6 induction was conducted by treatment of the cell culture with 1 μ g/ml doxycycline hyclate (DOX) (Sigma). Where applied, 5,6-dichloro-1- β -D-ribofuranosylbenzimidazole (DRB, Merck) was used at a final concentration of 100 μ M and it was added directly in the growth media for the indicated time periods. The cell lines used in this study were not found in the database of commonly misidentified cell lines that is maintained by ICLAC and NCBI Biosample. Its identity has been authenticated by STR profiling and is regularly tested for mycoplasma.

METHOD DETAILS

Plasmid generation

The pcDNA3-HA-BHLHE40 vector was obtained from Addgene (cat No 110154). The neomycin resistance cassette was replaced with a hygromycin coding one. The hygro insert was amplified through fusion-PCR from a pcDNA3 Hygro HA Akt2 vector (Addgene Cat No 16000). Moreover, a pcDNA3 Hygro vector with no insert was generated for mock experiments.

siRNA and plasmid transfections

For BHLHE40 silencing two different cocktails of 3 unique siRNA duplexes - 2 nmol each from OriGene Technologies, Inc, (Cat No SR305619) and from Thermo Fisher Scientific (#1299001: HSS112516, HSS112517, HSS112518) were employed respectively, to secure off-target effects. siRNA gene silencing was performed as previously described, following also the manufacturer's instructions ([Galanos et al., 2016](#)). More specifically, 3 \times 10⁵ cells plated in 60mm dishes were transfected using Invitrogen Lipofectamine RNAiMAX Transfection Reagent (#13778150) with the appropriate RNAi pool (set of three siRNAs) or the corresponding RNAi negative control. Cells were harvested 48h after transfection for further analysis.

Selection of escaped clones

Initially, 5 \times 10⁵ cells were plated. One day after the plating, CDC6 expression is induced by adding doxycycline in the culture media. Following the induction, cells fully senesce at day 6. At about day 30, senescence-evading cells start forming roughly 50 distinct colonies. Eventually, colonies were collected and they were transferred to 6-well plates, where they independently propagated.

Protein extraction, cell fractionation and immunoblot analysis

Total protein extracts were obtained by resuspension in 50 mM Tris/HCl pH 8.0, 150 mM NaCl, 0,1% SDS, 0,5% sodium deoxycholate, 1% NP-40 adjusted with protease and phosphatase inhibitors and rotation for 1 h at 4°C. The lysate was centrifuged at 13,400 rpm at 4°C for 15 min. The supernatant was collected and proteins quantified using Protein assay dye concentrate (BIO-RAD). Thirty micrograms of protein from total extracts per sample were adjusted with Laemmli buffer (Merck, 38733) and loaded on acrylamide/bis-acrylamide gels. Gel electrophoresis was followed by transfer to PVDF membrane (Macherey-Nagel, 741260), while signal

development was carried out by Clarity Western ECL Substrate (Bio-rad, 1705060) chemiluminescence and captured by using either autoradiography films (Kodak® BioMax® MS film) or on an iBright CL750 Imaging System (Thermo Fisher Scientific). Horse Radish Peroxidase conjugated anti-mouse and anti-rabbit secondary antibodies (1:1000 dilution) (Cell Signaling) were used.

Primary antibodies utilized were: anti-CDC6 (mouse, Santa Cruz, sc9964, 1:500), anti-BHLHE40 (mouse, Santa Cruz, sc101023, 1:200), anti-RAD52 (mouse, Santa Cruz, sc-365341, 1:100), anti-RAD51 (rabbit, Merck-Millipore, PC130, 1:100), anti-BRCA1 (mouse, Santa Cruz, sc6954, 1:500), anti-BRCA2 (mouse, Sigma (mfr. Calbiochem), OP95, 1:500), anti-p53 (mouse, Santa Cruz, DO7, 1:500), anti-MDM2 (mouse, Santa Cruz, SMP14, 1:500), anti-PER1 (rabbit, Abcam, ab136451, 1:500), anti- β -actin (rabbit, Cell Signaling, 4967L, 1:1000), anti-GAPDH (rabbit, Cell Signaling, 2118S, 1:2000), anti-vinculin (mouse, Sigma, V9131, 1:1000), anti-HA-Tag (C29F4 rabbit, Cell Signaling, 3724, 1:1000). All analyses were performed in triplicate.

Immunofluorescence analysis

Indirect immunofluorescence analysis was performed as previously described (Galanos et al., 2018). Specifically, cells were seeded and grown on 12-mm diameter autoclaved glass coverslips. To identify RAD52, RPA70, 53BP1 and γ H2AX foci, cells were pre-extracted on ice with cold PBS containing 0.1% Triton X-100 for 5 min before fixation in 4% cold formaldehyde solution for 15 min at room temperature. For the rest of the analyzed proteins, the pre-extraction step was skipped. When Click-iT EdU staining was performed, cells were incubated with 10 μ M EdU for 30 min, before fixation or pre-extraction. Detection of EdU was performed according to the manufacturer's recommendations (Click-iT Imaging Kit Alexa Fluor 647; Thermo Fisher Scientific, C10340) followed by incubation with primary antibodies. Cells were incubated with primary antibodies for 1 h at room temperature. Following washing steps with PBS, coverslips were incubated with the corresponding secondary antibodies (Thermo Fischer Scientific) supplemented with DAPI for an additional 1 h at room temperature before washed again and mounted. Image acquisition of multiple random fields was automated on a DM 6000 CFS Upright Microscope (Confocal Leica TCS SP5 II) or a ScanR screening station (Olympus) and analyzed with ScanR (Olympus) software, or a Zeiss Axiolab fluorescence microscope equipped with a Zeiss Axiocam MRm camera and Achroplan objectives, while image acquisition was performed with AxioVision software 4.7.1. In the case of RAD52, the representative images of foci formation (presented in Figure 3Ci) were acquired with a confocal LSM800 Zeiss microscope and processed with its Blue ZEN software. Primary antibodies utilized were: anti-CDC6 (mouse, Santa Cruz, sc9964, 1:500), anti-RAD52 (sheep, MRC-PPU Reagents, 1:100, kind gift from Drs. Jiri and Claudia Lukas), anti-53BP1 (rabbit polyclonal, Abcam ab36823, 1:250), anti-CDH1 (E-cadherin) (rabbit monoclonal, Cell Signaling #3195S, 1:100), anti-Vimentin (mouse monoclonal, Sigma V6630, 1:100), anti-RPA70 (rabbit, Abcam, ab79398, 1:100), anti- γ H2AX (mouse monoclonal, Abcam, ab22551, 1:100). All analyses were performed in triplicate.

Immunocytochemistry

For immunocytochemistry analysis cells were grown on coverslips and fixed with 100% ice-cold methanol or 4% formaldehyde (prepared from paraformaldehyde) for 10 min and stored at 4°C until staining was performed. Following, cells were permeabilized with 0.3% Triton X-100 in PBS for 5 min at RT. A 10% fetal bovine serum and 3% bovine serum albumin in PBS solution was used as a blocking buffer for 1 h at RT. Primary antibodies were diluted in blocking buffer and incubated overnight at 4°C. Secondary antibodies were: Ki-67 (rabbit, Abcam, ab16667, 1:250), caspase 3 (rabbit, Cell Signaling, 9662, 1:500). Nuclear signal was evaluated as a positive one. A minimum of 100 cells were counted at high power optical field (x 400).

Cell growth analysis

HBEC cells were seeded at day 0 on 6-well plates at a density of 8×10^4 cells per well. Every day up to day 6, cells from one well at a time were trypsinized and counted using a standard Neubauer chamber (Marienfeld Superior, # 0640010).

3D (organotypic) culture

First, airway fibroblasts were embedded in type I collagen, allowing contraction of the gel mimicking the underlying submucosa, as previously described (Sato et al., 2006; Ramirez et al., 2003; Lagopati et al., 2021). Briefly, positively selected HBEC-CDC6 Tet-ON cells were seeded on top of the contracted layer and upon attachment of HBECs on the underlying stroma, the organotypic culture was submerged into Keratinocyte-Serum-Free Medium (#17005-075, Invitrogen) supplemented with 50 μ g/ml Bovine Pituitary Extract and 5ng/ml hEGF (#17005-075, Invitrogen) and then lifted to an air-liquid interface, while cell growth was performed at 37°C with 5% CO₂. Following, CDC6 induction was performed as per the 2D culture medium. Finally, matrigels were collected at 6 and 30 days post-induction, formalin fixed and paraffin embedded. Sections were obtained and processed for hematoxylin-eosin and GL13 staining and immunohistochemical analysis as described in previous section.

Senescence detection with SenTraGor

SenTraGor™ staining was performed and evaluated according to previous published protocols (Evangelou et al., 2017, Gorgoulis et al., 2019; Kohli et al., 2021). Specifically, fixed cells mounted on coverslips were rinsed sequentially in 50% and 70% Ethanol for 5 minutes at room temperature, respectively. Then the coverslips were incubated with the SenTraGor™ solution for 10 minutes. Following washings with 50% Ethanol and TBS at room temperature, the anti-biotin antibody ([Hyb-8] ab201341 Abcam, diluted 1:30 in TBS) was applied for 60 minutes at 37°C. Subsequently the signal was developed using the Ultravision Quanto Detection System

HRP DAB kit (Cat no: TL-125-QHD), according to the manufacturer's instructions. Finally cells were counterstained with Hematoxylin (diluted 1:4 in deionized water) for 40 s and observed under a light microscope.

Invasion assay

Invasion assay was performed as described elsewhere (Sideridou et al., 2011; Galanos et al., 2016). Cells were trypsinized and plated (1×10^5) into a cell invasion chamber (Corning, 354480) containing EGF-free medium and allowed to invade for 24h toward full medium. Cells were fixed with 4% paraformaldehyde, stained with Giemsa, photographed and counted. Data from three independent measurements were averaged, and the corresponding SDs are also reported.

Tumorigenicity assay

Tumorigenicity assay was performed as previously described (Liontos et al., 2007). In brief, ESC and OFF cells were collected, washed in PBS, and s.c. injected (2×10^6 cells) at two opposite sites in the abdominal region of the same male severe combined immunodeficient (SCID) mouse, respectively. Two animals were tested. Tumor growth was measured twice to thrice weekly.

Flow cytometry analysis (FACS) - Cell Cycle analysis

Cell cycle analysis was determined using a BD FACSVerse (BD Biosciences), following EdU incorporation, as previously published (Galanos et al., 2016). Briefly, cells were incubated with 10 μ M EdU for 30 min, and they were then fixed with 70% of ice cold ethanol and were incubated on ice for at least 30 min or kept at -20°C until the day of staining and analysis. Afterward, the samples were centrifuged (1500 rpm, 5 min at room temperature) and washed sequentially with PBS and PBS⁺ (PBS, 1% BSA and 0,1% Tween). Detection of EdU was performed according to the manufacturer's recommendations (Click-iT Imaging Kit Alexa Fluor 647; Thermo Fisher Scientific, C10340) and subsequently samples were incubated with Hoechst 33342 (1:1000 in PBS) followed by a final wash with PBS⁺. Cells were then analyzed on BD FACSVerse (BD Biosciences) and acquired data were processed using the FlowJo software.

5'-EU incorporation based nascent RNA assay

In situ detection of nascent RNA was performed with the Click-iT Alexa Fluor 488 Imaging Kit (Thermo Fisher Scientific) as described elsewhere (Komseli et al., 2018).

QIBC analysis

Quantitative image-based cytometry (QIBC) analysis (Figure S2) was performed essentially as previously described (Ochs et al., 2016). In brief, images were taken with a ScanR inverted microscope High-content Screening Station (Olympus) for Life Science that was equipped with wide-field optics, 20x or 40x dry objectives were used, fast excitation and emission filter-wheel devices for 6 different spectral wavelength areas, an MT20 illumination system, and a digital monochrome scientific CMOS camera with sensor chip FL-400. Images were obtained in an automated fashion with the ScanR acquisition software (Olympus, 3.2.0). For each condition, 81 to 100 images were acquired containing at least 2,000 cells per condition. Acquisition times for the different channels were adjusted for non-saturated conditions, and same settings were applied to all the samples within one experiment. Images were processed and analyzed with the corresponding ScanR analysis software. In brief, the DAPI signal was used for the generation of an intensity-threshold-based mask to identify individual nuclei as main objects. This mask was then applied to analyze pixel intensities in different channels for each individual nucleus. For analysis of DNA damage-induced foci, additional masks were generated by segmentation of the respective images into individual spots with intensity-based or spot-detector modules provide by the software. Foci were defined as sub-objects, and the generated mask was used for quantification of pixel mean intensities in foci. Based on the distinguished objects and sub-objects, the desired parameters (mean and total intensities, area, foci count, and foci intensities) for the each nuclei or foci were quantified, as well as derived parameters (sum of foci intensity per nucleus). These values were then exported as .txt files and analyzed with TIBCO Software (version 10.10.0). This software was used to quantify absolute, median, and average values in cell populations and to generate all color-coded scatterplots. Within one experiment, similar cell numbers were compared for the different conditions. Primary antibodies utilized were: anti-53BP1 (rabbit, Abcam ab36823, 1:250), anti- γ H2AX (pSer139/140) (rabbit, Abcam, ab36823, 1:100), anti-RPA (rabbit, Abcam, ab79398, 1:100), anti-RAD52 (sheep, MRC-PPU Reagents, 1:100, kind gift from Drs. Jiri and Claudia Lukas).

DR-GFP, SA-GFP and BIR-GFP reporter assays

HBEC-CDC6 Tet-ON cells were transiently transfected with the GFP based reporter constructs for synthesis-dependent strand annealing (DR-GFP), single strand annealing (SA-GFP) and break induced replication (BIR-GFP), as previously described (Galanos et al., 2018). To monitor repair of I-SceI-generated DSBs, cells were transiently co-transfected with 1 μ g of the I-SceI expression vector HA-ISceI44A (Addgene #59424) using the Effectene reagent (QIAGEN). DSB repair efficiency upon CDC6 induction was determined by quantifying GFP-positive cells via flow cytometry FACS Calibur (Becton Dickinson) 48h after transfection, under non-chromatinized conditions.

DNA fiber fluorography (combing assay)

The assay was conducted as previously described (Galanos et al., 2016). Briefly, HBEC-CDC6 Tet-ON cells were grown in the presence or absence of doxycycline for the indicated time points (see Figure 2B) and then pulsed-labeled with 25 μ M CldU for 20min, and

then labeled with 250 μ M IdU for 20min (1:1000, I7125, Sigma-Aldrich). Cells were then harvested and lysed on glass slides in spreading buffer, DNA was denatured and stained using rat anti-BrdU/CldU (1:1000, C6891, B5002, Sigma-Aldrich) and mouse anti-IdU/BrdU (1:500, clone B44, Becton Dickinson) antibodies.

Breaks Labeling *In Situ* and Sequencing (BLISS)

“Breaks Labeling *In Situ* and Sequencing” (BLISS) analysis was performed as previously described (Yan et al., 2017; Bouwman et al., 2020). Briefly, the method consists of following main steps: i) upon harvesting of cells from multi-well plates, approx. 2 million cells were fixed in suspension with 4% formaldehyde for 10 min at room temperature, ii) DSBs ends were *in situ* blunted, iii) next they were tagged with dsDNA adapters containing sample barcodes, UMIS (unique molecular identifiers), RA5 adaptor and T7 promoter, iv) tagged DSB ends were linearly amplified using *in vitro* transcription and v) the resulting RNA was used for library preparation and sequencing. BLISS data were analyzed as described below.

Next Generation Sequencing and Bioinformatics analysis

For whole-genome sequencing (WGS), library preparations were as described previously (Galanos et al., 2018). SAMtools *mpileup* and *bcftools* (Li et al., 2009), *GATK tools*, the GATK source bundle and the GATK best practices guide (Van der Auwera et al., 2013), were used for identification and filtering of the SNPs and INDELS. Variations that were unique in the “escaped” cells were normalized based on the sequencing depth of each experiment. Copy number and structural variants were determined using MANTA (Chen et al., 2016) and annotated on the Human reference genome using ANNOVAR (Wang et al., 2010). As shared CNVs (or overlapped regions) we characterized the common intersected variations between the escape replicates, (using *intersectBed -wa -u* from BEDtools), after extracting the variations that are present in the OFF samples (*intersectBed -v*). A detailed description, on the intersected CNVs, among the precise coordinates of all CNVs is reported in the new Table S1. The depth of coverage that was obtained for each sample is described in Table S4B.

For BLISS data, DNA Double Stranded Breaks (DSBs) were normalized for total mapped reads and for the total number of used cells for each replicate. The aggregation of Unique Molecule Identifiers (UMIs) and the frequency of DSBs in various genomic regions were calculated using in-house R scripts (available on request).

BLISS signal data and CNV regions were compared with *intersectBed*, a subcommand from BEDtools suite in order to determine the distribution of expected overlaps. As a control we used a randomly selected set of loci by applying the *randomBed* and *shuffleBed* subcommands in order to permute these genomic locations repeatedly (10000 times).

RNA isolation, sequencing, and data analysis

6-day ON and senescence-bypass “inverted” HBECs were harvested in Trizol (Thermo Fisher Scientific, 15596026) and total RNA was isolated and DNase-treated using the Direct-zol RNA miniprep kit (Zymo Research) as per manufacturer’s instructions. cDNA libraries were next generated using the TruSeq RNA library kit (Illumina) via selection on poly(dT) beads. The resulting libraries were single-end sequenced to > 50 million reads on a HiSeq4000 platform (Illumina). Raw reads were mapped to the human genome (hg19) using STAR aligner (version 2.5.3a) (Dobin et al., 2013). Samtools (version 0.1.19) (Li et al., 2009) were used for data filtering and file format conversion, while HTseq count (version 0.5.4p3.) algorithm (Anders et al., 2015) was used to assign aligned reads to exons using the following command line `<htseq-count -s no -m intersection -nonempty>`. Normalization of reads and removal of unwanted variation was performed with RUVseq (Risso et al., 2014). Differential gene expression was computed using DESeq (Anders and Huber, 2010), and significantly deregulated genes (fold change cut-off 1.5 and P value \leq 0.05) are listed in Table S5.

Chromatin immunoprecipitation (ChIP), sequencing, and data analysis

ChIP was performed on 10-15 million cells crosslinked in 1% PFA/PBS at RT for 10 min, and quenched in 0.125M ice-cold glycine. ChIP material was prepared as previously described (Ford et al., 2014), and sonication was performed using a Bioruptor sonicator and adjusting fragment size to 200-500 bp. For the IP the following polyclonal antisera were used: anti-CTCF (61311, Active Motif), anti-H3K27ac (39133, Active Motif), anti-H3K27me3 (39155, Active Motif) and anti-BHLHE40 (#NB100-800, Novus Biologicals). ChIP-seq libraries were sequenced on a HiSeq4000 platform (Illumina) to at least 25 million reads per sample, and analyzed using the ENCODE pipeline (https://www.encodeproject.org/chip-seq/transcription_factor/).

Genome-wide chromosome conformation capture (Hi-C) and data analysis

In situ Hi-C on HBECs of different states and genotypes was performed and controlled for quality using the Arima Hi-C kit as per manufacturer’s instructions. All resulting libraries that met the QC criteria set by the manufacturer were paired-end sequenced on a NovoSeq6000 platform (Illumina) to at least 0.5 billion reads. For data analysis, reads were mapped to the reference human genome (GRCh37/hg19) using Bowtie (ver. 23.4.1) (Langmead and Salzberg, 2012) with the “-reorder” flag. Local mapping was used to increase mapping rates due to the inherent presence of chimeric reads. All preprocessing and downstream analysis was performed using HiCExplorer (ver. 3.2) (Ramírez et al., 2018) to remove unmappable reads, non-uniquely mapped reads and low-mapping-quality reads, as well as duplicated pairs (i.e., starting and ending with exactly the same location), dangling-ends (i.e., digested but not ligated), self-circularized (i.e., reads pairing within < 25 Kbp and facing outward), same-fragment (i.e., read pair locating in the same restriction enzyme fragment) or self-ligated reads (i.e., having a restriction site in between the read pair within < 800 bp). Next,

genome-wide contact matrices were generated in the form of *.cool* files, in which the genome was binned into different sizes (resolution) — 10 kb, 20 kb, 50 kb and 100 kb — for different downstream usage. To facilitate comparison between different samples, all Hi-C interaction counts were normalized and then balanced using the Knight-Ruiz (KR) matrix balancing algorithm (Knight and Ruiz 2013). Hi-C matrices stored in *.cool* files were visualized using HiGlass (Kerpedjiev et al., 2018) as interactive heatmaps. To make zooming-in and -out possible, normalized and balanced *.cool* files at 10 Kbp resolution were converted to multi-resolution cooler files called *.mcool* files using Cooler (Abdennur and Mirny 2020). For calling A/B compartments, 100 kbp-resolution and Pearson-transformed matrices were used to calculate the first eigenvector, which was then integrated with own H3K27ac ChIP-seq data to mark A-compartments. TADs were assigned using 20 kbp-resolution matrices using the function embedded in HiCExplorer based on deduced z-scores and with a *P*-value cutoff of 0.01. Finally, loops we detected as previously described (Rao et al., 2014) by computing a negative binomial distribution of 10 kbp-resolution Hi-C data and using Anderson-Darling/Wilcoxon rank-sum tests and a *P*-value cutoff of 0.05; loop lengths were restricted to 0.1–2 Mbp (to avoid signal contamination from the diagonal of Hi-C matrices), and compared to CTCF ChIP-seq data to identify loops with CTCF-bound anchors.

CRISPR/Cas9 inversion generation

Design of gRNAs

Based on the WGS data (see corresponding section), 20-nt sgRNAs were designed around each breakpoint. Two complementary DNA oligos for each sgRNA were annealed generating 5' overhangs consisting of CACC(G) and AAAC. gRNA1 and gRNA2 were chosen due to high specificity and small distance from the exact breakpoints (Table S4). They were cloned into – Cas9 expression plasmids – pSpCas9(BB)-2A-GFP (PX458) and pU6-(BbsI)_CBh-Cas9-T2A-mCherry, respectively, which had been already digested with BbsI. In this way, sgRNAs were integrated next to the gRNA scaffold of the particular vector (Figure S6A) (Table S4).

Transfection and FACS sorting

HBECs were cultured in Keratinocyte (serum free medium) (#17005042) without antibiotics supplemented with 25 mg Bovine Pituitary Extract and 2.5 μ g EGF, Human Recombinant. Delivery of 2.5 μ g from each plasmid, coding for one sgRNA and Cas9, was performed via double transfection of HBECs two days after plating 8×10^4 cells per well in a 6-well plate (reaching 80% confluency) with FuGENE® HD Transfection Reagent (Promega #E2311) (4:1 FuGENE® HD Transfection Reagent: DNA Ratio). FACS sorting of double positive (GFP and mCherry) cells gave rise to a large number of clones, subsequently cultured in 96-well plates (Figure S6A).

DNA extraction and PCR screening

After harvesting cells from 96-well plates in 30 μ L Trypsin/EDTA 1x (stock 10X, Thermo Fisher Scientific, #15400054), followed by a neutralization step with an equal volume of Trypsin Neutralizer Solution (Thermo Fisher Scientific, #R002100), half of the cells were lysed by adding 30 μ L of Lysis Buffer (50 mM KCl, 10 mM TRIS pH: 8.3, 2.5 mM MgCl₂, 0.45% NP40 and 0.45% Tween20) containing Proteinase K (1 μ L of 20 μ g/ μ L Proteinase K for every 50 μ L of Lysis Buffer), and heating for 45 min at 60°C followed by 10 min at 80°C to inactivate Proteinase K. The other half of the cells were kept in culture. 4 μ L of the lysate were used as genomic DNA for PCR. Two pairs of forward and reverse primer were designed around each breakpoint (Table S4). PCR product of F1/R1 and F2/R2 manifest the wild-type genomic DNA, while F1/F2 and R1/R2 give product in case that the area has been inverted. PCR products were submitted for Sanger sequencing verification (Figure 6A and S6A).

Sanger sequencing

PCR products were purified using the QIAquick PCR Purification Kit (#28104) and submitted for Sanger sequencing. Parental HBEC-CDC6 Tet-ON cells were used as a reference. Primers and full Sanger sequences are available in Table S4.

Survival data analysis

Data on survival analysis was obtained from a public database Kaplan-Meier plotter (<http://www.kmplot.com>; Nagy et al., 2018), except for breast and prostate cancer data for which a separate Log-rank (Mantel-Cox) survival analysis, with Bonferroni correction, was performed on data retrieved from Metabric and TCGA, respectively.

QUANTIFICATION AND STATISTICAL ANALYSIS

Two-tailed unpaired Student's *t* test was employed to compare data obtained by DNA fiber fluorography, QIBC assay, immunofluorescence imaging, reporter assays and differences in cell proliferation and invasion assay.

Super Exact test was used to assess whether common CNVs were significantly more than expected by chance.

The hypergeometric test was applied to estimate the significance of the upregulated genes which were identified as both BHLHE40 target genes and differentially expressed genes during escape.

Fisher's exact test was used to assess the significance of the increased cell death in FACS-based cell cycle profiling and in the immunostaining for Caspase-3.

Wilcoxon-Mann-Whitney test was used to examine changes in the distribution of lengths for the loops observed.